ABSTRACT

Title of Dissertation: YEAR-ROUND DETERMINATION OF METHANE (CH_4) SOURCES AND SINKS IN ARCTIC LAKES USING CONTINUOUS AND AUTONOMOUS SAMPLING

Hadley Allaben McIntosh Marcek, Doctor of Philosophy, 2020

Dissertation directed by: Dr. Laura Lapham
Associate Professor, University Maryland Center for Environmental Science

Methane (CH_4) is a potent greenhouse gas and its concentration has been increasing in the atmosphere. While natural emissions from inland water bodies are known to be important, there is large uncertainty in the amount of methane released from lakes to the atmosphere, especially from Northern latitudes. Part of this is due to limited sampling in these systems during dynamic periods, such as ice-over and ice-melt. To better understand these temporal dynamics, I used autonomous, continuous samplers (OsmoSamplers) to collect lake water year-round over two years (2015-2017). Lake water was collected at a fine temporal resolution to provide time-integrated (~1 week) samples from multiple Arctic lakes within the Mackenzie Delta. The Mackenzie Delta is a lake-rich, productive environment that is expected to be a significant source of methane to the atmosphere. Lakes spanning the central delta and outer delta were sampled for methane concentration and stable carbon isotope ratio ($\delta^{13}C$-CH_4) changes, ion

concentrations, and water column characteristics were measured with continuous sensor data (temperature, water pressure, conductivity, light, and dissolved oxygen). These unique time-series datasets show lakes exhibit a close coupling of dissolved oxygen, and other electron acceptors, with the timing of methane increasing during ice-cover. The increase in methane concentrations is primarily from diffusion out of sediments and possibly water-column methanogenesis. One lake in the outer delta exhibited thermogenic gas bubble dissolution that contributed to under-ice methane concentration increases. Following ice-melt, lake depth appears to impact methane release to the atmosphere. Shallower lakes exhibit rapid fluxes followed by significant microbial methanotrophy. Deeper lakes in the central delta are connected to groundwater, though it does not appear groundwater transports methane. This is the first study of dissolved methane and gas bubble ^{14}C-age in the Mackenzie Delta and shows that dissolved methane is produced primarily from modern carbon sources, such as macrophyte biomass and terrestrial material, but some methane transported in gas bubbles is significantly older, with seeps in the outer delta rapidly releasing radiocarbon-dead, thermogenic methane. This study demonstrates the importance of multi-lake studies particularly with fine scale temporal sampling to understand methane processes in seasonally ice-covered lakes.

YEAR-ROUND DETERMINATION OF METHANE (CH_4) SOURCES AND SINKS IN ARCTIC LAKES USING CONTINUOUS AND AUTONOMOUS SAMPLING

by

Hadley Allaben McIntosh Marcek

Dissertation submitted to the Faculty of the Graduate School of the

University of Maryland, College Park, in partial fulfillment

of the requirements for the degree of

Doctor of Philosophy

2020

Advisory Committee:
Professor Laura Lapham, Chair
Professor Lee Cooper
Professor Michael Gonsior
Dr. Ann McNichol
Professor Karen Prestegaard

Acknowledgements

Science and education cannot be alone and this dissertation is a testament to that. Behind me is a team of people who helped to make my dissertation possible and there are many hours of support and assistance by colleagues, friends, and family.

The research in this project was done with the support of many people both through their contributions to logistics, field work, and data analysis. First and foremost I need to thank the field team of Mitchell Bergstresser, Michelle Côté, Scott Dallimore, Trevor Fournier, Kim Geeves, Laura Lapham, Lance Lesack, Roger MacLeod, Beth Orcutt, Nilou Rajaei, and Geoff Wheat. Lance provided a tremendous amount of guidance about these lake systems to help me to better understand the Mackenzie Delta and provided invaluable assistance in completing this work. The Aurora Research Institute and its staff made a fantastic research station in this fairly remote part of Canada. I also thank the First Nation people for letting us sample their lands and water. The Mackenzie Delta will forever hold a special place in my heart.

A HUGE thanks is given for those who helped me with lab work: cutting kilometers of copper coil, squeezing liters of lake water, and spending days analyzing samples on the ion chromatograph, gas chromatograph and Picarro. Aimee Beardmore, Jessica Loveless, Mary Oster, and Maureen Strauss your help will never be forgotten. Without you I do not know if I could have processed so many samples in the amount of time I did.

I acknowledge the many agencies that funded this work and provided the grants that allowed this dissertation and made my time as a graduate research assistant possible. This includes the National Science Foundation and grants directly to me from the Geological Society of America Charles A. & June R.P. Ross Research Fund, an American Geophysical Union Horton Research Grant, an UMCES Presidential Fellowship, and the Ann G.Wylie Dissertation Fellowship from University of Maryland, College Park.

I extend a thank you to my committee, Lee Cooper, Michael Gonsior, Ann McNichol, and Karen Prestegaard. You each added to this project, data analysis and write-up in your own way. Laura Lapham was a gracious advisor and gave me the flexibility to lead a great life while working on my Ph.D. I am grateful for her life and science advice, editing, and letters of support. I accomplished a lot while Laura's student and that is a reflection of her mentorship and support. I look forward to continuing our collaborations in the future.

Thank you to my friends and family for supporting me the past 5 years. A lot has happened during this time in my life and your love has been so helpful. Stacy Aguilera-Peterson, Lauren Kuschner, Jenna Luek, Sara Shen, Jenna Spackeen, and 'Estrofest' – Alex Atkinson, Aimee Doyle, Christina Goethel, Amy Griffin, Katie Lecorchick, and Leanne Powers – you have made my life a great one. Your constant pushing and uplifting words of encouragement were not lost on deaf ears. I am truly blessed to have such a great support system in my family of Mom, Dad, Alex, and the whole Marcek family. My parents are always there to lend an ear and provide unending levity. I cannot express enough how thankful I am to have grown up in a family that

encouraged my creativity and got me to where I am today. Though, I am still trying to pay attention to the details and keep my antecedents clear. Put it together, take it apart, and finish it; what a great mantra for life and this dissertation.

Finally, I could not have done this without Luke and Remy. Life has been crazy the last few years and you kept me fed, entertained, and relaxed (as much as you could) during the process. As my Mom said, I did this PhD for love – love of a guy and love of science.

Table of Contents

List of Tables

List of Figures

Chapter 1

Introduction

Methane Budgets

Global methane (CH_4) concentrations in the atmosphere have increased significantly to 2.6 times pre-industrial concentrations and were ~1850 ppb in 2018 (Figure 1-1a; Kirschke et al., 2013; Nisbet et al., 2019; Saunois et al., 2016; Saunois et al., 2019). Most of the atmospheric increase in the past few centuries has been from anthropogenic fossil fuel sources (Nisbet et al., 2016). Since 2008, however, global atmospheric CH_4 concentrations have continued to increase, but atmospheric stable carbon isotope ratios ($\delta^{13}C$-CH_4) have changed indicating a shift in CH_4 source (Figure 1-1).

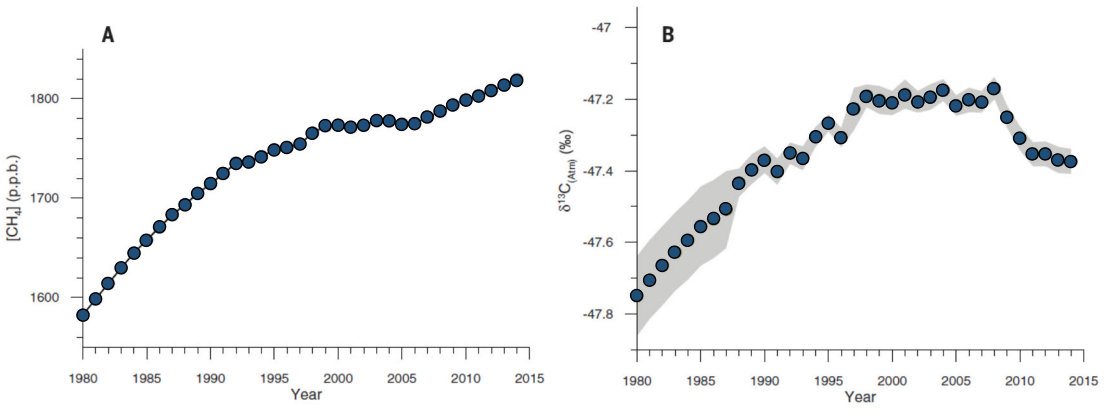

Figure 1-1. Global atmospheric CH_4 concentration increases (a) and their associated $\delta^{13}C$-CH_4 (b) changes since 1980. Data are from the National Oceanic and Atmospheric Administration Earth Systems Research Laboratory (NOAA ESRL) global monitoring network and the Global Atmospheric Watch. Gray shading in b) indicates a confidence interval of ±1 σ. Figure modified from its original version in Schaeffer et al. (2016).

Measurements of $\delta^{13}C\text{-}CH_4$ can be used as a tool to determine CH_4 sources because certain biological and physical processes can deplete or enrich the $^{13}C\text{-}CH_4$ pool. Microbial methanogenesis results in ^{13}C depleted CH_4 and more negative $\delta^{13}C\text{-}CH_4$ values (~-60‰), whereas catagenesis fractionates organic carbon precursors less and results in thermogenic CH_4 enriched in ^{13}C and more positive $\delta^{13}C\text{-}CH_4$ values (~-45‰) (Etiope & Klusman, 2002; Whiticar et al., 1986; Whiticar, 1990). Figure 1-1b shows atmospheric $\delta^{13}C\text{-}CH_4$ values were increasing in concert with atmospheric CH_4 concentrations until ~2000, at which point $\delta^{13}C\text{-}CH_4$ values plateaued around -47.2‰. Since the plateau in the early 2000's, atmospheric $\delta^{13}C\text{-}CH_4$ values have been decreasing, indicating that sources other than fossil fuels may be contributing to the observed increase of CH_4 in the atmosphere (Figure 1-1, Howarth, 2019; Nisbet et al., 2016; Schaefer et al., 2016). The recent atmospheric CH_4 increases, which consist of more ^{13}C depleted CH_4, are attributed to microbial sources from inland waterbodies (Nisbet et al., 2016; Schaefer et al., 2016). Inland waterbodies, which include wetlands, lakes, ponds, and rivers, are already one of the largest natural sources of CH_4 to the atmosphere (Bastviken et al., 2011; Manning et al., 2019; Striegl et al., 2012; Whitfield et al., 2015). Increased microbial emissions from boreal and northern inland waterbodies are offered as one explanation for the global increase in CH_4, although their contribution to total global emissions is thought to be small (Schaefer et al., 2016).

Although boreal and northern emissions only partly explain the observed increase in atmospheric CH_4, it is important to fully understand the CH_4 dynamics and resulting emissions to the atmosphere from these regions, particularly lakes. Lakes are ubiquitous in the Arctic (Verpoorter et al., 2014) representing up to 30% of the land surface in

permafrost covered areas (Walter et al., 2008) with 24% of global lakes found north of 60ºN (Downing et al., 2006). Arctic lakes contribute an estimated 16.5 Tg CH_4 yr^{-1} or 6% of the global natural CH_4 emissions (Bastviken et al., 2011; Kirschke et al., 2013; Wik et al., 2016b). Since CH_4 is a potent greenhouse gas with ~25 times the heating capacity of carbon dioxide (CO_2), increasing concentrations in the atmosphere will create a positive feedback on natural CH_4 emissions in northern lakes through higher rates of methanogenesis, gas-hydrate (CH_4 enclosed in frozen water) dissolution, and permafrost thaw (Boucher et al., 2009; Myhre et al., 2013; Schuur et al., 2015; Wuebbles & Hayhoe, 2002; Yvon-Durocher et al., 2014). Therefore, it is important to determine the processes that affect current CH_4 fluxes to the atmosphere from Arctic lakes, both to gain insight into the past contributions and to be able to predict future changes.

Arctic Freshwater Methane Production and Consumption

Northern lakes and their associated CH_4 fluxes are subject to the Earth's changing climate (Thornton et al., 2015; Walter Anthony et al., 2012; Wik et al., 2016b). In particular, the release of CH_4 to the atmosphere is predicted to increase from increasing temperatures due to 1) increasing microbial production of CH_4 (Blake et al., 2015; Duc et al., 2010; Lofton et al., 2014; Yvon-Durocher et al., 2014), 2) thawing of permafrost increasing labile carbon sources for microbial production (Heslop et al., 2019; Lara et al., 2019; Schuur et al., 2015; Treat et al., 2015), and 3) thawing of permafrost reducing the "cryosphere cap" that is keeping thermogenically produced CH_4 below-ground (Walter Anthony et al., 2012). The mechanisms for how microbial CH_4 production, permafrost

degradation, and thermogenic CH_4 release influence CH_4 flux from Arctic lakes are explained in detail below.

Methane fluxes from lakes are either from *in situ* microbially produced (methanogenic microbes) CH_4 in anoxic sediments and anoxic water columns or advected from thermogenically produced CH_4 stored below bedrock or gas hydrate dissociation (Collett & Dallimore, 1999; Etiope & Klusman, 2002; Walter Anthony et al., 2016; Walter et al., 2008). Lake conditions and characteristics dictate the migration pathway for CH_4 and whether CH_4 is released from sediments to the atmosphere. Exchange of CH_4 out of sediments is controlled by molecular diffusion (Martens & Val Klump, 1980), bubbling or ebullition from oversaturated sediment (Casper et al., 2000; Walter et al., 2006; Wik et al., 2013), and transfer through emergent macrophyte plant stems (Chanton, 2005; Knoblauch et al., 2015). The magnitude of CH_4 emissions from Arctic lakes through diffusive and bubble fluxes are negatively correlated to lake depth (Bastviken et al., 2008; MacIntyre et al., 2010), reduced when lakes are thermally stratified (Bastviken et al., 2004; Kankaala et al., 2006; López Bellido et al., 2013), and enhanced when conduits are present to transport thermogenic CH_4 that is stored beneath lakes (Walter Anthony et al., 2012). In addition, microbial CH_4 production rates are expected to vary between lakes depending on the quantity and quality of carbon in the sediment (Bastviken et al., 2004; Blake et al., 2015; Cunada et al., 2018; Hershey et al., 2014; Lundin et al., 2015; Wik et al., 2018). Specific to Arctic lakes, thermokarst activity increases CH_4 production rates (Heslop et al., 2015; Matheus Carnevali et al., 2015; Matveev et al., 2016; Walter et al., 2008). As a result of all of these factors influencing

CH_4 release, multi-lake studies are necessary to better integrate the impact of CH_4 production on larger scales across the Arctic.

Within the Arctic there are regions with large reservoirs of thermogenic gas and oil, especially along the North American Arctic Ocean coastline (Collett & Dallimore, 1999; Gautier et al., 2009). Long-term thermogenic gas bubble seeps are found where lake sediments are linked to these deeper geologically formed gas or carbon-rich deposits through faults or fissures in bedrock and permafrost (Etiope, 2009). Thermogenic bubble seeps typically have $\delta^{13}C$-CH_4 values from -30‰ to -50‰ and radiocarbon-dead CH_4, indicating geologically produced, thermogenic CH_4 was broken down from its precursor organic matter >50,000 years before present (YBP, Walter Anthony et al., 2012; Whiticar, 1990). Hotspots of thermogenic CH_4 are often locations of rapid, voracious bubbling and can maintain open holes up to 300 m^2 in 0.2-2 m thick ice (Walter Anthony et al., 2012). Hotspots of geologic CH_4 release and sites of gas hydrate formation are often heterogeneous within Arctic lakes (Collett & Dallimore, 1999; Dallimore & Collett, 1995; Dallimore & Matthews, 1997). For example, in the Mackenzie River Delta hotspots, believed to be from a geologic source of CH_4, were only noted in a small portion (1%) of the delta, but were a disproportionately large component (17%) of the delta's atmospheric CH_4 flux (Kohnert et al., 2017; Kohnert et al., 2018). Studies are needed at both greater spatial and temporal scales to investigate the heterogeneous nature of thermogenic CH_4 release from Arctic lakes.

In addition to heterogeneous thermogenic CH_4 fluxes, release of microbial CH_4 from permafrost thaw lakes (thermokarst lakes) is inconsistent across the landscape. Permafrost is present across the majority of the land surface above 60ºN with continuous

permafrost across most of Siberia and northern Canada (Westermann et al., 2015). As permafrost thaws, it creates depressions in the landscape that are then filled with groundwater and precipitation and form lakes (Bouchard et al., 2013). Once these lakes are deep enough to no longer freeze to the sediment during winter, thaw bulbs underneath the lakes form (Johnston & Brown, 1964). Thermokarst lakes continue to expand as permafrost thaws from the warmer lake water. As thermokarst lakes expand, their CH_4 emissions increase from the high quantity and quality of carbon being exposed in lake sediments and result in hotspots of CH_4 bubbling in some locations (Heslop et al., 2019; Tarnocai et al., 2009; Walter Anthony et al., 2014). Eventually, the thermokarst lakes may shrink from evaporation, drainage through groundwater or shoreline breaches, and/or sediment accumulation at which point the landscape refreezes (Andresen & Lougheed, 2015; Bouchard et al., 2013; Jepsen et al., 2013; Jones et al., 2011; Smith et al., 2005; Yoshikawa & Hinzman, 2003). Microbial incorporation of permafrost carbon leads to CH_4 that has a similar $\delta^{13}C\text{-}CH_4$ as the CH_4 that is formed from other precursor carbon sources, between -60‰ and -75‰, but it is isotopically distinct with a $^{14}C\text{-}CH_4$ age between 15,000-40,000 YBP (Walter et al., 2008). Hence, the influence of permafrost thaw on atmospheric CH_4 flux across the Arctic landscape can be constrained using $\delta^{13}C\text{-}CH_4$ and $\Delta^{14}C\text{-}CH_4$ (Walter et al., 2006; Walter et al., 2008).

While there are large amounts of CH_4 produced in or transported through lake sediments, not all the CH_4 in lakes is emitted to the atmosphere. Some is consumed by methanotrophs via CH_4 oxidation (MOx). Aerobic MOx rates depend on dissolved oxygen concentrations in the winter and CH_4 concentrations in the summer, temperature, and the permafrost environment, e.g. permafrost thaw lakes have greater MOx than other

lake types possibly due to higher organic carbon inputs (Bastviken et al., 2002; Kankaala et al., 2006; Martinez-Cruz et al., 2015). Aerobic oxidation occurs at the ice-water interface during winter, sediment-water interface in an oxic water column, and at the anoxic/oxic boundary in a stratified water column (Bastviken et al., 2002; Huttunen et al., 2006; Martinez-Cruz et al., 2015; Ricão Canelhas et al., 2016; Whiticar & Faber, 1986). Anaerobic MOx, prevalent in some Arctic lakes (Martinez-Cruz et al., 2018), can take place through the use of nitrate or iron reduction (Ettwig et al., 2010; Ettwig et al., 2016). Although, aerobic MOx rates are generally greater than anaerobic oxidation rates (e.g., Zigah et al., 2015). MOx can mitigate CH_4 emissions globally from freshwater environments to the atmosphere by 30 – 99% (Bastviken et al., 2002). In northern lakes MOx removes up to 80% of the CH_4 diffused from sediments into the water column (Kankaala et al., 2006). MOx acts as a natural emission buffer to high rates of CH_4 produced in lakes.

Methane loss due to MOx can be identified using $\delta^{13}C\text{-}CH_4$ since ^{13}C is enriched in the residual CH_4 pool when $^{12}C\text{-}CH_4$ is preferentially consumed by methanotrophs (Whiticar, 1999). To identify this enrichment, carbon isotope fractionation factors, α or enrichment factors, are calculated to determine how quickly ^{12}C is assimilated compared to ^{13}C (Coleman et al., 1981). α for microbial oxidation (α_{ox}) of CH_4 ranges from 1.0088 in anaerobic oxidation of Arctic sediments (Alperin et al., 1988), 1.0184 to 1.0208 in oxic water columns of Arctic lakes (Bastviken et al., 2002), and extreme enrichment of 1.030 in Greenland lakes (Cadieux et al., 2016). Alternatively, diffusive isotope fractionation is assumed to be small in water and Preuss et al. (2013) showed an α of 1.001 from diffusion (α_{diff}) in saturated Arctic wetland soils. Utilizing α_{ox} and α_{diff} in a $\delta^{13}C\text{-}CH_4$

mass balance can assess the proportion of CH_4 in the water column lost through MOx or diffusion (Chanton & Liptay, 2000). Complications can arise with mass balance calculations if thermogenic CH_4 sources are present due to the similarity of $\delta^{13}C$-CH_4 between oxidized CH_4 and thermogenic CH_4 (Whiticar, 1990; Whiticar, 1999). This means the source $\delta^{13}C$-CH_4 needs to be known in order to assess the impact MOx has on CH_4 release from lakes. Source $\delta^{13}C$-CH_4 can be determined when CH_4 concentrations are the highest by measuring changes during the year.

Over the past two decades, an extensive body of knowledge has developed that focuses on seasonal changes in dissolved CH_4 and diffusive fluxes from surface water in northern (>50^{o}N) lakes (33 studies, Figure 1-2 and references therein). Most sampling has occurred in the ice-free times (white space on Figure 1-2), but a handful of studies have focused on the period immediately before ice-out (gray shading to the left) and even fewer studies have persistent sampling through the winter. Overall, these studies show that CH_4 concentrations increase under ice and the spring thaw is a crucial period for CH_4 release from lakes. As ice-melts and lake water overturns, CH_4 from ice-trapped bubbles is released and winter-derived CH_4 accumulated in the lower water column is mixed and brought to the surface waters (Boereboom et al., 2012; Jammet et al., 2017; Jammet et al., 2015; Walter Anthony et al., 2010; Wik et al., 2011). During this period, 3 to 100% of total annual lake CH_4 emissions are released to the atmosphere (Jammet et al., 2015; Jansen et al., 2019; Karlsson et al., 2013; Phelps et al., 1998), suggesting that the majority of winter-derived CH_4 evades oxidation (Jansen et al., 2019). High variability in spring thaw and CH_4 emissions suggest regular sampling in seasonally ice-covered lakes is needed to better account for this important component in Arctic lake CH_4 budgets.

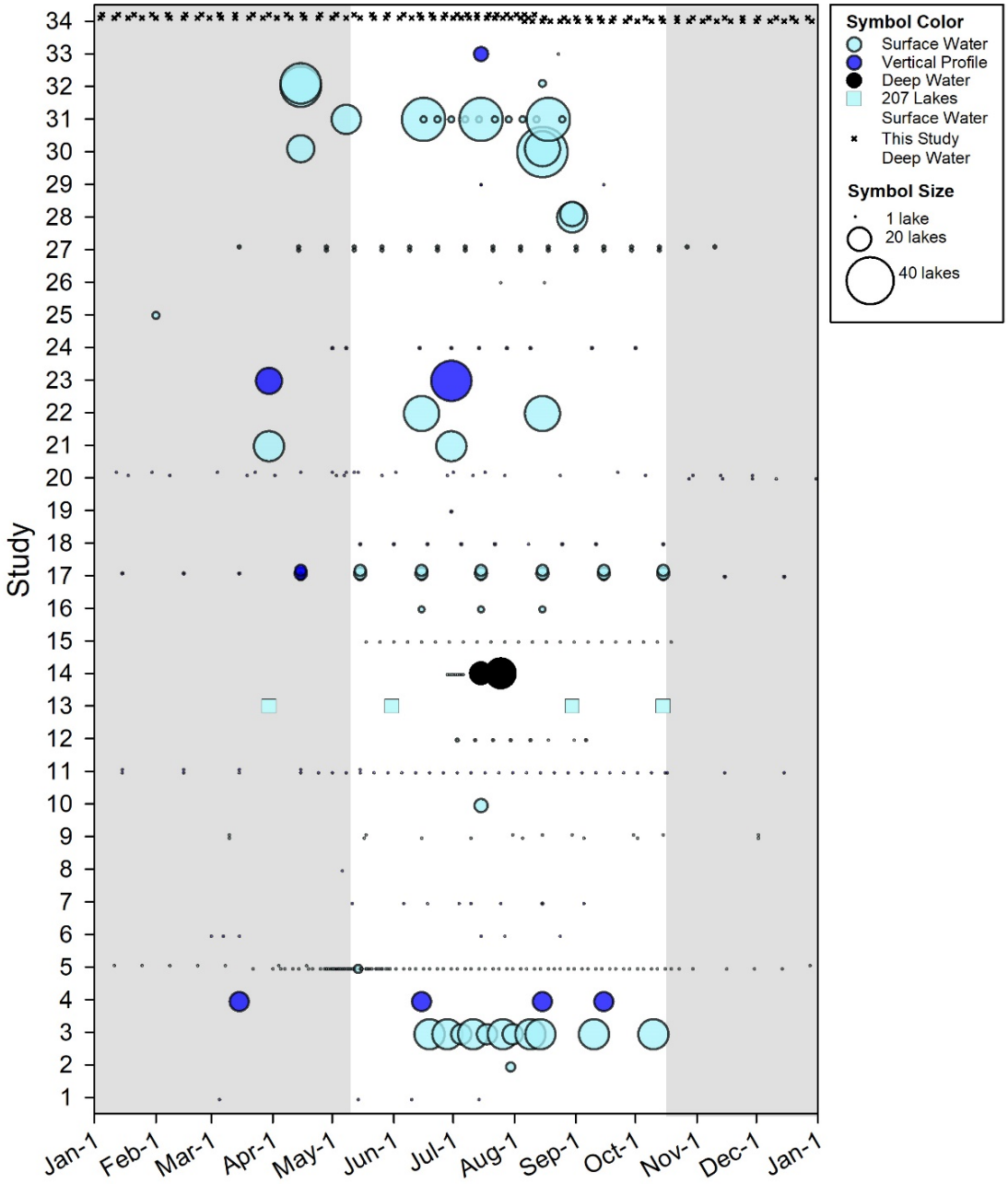

Figure 1-2. Distribution of sampling occurrence throughout the entire year in 33 studies where dissolved CH_4 was measured in surface water (light blue circles), deep water (black circles), or vertical profiles (dark blue circles) in northern lakes (>50°N). Gray bars indicate general timing of ice-cover in northern latitudes (mid-October to May). Ice-cover may be shorter or longer depending on exact study location. Dot size corresponds to the number of lakes sampled and each dot is a separate sampling event. Study number goes from the oldest study to the current study. 1. Rudd & Hamilton, 1978, 2. Kling et al., 1992, 3. Hamilton et al., 1994, 4. Zimov et al. 1997, 5. Phelps et al. 1998, 6. Bastviken et al. 2002, 7. Huttunen et al., 2002, 8. Huttunen et al. 2003b, 9. Huttunen et al. 2003a, 10. Bastviken et al. 2004, 11. Kankaala et al. 2006, 12. Repo et al. 2007, 13. Juutinen et al. 2009, 14. Laurion et al. 2010, 15. López Bellido et al. 2011, 16. Kankaala et al. 2013, 17. Karlsson et al. 2013, 18. López Bellido et al. 2013, 19. Lofton et al. 2014, 20. Greene et al. 2014, 21. Martinez-Cruz et al. 2015, 22. Rasilo et al. 2015, 23. Sepulveda-Jauregui et al. 2015, 24. Tan et al. 2015, 25. Denfeld et al. 2016, 26. Garcia-Tigreros Kodovska et al. 2016, 27. Natchimuthu et al. 2016, 28. Sasaki et al. 2016, 29. Lecher et al. 2017, 30. Townsend-Small et al. 2017, 31. Cunada et al. 2018, 32. Elder et al. 2018, 33. Thottathil et al. 2018, 34. This study.

Mackenzie River Delta

The Mackenzie River Delta was used as a model system to examine the temporal variability of methanogenesis, CH_4 oxidation, thermokarst impacts, and thermogenic CH_4 sources on the release of CH_4 from Arctic lakes (Figure 1-3). The Mackenzie River Delta is a lake-rich, productive ecosystem (Emmerton et al., 2007) and a portion of it extends over thermogenic gas reserves (Dallimore & Matthews, 1997; Todd & Dallimore, 1998). Delta lakes exhibit a wide range of size and depth, with surface areas ranging from $3.0x10^{-4}$ ha to 4270 ha, skewing toward smaller lakes, and average depths commonly between 1 and 2 m (Emmerton et al., 2007; Marsh et al., 1999). Water balances in delta lakes are expected to be primarily influenced by their connection to the Mackenzie River as well as evaporation (Bigras, 1990; Lesack & Marsh, 2010; Marsh & Bigras, 1988; Marsh & Lesack, 1996). Lakes in the Mackenzie Delta are flooded in the spring by the Mackenzie River at differing intervals and are dependent on the sill height between the lake and river (Lesack & Marsh, 2010; Lesack et al., 2013; Marsh & Hey, 1989; Marsh & Hey, 1994).

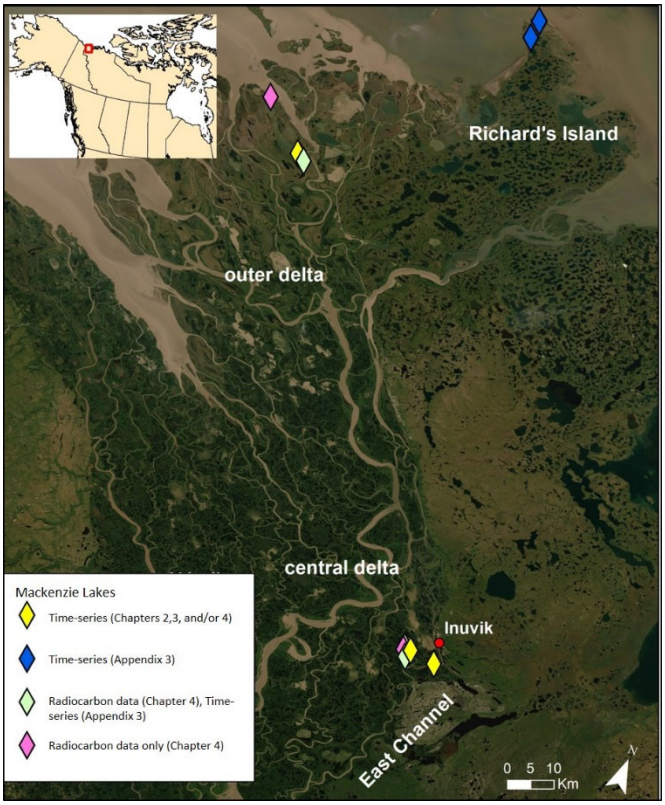

Figure 1-3. Mackenzie Delta lake sampling sites. Yellow diamonds indicate where CH_4 and $\delta^{13}C$-CH_4 time-series data are presented in Chapters 2, 3, and/or 4. Blue diamonds indicate where samples were collected and only presented in Appendix 3. Green diamonds indicate radiocarbon data presented in Chapter 3 and time-series of CH_4 and $\delta^{13}C$-CH_4 are presented in Appendix 3. Pink diamonds indicate lakes that were only sampled for $\Delta^{14}C$-CH_4. Inset shows the extent of the Mackenzie Delta in the Northwest Territories, Canada.

Connection times for lakes to the Mackenzie River vary yearly from 120-153 days for no-closure lakes (<1.5 m sill height), 20-129 days for low-closure lakes (1.5 to 4 m sill height), and an interannual connection of 0.9-14 days for high-closure lakes (>4 m sill height) (Marsh & Hey, 1989). These annual flooding events are a major source of oxygenated water, sediment, organic matter, and nutrients into lakes, which affect microbial CH_4 production (Cunada et al., 2018; Emmerton et al., 2008; Gareis & Lesack, 2017; Lesack et al., 1998; Lesack & Marsh, 2010; Marsh et al., 1999; Tank et al., 2011).

The Mackenzie River Delta is a post-glacial feature that began forming 14,500 year ago after the Laurentide ice-sheet receded and drainage shifted from the Atlantic Ocean to the Arctic Ocean (Murton, 2009). During the height of the Wisconsian glaciation (~ 16,000 to 22,000 YBP) the Laurentide Ice Sheet extended across the majority of the Mackenzie Delta, but left portions of Richard's Island ice-free (Murton, 2009). At this time, while sea levels were low, permafrost developed across the delta. Thinner permafrost is found where glaciers were present since they isolated the underlying ground from cold atmospheric temperatures. The permafrost regime differs between the western (<100 m) and eastern (>600 m) of the Mackenzie Delta with the thickest permafrost found on Richard's Island where the delta was unglaciated during most of the Pleistocene (Collett & Dallimore, 1999; Taylor et al., 1996). In the early Holocene, the outer delta became submerged as sea-level increased. Since then, the outer delta has been prograding into the ocean from fluvial sedimentation, both laterally and vertically, as the land surface has built up and risen above sea level (Carson et al., 1999; Marsh et al., 1999; Ritchie, 1985). Additionally, lakes in the outer delta overlie known natural gas and oil reservoirs (Dallimore & Matthews, 1997; Todd & Dallimore, 1998).

Differences in permafrost regimes of the delta impact the release of thermogenic CH_4 and necessitate examining the impact of geology and permafrost cover on microbial and thermogenic CH_4 release into Mackenzie Delta lakes.

Permafrost extent and the geological features beneath a lake in Mackenzie Delta near Inuvik, Northwest Territories, Canada were described by Johnston & Brown (1964) who conducted a coring program. Sediments were found to consist of up to 60 m of Holocene deltaic silt and silty sand with heterogeneous detrital organic material, underlain by glaciomarine clays (60-80 m soil depth) that sit on top of bedrock (Johnston & Brown, 1964). Terrestrial areas of the modern delta are underlain by continuous permafrost (Burn & Kokelj, 2009; Johnston & Brown, 1964; Nguyen et al., 2009). However, the mean annual temperature of water bodies can be above 0°C and thawed zones or taliks can form beneath lakes and river channels, leading to discontinuous permafrost. For example, a lake to the southwest of Inuvik had no frozen ground extending to the bedrock, but permafrost was up to 100 m deep surrounding the lake (Johnston & Brown, 1961). Within the central delta where there is regular river flooding, the active layer thaw depth is ~100-130 cm during the warm season (Smith et al., 2009). With increased air temperatures in the last several decades, the permafrost in the Inuvik area has warmed approximately 1.5ºC (Burn & Kokelj, 2009), and this warming trend is continuing. As permafrost thaws, the active layer depth increases and thermokarst lakes expand (Mackay, 1995). Deepening and lateral expansion of water bodies cause erosion of permafrost along the shoreline, which has the potential to provide a large and labile carbon source to these lakes (Burn & Kokelj, 2009; Tank et al., 2011; Zolkos et al., 2019).

Prior to this dissertation, Pipke (1996) examined under-ice CH_4 within Mackenzie Delta lakes, while Cunada et al. (2018) examined open-water spatial and temporal CH_4 dynamics. Both studies found the connection between lakes and the Mackenzie River are important factors in the lake-to-lake variability of CH_4 concentrations. Shorter river connections are associated with greater CH_4 production due to more labile macrophyte biomass, which is produced in clearer lakes that are more isolated from the river (Cunada et al., 2018; Pipke, 1996). Despite this, thermokarst lakes have CH_4 concentrations lower than nearby lakes with significant macrophyte-derived carbon (Cunada et al., 2018; Tank et al., 2011). My study presented here provides new insights because no prior study has looked at CH_4 dynamics in these lakes over multiple years or included outer (lower) delta lakes.

Dissertation Objectives, Questions, and Approaches Used

In this dissertation, I delve deeper into understanding the processes that influence the variability of spring and open-water fluxes from Arctic lakes to the atmosphere. The overall objective was to understand the sources and processes (e.g. methanogenesis, CH_4 oxidation, diffusion, and thermogenic source) that contribute to changes in CH_4 concentrations in lakes throughout the year within the Mackenzie River Delta (Figure 1-4). To do this, I collected samples regularly during the entire year to provide perspective on the sources (microbial CH_4, permafrost degradation, thermogenic CH_4) and sinks (MOx, diffusive or advective release) affecting dissolved CH_4 concentrations. Figure 1-4 is the conceptual model that guided my work, and is outlined below.

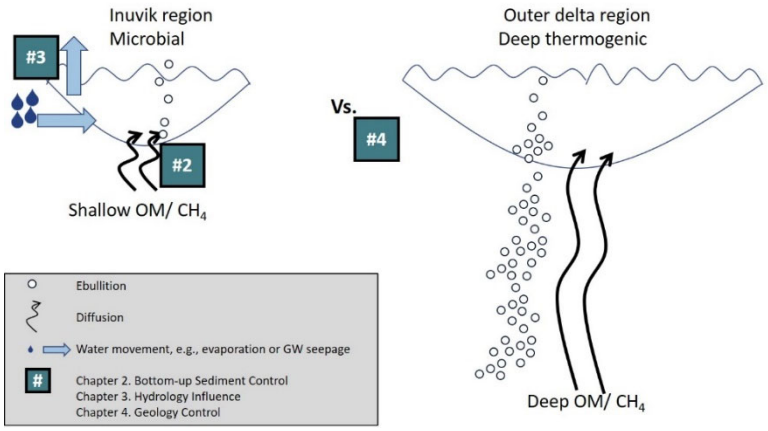

Figure 1-4. Schematic depicting the sources and processes expected to control CH_4 emissions from lakes in the Mackenzie Delta.

Dissertation Synopses

Chapter 2 "*Year-round quantification of dissolved CH_4 concentrations and stable- and radiocarbon isotopes in a small Arctic lake (Mackenzie Delta)*" was submitted to the Journal of Geophysical Research: Biogeosciences in December 2019. The questions asked were: during the ice-cover period, what is the source of the CH_4 to the under-ice build-up (e.g. thermogenic CH_4 or microbial CH_4)? Is this CH_4 diffusing from the sediments or is there an ebullitive flux? Do those migration pathways result in different amounts of CH_4 in the water column? Once the lake-ice melts, how do bottom-water CH_4 concentrations change in response to MOx and flux to surface water? These questions are denoted by the #2 in Figure 1-4. My approach was to measure the dissolved CH_4 concentration and $\delta^{13}C$-CH_4 in bottom water and surface water over a year to describe the interplay between CH_4 production, CH_4 oxidation, and CH_4 efflux to the atmosphere in one lake. A 1-D model of CH_4 diffusion revealed the under-ice CH_4 increases were primarily from sediment diffusion, and there was a possibility of water-column methanogenesis. $\delta^{13}C$-CH_4 isotope modeling during the open water period indicated the

majority of CH_4 removed from bottom water was oxidized, rather than emitted to the atmosphere. Surprisingly, in this lake the carbon precursor for microbially produced CH_4 was a modern carbon source, probably degraded macrophyte biomass.

Chapter 3 "*Determining evaporation, groundwater, and ice cover influences on lake chemistry and methane (CH_4) dynamics in multiple Arctic lakes (Mackenzie Delta)*" is in preparation for peer review. This chapter focused on understanding how the CH_4 dynamics during the open-water period could be impacted by local hydrology, a topic that has not been thoroughly examined in the literature. If all lakes are evaporative basins, does the decrease in water level through the open-water period result in greater CH_4 losses to the atmosphere? Alternatively, do thermokarst lakes that thaw into ice-rich permafrost have a groundwater connection through the thaw bulb and does groundwater carry CH_4 into lakes? As thermokarst lakes expand, does permafrost from shoreline erosion or the organic carbon in thawing permafrost sediments get consumed by microbes? These questions were addressed for three lakes in the Mackenzie Delta. The approach was to analyze the hydrologic setting during open-water and ice-cover to establish the influence of evaporation and groundwater contributions on lake chemistry and CH_4 dynamics (denoted figuratively as #3 in Figure 1-4). Water depth, converted from water pressure sensors, during open water was observed during two partial open water periods (2015, 2017) and one full ice-melt to ice-cover open water period (2016). Ion data were expected to be used to indicate evaporative lake level decline, but instead showed the significant effect of the expulsion of ions during ice formation. The two lakes with groundwater contributions during open-water were deeper and had slower declines in dissolved CH_4 following ice-melt than the lake that was influenced primarily by

evaporation. Finally, modern CH_4 in all three lakes suggests labile permafrost carbon is not transported through groundwater to any of the lakes.

Chapter 4, "*Radiocarbon and stable carbon isotopes to discern source, age and migration pathways of methane from lakes in the Mackenzie River Delta, Northwest Territories, Canada*" is in preparation for peer review. The key questions framing this chapter included: what is the source(s) of CH_4 within surface water (e.g. thermogenic CH_4 or microbial CH_4) that is emitted to the atmosphere? Does the source change during the year? The approach was to utilize radiocarbon measurements to determine how underlying geology and organic carbon sources impact CH_4 in nine lakes and in the Mackenzie River (denoted figuratively as process #4 in Figure 1-4). Dissolved CH_4 from surface water (8 lakes) and CH_4 captured in gas bubbles (3 lakes) were analyzed for $\Delta^{14}C\text{-}CH_4$ to discern the source(s) of CH_4. Methane diffusing out of the lakes was found to be near-modern in age, while CH_4 in gas bubbles was significantly older and from the outer delta sites formed via thermogenic processes. $\Delta^{14}C\text{-}CH_4$ data compared with previous work by Kohnert and colleagues (2017) showed that locations with an enhanced CH_4 flux were from delta areas with natural gas and oil reservoirs, and the CH_4 was of thermogenic origin. Within one lake near a CH_4 seep location, a two-year time-series showed CH_4 increases under-ice are linked to dissolved oxygen concentrations. Bubbles from thermogenic CH_4 rapidly increase CH_4 concentrations after dissolved oxygen is depleted during ice-cover, and then bubble release decreases as ice thickness increases hydrostatic pressure. This is the first study to analyze $\Delta^{14}C\text{-}CH_4$ in the Mackenzie Delta lakes and expands our knowledge of CH_4 source and migration pathways within these systems.

Chapter 2

Year-round quantification of dissolved CH_4 concentrations and stable- and radiocarbon isotopes in a small Arctic lake (Mackenzie Delta)

Submitted to *Journal of Geophysical Research: Biogeosciences* December 2019

Hadley A. McIntosh Marcek, Lance Lesack, Beth Orcutt, C. Geoff Wheat, Scott Dallimore, Kimberly Geeves, Laura Lapham

Contribution: Experimental design, all sample analysis, data analysis and interpretation, and all text and figures; Text has been edited by all co-authors

Abstract

Seasonally ice-covered permafrost lakes in the Mackenzie River Delta (western Canadian Arctic) emit methane to the atmosphere during periods of open water. However, the processes contributing to methane cycling under-ice have not been thoroughly addressed. We studied annual dissolved methane dynamics within a small delta lake (0.2 ha) using sensor and water sampling packages that autonomously and continuously collected lake water samples for two years at multiple water column depths. Lake physical and biogeochemical properties (temperature; light; concentrations of dissolved oxygen, manganese, iron, and dissolved methane, including the stable carbon and radiocarbon isotope composition of the methane) yielded a complex dataset. Data showed that dissolved methane concentrations increase under-ice after electron acceptors

(oxygen, manganese and iron oxides) are depleted or inaccessible from the water column. The radiocarbon age of dissolved methane suggests a source from recently decomposed carbon as opposed to thawed ancient permafrost. Sources of dissolved methane to the water column include a diffusive flux from the sediment and water column methanogenesis. Following ice-melt, the water column partially mixes and dissolved methane concentrations decline slowly, allowing a portion of the winter-derived retained methane to be microbially oxidized. Despite methane oxidation, surface water was a source to the atmosphere. The greatest diffusive fluxes out of the lake to the atmosphere occurred following ice-melt (75 mmol CH_4 m^{-2} d^{-1}) and in mid-July when the entire water column mixed. This study demonstrates the importance of fine scale temporal sampling to understand dissolved methane processes in seasonally ice-covered lakes.

2.1. Introduction

Methane (CH_4) is a potent greenhouse gas with at least 25 times the heating capacity of carbon dioxide over a 100-year time period (Boucher et al., 2009; Myhre et al., 2013). While there are large sources of CH_4 to the atmosphere from anthropogenic activities, one of the largest sources of natural emissions is freshwater lakes (Bastviken et al., 2011; Kirschke et al., 2013; Saunois et al., 2016). In general, lakes have large amounts of labile organic matter from *in situ* production or terrestrial inputs (Cole et al., 2007; Tank et al., 2011; Tranvik et al., 2009). Microbes (methanogens) break down that organic matter through a series of thermodynamically favorable processes that terminate in the production of CH_4 (Jørgensen, 2000 and references therein; Whiticar et al., 1986). Studies show lakes in the Arctic could release more CH_4 than previously thought as

underlying permafrost soils thaw and unlock carbon reserves that are potentially usable as energy sources by methanogens (Knoblauch et al., 2018; Matveev et al., 2018; Walter Anthony et al., 2016). As models predict greater CH_4 release with projected increasing global temperatures, it is imperative to understand CH_4 dynamics and processes leading to CH_4 release from Arctic lake systems (Tan et al., 2015).

Most Arctic lake systems are ice covered in winter, thus have a seasonality in CH_4 production and oxidation processes (Michmerhuizen et al., 1996). For example, in Arctic lakes in the western Canadian Arctic, the lake surfaces begin to ice over in fall (~October) and remain ice-covered until spring (April or May), forming a barrier to gas exchange with the atmosphere. This barrier leads to bottom water anoxia as available oxygen is consumed via heterotrophic activity (Denfeld et al., 2016; Deshpande et al., 2015; Rudd & Hamilton, 1978). Bottom water anoxia, and the lack of sulfate in lake systems, results in the formation of CH_4 within centimeters of the sediment-water interface in anaerobic lake sediments (Whiticar & Faber, 1986). Then CH_4 either diffuses (Greene et al., 2014) or bubbles-out of the sediment (Walter et al., 2008), if sediment pore-water CH_4 concentrations exceed solubility, to the overlying water column (Casper et al., 2000; Tan et al., 2015; Wik et al., 2016b). Once in the water column, CH_4 can be oxidized anaerobically via nitrate or iron reduction (Ettwig et al., 2010; Ettwig et al., 2016) or build-up to levels above atmospheric equilibrium under ice-covered conditions (Cunada et al., 2018; Elder et al., 2018; Martinez-Cruz et al., 2015; Sepulveda-Jauregui et al., 2015; Townsend-Small et al., 2017).

Of the different CH_4 emission pathways in lakes, an extensive body of knowledge has developed over the past two decades that focuses on seasonal changes in dissolved

CH_4 and diffusive fluxes from surface water in boreal and arctic (>50ºN) lakes (33 studies, see Figure 1-2 and references therein). As the ice melts in spring, the previously ice-trapped CH_4 is released to the atmosphere (Denfeld et al., 2018; Karlsson et al., 2013; Walter et al., 2006). This can either be a rapid release of CH_4 to the atmosphere when lakes are shallow enough for their water column to be fully mixed by the available wind energy (Jammet et al., 2017; Jammet et al., 2015; Phelps et al., 1998) or the CH_4 may only be partially released if the water column is deep enough to thermally stratify as surface waters warm through the spring and summer (Vachon et al., 2019). In such cases, the additional CH_4 may not be released completely until either a sufficiently strong wind event fully mixes the water column, or the water column cools and destratifies prior to the onset of a surficial ice layer (Bastviken et al., 2004; Greene et al., 2014; Kankaala et al., 2007). The removal of the ice barrier also allows atmospheric oxygen to penetrate into the water column. This dissolved oxygen can be utilized by aerobic CH_4 oxidizing bacteria (methanotrophs) to consume CH_4 (Kankaala et al., 2006). Aerobic CH_4 oxidation is efficient, reducing the amount of CH_4 produced from the sediments by 30-99% (Bastviken et al., 2002). Recognizing physical and biogeochemical controls on CH_4 cycling during under-ice and open-water conditions is key to predicting how Arctic lakes will respond to shorter ice-covered periods in the future (Wik et al., 2016b).

For this study, we used sampler systems called OsmoSamplers (Jannasch et al., 2004; Wheat et al., 2011) to continuously collect bottom water samples over two years in a seasonally ice-covered Arctic lake. The samplers allowed us to integrate dissolved CH_4 concentrations from bottom water collected over ~5-day periods, including dynamic times such as the onset of ice-cover and during ice melt. The goals of this study were to

determine to what extent and rate dissolved CH_4 concentrations increases in the lake under ice-cover, the source(s) of dissolved CH_4, the diffusive flux of CH_4 to the atmosphere during open water, and the biogeochemical reactions that effect dissolved CH_4 concentrations.

2.2. Study Location

We studied dissolved CH_4 and diffusive flux CH_4 dynamics within a lake in the Mackenzie River Delta (Figure 2-1). The Mackenzie River Delta is the second largest delta in the Arctic with an area of 13,000 km^2 and contains over 45,000 lakes (Emmerton et al., 2007). Lakes in the delta are impacted by spring flooding at different intervals, due to their sill elevations in relation to the river height (Lesack & Marsh, 2010; Marsh & Hey, 1989). High closure lakes (>4.0 m sill height) are connected to the river a few days a year and on an internannual basis (0 to 20 days per year). The extent of exchange with river water is

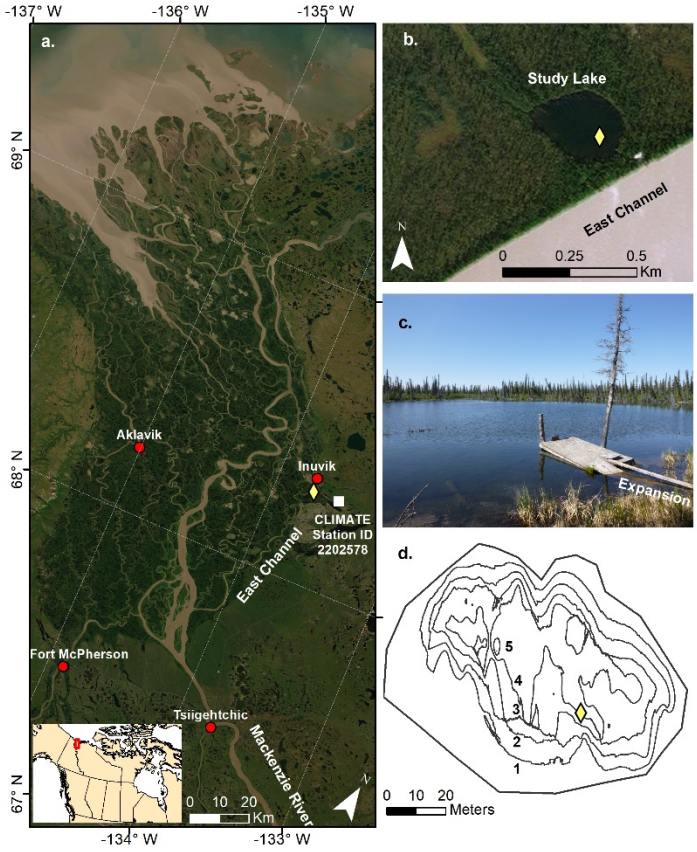

Figure 2-1. Map of Lake 520 sampling site in Mackenzie River Delta, Northwest Territories, Canada. a) Satellite image (ESRI) with the major towns (red circles), the study lake (Lake 520, yellow diamond), and weather station at the Inuvik Airport (white square) identified. b) Satellite image of Lake 520 adjacent to the East Channel of the Mackenzie River with sampling location (diamond). c) Photograph of Lake 520 in August 2015 from shore facing North showing shoreline expansion since the dock was originally built. d) Lake 520 bathymetry with meter contours (deepest point 5.5 m) and sampling location.

typically enough to offset the negative water balance of the Mackenzie River Delta region (Lesack & Marsh, 2010; Marsh & Hey, 1989; Marsh & Hey, 1994). The limited connection of high closure lakes to the Mackenzie River increases their water clarity, due to less suspended sediment input, and allows for large mats of macrophytes to grow on the lake bed (Marsh et al., 1999; Squires et al., 2002; Squires & Lesack, 2003; Squires et al., 2009). Hence, high closure lakes have a highly labile source of carbon from macrophyte exudates and wintertime macrophyte senescence (Cunada et al., 2018; Tank et al., 2011). Within the Mackenzie Delta, high closure lakes are <15% of total lake area (Emmerton et al., 2007; Lesack & Marsh, 2007).

The lake chosen for this study – informally known as Lake 520 (68º 18.826', -133º 42.931') – is a small (0.2 ha), freshwater, high closure lake (Lesack & Marsh, 2010). Lake 520 is impacted by thermokarst (permafrost thaw) processes, based upon its water column over-saturation of pCO_2 throughout open water (Cunada et al., 2018; Tank et al., 2009) and shoreline erosion. Shoreline and lake area are expanding as indicated by numerous recently fallen trees along the lake margins (Figure 2-1c; Burn & Kokelj, 2009). It is located close to the East Channel of the Mackenzie River near Inuvik, Northwest Territories, Canada (Figure 2-1). Lake bathymetry was determined by interpolating measured water depths from June 2017 (handheld depth meter) with kriging in ArcGIS (ArcMap version 10.5.0.6491, ESRI). Lake 520 was deepest at 5.5 m (Figure 2-1). Additionally, this lake has been connected to the Mackenzie River three out of every four years since the 1960s with a mean spring flooding depth of 0.589 m (Lesack & Marsh, 2010). The short river connection of less than 19 days each spring and clear water supports a substantial macrophyte community. The primary macrophyte is the algae

Chara vulgaris L., which persists in the lake bottom over multiple years, and in Lake 520 it develops to the highest mean aboveground macrophyte biomass by a factor of 10 compared to lakes nearby (2446 g m^{-2}; Squires & Lesack, 2003). While bubbles have been observed trapped in ice (Cunada, 2016), during the open water season we observed no evidence of bubbles spontaneously breaking the lake surface.

2.3. Materials and Methods

Lake water and sediment cores were collected from Lake 520 from August 2015 through August 2017 during four field campaigns. During open water, the lake was accessed by small boat from a base of operations at the Aurora Research Institute (ARI, Inuvik, Canada); during winter, the lake was accessed via snowmobile travel. As described in more detail below, water was collected from the deeper water column continuously by OsmoSampler packages (Jannasch et al., 2004) and discretely from the near-surface (Magen et al., 2014). Methane concentrations and stable carbon isotope ratios ($\delta^{13}C$-CH_4) were measured on lake water and sediment pore-water. The source of CH_4 into the water column was probed by modeling diffusion of CH_4 from sediments and measuring radiocarbon age of surface water CH_4. Ancillary water column characteristics (i.e. temperature, dissolved oxygen, and light) were measured by commercially-available sensors, and sediment characteristics (i.e. porosity, sediment organic carbon) were quantified from sediment cores.

2.3.1. Continuous Bottom Water Sampling with OsmoSamplers

Bottom water at Lake 520 was collected continuously using OsmoSamplers, which are osmotically powered sampling pumps continuously drawing in water via

diffusion and storing that water in a coil of small diameter tubing (Appendix 1 Figure S1-1; Jannasch et al., 2004; Orcutt et al., 2017b; Wheat et al., 2011). The pumps are powered by an osmotic gradient produced when semi-permeable membranes (Alzet Osmotic Pumps, Model 2ML1, Cupertino, CA, USA) are sandwiched between a supersaturated salt water chamber, referred to as the "salt" chamber, and a chamber filled with milli-Q water, referred to as the "fresh" chamber (Jannasch et al., 2004). The "fresh" chamber was modified by using low-salinity water (40 mg L^{-1} NaCl solution) instead of milli-Q water, so that the pumps could withstand freezing temperatures, if needed. Pumping rates were 0.88 – 2.07 mL day^{-1} at 21°C, for 8-membrane pumps, and varied with temperature (Jannasch et al., 2004). Pumps were deployed either to collect dissolved gases or total ions. Gas OsmoSamplers were connected in series with gas-tight fittings to a sample coil of 300-m-long, small-bore copper tubing of either 0.8 mm inner diameter (ID) or 1.1 mm ID that was filled with 40 mg L^{-1} NaCl solution prior to deployment. One side of the copper tubing was connected to the "fresh" side of the pump and the other side of the copper tubing was connected to a Rhizon filter (Rhizosphere Research Products, 0.15 μm mean pore size, Wageningen, NLD) to exclude microbes that could alter sample during storage (Hahn, 2004). Total ions were collected from an Acid OsmoSampler that had two pumps and two Teflon coils (1.1 mm ID and 10% hydrochloric acid (HCl) rinsed). One 300-m-long coil was filled with 40 mg L^{-1} NaCl solution prior and the second was filled with 0.02 M subboiled HCl. A 2-membrane OsmoPump was used to pump acid out of the acid-filled coil into the larger coil to acidify the sample *in situ* (Wheat et al., 2011). An 11-membrane pump pulled in the lake water sample that was then mixed with the acid at the intake and diluted the acid 5.5 times.

OsmoSamplers were set up at ARI several days prior to deployment. Three Gas OsmoSamplers were secured to a plastic crate (33 cm x 47.5 cm x 28 cm) with intakes set at three different heights on the outside of the plastic crate. When deployed in 3.10 m of water, the intakes correspond to 2.70 m and 2.90 m water depth (40 cm and 20 cm above the sediments, respectively) and at the base of the plastic crate at 7 cm below the sediment-water interface (cmbsf) in 2015-2016 and 2.90 m and 3.04 m water depth (20 cm and 6 cm above the sediments, respectively) and at 7 cmbsf in 2016-2017 (Appendix 1 Figure S1-1). These depths account for the plastic crate settling into sediments (~ 7 cm, based on visual mud markings on crate). The single Acid OsmoSampler had an intake at 2.90 m water depth (20 cm above the sediment) from 2015-2017. Sensors were also used to collect continuous water temperature (Tidbit V2 temperature Model UTB1-001 logger, 30-minute increment), water pressure (HOBO Model U201L-01 logger, 1-hour increment), light (HOBO Temp/Light Model UA-002-64 logger, 30-minute increments), and dissolved oxygen (HOBO DO Model U26-001 logger, 1-hour increments for 6 months until the battery fully drained) data and were mounted at 2.90 m water depth (20 cm above the sediments). Additional temperature sensors were mounted along a float line for the 2016-2017 deployment at 2.41 m and 2.66 m water depth (69 cm and 43 cm above the sediments, respectively).

Plastic crates were deployed in 3.10 m water (measured with a handheld depth meter) from a small boat, anchored under their own weight (> 13.5 kg), from 3 August 2015 to 9 August 2016, and again from 13 August 2016 to 12 August 2017. The location for deployment was meant to be mid-lake, but later collection of the lake bathymetry shows that the location chosen does not represent the deepest part of Lake 520 (Figure

2-2d). Deployments were as spatially close as possible, although subtle changes in location could have occurred between the 2015-2016 and 2016-2017 deployments. Upon recovery, the two ends of the copper tubing were crimped immediately and stored at 4ºC until processing at Chesapeake Biological Laboratory (Solomons, MD, USA). Processing of copper tubing was done within one year of recovery, and during this time dissolved CH_4 and ions diffused less than 1 m in each direction (Jannasch et al., 2004). Teflon tubing was capped upon recovery, and sectioned into 1 m increments and liquid expelled into acid-cleaned 2mL microcentrifuge tubes (Wheat et al., 2017) at ARI. Sensors were detached and data downloaded within 24 hours.

2.3.1.1. Subsampling Copper Tubing

Copper tubing was sectioned to give ~5-day resolution of time-integrated samples, which alternated between short segments for salinity and long segments for dissolved CH_4 measurements (Gelesh et al. 2016). This continued until the transition from the sample (fresh lake water) to the saline filling solution (40 mg L^{-1} NaCl) was reached. Samples for salinity determinations (Extech RF20 refractometer, 1‰ precision) were obtained from either 0.5 m or 1 m of copper coil squeezed using a benchtop roller to extracted fluid from the coils. Samples for CH_4 analyses were extracted from either 2 m or 4.5 m segments. Segments for dissolved CH_4 measurements were squeezed under gas tight conditions using the same bench-top roller into pre-flushed (air, Ultra High Purity (UHP) Airgas, flushed 10-20 times vial volume) glass serum vials (13.5 mL, Wheaton) with butyl rubber stoppers (1.5 cm thick, GMT Stoppers Item #1313) and crimped aluminum caps. This process introduced ~2 mL of sample to the vials, which were stored

upside down at -20ºC until CH_4 analysis. At the most intensely sampled water depth, 2.90 m, there were 115 samples collected from 2015 to 2017.

2.3.1.2. Determination of Sample Date Assignment

Date assignments for samples collected with OsmoSamplers are typically determined by assigning evenly distributed dates across the deployment period. However, pumping rates vary as a function of temperature (Jannasch et al., 2004), and lake bottom water temperature from the 2.90 m water depth sensor varied between 2ºC and 18ºC. Dates were assigned with a temperature correction (Appendix 1 Text S1-1, Appendix 1 Figure S1-2) following methods described in Gelesh et al. (2016).

2.3.2. Discrete Lake Water Samples

Discrete near-surface water samples (within 0.5 m of the lake surface) were gently collected in duplicate during open-water conditions in August 2015; June, July and August 2016; and August 2017; and under-ice in March 2016 and May 2016 (Appendix 1 Table S1-1). Water samples were collected into 160 mL glass serum vials (Wheaton) with a submersible pump or direct submergence. Briefly, once filled, vials were capped immediately (1.5 cm butyl rubber, GMT Stoppers), a 10 mL headspace of air (UHP, Airgas) was added, and back at ARI samples were basified (0.5 mL 8 M potassium hydroxide, KOH) following Magen et al. (2014). Samples were stored at ~22ºC and analyzed for dissolved CH_4 concentrations and $\delta^{13}C\text{-}CH_4$ at the Chesapeake Biological Laboratory.

2.3.3. Surface Water Methane Radiocarbon Age

In August 2016 and August 2017, near-surface water samples were collected from the center of the lake from a small boat in duplicate 10 L air-tight bags (Tedlar, Restek,

Bellefonte, PA, USA) with a submersible pump. After retrieval, 140 mL of air (UHP, Airgas) was added to each bag, bags were shaken for three minutes (Garnett et al., 2016), headspace transferred to 160 mL serum vials (Wheaton), and then vials were capped (butyl rubber stoppers and crimped aluminum caps). Headspace extraction was repeated to produce two serum vials per sample bag. Extracted CH_4 gas was purified from other gases (e.g. water vapor, carbon dioxide) using a vacuum line and cryogenic traps and converted to CO_2 by passing the CH_4 over a heated copper oxide column at Florida State University (Chanton et al., 1995). Purified CO_2 was reduced to graphite and formed into graphite targets for ^{14}C analysis in the accelerator mass spectrometer (AMS) at the National Ocean Sciences AMS radiocarbon facility (McNichol et al., 1992). A split (10%) of the purified CO_2 was analyzed on a stable isotope mass spectrometer (VG PRISM series II) for $\delta^{13}C$-CH_4. Stable carbon isotope ratios are presented using per mil (‰) notation and radiocarbon data are presented as radiocarbon ages (McNichol & Aluwihare, 2007; Stuiver & Polach, 1977). A process blank of air (UHP, Airgas) was treated in the same way as samples and a correction for carbon added during processing was made using isotopic mass balance (Appendix 1 Table S1-2).

2.3.4. Sediment Sampling

Sediment cores were collected alongside OsmoSampler package deployments and recoveries (August 2015, 2016, 2017), and through a hole cut in the ice in May 2017, using a 9-cm diameter, hand-held gravity corer (Uwitec Corer, Mondsee, AUT). Cores were transported to ARI by small boat during open-water and by helicopter and truck during ice-cover with minor disturbance and immediately sectioned into 2, 3, or 4 cm depth intervals. From each section, subsamples were collected for pore-water CH_4

concentration and $\delta^{13}C\text{-}CH_4$ ($CH_{4\text{-}Sed}$), sediment porosity and sediment organic carbon (SOC) concentrations. For the $CH_{4\text{-}Sed}$ samples, a 3 mL plug of sediment was placed in a 13.5 mL glass serum vial, capped (1.5 cm thick butyl rubber stopper and aluminum seal), basified (3 mL 1M KOH) to arrest microbial activity, and stored at -20°C until analysis (Lapham et al., 2008). For the porosity and SOC samples, multiple aliquots of sediment were transferred to pre-muffled (500°C, 4 hours) 20 mL borosilicate scintillation vials, capped with methanol rinsed caps and stored at -20°C until analysis.

2.3.5. Analytical Analyses

Methane concentrations were measured by headspace equilibration with air (UHP, Airgas) at ~22°C (Magen et al., 2014). The diluted headspace was introduced to a gas chromatograph (SRI 8610C, Torrance, CA, USA with HayeSep D (1.83 m, 3.2 mm ID) and Molecular Sieve (1.83 m, 3.2 mm ID) columns and flame ionization detector) through a loop injector. Sample areas on PeakSimple Chromatography software were compared to CH_4 gas standard areas ranging from 30 ppm to 9.0% CH_4 (Airgas, balance helium). Replicate standards and duplicate discrete surface water vials had coefficients of variance (CV) <2%. For calculating sediment CH_4 concentrations (moles of CH_4 per cubic centimeter), porosity was determined by weighing dried sediments at 60°C and comparing to wet sediment weight. Sample CH_4 concentrations were calculated with Henry's law as described in Magen et al. (2014).

Methane stable carbon isotope ratios ($\delta^{13}C\text{-}CH_4$) from time-integrated bottom water, discrete surface water, and sediment pore-water were measured using a Cavity Ring-Down Spectrometer (CRDS G220l-i, Picarro, Santa Clara, CA, USA) using the same headspace samples described above. Samples with headspace greater than 420 ppm

CH_4 had gas aliquots of variable volumes diluted to 15-500 ppm in 100-140 mL air (UHP, Airgas). Samples were introduced into the CRDS intake through a Drierite-filled tube under the machine's vacuum. Samples with CH_4 headspace between 30 and 420 ppm were introduced to the CRDS via a Small Sample Isotope Module (Model #A0314 Picarro, Santa Clara, CA, USA). Raw isotopic ratios were averaged over three minutes for each injected sample and compared to certified CH_4 standards (T-iso1, L-iso1, and H-iso1, Isometric Instruments, Victoria, BC, CAN). Isotopic results are reported using the $\delta^{13}C$ notation in per mil (‰). Precision was ±1‰.

Ion analysis was performed on the acidified Teflon coil samples diluted 1:20 in 1% nitric acid using an ICPOES/MS for iron (Fe) and an ICPOES for manganese (Mn) (Wheat et al., 2017). The detection limit was 0.5 μmol L^{-1} for Fe and 0.1 μmol L^{-1} for Mn. Precision was ±2% for Fe and <2% for Mn.

Sediment organic carbon and total nitrogen (OC, TN) were quantified on the dried sediment after porosity determinations. An aliquot of sediment was acidified with 1 M HCl until bubbles ceased and then dried at 60ºC overnight (Hedges & Stern, 1984). Acidified (OC) and unacidified (TN) sediment were measured on an elemental analyzer (Costech elemental combustion system). Precision was <5%.

2.3.6. Methane Diffusion Model

A one-dimension (1-D) model was used to describe CH_4 diffusing from the surface sediments into the water column, assuming that dispersion in the water column is negligible. First, η was calculated using the following equation:

$$\eta = \frac{X\ (cm)}{2 * \sqrt{Porosity * Diffusion\ Coefficient * Time\ (sec)}} \quad (2.1)$$

where x (cm) is the distance from the sampling intake to the sediment for samples collected at 2.90 m water depth. Mean sediment porosity of 0.65 mL water mL sediment^{-1} was used (Appendix 1 Figure S1-3). The diffusion coefficient (9 x 10^{-6} cm^2 s^{-1}) was corrected for *in situ* temperature (°C), pressure (atm), and salinity (psu) (Riley & Skirrow, 1975). Time (sec) corresponds to time elapsed in the model beginning when DO was 0 mg L^{-1} (e.g., 25 October 2015, Figure 2-2b).

To calculate the dissolved CH_4 concentration at distance x (cm) over time, η was entered into equation 2.2:

$$CH_4 \text{ Concentration } (\mu M) = \text{Saturated Concentration } (\mu M) * (1 - \text{Error Function } (\eta)) \quad (2.2)$$

where the saturated concentration of CH_4 is set as the boundary condition at the surface of the sediment. Three different concentrations were used for the surface sediment concentration and are referred to as scenarios 1-3. Scenario (1) utilized 5800 μM CH_4, similar to sediment pore-water in May 2017 (Appendix 1 Figure S1-4); scenario (2) used 4500 μM CH_4; and scenario (3) used 2000 μM CH_4, similar to sediment pore-water in August 2015 (Appendix 1 Figure S1-4). For scenario (2), the concentration used was found iteratively to be the best fit to the observed CH_4 data at 2.90 m water depth during winter 2015-2016 (Figure 2-5). In equation 2.2, the "1-Error Function" is the complementary error function (erf) which describes diffusion through a sigmoid shape over time, t (Lapham et al., 2014):

$$\text{erf}(x) = \frac{2}{\sqrt{x}} \int_0^x e^{-t^2}\, dt \quad (2.3)$$

2.3.7. Spring River Flood Intrusion

To determine the intrusion of the spring Mackenzie River flood, both lake depth changes and river height were reviewed. Lake depth (h) was estimated from water

pressure sensor measurements (p_w) and atmospheric pressure (p_a) during the ice-free period using:

$$p_w - p_a = \rho g h \quad (2.4)$$

where p_w and p_a are in pascals (kg m^{-1} s^{-2}), ρ is water density in kg m^{-3}, g is gravity as 9.8 m s^{-2} and h is lake level or water height in m (raw pressure accuracy of 0.62 kPa and a water level accuracy of 1.0 cm noted in the manufacturer specifications). Atmospheric pressure was measured at the airport in Inuvik, NT, Canada (CLIMATE Station ID 2202578, Environment and Climate Change Canada, http://climate.weather.gc.ca/) which is 9.1 km from Lake 520 (Figure 2-1). Daily river height for the Mackenzie River at the East Channel at Inuvik, NT, Canada (Station 10LC002, Water Survey Canada, https://wateroffice.ec.gc.ca/index_e.html) was used to determine if flood waters breached the lake sill in 2016 and 2017. Following Lesack and Marsh (2010), 10.00 m was subtracted from the water gauge data to account for the sea level contribution to the river height. The sill at Lake 520 was breached when the Inuvik gauge rose above 4.91 m above sea level (asl). The river-to-lake connection ended when the river level fell below the summer sill height of 4.59 m asl (Lesack & Marsh, 2010).

2.3.8. Surface Water CH_4 Diffusive Flux

Surface water CH_4 diffusive fluxes were calculated following Cunada (2016) and utilizing Fick's first law:

$$F = k_{CH4} * (C_w - C_A) \quad (2.5)$$

where F is the diffusive flux (mg CH_4 m^{-2} d^{-1}), k_{CH4} is the transfer coefficient of CH_4 across the air-water interface, C_w is the concentration of CH_4 measured in the surface water, and C_A is the concentration of CH_4 measured in the atmosphere from 2015 to 2017

(1.9 ppm, Dlugokencky et al., 2018). The transfer coefficient k_{CH4} is obtained in equation 2.6 from the Schmidt number for CH_4, (Sc_{CH4}) a unitless ratio of the kinematic viscosity of water to molecular diffusion of CH_4 calculated following Cunada (2016):

$$k_{CH4} = k_{600} * (Sc_{CH4}/600)^{-n} \quad (2.6)$$

An exponent of n = 0.5 was used, based on local wind speeds (Ledwell, 1984). k_{600} is the gas transfer coefficient normalized to the Sc_{CH4} of CO_2 at 20ºC (Cole & Caraco, 1998) and calculated by:

$$k_{600} = 2.07 + 0.215u^{1.7} \quad (2.7)$$

where u is average monthly wind speed (between 2.8-3.3 m s^{-1}) measured at 10 m height at the airport in Inuvik, NT, Canada (CLIMATE station 2202578; Environment and Climate Change Canada), following Cunada (2016). Cunada (2016) found equation 2.7 best replicated the k_{600} measured in floating chambers on lakes in the Inuvik region of the Mackenzie River Delta (mean difference = 17%). Their analysis included Lake 520 where a floating chamber diffusive CH_4 flux was <8% greater than the Cole & Caraco (1998) calculation based on wind speeds measured at the Inuvik airport.

2.3.9. Data Visualization and Comparison of Reactions Influencing CH_4 Storage

A visualization of the processes which contribute to the CH_4 dynamics captured in the time-series was carried out within the 2.90 m water layer during 2015-2016 (equation 2.8). For this comparison, concentration changes measured (Δ_{CH4}) were a balance of diffusion from surface sediments ($Diff_{sed\text{-}CH4}$), any attributable CH_4 oxidation (MOx) that might occur in the water column, and an unknown residual term:

$$\Delta_{CH4}\ (\mu mol\ L^{-1}\ d^{-1}) = Diff_{sed\text{-}CH4}\ (\mu mol\ L^{-1}\ d^{-1}) - MOx\ (\mu mol\ L^{-1}\ d^{-1}) + Residual\ Reaction\ (\mu mol\ L^{-1}\ d^{-1}) \quad (2.8)$$

To obtain the Δ_{CH4} term, a 3-point average was used for the CH_4 concentrations and $\delta^{13}C\text{-}CH_4$ values to reduce the noise in the measured data while still maintaining the integrity of the large changes visible in the dataset. $Diff_{sed\text{-}CH4}$ was determined for the three 1-D diffusion model scenarios (section 2.3.6). MOx was calculated using isotope data with a modified open-system isotope model of Chanton & Liptay (2000):

$$F_o = (\delta^{13}C\text{-}CH_{4,t2} - \delta^{13}C\text{-}CH_{4,t1})/[(\alpha_{ox} - \alpha_{diff})*(1000)] \quad (2.9)$$

where F_o is the fraction of CH_4 oxidized between integrated samples at 2.90 m water depth and $\delta^{13}C\text{-}CH_4$ values are rounded to the closest integer for adjacent 3-point averaged data, time 2 (t2) and time 1 (t1). The isotopic fractionation factors, α_{ox} and α_{diff}, represent aerobic microbial CH_4 oxidation and CH_4 diffusion, respectively. We used α_{ox} = 1.020 and α_{diff} = 1.000, due to negligible fractionation during water column diffusion (Chanton & Liptay, 2000). An α_{ox} value of 1.020 was chosen after iteratively adjusting α_{ox} in equation 2.9 to get the lowest difference between F_o and the observed CH_4 decline (Appendix 1 Text S1-2). Calculated oxidation is likely conservative because the fractionation factor used was not measured directly through CH_4 oxidation experiments and CH_4 substrate and microbial community could influence the actual extent of CH_4 oxidation in the water column (He et al., 2012; Lofton et al., 2014). With that caveat, F_o was calculated and converted to a MOx rate by multiplying it by the change in CH_4 concentration between averaged time-points and dividing by the time elapsed between them.

Once MOx was determined, equation 2.8 was rearranged to solve for the residual reaction term. Measurement uncertainty should be randomly distributed around zero, whereas we interpreted substantial negative or positive residual values to suggest the

presence of unaccounted processes. A negative residual reaction value indicates greater CH_4 removal than CH_4 production, which could be due to evasion to the atmosphere or dilution with overlying water of lower CH_4 concentration. A positive residual reaction value indicates CH_4 production occurring at greater rates than CH_4 removal, which could be due to ebullition and bubble dissolution, water column methanogenesis, and/or the result of vertical or horizontal mixing with water of a higher CH_4 concentration.

2.4. Results

All sensor data, dissolved CH_4, $\delta^{13}C$-CH_4, ^{14}C-CH_4 age, and total ion data are freely available (Orcutt 2017a) and discussed in detail here.

2.4.1. Sensor data

Lake 520 bottom water temperatures from August 2015 to August 2017 were lower in the ice-covered months (2.9 ± 0.4ºC, mean ± standard deviation (S.D.)) and higher in the summer months (10.0 ± 4.5ºC) (Figure 2-2a). Shoulder seasons generally showed a linear increase or decrease in bottom water temperature consistent with the season. Initially after ice-out, water temperatures were similar at each of the near-bottom depths. Then a thermal gradient formed between 2.41 m and 2.90 m of ~3ºC by mid-July (Figure 2-2a insert). The water column mixed in mid-July, and temperatures became similar at the three depths (Figure 2-2a inset).

From these temperature data, ice-cover was determined to start on 30 September 2015 and 10 October 2016 as the temperature reached a minimum, and the lake was ice-free by 18 May 2016 and 24 May 2017 (shaded boxes in figures). Light data support this timing since light was reduced to 0 lux on 20 October 2016 as ice formed and

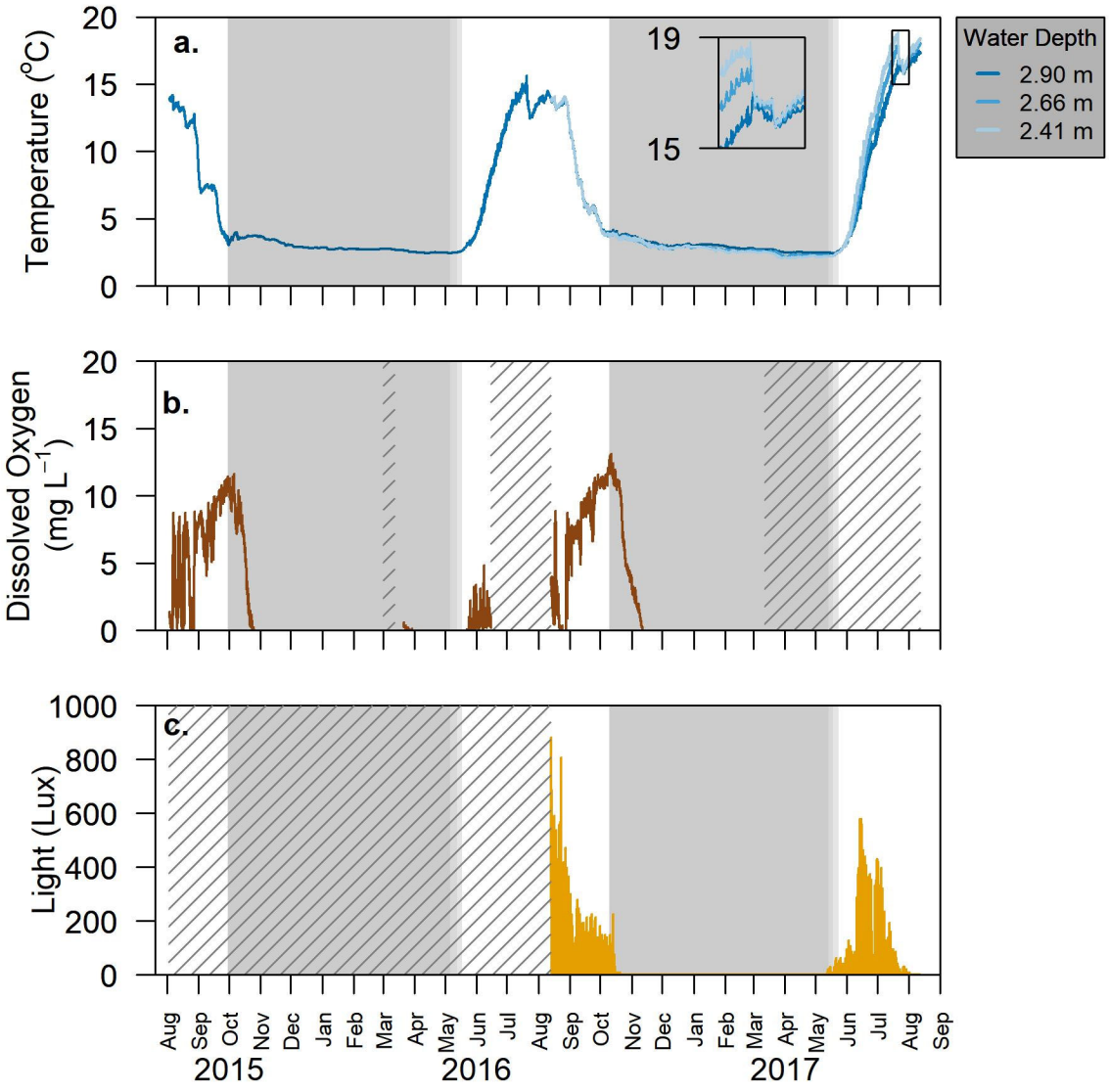

Figure 2-2. Sensor measurements in Lake 520 from August 2015 to August 2017. a) Water temperature at 2.90 m water depth (dark blue line), 2.66 m (medium blue line), and 2.41 m (light blue line) with the insert detailing 15 July to 1 August 2017. b) Bottom water dissolved oxygen and c) light intensity at 2.90 m water depth. Gray shaded boxes indicate when ice covered the lakes and lighter gray indicates when ice began thinning. Areas of no data collection are indicated by diagonal stripes

returned to measurable lux values on 12 May 2017 (Figure 2-2c). There was no similar sensor measuring light to verify the 2015-2016 dataset. Timing of ice melt was also determined from satellite images for 2016. Satellite images in the region near Inuvik show snow began to melt in early May 2016 and there was no snow on the ground by mid

May 2016 (https://worldview.earthdata.nasa.gov/). Most lakes in the region appear to be ice free following the Mackenzie River freshet. Consequently, we define the melt-period to be between 6 May to 18 May 2016 and similarly from 14 May to 24 May 2017 (gray gradient in figures).

Dissolved oxygen (DO) concentrations peaked prior to ice-cover on 6 October 2015 (11.62 mg L^{-1}) and 11 October 2016 (13.12 mg L^{-1}) and decreased to 0 mg L^{-1} on 25 October 2015 and 5 November 2016 (Figure 2-2b). Following ice melt and an increase in bottom water temperature, DO returned into the bottom water on 24 May 2016. We did not deploy a sensor measuring DO in spring 2017.

Pressure sensor data did not indicate a significant Mackenzie River flood in spring 2016 and indicated a minor intrusion into the lake in spring 2017 (Appendix 1 Figure S1-5). The Mackenzie River gauge height of the East Channel at Inuvik showed the lake flooded over 4 days in late May 2016 and 9 days in late May 2017, similar to connection times from 1964 to 2005 (Lesack & Marsh, 2010). The peak spring flood in Lake 520 was 0.09 m in 2016 and was 0.60 m in 2017 (Appendix 1 Figure S1-5).

2.4.2. Discrete Surface Water CH_4 Concentration, $\delta^{13}C$-CH_4, and CH_4 Radiocarbon Age

Near-surface dissolved CH_4 reached ~250 µM CH_4 under the ice in early May 2016 (Figure 2-3a, Appendix 1 Figure S1-6) prior to the peak in dissolved CH_4 at 2.70 and 2.90 m water depth (Figure 2-3b). Throughout the open-water period in 2016, surface water CH_4 concentrations decreased, except for an increase in mid-July 2016 to 34 µM CH_4 (Figure 2-3a). The $\delta^{13}C$-CH_4 values were ~-60‰ before ice-melt and quickly increased to ~-45‰ from June to August 2016 (Figure 2-3c), indicating a change from microbially produced CH_4 to highly oxidized residual CH_4 (Whiticar, 1999). Late

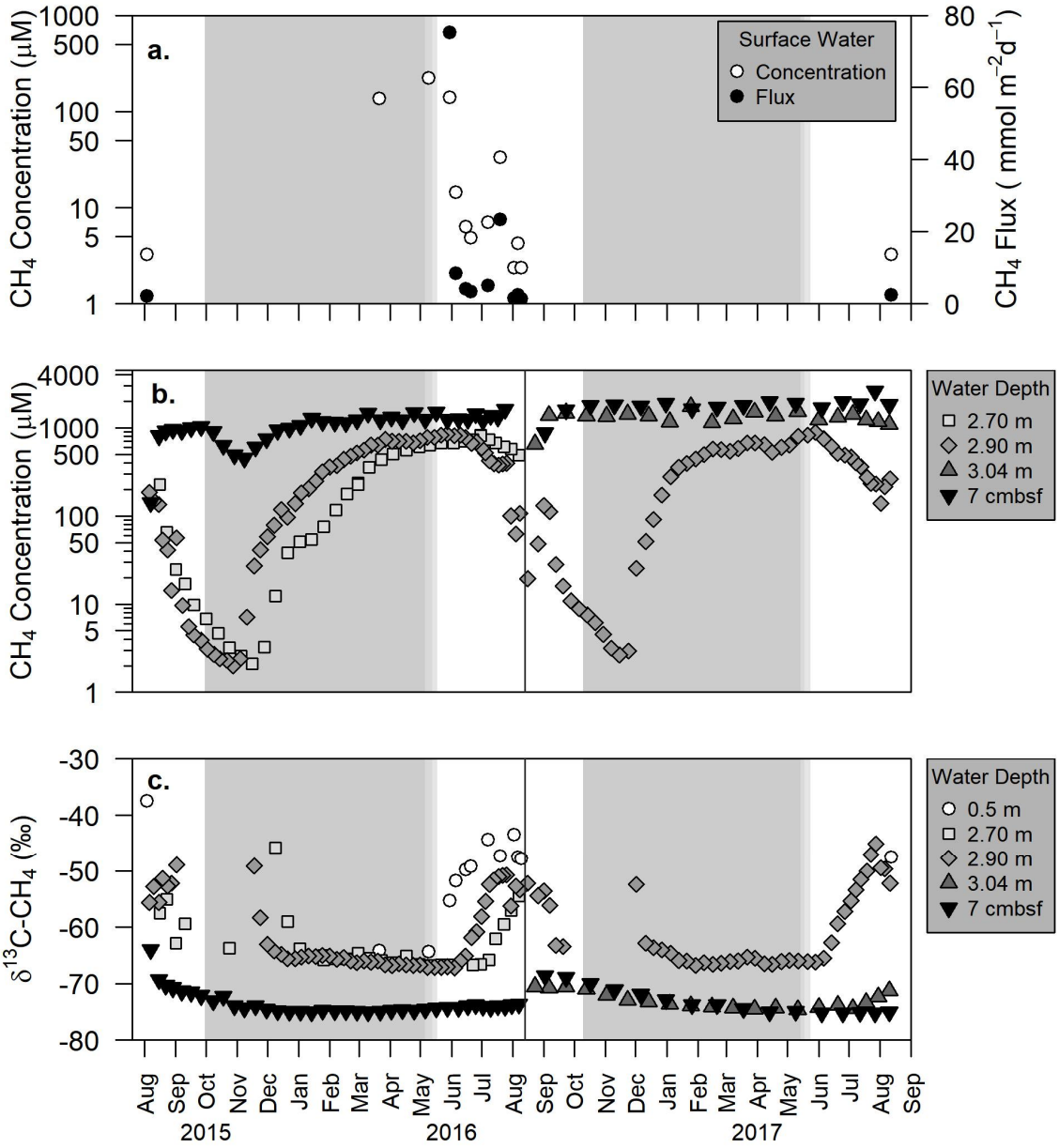

Figure 2-3. Dissolved CH_4 concentration and stable isotope patterns in Lake 520 from August 2015-August 2017. a) Discrete surface water (0.5 m) CH_4 concentration (white circles) and surface water CH_4 diffusive flux (gray circles), b) time-integrated sample dissolved CH_4 concentrations and c) $\delta^{13}C$-CH_4 from surface and bottom water. Discrete samples of surface water were taken at 0.5 m, and continuously collected samples were taken from 2.70 m (40 cm from sediments), 2.90 m (20 cm from sediments), 3.04 m water depth (6 cm from sediments) and 7 cm in the sediments (cmbsf). Note the difference in CH_4 concentration scale between a and b, and that concentrations scales are logarithmic. Gray shaded boxes indicate when ice covered the lakes and lighter gray indicates when ice began thinning. A solid vertical line separates the two deployments in August 2016.

summer (August 2015, 2016, 2017) surface water CH_4 had the lowest concentration (2-3 μM CH_4) and $\delta^{13}C$-CH_4 values were the highest (-37, -48, and -47‰, respectively). These

late summer surface water CH_4 concentrations were three orders of magnitude higher than if surface water was in equilibrium with the atmosphere (3-4 nM at air temperatures of 7-15ºC; Yamamoto et al., 1976). From the concentration gradient between the atmosphere and surface water, we calculated diffusive fluxes to the atmosphere ranging from 1.5 to 75 mmol CH_4 m^{-2} d^{-1} (Figure 2-3a). The highest flux was calculated during the week following ice-melt. While fluxes generally decreased during the open-water period in 2016, there was a second peak of 23 mmol m^{-2} d^{-1} in July. The radiocarbon age of dissolved CH_4 in Lake 520 was 0 ± 27 YBP in 2016 (n=4) and 6 ± 27 YBP in 2017 (n=2), which are both within error of a modern age (Appendix 1 Table S1-2).

2.4.3. Continuous Bottom Water CH_4 and $\delta^{13}C$-CH_4

In general, the high-resolution time-integrated samples had dissolved CH_4 concentrations that increased with water depth, increased during ice-cover, and decreased during open-water time periods (Figure 2-3b, Appendix 1 Figure S1-6). An exception to this is the sediment pore-water time-series at 7 cmbsf, where there appears to be a trend of increasing CH_4 over the sampling period from a minimum of ~700 µM in the fall of 2015 to nearly 2 mM CH_4 in August 2017 (Figure 2-3b). This could be an artefact of the second deployment being in a slightly different location and possible differences in the depth the plastic crate settled in the sediments, but the concentration trend is mirrored by the results at 3.04 m (at somewhat lower concentrations). Generally, at 3.04 m water depth and 7 cmbsf pore-water, dissolved CH_4 concentrations were near saturation of 1700-2300 µM CH_4 (assuming 2-14ºC water temperature and 1 atm pressure). $\delta^{13}C$-CH_4 values averaged -73 ± 2‰ at 3.04 m water depth and 7 cmbsf.

At 2.70 m and 2.90 m water depth, dissolved CH_4 concentration and $\delta^{13}C$-CH_4 value trends are similar although slightly offset in timing (Figure 2-3b and 2-3c). During ice-cover, the shallow depths reached minimum CH_4 concentrations in November 2015 and December 2016 (Figure 2-3b). Following the minimum CH_4 concentrations under-ice, the rate of CH_4 concentration increase accelerated with time for 2.70 m and 2.90 m water depth in both years (Figure 2-3b). Peak CH_4 concentrations were observed in late May in both years (~ 860 µM CH_4), and concentrations decreased through the summer at a rate of ~10 µmol L^{-1} d^{-1}. Methane was more enriched in ^{13}C when CH_4 concentrations were low during open-water conditions and then $\delta^{13}C$-CH_4 values quickly decreased and plateaued to ~-66‰ during ice-cover as CH_4 concentrations increased (Figure 2-3c).

2.4.4. Ion concentrations

Total Fe and Mn concentrations measured at 2.90 m water depth were low during open-water and increased following ice-cover and the removal of DO (Figure 2-4a). Fe was 7 ± 4 µmol L^{-1} in open-water in 2015 and increased to 195 µmol L^{-1} under-ice in 2015-2016. Mn was below detection

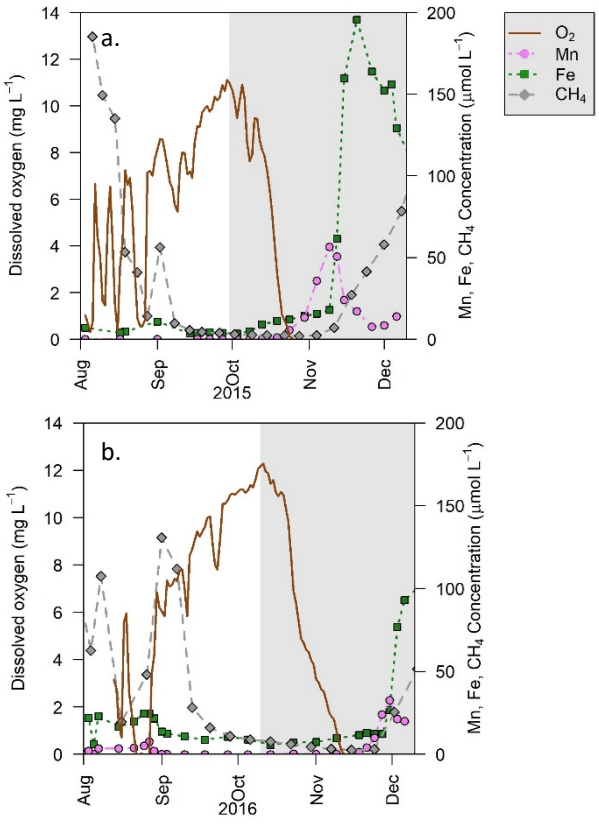

Figure 2-4. Patterns in Lake 520 dissolved CH_4 concentration dependence on electron acceptors in a) 2015 and b) 2016. Dissolved CH_4 (gray diamonds) at 2.90 m water depth in comparison to dissolved oxygen (O_2, brown), manganese (Mn, pink), iron (Fe, green), and ice-cover indicated by gray shading.

during open-water 2015 and increased to 56 μmol L^{-1} under-ice in 2015-2016. A similar pattern was observed in 2016-2017 (Figure 2-4b).

2.4.5. Sediment Pore-water CH_4 and $\delta^{13}C$-CH_4 and Sediment OC/ TN

Methane dissolved concentrations in sediment pore-water were above saturation at 1 atm in May (4 to 8 mM CH_4) and $\delta^{13}C$-CH_4 values averaged -72 ± 2‰ throughout the core (Appendix 1 Figure S1-4). In contrast, August pore-water dissolved CH_4 concentrations were lower and ranged from 1 to 3 mM (Appendix 1 Figure S1-4). $\delta^{13}C$ values increased from ~-65‰ to ~-73‰ below 6 cmbsf (Appendix 1 Figure S1-4). Surface sediments (0-2 cm) in Lake 520 had an organic carbon content of 9.3-13.0% OC and a total nitrogen content of 0.2-1.1% TN (Appendix 1 Table S1-3).

2.4.6. Diffusion Model Scenarios

Results of the 1-D diffusion model are shown in Figure 2-5 for the three scenarios relative to dissolved CH_4 concentrations observed at water depths of 2.90 m and 2.70 m water depth (20 and 40 cm above the sediments, respectively). Scenario (1) predicted CH_4 concentrations that are slightly lower than those observed at the 2.90 m water depth, except when the observed CH_4 concentrations decreased in April 2016; however, scenario 1 did not predict the CH_4 concentrations observed at 2.70 m water depth. Again, scenario (2) did not predict accurately the CH_4 concentration at 2.70 m. Scenario 3 did a poor job of predicting the dissolved CH_4 concentrations at either depth and a supplemental source of CH_4 would be necessary under this scenario.

2.4.7. Bottom Water CH_4 Mass Balance and Data Visualization

The data visualization carried out with equation 2.8 shows the balance between CH_4 diffusing in from the sediments, MOx in the water column, and a residual term

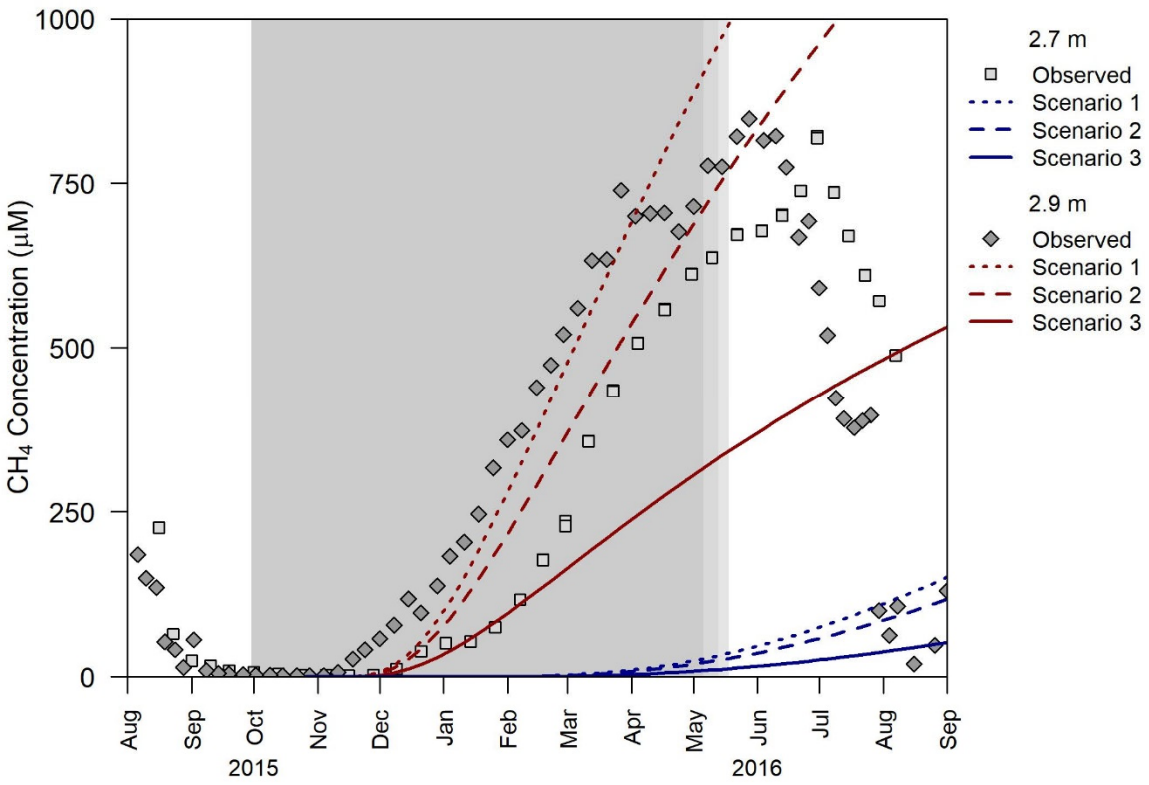

Figure 2-5. Observed (symbols) and modeled (dashed and solid lines) dissolved CH_4 concentrations in Lake 520 at two depths (2.70 m and 2.90 m) for ice-cover (gray shading as in other figures) during the winter of 2015-2016. Model scenarios were: (1) with 5800 µM CH_4 (dotted lines), (2) 4500 µM CH_4 (dashed lines), and (3) 2000 µM CH_4 (solid lines). The 1-D models were initiated when dissolved oxygen in the bottom water was negligible (25 October 2015).

which accounts for processes not constrained with the observed changes in CH_4 concentration data at 2.90 m water depth for 2015-2016 (Figure 2-6, Appendix 1 Figure S1-7). Different processes influenced the CH_4 inventory during ice-cover and open-water. During ice-cover, predicted MOx reaction rates were negligible with CH_4 becoming ^{13}C-depleted rather than enriched. Scenarios (1) and (2) were relatively close in predicting CH_4 concentrations at 2.90 m (Figure 2-6, Appendix 1 Figure S1-7). In scenario (3) the dominant component of the mass balance was a consistently positive residual rate. April 2016 coincided with a minor decline in observed water column CH_4 storage (Figure 2-6). The only component of the mass balance that could account for the

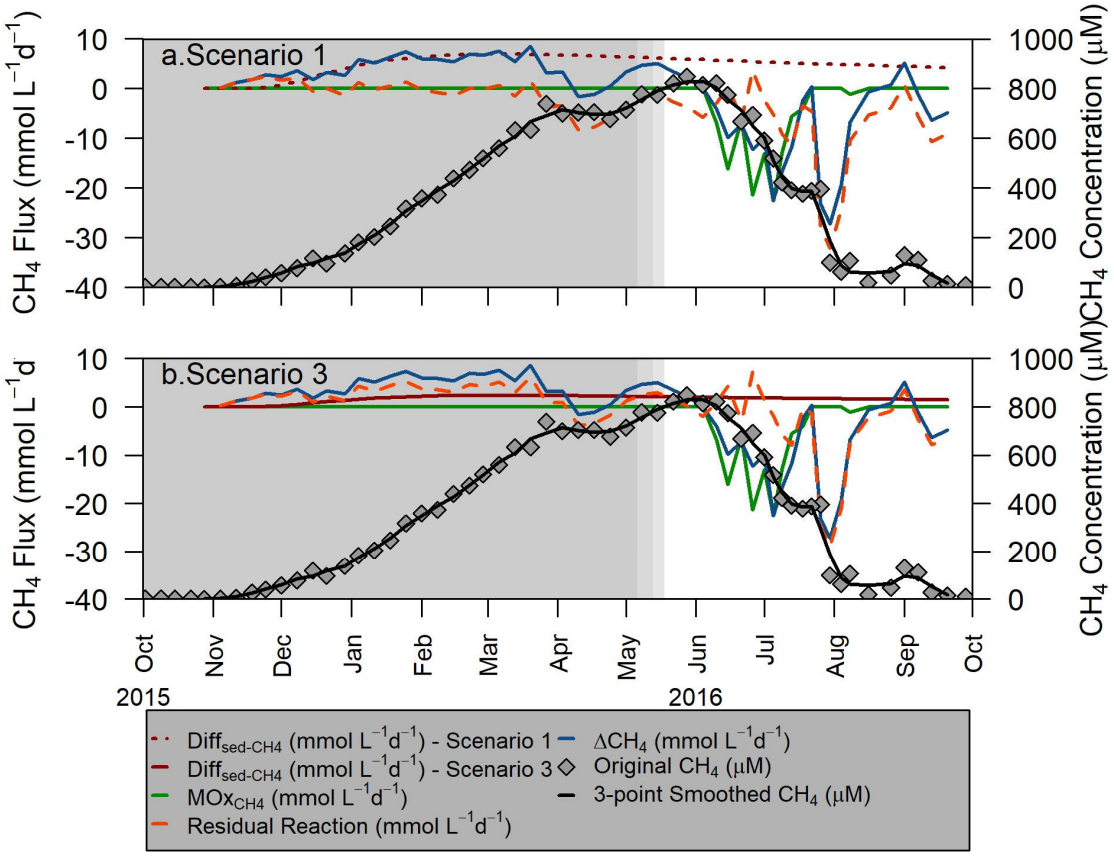

Figure 2-6. Comparison of dissolved CH_4 concentration and fluxes at 2.90 m water depth. Dissolved CH_4 concentration (grey diamonds plotted on right-hand y-axis), 3-point average smoothed dissolved CH_4 concentrations (black line), and fluxes of CH_4 (overall change in dissolved CH_4 concentration, blue line; diffusive flux, red line; CH_4 oxidation flux, green line; residual reaction flux; orange line; all plotted on left-hand y-axis) for a) scenario (1) and b) scenario (3). Gray shading indicates ice-cover as in other plots.

decline in the dissolved CH_4 concentration was a negative residual rate. During open-water until mid-July, observed CH_4 at 2.90 m steadily decreased from about 850 µM to 400 µM and calculated rates of MOx became substantial (as much as -23 µmol L^{-1} d^{-1}) (Figure 2-6). Late-July coincided with a considerable decline in observed CH_4 at 2.90 m (Figure 2-6). MOx declined to low rates at that time (<-5 µmol L^{-1} d^{-1}) counter-balanced by sediment diffusion rates during the whole open-water period (scenario 1: ~5 µmol L^{-1} d^{-1}, scenario 3: ~2.0 µmol L^{-1} d^{-1}). Therefore, the only component of the mass balance that could account for the dissolved CH_4 decline was a

large negative residual rate during this period (scenario 1: -29 μmol L^{-1} d^{-1}, scenario 3: -26 μmol L^{-1} d^{-1}). Following the late-July drop in observed CH_4, there were episodes where CH_4 concentrations moderately increased in early-August and again at the end of August (Figure 2-6). These increases were too large to be accounted for by the sediment diffusion flux. Significant positive residual fluxes, such as unaccounted for CH_4 sources, were needed to account for these changes (Figure 2-6). Overall, sediment diffusion and methanogenesis dominated in the ice-cover period, and MOx and removal via diffusion and mixing dominating during open-water.

2.5. Discussion

Over the last few decades, in high latitude lakes, emphasis has been placed on measuring open water CH_4 emissions while the influence of under-ice CH_4 processes on annual CH_4 budgets remains largely unexplored (Figure 1-2). Our high-resolution year-round sampling of dissolved CH_4, using OsmoSampler technology, provides new insights about *in situ* dissolved CH_4 dynamics under-ice and during open-water in an Arctic lake. After the lake iced-over and electron acceptors (DO, Mn, Fe) were depleted, water column dissolved CH_4 concentrations progressively increased from sediment diffusion and water column methanogenesis (Figure 2-4). Following ice-melt, dissolved CH_4 slowly decreased to lower concentrations over weeks to months, due to incomplete mixing of the water column until mid-summer. This is in contrast to what might be expected for a shallow lake that was well mixed quickly after ice removal. Surprisingly, even though Lake 520 exhibits thermokarst characteristics, the carbon source for the dissolved CH_4 did not originate from thawing permafrost but instead from modern carbon

sources, likely macrophyte biomass. Lake 520 exhibits CH_4 dynamics that might be important for understanding more broadly CH_4 cycling in Arctic lakes.

2.5.1. Under-ice CH_4 is from Lake Sediments and Water Column Methanogenesis

Within Lake 520, dissolved CH_4 concentrations increased under-ice from the time DO was exhausted until ice-melt in late spring, consistent with earlier observations (Cunada et al., 2018; Pipke, 1996). Patterns of dissolved CH_4 concentrations provide important new information about the source of dissolved CH_4, such as sediment diffusion (due to high rates of methanogenesis in underlying anoxic sediments), water column methanogenesis, and bubble dissolution. First, the close-coupling of redox elements (e.g. DO, Mn, Fe; Figure 2-4) through time to dissolved CH_4 concentrations suggests sediments are a primary source (Joung et al., 2017). Following ice-cover, DO was depleted, total Mn increased and was followed by an increase in total Fe in bottom water (Figure 2-4). Peak Mn and Fe concentrations are higher than seen in bottom water (e.g. Joung et al., 2017; St. Pierre et al., 2019) and in pore-water (e.g. Cornwell & Kipphut, 1992) of other ice-covered lakes. High Fe in the water column is from reduction of suspended iron oxides likely from pyrite-oxidation transported by the Mackenzie River (Calmels et al., 2007). Continuous measurements within Lake 520 provide a clear example of the electron acceptor cascade and biogeochemical dynamics through time in the water column. Time-series of dissolved CH_4 and $\delta^{13}C$-CH_4 data indicate that during the ice-free period, rates of aerobic MOx are high enough in the near bottom waters and/or surface sediments to control the diffusive release of CH_4 from lake sediments. Second, CH_4 accumulated first in deeper water before reaching the upper water column (Figure 2-3). This pattern is inconsistent with ebullition contributing substantially to the

CH_4 signal in lake-water by re-dissolution of CH_4 from bubbles trapped under the ice, as reported elsewhere (Greene et al., 2014). Third, measured concentrations cannot be accounted for solely by diffusion out from the lake sediments. Our 1-D diffusion model showed that there was an additional source of CH_4 to account for the observed pattern of winter-time CH_4 accumulation (Figure 2-5). We inferred the additional source of CH_4 was microbial methanogenesis in the water column, and discuss its plausibility below.

2.5.5.1. Plausibility of Under-ice Water Column Methanogenesis

While sediment diffusion provides a substantial portion of CH_4 to the water column, the data visualization exercise shows that it does not explain all the variability in dissolved CH_4 (Figure 2-6). Of the 3 scenarios explored, scenario (3) seems to be the most plausible. It represents the average August CH_4 gradient from the sediment pore-water to the overlying lake-water (Figure 2-5, Appendix 1 Figure S1-4). The model for scenario (3) yielded CH_4 diffusion curves that differed from observed trends, but there was similarity in the rate of increase in the difference between the model and the measured CH_4 contributing to water column CH_4 (Figure 2-5, solid lines). Water column methanogenesis would be expected to be roughly similar between the two depths because the available methanogenic substrate (i.e. dissolved organic matter, DOM, from various lake processes) would be similar. Average inferred methanogenic rates (observed CH_4 minus diffusion-derived CH_4) in the water column were 2.5 and 3.0 $\mu mol^{-1}\ L^{-1}\ d^{-1}$, respectively at 2.90 m and 2.70 m water depth, for scenario (3). These rates could have converged even closer by setting the 1-D model gradient to <2000 μM CH_4, but a value <2000 μM CH_4 was inconsistent with observed pore-water CH_4 in the top 5 cm of our sediment cores (Appendix 1 Figure S1-4). As a result, we concluded that methanogenesis

in the water column contributed around 60-70% of the CH_4 at 2.90 m, and 97-99% of the CH_4 at 2.70 m during the under-ice period in scenario (3).

Water column methanogenesis could be fueled by high quality DOM substrate that is present in the water column of Lake 520 during winter (Cunada, 2016; Tank et al., 2011). These results are consistent with other work that detected water column methanogenesis (0.4 to 0.6 μmol L^{-1} d^{-1}) during summer in Lake 520 under aerobic conditions (Bergstresser, 2018). Our study showed higher rates of methanogenesis (2.5 to 3.0 μmol CH_4 L^{-1} d^{-1}) while the lake was anoxic during ice-cover. Moreover, CH_4 in this lake had a modern radiocarbon age (Appendix 1 Table S1-2), which is consistent with CH_4 produced from decomposition of modern carbon in surface sediments or modern DOM in the water column (Martens et al., 1992; Nakagawa et al., 2002). Our finding of significant bottom water methanogenesis is important, yet an unexplored element of CH_4 cycling in Arctic lakes.

2.5.2. Methane has a predominantly modern (non-permafrost) origin

On the basis of radiocarbon dating, we establish the CH_4 found in the surface water of Lake 520 is modern in age. This finding is surprising for a thermokarst lake in which we expected a mixture of modern and aged carbon. Lake 520 receives aged sediments from thermokarst activity through modest shoreline expansion (Figure 2-1c, <3 m over 17 years) and an underlying thaw bulb into the permafrost (Johnston & Brown, 1964). The influence of bank erosion on lake geochemistry is a topic of interest as there is a reservoir of soil organic carbon that can be mobilized from Mackenzie Delta permafrost (>50 kg m^{-2} soil organic carbon content; Tarnocai et al., 2009). This potentially provides a large, labile carbon source to Mackenzie Delta lakes (Burn &

Kokelj, 2009; Tank et al., 2011; Zolkos et al., 2019). Our results may be explained by shoreline expansion that is episodic and may only contribute aged carbon to lake-water on an intermittent basis. Similarly, river flooding may not contribute a substantial amount of aged sediment (~5000 YBP; McClelland et al., 2016), especially given the average annual river-to-lake connection for Lake 520 is short and connections do not necessarily occur every year (Lesack & Marsh, 2010). We postulate that older-carbon from imported river sediments and within-lake thermokarst activity was not detected in our CH_4 samples because of the intermittent and heterogeneous nature of these carbon sources.

On the other hand, there are other important carbon sources that could yield CH_4 with a modern carbon-age. In other work, regular fresh organic matter inputs have been shown to produce CH_4 with a modern age (Martens et al., 1992; Nakagawa et al., 2002). Lake 520 has the highest density of submerged macrophytes of any lake nearby (Squires & Lesack, 2003). Over a multi-year time-scale, macrophyte biomass may be quantitatively the primary source of modern carbon. The high macrophyte density corresponds with high organic carbon in surface sediments (9 to 13%) as some decomposed macrophyte biomass is deposited annually following winter senescence and is a higher quality microbial substrate than river DOM (Tank et al., 2011). Other modern-age carbon sources to the lake beside the macrophyte biomass in Lake 520 and its exudates include: DOM in the spring Mackenzie River flood has been characterized as modern (Gareis, 2018) and fallen trees. Short river-to-lake connection times and shallow flooding in 2016 and 2017 with the <0.6 m spring flood limit the modern DOM in river-water transported into the lake (Appendix 1 Figure S1-5). Fallen trees surrounding Lake 520 show a range of decomposition stage (Figure 2-1c), which can also add modern

organic matter (<182 yr, Black & Bliss, 1980) to the lake. Hence, the autochthonous and allochthonous sources of modern carbon in Lake 520 represents abundant and high-quality substrate that can be rapidly decomposed by methanogens to produce the high bottom water CH_4 concentrations measured.

2.5.3. Incomplete Water Column Mixing Weakens Atmospheric CH_4 Flux

Previous work has shown that at ice-melt, any CH_4 frozen in ice or dissolved in the lake water under the ice would be quickly released to the atmosphere (Jammet et al., 2015; Jammet et al., 2017; Phelps et al., 1998). Conversely, Lake 520 retains dissolved CH_4 in bottom waters for more than two months after ice-out. We posit this is because of incomplete water column mixing, visualized by a temperature gradient in bottom water (Figure 2-2a insert). Typically, after ice-out, moderate wind energy should be sufficient to fully mix the water column of 2.23 m average depth (Lesack & Marsh, 2010). Thermal resistance to the entire water column mixing should have been low since lake water was still relatively cold. Deshpande et al. (2015) documented incomplete water column mixing following spring ice-out in some comparably shallow thermokarst lakes in sub-Arctic Quebec, but those lakes were smaller in area and with shorter wind fetches. Beyond the physical processes affecting water column mixing, it is possible that macrophytes in this lake inhibit mixing. Lake 520's macrophyte community grows to substantial height above the lake bottom (Squires & Lesack, 2003). The OsmoSampler intakes (20 and 40 cm above the lake bottom) were located below the height of the macrophyte canopy, so our observations may be limited because they were below where winter-derived CH_4 was retained. Our work highlights the need to understand lake water circulation impacts on the release of CH_4 from lakes to the atmosphere and why it is

important to understand these processes to scale up individual and regional lake fluxes to global estimates.

2.5.3.1. Electron Acceptors to Facilitate MOx

The consequence of incomplete mixing was that winter-derived CH_4 was not all released upon ice-out and lingered in the bottom water through the summer. This time delay allowed the retained CH_4 to be microbially oxidized and is consistent with our observations of dissolved CH_4 enrichment in ^{13}C as dissolved CH_4 concentrations decreased over time (Figure 2-3; also see Whiticar et al., 1986) and with our MOx model (Figure 2-6). MOx rates at 2.90 m became substantial after the first two weeks of open water, similar to the induction period for methanotrophy in other Arctic lakes (Greene et al., 2014 and references therein). There were modest levels of DO, which likely served as electron acceptor in late May and early June; either from atmospheric exchange or macrophyte photosynthesis after ice-melt and waters warmed. At the same time that MOx occurred, the mass balance residual reaction rates varied from positive to negative to varying degrees throughout open-water, indicating that dissolved CH_4 declined faster than MOx alone and there was occasionally an unaccounted for CH_4 source. We interpret these negative residual spikes as low magnitude episodes of deep mixing (except for the large magnitude event in late July) that diluted the concentration of dissolved CH_4 at 2.90 m by minor amounts and also supplied DO to the deep water, which in addition to photosynthesis would sustain MOx. Similarly, mixing events could result in the positive residuals in August and bring up deeper, high dissolved CH_4 concentration water to the 2.90 m water depth. Oxidation early in the summer led to less dissolved CH_4 being

transported to surface water and ultimately led to a decrease in the diffusive flux of CH_4 to the atmosphere.

The large negative spike of the mass balance residual in late July 2016 appears to represent a substantial deep-mixing of the water column, dilution of the water at 2.90 m, and a ventilation of dissolved CH_4 from bottom waters to surface waters (Figure 2-6). Late July deep water-column mixing events likely occur annually as similar dips in bottom water temperature were seen in both late July 2016 and late July 2017 (Figure 2-2a). The mixing episode in 2016 diluted the dissolved CH_4 at 2.90 m from 400 to 100 μM within four days, resulting in near-surface water increasing from 6 to 40 μM (Figure 2-3) and becoming more depleted in ^{13}C (-44‰ to -47‰) as it mixed with bottom water (-51‰) with an elevated dissolved CH_4 concentration. At this point, MOx rates declined substantially at 2.90 m (Figure 2-6) presumably because of much lower CH_4 substrate concentration (Lofton et al., 2014). MOx rates in the upper waters could have increased following the mixing event because of the sudden increase in near-surface water dissolved CH_4 concentrations (Cunada, 2016), but we did not measure what occurred in this case.

2.5.3.2. Multiyear CH_4 Accumulation

Despite the high concentrations of CH_4 at 2.90 m being mostly mixed into the lake water column by the end of July, an important observation is the increasing CH_4 concentration in the sediment 7 cmbsf pore-water spanning our 2-year data window (from 500 to 1300 μM in year 1 and 1300 to 2000 μM in year 2). The trend is also consistent with the CH_4 time-series at 3.04 m in the second year (Figure 2-3b). While the increasing CH_4 concentrations cannot continue indefinitely, it raises the question of how and when

the bottom-water layer mixes and resets to lower concentrations. We postulate that such reset may not occur every year, but only when sufficiently vigorous water column mixing occurs. This could correspond to years of higher-level river-flooding, which could deepen the lake sufficiently to more broadly connect it to the surrounding delta floodplain and greatly extend the wind fetch and effective energy for water mixing.

2.5.4. Large Surface Water Diffusive Evasion Flux from Lake Despite Oxidation

While a large amount of winter-derived CH_4 is retained in the bottom water and oxidized during open water, the surface waters of Lake 520 still produced a flux of 1.5-75 mmol CH_4 m^{-2} d^{-1} to the atmosphere-through the open-water period of 2016 (Figure 2-3a, black circles). Interestingly, the surface water discrete sampling detected two significant releases of CH_4 to the atmosphere: one following ice-out and a second one in mid-July, which was not predicted and would not have been observed without bi-weekly sampling. Excluding the highest CH_4 diffusive flux, which captured the ice-melt period on 30 May 2016, these rates (1.5 to 23 mmol CH_4 m^{-2} d^{-1}) are similar to previously measured rates in Lake 520 during 2014 (3.2-22 mmol CH_4 m^{-2} d^{-1}, Cunada, 2016). Our sampling captured surface water efflux ~16 days earlier in the year and closer to the time of ice-melt. In late-July the diffusive flux was 22 mmol m^{-2} d^{-1}, which is consistent in both timing and magnitude to that measured in 2014 (Cunada, 2016). These annual evasion episodes seem to be driven by a more complete mixing of the lake water column later in the summer. It is not clear why the annual evasion episodes occur in mid-July in Lake 520 and are not observed in other nearby lakes (Cunada, 2016).

The diffusive flux of CH_4 from Lake 520 was considerably higher compared with other lakes in the circumpolar region. For example, Wik et al. (2016b) estimated mean

thermokarst lake diffusive fluxes of 2.1 mmol CH_4 m^{-2} d^{-1} (range: 0.19-2.3 mmol CH_4 m^{-2} d^{-1}), though their estimate does not include any lakes in western Canada. Matveev et al. (2018) reviewed the range of CH_4 diffusion in other circumpolar lakes and found thermokarst peatland lakes (0.01-12.8 mmol CH_4 m^{-2} d^{-1}, Matveev et al., 2016) to have the highest diffusive fluxes, which are lower than those found in Lake 520. The river floodplain setting is an important driver of the macrophyte community in Lake 520 that appears to ultimately fuel the high emissions of CH_4.

We extrapolate the calculated diffusive fluxes in Lake 520 to all high-closure lakes in the Mackenzie Delta during open-water (post-flood to October 1) period. The calculated diffusive flux from each time-point was applied to the days in-between time-points, and after summing the open-water diffusive flux for Lake 520, the calculated diffusive flux was scaled-up based on the area of all high-closure lakes. High closure lakes cover ~376 km^2 in the Mackenzie Delta (Emmerton et al., 2007). Assuming all high closure lakes behave similarly to Lake 520, we estimate a release of 6.6 Gg CH_4 during open-water (post-flood to October 1). This value is approximately one-fifth the CH_4 open-water estimate across the whole delta (Kohnert et al., 2017), which is greater than their areal coverage of 11% of the Mackenzie Delta (Emmerton et al., 2007). It is possible that this estimate is an underestimate because of the winter-derived CH_4 that stays retained in bottom water. Quantifying the diffusive flux of CH_4 across the lake-rich Mackenzie Delta landscape provides a preliminary estimate for future assessments of CH_4 emissions from Arctic lakes.

2.5.5. Uncertainties and New Issues

2.5.5.1. Isotopic Fractionation by MOx

An important uncertainty in our estimated MOx rates for the 2.90 m water layer was the fractionation factor chosen for the calculation. The $\alpha_{ox} = 1.020$ was iteratively chosen, which resulted in an average oxidation of 15 μmol L^{-1} d^{-1} from mid-June to mid-July 2016 (Figure 2-6), and was similar to other Arctic lakes (1.0184-1.0208, Bastviken et al., 2002; 1.013, Ricão Canelhas et al., 2016; 1.020-1.027, Thottathil et al., 2018). The α_{ox} value used is also within the range of aerobic CH_4 oxidizing bacterial cultures (1.005 to 1.031) reported by Whiticar (1999). The effect of lowering α_{ox} to 1.011, which was the highest fractionation factor value obtained by Geeves (2019), would increase MOx rates by a factor of ~2 times and would result in a much larger positive residual rate in the mass balance with the source of that CH_4 being uncertain. This highlights the need for more precise measurements of *in situ* α_{ox} to accurately quantify MOx rates and should be pursued during future work.

2.5.5.2. Adequacy of 1-D diffusion Model

Our 1-D model is an oversimplified representation of sediment diffusion that has important uncertainties relevant to our findings. Our application of the model assumes that the pore-water CH_4 concentrations remained constant over time, and based on the sediment cores we collected, is not realistic. For example, the pore-water CH_4 profiles in the top 5 cm of sediment at the end of winter were 5800 μM, which is much higher than the ~2000 μM CH_4 value measured prior to ice-cover and used in the model (Appendix 1 Figure S1-4). The winter sediment core was collected to avoid hitting the plastic crate with OsmoSamplers in Lake 520 and represents the high end of sediment pore-water

concentrations within the lake. Recent work in Lake 520 suggests the pore-water CH_4 has appreciable spatial variability over the lake bottom, possibly because of heterogeneous macrophyte community coverage (Geeves, 2019). Similarly, sediment from interannual flooding could be deposited unevenly depending on macrophyte detritus distribution within sediments. Conversely, the time-series data from 3.04 m water depth (6 cm above sediments) and 7 cmbf suggest that constant pore-water CH_4 concentrations during ice-cover is a realistic assumption. The 7 cmbsf pore-water, with different CH_4 concentrations between the 2015-2016 and 2016-2017 deployments, had minimal CH_4 change during ice-cover (1070 ± 330 μM CH_4 and 1800 ± 100 μM CH_4, respectively; Figure 2-3). Similarly, the 2016-2017 time-series data from just above the sediment-water interface at 3.04 m water depth indicate minimal dissolved CH_4 concentration change during ice-cover at that single location (1370 ± 170 μM CH_4; Figure 2-3). The time-series data provide good evidence that our assumption was correct and highlight how important continuous measurements are to fully understand the biogeochemical dynamics in Arctic lakes. Future use of OsmoSamplers would be aided by collecting sediment cores within a close proximity periodically during the year and collecting time-series of dissolved CH_4 in pore-water directly at the sediment-water interface to constrain the starting CH_4 concentrations used in the 1-D diffusion model.

2.5.5.3. Under-ice Mass Balance Anomaly and Hydrodynamics

While the water column dissolved CH_4 concentrations increased during most of the ice-covered period, towards the end of the winter, the CH_4 concentrations reached a maximum in April (Appendix 1 Figure S1-6). It is possible there was under-ice MOx that would explain the leveling off of CH_4 concentrations, but there was no evidence for

oxidation in the $\delta^{13}C\text{-}CH_4$ values (Figure 2-3c). There was a period during April 2017 when the $\delta^{13}C\text{-}CH_4$ values briefly increased by a small amount before resuming their declining trend. If oxidation were occurring $\delta^{13}C\text{-}CH_4$ values would become enriched over time by as much as a 13‰ (Ricão Canelhas et al., 2016). For that reason, the plateau in dissolved CH_4 in April each year was not likely due to oxidation. Our hypothesis is that an episode of under-ice water circulation may have occurred that diluted the bottom water CH_4 with lower concentration water from higher in the water column. In the first week of April 2017, our uppermost water column sensor reached its coldest temperature of the winter (~2.1ºC) (Figure 2-2a). After that point, spring solar warming of the upper water column water just beneath the ice would increase its density relative to water beneath it and sink. Other prior work has established that vertical and horizontal mixing occurs in Arctic lakes beneath ice (Welch & Bergman, 1985; MacIntyre et al., 2018).

Our findings above along with the apparent incomplete vertical mixing (Figure 2-3b) during open-water periods suggest a highly important role of water column hydrodynamics in Lake 520. It is not known to what degree incomplete vertical water column mixing occurs in parts of the lake deeper than our deployment location and to what extent macrophytes may be involved. It is also unknown to what extent water column mixing may be occurring under-ice. Hydrodynamics of this lake need to be investigated in future work combining OsmoSampler technology with temperature, conductivity and DO measured at multiple depths throughout the entire water column, similar to MacIntyre et al. (2018).

2.5.5.4. Necessity of More Observations Prior to Freeze-up

The CH_4 dynamics and transformations occurring in Lake 520 from early August until freeze-up in early October are limited by the available data. We did not sample near-surface water after August so estimates of diffusive evasion are not available. During this period, dissolved CH_4 concentrations steadily declined at 2.90 m but concurrently became more depleted in ^{13}C. Availability of dissolved CH_4 and abundant electron acceptors (e.g. DO, Figure 2-2b) suggests MOx should be occurring, though the ^{13}C changes suggest it is not. On the other hand, the progressively depleted ^{13}C content in CH_4 could be a result of more vigorous deep mixing. Water temperatures cooled and lowered the thermal resistance to mixing. As a result, mixing dispersed the more strongly ^{13}C-depleted CH_4 from waters at 3.04 m and in 7 cmbsf pore-water (e.g. 2015, Figure 2-3b) through the water column, while also causing the concentration at 2.90 m to decline. Depending on the balance between these two processes, our open-water average of MOx may be too low or diffusive evasion to the atmosphere prior to freeze-up may be higher that we expect (Kankaala et al., 2007), particularly if deep mixing is able to disperse the high CH_4 water. Further surface water sampling and diffusive CH_4 flux measurements should be conducted during the fall, near the time of freeze-up, to determine if the decrease in bottom-water CH_4 leads to a flux of CH_4 to the atmosphere at that time.

2.6. Conclusion

Our use of OsmoSamplers and their high temporal resolution sampling yielded new insights about under-ice CH_4 dynamics in an Arctic lake with active thermokarst

processes. The findings highlight the importance of sediment diffusion augmented by water column methanogenesis and bottom water MOx processes influencing the concentration of dissolved CH_4 during ice-cover and open-water, respectively. Despite being a thermokarst lake with potential sources of modern and aged carbon substrates, dissolved CH_4 was modern with methanogens primarily using macrophyte detritus or other recently fixed organic carbon to fuel the high rates of methanogenesis. The potential dual role of macrophytes inhibiting full water column mixing, and facilitating provision of electron acceptors for methanotrophic biomass and thereby fueling foodwebs, may represent an important CH_4 and carbon cycling pathway that should be further investigated in Arctic lakes. It is also uncertain how widespread incomplete water column mixing is and the role of macrophytes when scaling up the amount of CH_4 released from specific lakes to the broader Arctic region. Our findings emphasize the need for greater resolution of sampling, especially prior to and during ice-cover, to better understand CH_4 dynamics within Arctic lakes.

2.7. Acknowledgements

We would like to thank Mitchell Bergstresser, Michelle Côté, Trevor Fournier, Roger MacLeod, and Nilou Rajaei for field assistance; Aimee Beardmore and Mary Oster for laboratory assistance; Christopher Cunada for assistance with surface water flux data analysis; Jeff Chanton and Ann McNichol for radiocarbon analysis assistance; and the Gwich'in Renewable Resources Board and entire team at the Aurora Research Institute (Western Arctic Research Centre) for critical logistical, technical, financial, and lab and field support, especially Edwin Amos, Elye Clarkson, and Andrew Gordon. Financial

support was provided by a University of Maryland Center for Environmental Science Presidential Fellowship (HAMM), University of Maryland Ann G. Wylie Dissertation Fellowship (HAMM), American Geophysical Union Horton Research Grant (HAMM), Geological Society of America Charles A. and June R.P. Research Fund (HAMM), U.S. National Science Foundation grants PLR-1416961 (BNO), PLR-1417128 (LLL) and PLR-1417815 (CGW), NSERC Discovery Grant and Northern Research Supplement programs (LFWL), and Polar Knowledge Canada (KG). This research was conducted under Northwest Territories Research licenses numbers 15724, 15851, and 16066. The data supporting the conclusions in this paper are available at the NSF Arctic Data Center (Orcutt 2017a).

Chapter 3

Determining evaporation, groundwater, and ice cover influences on lake chemistry and methane (CH_4) dynamics in multiple Arctic lakes (Mackenzie Delta)

Abstract:

Lake water was collected from the lower water column (25 cm from sediment surface) using autonomous, continuous samplers (OsmoSamplers) of three lakes in the central Mackenzie Delta near Inuvik, Northwest Territories, Canada. The lakes are all small (0.2 – 3.1 ha), and have variable depths (1.5 m – 5.5 m). Time-integrated lake water samples represent ~7 day intervals over a two-year time period (August 2015 to August 2017). At the same time, lake level was continuously measured using pressure transducers to calculate water balance. Under-ice dissolved methane and inorganic ion concentrations (Cl, Ca, Mg) increased in all three lakes with the greatest increase measured in the shallowest lake. During open water, the shallowest lake exhibited lake level decline consistent with evaporation and low dissolved CH_4 concentrations, but the two deeper lakes had groundwater influxes during the same time-period and variable dissolved CH_4 concentrations. Surprisingly, the groundwater connection to permafrost in two lakes did not warrant permafrost carbon being incorporated. Dissolved CH_4 was primarily of microbial origin with a near-modern carbon source from all three lakes. The results indicate that lake depth is a primary influence on both the amount of dissolved

CH_4 present in bottom water and the hydrologic processes of evaporation and groundwater seepage within some Mackenzie Delta lakes.

3.1. Introduction

Lakes can be hotspots of biological activity and greenhouse gas production (e.g. carbon dioxide (CO_2) and methane (CH_4); Cole et al., 2007; Raymond et al., 2013; Tranvik et al., 2018). They represent approximately one-fifth of the global CH_4 emissions releasing 103 Tg CH_4 yr^{-1} of the 560 Tg CH_4 yr^{-1} global budget (Bastviken et al., 2011; Saunois et al., 2019). Northern lakes (>50 ^{o}N), specifically, contribute up to 16.5 Tg yr^{-1} CH_4 to the atmosphere (Bastviken et al., 2011; Wik et al., 2016b). Most of the release from these seasonally ice-covered lakes occurs rapidly after ice-melt in the late spring (Jammet et al., 2017; Jammet al., 2015; Jensen et al., 2019; Phelps et al., 1998), and continues through the open water season via wind-influenced evasion to the atmosphere (Repo et al., 2007; Sasaki et al., 2016). Open water CH_4 emissions are mediated by saturated or near-saturated dissolved oxygen concentrations in the water column that enable microbial methanotrophy (Bastviken et al., 2002; Kankaala et al., 2006; McIntosh Marcek et al. *Submitted*). Potential sources of CH_4 in northern lakes, specifically in the Arctic and sub-Arctic, that feed surface water fluxes include methanogenesis in anoxic lake sediments (Cunada et al., 2018; Duc et al., 2010; Hershey et al., 2014) and groundwater CH_4 transported through the thawed active layer along the lake perimeter (Lecher et al., 2017; Paytan et al., 2015). When the active layer thaws, groundwater is generated, which can transport CH_4 produced in the saturated, anoxic active layer zones laterally to surface waters (Lecher et al., 2017; Paytan et al., 2015). Therefore, CH_4

emissions from northern lakes to the atmosphere are dependent on *in situ* methanogenesis and methanotrophy and their hydrologic connectivity.

The greatest influence on hydrologic connectivity in Arctic and subarctic lakes is permafrost presence and active layer formation (Lamontagne-Hallé et al., 2018; Walvoord & Kurylyk, 2016). Lakes surrounded by permafrost are disconnected from groundwater, since the frozen ground is a barrier to water movement (Lecher, 2017; Mackay, 1983). For this reason, Arctic lakes are isolated from one another and thus have been characterized as evaporative basins (Bigras, 1990; Gibson & Edwards, 2002; Marsh & Bigras, 1988; Oswald & Rouse, 2004). However, in a warmer climate, the active layer could deepen and taliks (thawed zones under lakes) form, which can promote more lateral groundwater movement and vertical connections, respectively (Jepsen et al., 2013; Lamontagne-Hallé et al., 2018; Wellman et al., 2013). As these types of lake-groundwater connections increase, they facilitate greater water fluxes both into and out of lake systems (Andresen & Lougheed, 2015; Connon et al., 2014; Jepsen et al., 2013; Smith et al., 2005; Yoshikawa & Hinzman, 2003). For instance, deepening of the active layer has enhanced groundwater flow to streams and increased winter-time baseflow and annual discharge in northern rivers such as the Mackenzie in western Canada (Lesack et al., 2013; McClelland et al., 2004; St. Jacques & Sauchyn, 2009; Toohey et al., 2016; Walvoord & Striegl, 2007). Hence, understanding hydrologic connections between lakes and groundwater resources is necessary to determine their impact on biogeochemical processes in a warmer and wetter Arctic (Lecher, 2017) with increased evaporation (Zhang et al., 2000) and increased hydrologic connectivity (St. Jacques & Sauchyn, 2009).

While groundwater connectivity may be limited, northern lakes can be hydrologically connected through surface water to rivers and channels in delta systems, and the example in my study is the lake-rich Mackenzie Delta. Within the Mackenzie Delta springtime flooding is particularly important because it affects both water balances and water chemistry. River-to-lake connections are controlled by the height of floodwaters relative to the ground (sill) elevations that separate rivers from lakes. Lakes in the Mackenzie Delta have varying connections to river channels, ranging from a) regularly connected (termed "no closure", <1.5 m sill), b) lakes only connected during the spring flood ("low closure", 1.5 to 4 m sill) to c) lakes inter-annually connected during the spring flood ("high closure", > 4 m sill) (Marsh & Hey, 1989; Marsh & Hey, 1994). In summer months, evaporation from lakes in the Mackenzie Delta often exceeds precipitation, leading to frequent negative water balances for lakes that are not flooded annually (Bigras, 1990; Lesack & Marsh, 2010; Marsh & Bigras, 1988). The springtime Mackenzie River connection provides nutrients, dissolved organic carbon, and high concentrations of fluvial, reworked sediment to lakes (Emmerton et al., 2008; Gareis & Lesack, 2017; Marsh et al., 1999). In contrast, summer evaporation causes the concentration of solutes in disconnected lakes (Lesack et al., 1998; Sokal et al., 2010). Furthermore, shorter river-to-lake connections, e.g. high closure lakes, are associated with greater CH_4 production (Cunada et al., 2018; Pipke, 1996). The interplay between the hydrologic influences of the Mackenzie River and evaporation is important to better understanding biogeochemical dynamics such as lake chemistry and dissolved CH_4 cycling within Mackenzie Delta lakes.

In this study of Mackenzie Delta lakes, the effects of winter freezing and summer open-water evaporation and groundwater contributions on lake chemistry and CH_4 dynamics in multiple lakes were examined. The lakes studied had different characteristics (shallow vs. deep water depth, low vs. high closure, thermokarst vs. non-thermokarst; Table 3-1) which were expected to impact the CH_4 dynamics of the individual lakes. Lake closure was hypothesized to be the greatest influence on CH_4 concentrations, meaning the highest dissolved CH_4 concentrations would be expected in the high closure lakes during both ice-cover and open-water. All lakes were expected to be evaporative basins showing an increase in inorganic ion concentrations and to have no groundwater contributions.

Table 3-1. Lake characteristics for study lakes near Inuvik, Northwest Territories, Canada.

	Lake		
	56	**280**	**520**
Latitude (°N)	68° 19.417’	68° 19.276’	68° 18.826’
Longitude (°W)	133° 50.805’	133° 50.309’	133° 42.931’
Lake Area[a]	3.1 ha	2.4 ha	0.2 ha
Spring Sill Height[a]	4.623 m	3.838 m	4.913 m
Deployment Depth	1.5 m	2.9 m	3.1 m
Mean Depth[a]	1.08 m	1.64 m	2.23 m
1st Deployment	2 August 2015	4 August 2015	3 August 2015
1st Retrieval/2nd Deployment	12 August 2016	12 August 2016	9 August 2016/ 13 August 2016
2nd Retrieval	9 August 2017	9 August 2017	12 August 2017
Ice-Cover dates	28 Sept. 2015-17 May 2016 5 Oct. 2016-22 May 2017	1 Oct. 2015-4 June 2016 2 Oct. 2016-31 May 2017	30 Sept. 2015-18 May 2016 10 Oct. 2016-24 May 2017
Flooding Duration	19 May to 27 May 2015 17 May to 25 May 2016 22 May to 2 June 2017	17 May to 1 June 2015 13 May to 30 May 2016 21 May to 7 June 2017	20 May to 26 May 2015 20 May to 23 May 2016 24 May to 1 June 2017
Lake Description	High Closure, Shallow	Low Closure	High Closure, Thermokarst

[a] Lake area, spring sill height, and mean depth came from Lesack & Marsh (2010).

3.2. Study Location

The Mackenzie Delta is a lake-rich flood-plain system, overlying discontinuous permafrost south of the tree line (Burn & Kokelj, 2009; MacDonald & Gajewski, 1992).

Within the central Mackenzie Delta the terrestrial landscape forms an active layer seasonally to a depth of 109-130 cm (Smith et al., 2009). The delta hosts ~45,000 lakes (Emmerton et al., 2007). Some of these lakes are too deep to freeze to the lake bed during the winter and can maintain a talik into underyling permafrost (Johnston & Brown, 1964), although it has not been shown if these lakes have a connection to subpermafrost groundwater supplies (Marsh & Bigras, 1988; Marsh & Lesack, 1996).

The three lakes selected for this study – informally named Lakes 56, 280, and 520 – are located in the central Mackenzie Delta adjacent to the East Channel of the Mackenzie River near Inuvik, Northwest Territories, Canada (Figure 3-1). Lake 280 is a low-closure lake and Lakes 56 and 520 are high-closure lakes (Table 3-1). Lake 56 is the shallowest lake in this study with a maximum depth in August 2015 of 1.5 m, while the other two lakes are deeper with maximum depths of 3.1 m for Lake 280 and 5.5 m for Lake 520 (McIntosh Marcek et al., *Submitted*; Lesack & Marsh, 2010). These lakes are south of the tree line and are located in white spruce (*Picea glauca*) and black spruce (*Picea mariana*) forests with an understory of sedges,

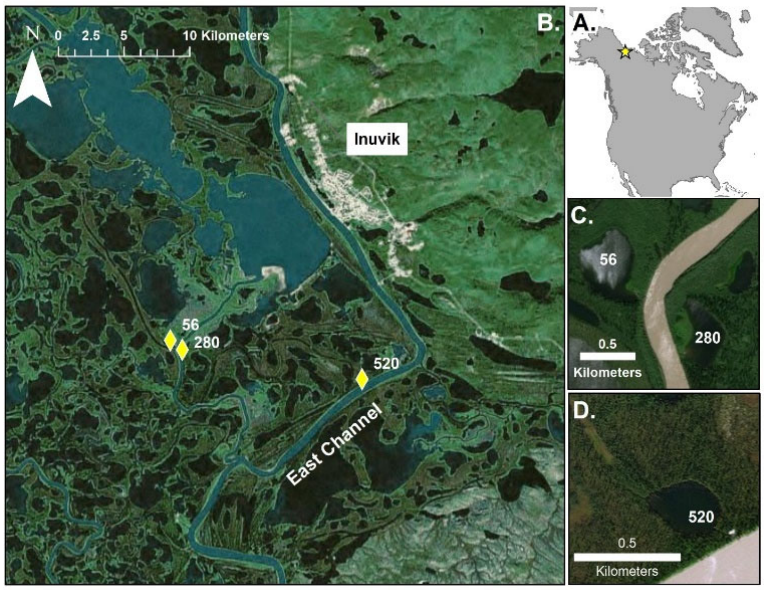

Figure 3-1. Location of three study lakes in the Mackenzie Delta, western Canadian Arctic. a) North American continent with Mackenzie Delta highlighted by the yellow star. b) Mackenzie Delta region near Inuvik, NT, Canada with the study lakes noted by yellow diamonds. c) Aerial image of Lakes 56 and 280. d) Aerial image of Lake 520 and a dried channel with lighter vegetation to the northwest. The small white box between Lake 520 and the East Channel (gray in lower right) is a hunting cabin. All aerial images courtesy of ESRI World Imagery Map (ESRI, 2018).

ericaceous shrubs and mosses (Black & Bliss, 1980; Mackay, 1995; Nguyen et al., 2009; Pearce et al., 1988). Lake 280 has water horsetails (*Equisetum fluviatile and Equisetum arvense*) between the river bank and western lake edge (Gill, 1973). Marsh surrounds Lake 280 on the southwest side and an abandoned stream channel is on the northwest side of Lake 520 (Figure 3-1). Additionally, Lakes 280 and 520 exhibit active thermokarst processes (permafrost thaw) with elevated pCO_2 (Cunada et al., 2018; Tank et al., 2009). Permafrost thaw is visible around Lakes 280 and 520 as trees collapse along lake shores (Figure 2-1c).

3.3. Methods

To test our hypotheses regarding ion and dissolved methane concentrations, time-integrated lake water samples were collected from the lower water column in three seasonally ice-covered lakes in the central Mackenzie Delta using autonomous and continuous samplers (Jannasch et al., 2004, McIntosh Marcek et al., *Submitted*). Dissolved CH_4 and solute concentrations (calcium, Ca^{2+}, chloride, Cl^-, magnesium, Mg^{2+}) were measured on lake water collected over two years. Continuous measurements of lake level were used to determine evaporation loses and groundwater contributions during open-water conditions. Finally, the age of dissolved CH_4 in surface-water samples was measured to evaluate whether groundwater transported "old" thawed permafrost carbon.

3.3.1. Autonomous Sampling

Lake water was collected from August 2015 through August 2017 from Lakes 56, 280, and 520 using osmotic pumps (OsmoSampler, Jannasch et al., 2004; Wheat et al., 2011) following similar methods as described in Chapter 2. Thin bore copper tubing (300

m, 0.8 mm inner diameter (ID) or 1.1 mm ID) for CH_4 analyses and thin Teflon tubing (300 m, hydrochloric (HCl) acid cleaned, 1.1 mm ID) for ion analyses were filled with a low salinity salt solution (44 mg L^{-1} NaCl) and attached to the intakes of separate osmotic pumps to make Gas and Acid OsmoSamplers, respectively. On the sample intake side of the copper tubing a rhizon filter (Rhizosphere Research Products, 0.15 μm mean pore size, Wageningen, NLD) was attached to reduce microbial alteration of samples while in the copper tubing. The Acid OsmoSampler Teflon tubing was connected to an additional osmotic pump that acidified (0.1 M HCl acid) the collected lake-water sample with a ratio of ~2 parts HCl acid solution to 11 parts lake water (Wheat et al., 2011; McIntosh Marcek et al., *Submitted*). OsmoSamplers and commercially-available sensors (water pressure: HOBO Model U201L-01 logger, 1-hour increment, kPa; water temperature: Tidbit V2 temperature Model UTB1-001 logger, 30-minute increment, ºC) were secured to plastic crates as sampling packages. A conductivity sensor (HOBO Model U24-001 logger, 2-hour increment, μS cm^{-1}) was also attached to the Lake 280 plastic crate for the 2015-2016 deployment. Sensors and the tubing intakes were ~ 25 cm above the lake bed when attached to sampling packages to collect from the lower water column. A sampling package with a Gas OsmoSampler and sensors was deployed to the bottom of Lake 280 in August 2015. Packages had both Gas and Acid Osmosamplers for both deployments in Lake 56 and 520 and in August 2016 in Lake 280 (Table 3-1).

Sampling packages were retrieved by Global Positioning System (GPS) location and by visualizing floats extending 1 m above the sampling packages. Immediately after retrieval, copper tubing was crimped and kept at 4ºC until processing. Sensor data was downloaded to a computer within 48 hours of collection. Upon retrieval, Teflon tubing

was sectioned into 1 m segments at the Aurora Research Institute, Inuvik, Canada. Sample water was drained into trace metal cleaned plastic microcentrifuge tubes as described in Wheat et al. (2017). Salinity was measured on aliquots with a refractometer (Extech RF20 refractometer, 1‰ precision) until the interface between fresh lake water and the saline filling solution was reached. Samples from Teflon tubing were kept at 20-25^{o}C until ion analyses at Monterey Bay Aquarium Research Institute (Moss Landing, CA, USA).

Copper tubing was brought back to the Chesapeake Biological Laboratory (Solomons, MD, USA) and sectioned into short (0.5 m or 1 m) and long (2 m or 4.5 m) segments for anion (Cl^- and sulfate, SO_4^{2-}) and CH_4 analyses, respectively, until the interface between fresh lake water and the saline filling solution was reached (Gelesh et al., 2016; McIntosh Marcek et al., *Submitted*). Long segments created time-integrated samples each representing ~7 days. Water was expelled from short copper segments using a benchtop roller into plastic vials (2 mL, Eppendorf) and from each a 400 µL aliquot of sample water was acidified (20-30 µL, 0.1 M HCl acid) for inorganic ion analyses. Long segments were squeezed for CH_4 analyses using gas tight connections into pre-flushed vials (13.5 mL, Wheaton, Ultra High Purity zero air 100-150 mL min^{-1} for 2 minutes) capped with butyl rubber stoppers (1.5 cm thick, GMT Stoppers Item #1313) and crimped aluminum seals.

Inorganic ion samples from the copper tubing were analyzed on an ion chromatograph (IC, Dionex ICS 1000) for Cl^- and SO_4^{2-} and matched to ion samples collected from Teflon tubing (Appendix 2 Figures S2-1 and S2-2). Date intervals were assigned for the time-integrated samples extruded from Teflon and copper tubing using a

temperature correction, because the rate of sample water pulled into the tubing varies as a function of temperature (Appendix 2 Text S2-1, Gelesh et al., 2016; Jannasch et al., 2004, McIntosh Marcek et al., *Submitted*).

3.3.2. Dissolved CH_4 Concentration and $\delta^{13}C$-CH_4 Analyses

Concentrations of dissolved CH_4 in the time-integrated samples were determined with a headspace equilibration method (Magen et al., 2014). Briefly, methane-free air (UHP, Airgas) was added to the sample headspace and shaken for 2 minutes to equilibrate CH_4 with the added gas. An aliquot of the diluted headspace was introduced via a loop injector to a gas chromatograph (SRI 8610C, Torrance, CA, USA with molecular sieve and HayeSep D columns and flame ionization detector). Sample concentrations were determined by comparing to CH_4 gas standards from 30 ppm to 9.0% CH_4 (Airgas, balance helium) and Henry's law following Magen et al. (2014). Standard replicates (n=3) run daily had coefficients of variance (CV) less than 2%.

Stable carbon isotope ratios of CH_4 ($\delta^{13}C$-CH_4) of time-integrated samples were measured on a Cavity Ring-Down Spectrometer (CRDS G220l-i, Picarro, Santa Clara, CA, USA) (McIntosh Marcek et al., *Submitted*). Samples with headspace between 30 and 420 ppm CH_4 were introduced to the CRDS via a Small Sample Isotope Module (#A0314 Picarro, Santa Clara, CA, USA). Raw isotopic ratios were averaged over three minutes per sample and compared to certified CH_4 standards (L-iso1 = -66.5 ± 0.2‰, T-iso1 = -38.3 ± 0.2‰, and H-iso1 = -23.9 ± 0.2‰, Isometric Instruments, Victoria, BC, CAN). Stable carbon isotope data are presented in the $\delta^{13}C$ notation in per mil (‰). Methane concentrations greater than 15 ppm have a precision of 1‰ on the CRDS.

3.3.3. Ion Tracer Analysis

Time-integrated samples from Teflon tubing were measured for Cl^- and SO_4^{2-} concentrations on an ion chromatograph (IC; Dionex ICS 1000) following standard methods (Wheat et al., 2010). Ca^{2+} and Mg^{2+} were measured with a 1:200 dilution in 1% nitric acid on an inductively coupled plasma optical emission spectrometer (ICP-OES, precision of <3%) following published protocols (Wheat et al., 2017). A few samples were concurrently measured on both the IC and ICP-OES. Under-ice concentration factors were calculated for all dissolved ions for both the 2015-2016 and 2016-2017 winters from these time-series data by taking the maximum under-ice concentration divided by the initial under-ice concentration.

3.3.4. $\Delta^{14}C$-CH_4 Measurement

Surface water (0.5 m below lake-surface) was collected into gas-tight Tedlar bags (10 L) from Lakes 56, 280, and 520 during field campaigns in August 2016 and 2017 and prepared for ^{14}C analysis following the procedure outlined in McIntosh Marcek et al. (*Submitted*). Gas was extracted from surface water in the Tedlar bags with methane-free air (UHP, Airgas) (Garnett et al., 2016). Methane in the extracted headspace was purified from other gases (e.g. water vapor, CO_2) and combusted to CO_2 on a copper oxide column at Florida State University (Chanton et al., 1995). CO_2 was purified and converted to graphite on iron filaments in a hydrogen atmosphere at the National Ocean Sciences Accelerator Mass Spectrometry (AMS) facility at Woods Hole Oceanographic Institution (McNichol et al., 1992). Graphite targets were analyzed on the AMS along with a process blank (McIntosh Marcek et al., *Submitted*) and traditional standards (NIST OxI, OxII) (Schneider et al., 1995). Splits (10%) of purified CO_2 were run on a VG

PRISM series II isotope ratio mass spectrometer for $\delta^{13}C\text{-}CH_4$ with a precision of 0.1‰. Data are presented as process blank corrected radiocarbon ages in years before present (YBP), where present is 1950 (McNichol & Aluwihare, 2007; Stuiver & Polach, 1977).

3.3.5. Mackenzie River Flood Duration

The duration of the spring river flood in the study lakes was determined as in McIntosh Marcek et al. (*Submitted*) from the daily water level gauge at the East Channel at Inuvik, NT, Canada (Station 10LC002, Water Survey Canada, https://wateroffice.ec.gc.ca/index_e.html). Sea level contribution (10.0 m) to river height was removed and the duration of the river-to-lake connection was calculated as the time interval when river height exceeded sill heights (Lesack & Marsh, 2010; Figure 3-2).

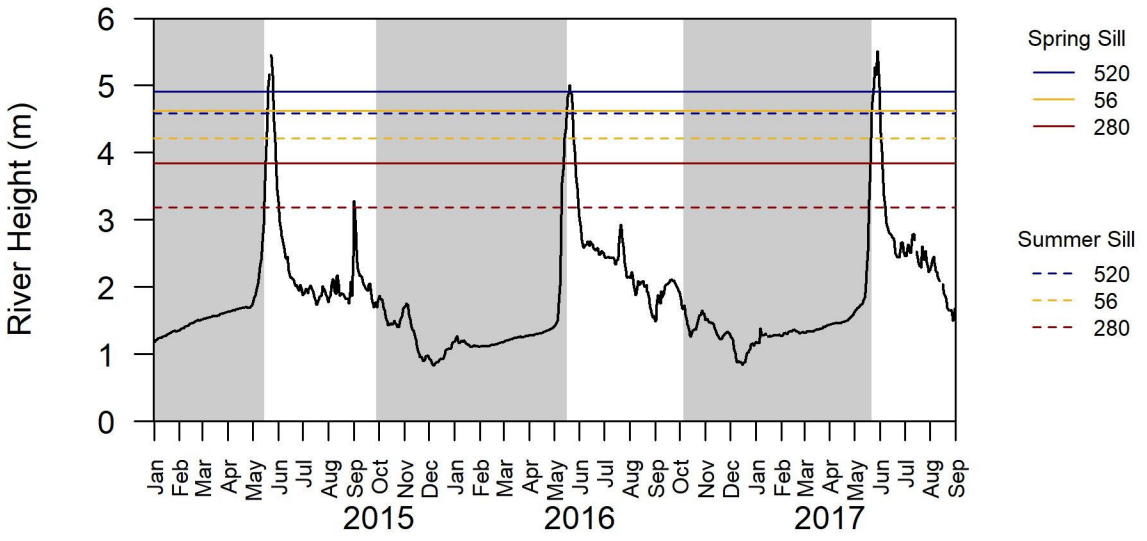

Figure 3-2. Mackenzie River hydrograph from the East Channel near Inuvik, Northwest Territories, Canada January 2015 to September 2017 with spring and summer sill heights for the study lakes noted. Solid lines are for spring sill heights and dashed lines are for summer sill heights (Lesack & Marsh, 2010). Gray shading indicates when the Mackenzie River was ice-covered.

3.3.6. Ice Cover and Thickness

The ice cover period was determined from bottom water temperature data. The presence of ice cover was determined to be the time between the measured temperature

minimum until the temperature began to increase in the spring. Ice melt started before lakes were completely ice free, based on satellite images in the region surrounding Inuvik (https://worldview.earthdata.nasa.gov/), and the ice melt period is presented as a gray gradient in Figures 3-2 to 3-6. The formation of ice and the exclusion of solutes in lake water was modeled with a cold summation relationship (Zubov, 1945) using air temperature data for Inuvik, NT, Canada (Environment and Climate Change Canada Meteorological Service of Canada (ECCC MSC)):

$$h^2 + h = 8 \sum T_{where\ T>0}, \tag{3.1}$$

where h is ice-thickness in cm and temperature is in ºC. A summation of temperature (ΣT) was calculated for the days where air temperatures were below 0ºC.

3.3.7. Weather Data

Hourly air temperature, wind speed, humidity, and atmospheric pressure, and daily precipitation data were obtained from the Environment Canada CLIMATE Station ID 2202578 in Inuvik, NT, Canada (ECCC MSC). The meteorological station was 9.1 km from Lake 520, 14.7 km from Lake 280 and 15.1 km from Lake 56. Hourly data were averaged together for mean daily temperature (ºC), mean daily relative humidity (%), mean daily atmospheric pressure (kPa), and mean daily wind speed (km h^{-1}) (Appendix 2 Figure S2-3).

3.3.8. Evaporation and/ or Groundwater Influence on Lake Level

A water balance was used to examine the influences on lake level:

$$\Delta LL = p - E + GW, \tag{3.2}$$

which was reorganized to determine evaporation (E) and/ or groundwater (GW) as a balance between measured lake level (LL) and precipitation (p) as LL_{-P}:

$$\Delta LL - p = -E + GW, \quad (3.3)$$

where weekly change in lake level (ΔLL) was determined by calculating LL on a weekly basis as the difference in water pressure (p_w) and atmospheric pressure (p_a) in pascals or kg m^{-1} s^{-2}, divided by the water density (ρ, in kg m^{-3}) and gravity (g as 9.8 m s^{-2}); following:

$$LL = \frac{p_w - p_a}{\rho * g} \quad (3.4)$$

Hourly water pressure (p_w) was averaged for daily water pressure for each lake's sensor. Average daily atmospheric pressure (p_a) was from weather data presented in section 3.3.7. Daily water density, ρ, was calculated as a function of water temperature, T, using the following equation (Jones and Harris 1992):

$$\rho = 999.85308 + 6.32693 * 10^{-2} * T - 8.523829 * 10^{-3} * T^2 + 6.943248 * 10^{-5} * T^3 - 3.821216 * 10^{-7} * T^4 \quad (3.5)$$

The average lake level was determined for each week of open water and represents lake level changes that were not due to the Mackenzie River flood or the onset of ice-cover based on dates determined in section 3.3.5 and 3.3.6. Cumulative weekly ΔLL was then taken as the difference between the previous weekly average lake level and the current weekly average lake level. Precipitation was from weather data presented in section 3.3.7. When ΔLL_{-P} decreased it was associated with evaporation, and where ΔLL-P increased it was associated with a source of water to the lake.

3.3.9. Groundwater Estimates

Groundwater contributions were calculated as a balance between lake level (LL) minus precipitation (p) plus evaporation (E), following:

$$GW = \Delta LL - p + E* \quad (3.6)$$

with ΔLL and p the same as in equation 3-2. Lake 56 was the only lake with continuous ΔLL_{-P} decrease during the full open-water period in 2016, and it is consistent with evaporation. Therefore cumulative decrease in LL_{-P} at Lake 56 was used as the reference open-water evaporation rate (E*) for Lakes 280 and 520, due to their close spatial proximity.

3.3.10. Comparison of Evaporation Estimates

Measured evaporation using LL_{-P} in Lake 56 (section 3.3.8) was compared to estimates calculated using three other methods. First, the mass-transfer method was used to calculate lake evaporation for each lake in 2016, where the mass transfer coefficient was based on lake area (Dingman, 1994, Appendix 2 Text S2-2). Second, lake evaporation was calculated with the Thornthwaite method for the entire open-water period in 2015, 2016 and 2017 for the region near Inuvik, NT, Canada (Thornthwaite, 1948, Appendix 2 Text S2-3). Third, I obtained an evaporation estimate based on data collected from satellite by Moderate Resolution Imaging Spectroradiometer (MODIS) from which evaporation was calculated using the Penman-Monteith equation for the area surrounding Inuvik, NT, Canada (University of Montana Evapotranspiration Web Viewer).

3.3.11. Statistical Analyses

Statistical comparisons for solutes were carried out using natural log transformed data as needed due to skewedness in the Cl^- raw data. Original data were used for Ca^{2+} and Mg^{2+} because of their normal distributions. Student's t-tests compared individual ion concentrations between Lakes 56 and 520 and between open-water and ice-cover.

Analysis was performed in RStudio (version 1.1.456). P-values less than 0.05 were treated as significant.

3.4. Results

3.4.1. Lake Water Temperature, Ice-Cover and Open-Water Periods

For all three lakes, the bottom water temperature averaged ~3°C during the ice-covered period and increased up to 20ºC after ice-melt (Figures 3-3a, 3-4a, 3-5a). All lakes show a mid-July decrease in bottom-water temperatures, which is likely due to water column mixing (McIntosh Marcek et al., *Submitted*). From the temperature data, ice-cover was determined to extend from early October to late May (Table 3-1). During that time, the depth of ice steadily increased to a maximum of 1.4 m in both March 2016 and 2017 (Figure 3-6).

All three lakes were connected to the Mackenzie River during the spring flood in 2016 and 2017 (Table 3-1, Figure 3-2). Lakes 520 and 56 were ice-free by the time the Mackenzie River flood receded (Figure 3-2). However, bottom water temperatures suggest that Lake 280 was not ice-free until after floodwaters receded (Figure 3-4a). The flood duration of the Mackenzie River ranged from 4 (Lake 520) to 18 days (Lake 280) and was within historical averages (Lesack & Marsh, 2010).

3.4.2. Conductivity and Inorganic Ion Concentrations in Lake 280

Conductivity was measured solely in Lake 280 during 2015-2016 and then ion concentrations were measured during 2016-2017 (Figure 3-4b). Under-ice conductivity measured in Lake 280 increased continuously to a maximum of 358 μS cm^{-1} in May 2016 (Figure 3-4b). Once the lake was ice-free, conductivity slowly decreased until mid-July

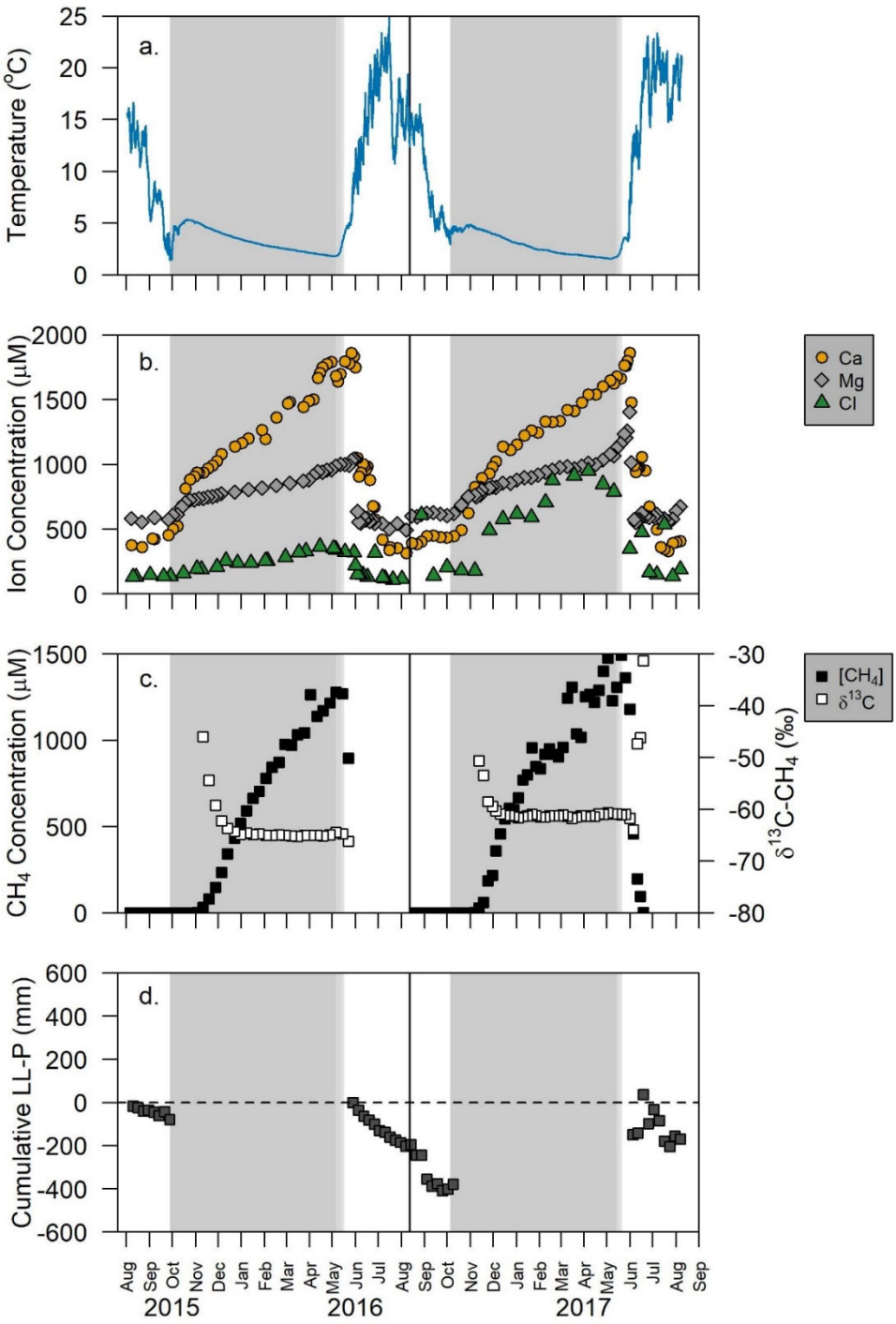

Figure 3-3. Lake 56 time-series of bottom-water characteristics and lake chemistry changes from August 2015 to August 2017 measured ~25 cm above the lake bed. a) bottom water temperature and b) lake chemistry – Ca^{2+} (gray circles), Mg^{2+} (blue diamonds), and Cl^{-} (yellow triangles) ion concentrations, c) dissolved CH_4 concentrations (black squares) and $\delta^{13}C$-CH_4 (white squares), and d) cumulative change in lake level minus precipitation. Gray bars indicate ice-cover. Vertical black lines indicate the switch from the first to second deployment.

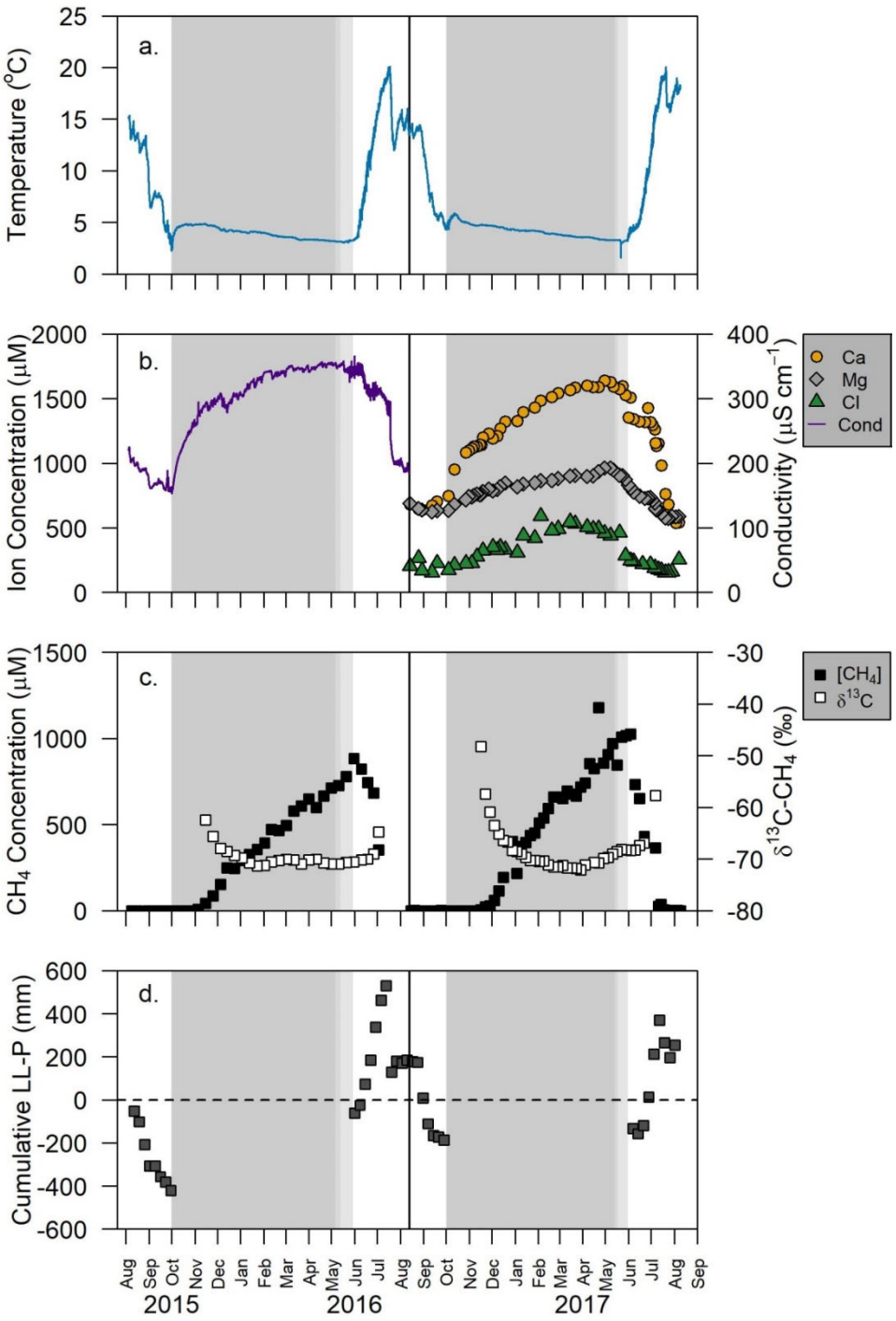

Figure 3-4. Lake 280 time-series of bottom-water characteristics and lake chemistry changes from August 2015 to August 2017 measured ~25 cm above the lake bed. a) bottom water temperature and b) lake chemistry – conductivity (purple line) and Ca^{2+} (gray circles), Mg^{2+} (blue diamonds), and Cl^{-} (yellow triangles), c) dissolved CH_4 concentrations (black squares) and $\delta^{13}C$-CH_4 (white squares), and d) cumulative change in lake level minus precipitation. Gray bars indicate ice-cover. Vertical black lines indicate the switch from the first to second deployment.

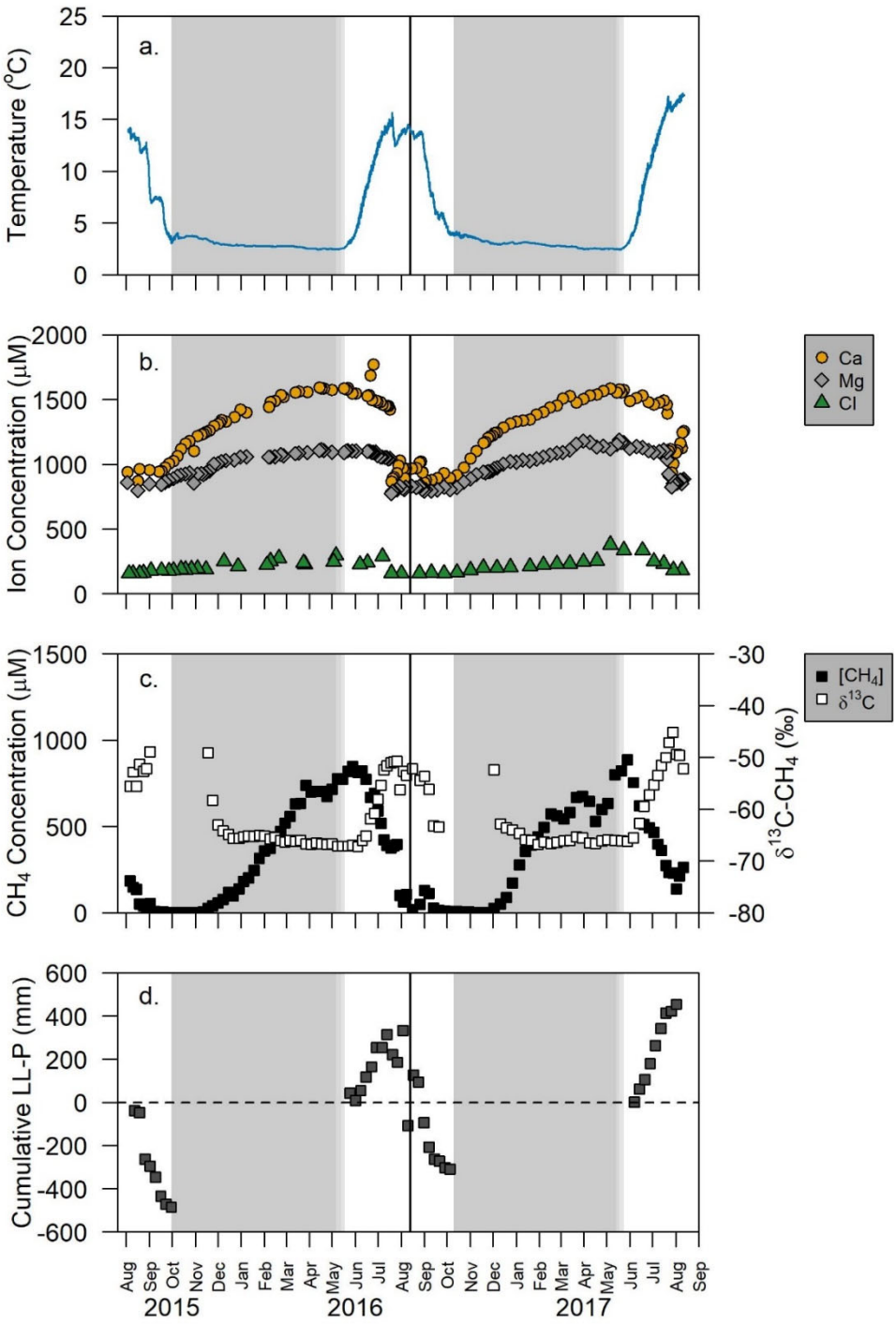

Figure 3-5. Lake 520 time-series of bottom-water characteristics and lake chemistry changes from August 2015 to August 2017 measured ~25 cm above the lake bed. a) bottom water temperature and b) lake chemistry – Ca^{2+} (gray circles), Mg^{2+} (blue diamonds), and Cl^{-} (yellow triangles) ion concentrations, c) dissolved CH_4 concentrations (black squares) and $\delta^{13}C$-CH_4 (white squares), and d) cumulative change in lake level minus precipitation. Gray bars indicate ice-cover. Vertical black lines indicate the switch from the first to second deployment.

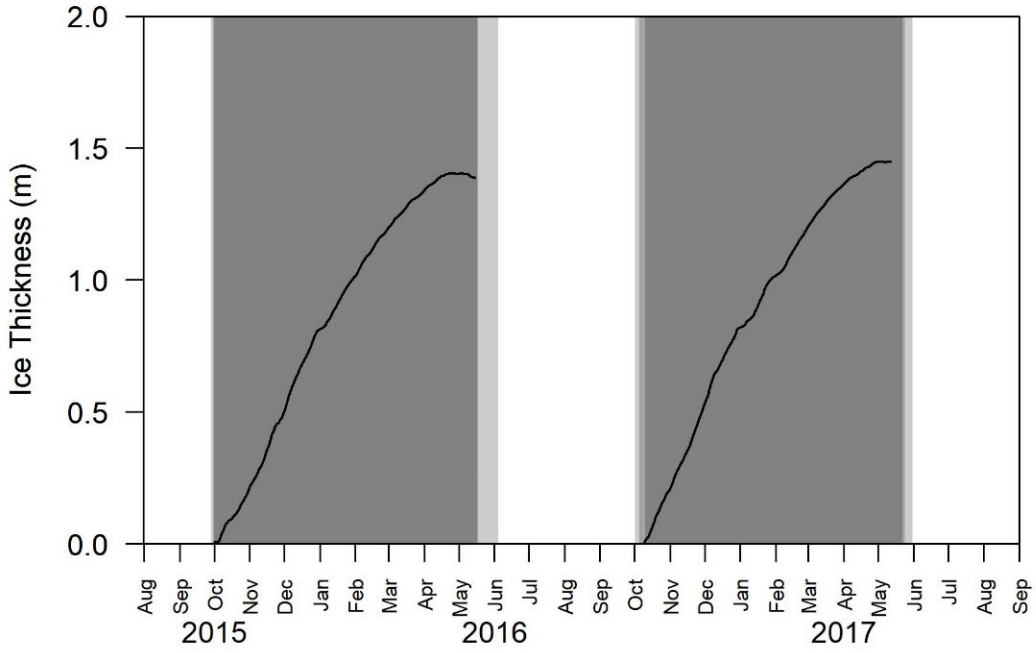

Figure 3-6. Ice thickness for lakes near Inuvik, NT, Canada was calculated using equation 3.1 based on air temperatures at Inuvik. Gray bars indicating ice-extent on Lakes 56, 520, and 280.

where it precipitously decreased to pre-ice values, which occurred simultaneously with a mid-summer temperature minimum (Figure 3-4a). Ion concentrations were significantly higher during ice-cover than during open-water for all ions ($p < 0.001$) with under-ice concentration factors of $Ca^{2+} = 2$, $Mg^{2+} = 2$, $Cl^{-} = 3$. Both Mg^{2+} and Cl^{-} had slow decreases in ion concentrations during open water, while the decrease for Ca^{2+} was more rapid in mid-July (200 µM drop from 11 to 15 July 2017).

3.4.3. Inorganic Ion Concentrations

Ion concentrations showed significant increases during ice-cover (all ions in Lakes 56 and 520 $p<0.01$, Appendix 2 Table S2-3; Figures 3-3b, 3-5b). There was not a significant difference in the concentrations of ions between Lake 56 and 520 (Student's t-tests, $Ca^{2+} << 0.001$, $Cl^{-} = 0.02$, $Mg^{2+} << 0.001$). Summer trends in ion concentration were different between the two lakes (Figures 3-3b, 3-5b). In Lake 56, immediately

following ice-melt and the Mackenzie River spring freshet, ion concentrations decreased to a minimum. This was followed by a ~30% concentration increase for most ions until ice-formation. Lakes 280 and 520 exhibited a different trend with the open-water decrease in dissolved ion concentrations delayed compared to Lake 56. Ca^{2+} and Mg^{2+} concentrations had a slight increase after the water column mixed in Lake 520 in mid-July, but Cl^- showed no change, even as lake levels declined in late summer (Table 3-2).

Table 3-2. Minimum open-water ion concentrations in 2016 and maximum ion concentrations prior to ice-formation in fall 2016. Ion concentrations fluctuated during open water for those with no minimum concentration. Data are presented graphically in Figures 3-3b and 3-5b.

Lake	Date	Ca^{2+} ($\mu mol\ kg^{-1}$)	Mg^{2+} ($\mu mol\ kg^{-1}$)	Cl^- ($\mu mol\ kg^{-1}$)
56	8/8/2016	313	491	No minimum
	10/1/2016	432	606	No maximum
520	7/19/2016	866	776	160
	10/5/2016	893	806	160 *

* Observed on 27 September 2016

There were strong correlations during the ice-cover period between ion concentrations and ice depth (R^2 >0.9; Figure 3-7). Under-ice concentration factors of ions were greater for Lake 56 (Ca^{2+} = 4 and 4, Cl^- = 2 and 5, Mg^{2+} = 2 and 2 for the winters of 2015-2016 and 2016-2017, respectively), than Lake 520 (Ca^{2+} = 2 and 2, Cl^- = 2 and 2, Mg^{2+} = 1 and 2 for the winters of 2015 2016 and 2016-2017, respectively). While ion concentrations increased in both lakes during ice-cover, the increase was greater in Lake 56. Overall, in these two lakes there was a greater influence on ion concentrations from salt-exclusion during ice formation than open-water evaporative concentration.

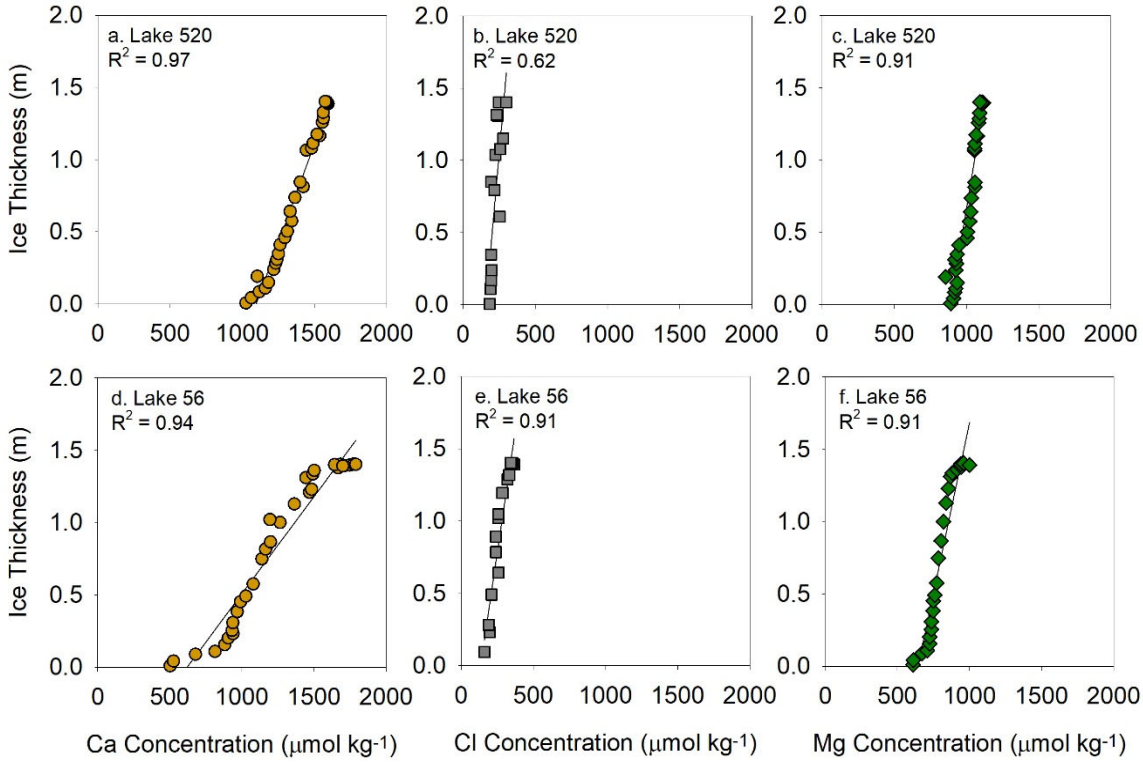

Figure 3-7. Ion concentrations compared to ice-thickness for Lakes 520 and 56 during ice-cover in the winter of 2015-2016. Lake 520 ions a) Ca^{2+}, b) Cl^-, and c) Mg^{2+} and Lake 56 ions d) Ca^{2+}, e) Cl^-, and f) Mg^{2+}.

3.4.4. Dissolved CH_4 Characteristics

Continuous dissolved CH_4 concentration data show similar trends over times. For example, in all three lakes, dissolved CH_4 concentrations increased during ice-covered intervals and decreased following ice-melt (Figures 3-3c, 3-4c, 3-5c). The rate and magnitude of these changes were variable between the lakes. No lake reached dissolved CH_4 saturation of 2300 µM CH_4 at 2ºC, 1 atm during ice-cover (Yamamoto et al., 1976), which is in agreement with the below-saturation August pore-water CH_4 concentrations (Appendix 3 Table S3-4). In Lake 56, under-ice dissolved CH_4 concentrations reached the highest values of 1300 µM, over 400 times higher than during open-water, and during ice-melt immediately decreased at a rate of 50 µM d^{-1}. Bottom water dissolved CH_4

concentrations were lowest in Lake 56 during late summer (mean = 0.7 ± 1.1 μM CH_4 in August to September). In Lake 280, dissolved CH_4 concentrations reached 900 μM, increasing by over 100 times from open-water, and decreased at ~20 μM d^{-1} during ice-melt. In Lake 520, dissolved CH_4 concentrations also reached ~900 μM, increasing by over 100 times from open-water, but CH_4 decreased more slowly following ice-melt than the other lakes and remained slightly elevated (19 to 591 μM CH_4) during the summer (July and August) both years. During open-water dissolved CH_4 concentrations in all three lakes were low (240 ± 330 μM CH_4) but exceeded than equilibrium with the atmosphere (3-4 nM at air temperatures of 7-15ºC; Yamamoto et al., 1976).

As with dissolved CH_4 concentrations, $\delta^{13}C$-CH_4 time-series data were collected to discern the production pathway of CH_4. $\delta^{13}C$-CH_4 data displayed similar patterns among the study lakes. Following ice-over, $\delta^{13}C$-CH_4 values decreased to -60 to -70‰ in all three lakes (Figure 3-3c, 3-4c, 3-5c). Once under-ice $\delta^{13}C$-CH_4 values reached ~-60‰ in Lake 56 and ~-66‰ in Lake 520, the $\delta^{13}C$-CH_4 values remained constant until ice-melt. Lake 56 exhibited a slight decrease in $\delta^{13}C$-CH_4 values immediately following ice-melt before a rapid increase to -30‰ (Figure 3-3c). $\delta^{13}C$-CH_4 values in Lake 280 were different than the other two lakes during ice-cover with a rapid depletion in ^{13}C following ice-over to ~-70‰, and then in mid-winter the CH_4 began to be enriched in ^{13}C (Figure 3-4c). Methane was relatively enriched in ^{13}C during open water periods, although most CH_4 concentrations were too low to undertake $\delta^{13}C$-CH_4 analysis.

Radiocarbon dating indicated surface water dissolved CH_4 was near-modern aged for Lakes 280 and 520. Dissolved CH_4 in Lake 56 was oldest, though in 2017 the large variability between samples resulted in error that encompassed a modern-age (Table 3-3).

Table 3-3. Dissolved CH_4 radiocarbon and stable carbon isotope ratios for large volume samples (10 L) taken from surface water in Lakes 56, 280, and 520 in 2016 and 2017.

Lake	Sample Date	Replicate vials (n)	Fm (mean ± s.d.)*	Age (YBP, mean ± s.d.)*	$\delta^{13}C$ (‰) (mean ± s.d.)**
56	15 August 2016	1	0.9813 ± 0.0034	150 ± 30	-40.4 ± 0.1
	10 August 2017	2	0.986 ± 0.045	120 ± 360	-49.9 ± 0.5
280	12 August 2016	1	0.996 ± 0.015	30 ± 130	-24.3 ± 0.1
	9 August 2017	1	1.002 ± 0.020	Modern ± 50	NA
520	13 August 2016	4	1.0081 ± 0.0035	Modern ± 30	-47.5 ± 1.2
	12 August 2017	2	0.9991 ± 0.0034	6 ± 30	-41.9 ± 1.4

*Fm or fraction modern and age in years before present (YBP) were process blank carbon corrected (1.6 μmol C, Fm = 0.7885). s.d. is the error propagated from the process blank mass balance or the standard deviation between replicate vials, whichever was larger.
**$\delta^{13}C$ were given include s.d., which is the standard deviation between replicate vials or instrument analytical error, whichever was larger

3.4.5. Cumulative Change in Lake Level Minus Precipitation

Precipitation totals during the open-water period of the three study years (2015: 230 mm, 2016: 145 mm, 2017: 162 mm; Table 3-4) were close to or higher than the 1981-2010 average of 147 mm (https://climate.weather.gc.ca/climate_normals/, CLIMATE ID 2202570). Patterns of cumulative lake level minus precipitation (LL_{-P}) were replicated among the three open water periods for each of the study lakes (Figure 3-3d, 3-4d, 3-5d). While constant LL_{-P} decline was seen in Lake 56 during the 2016 open-water period, Lakes 280 and 520 had increasing LL_{-P} in early summer followed by a large decrease in LL_{-P} in late summer. A rapid decrease in LL_{-P} was seen in Lake 280 between 13 July 2016 and 20 July 2016, and in September 2016 cumulative LL_{-P} became negative (-186 mm; Figure 3-4d). In Lake 520, a rapid decline in LL_{-P} was seen on 10 August 2016 and resulted in a negative LL_{-P} at the end of open-water (-308 mm; Figure 3-5d). By the end of the open-water period, all three lakes exhibited an overall decrease in cumulative LL_{-P}.

Table 3-4. Comparison of annual precipitation with total open-water evaporation for lakes near Inuvik, NT, Canada including the measured lake level and calculations using the Thornthwaite equation, mass transfer equation, energy balance, water balance, and NASA's MODIS satellite for the area encompassing Inuvik.

Total Annual Precipitation and Evaporation					
Method		Lake	Year	Annual (mm)	Source
Precipitation	Measured[o]	Not specific	2015	323	1
			2016	203	1
			2017	278	1
		Lake	Year	June to September (mm)	Source
Evaporation	Lake Level*	Lake 56	2016	409	2
	Thornthwaite[•]	Not specific	2015	468	2
		Not specific	2016	487	2
		Not specific	2017	509	2
	Mass Transfer[•]	Lake 520	2016	285	2
		Lake 56	2016	238	2
		Lake 280	2016	254	2
	MODIS[•]	Not specific		227	3
	Energy Balance[•]	NRC[a]	1984	247	4
		NRC	1985	243	4
		NRC	1986	200	4
	Water Balance Method[•]	Dishwater lake[a]	1982	349	4
		Dishwater lake	1983	322	4
		Dishwater lake	1984	387	4
		Dishwater lake	1985	310	4

[o] denotes measured precipitation in Inuvik, Northwest Territories, Canada (CLIMATE Station ID 2202578)

* denotes the water balance of lake level minus precipitation (LL-P) for Lake 56 and the measured decrease which is assumed to be primarily due to evaporation, [•] denotes a method where evaporation was calculated using equations and assumptions in the cited literature

[a]NRC Lake is spatially in-between Lake 520 and Lakes 56 and 280 while Dishwater Lake is in the southern Mackenzie Delta

1 = Environment and Climate Change Canada, 2 = This study, 3= NASA MODIS (University of Montana), 4 = Marsh & Bigras (1988)

3.4.6. Comparison of Evaporation Estimates

Evaporation estimates for all methods were generally higher than both summer and annual precipitation for the Inuvik region between 2015 and 2017 (Table 3-4;

Appendix Figure S2-3). MODIS (227 mm) and mass transfer (238 to 285 mm) calculated evaporation were closest to the precipitation in the region. Annual evaporation rate estimates were highest with the Thornthwaite method (468 to 509 mm). Measured evaporation is represented by the generally continuous LL_{-P} decrease in Lake 56 (Figure 3-3d). LL_{-P} decreased to a maximum of 409 mm in September and a final cumulative decrease of 380 mm at the end of September. Despite differences between the evaporation estimate methods, the measured evaporation in Lake 56 is within the range of the calculated evaporation estimates for this lake and region for 2016 (Table 3-4).

3.4.7. Evaluation of Groundwater Inputs

Groundwater inputs increased lake level in Lakes 280 and 520 (Figure 3-8). In 2016, groundwater input peaked in late July and early August at +668 mm and +517 mm in Lakes 280 and 520, respectively. Similar groundwater inputs were seen during the early open-water period in 2017 in both lakes. Cumulative groundwater contributions decreased after their initial peak and were positive (222 mm, 92 mm, respectively)

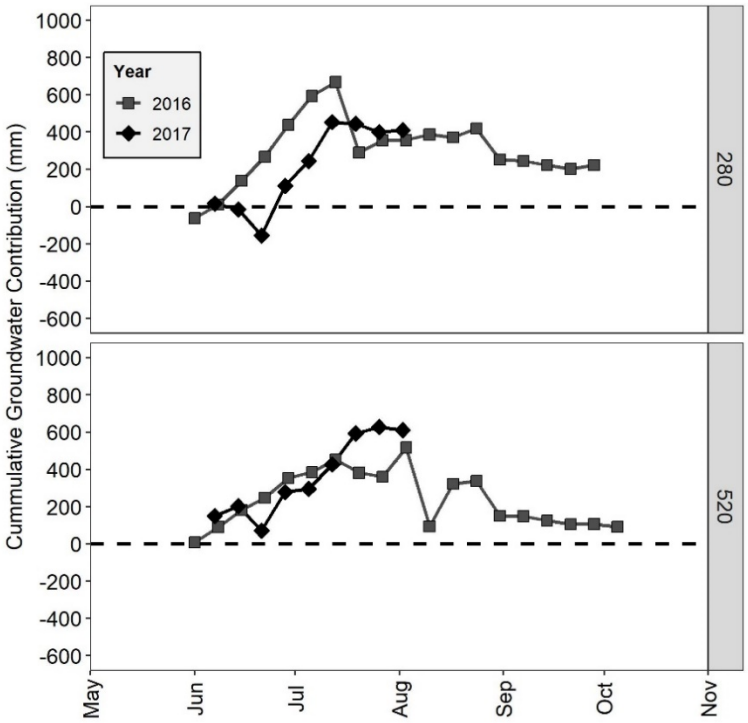

Figure 3-8. Cumulative groundwater contribution for Lakes 280 and 520. Lakes 280 (top) and 520 (bottom) cumulative groundwater contribution (mm) for the two time-series which start in the spring: 2016 (gray, squares) and 2017 (black, diamonds). Negative values indicate seepage out of the lake. Positive values indicate cumulative groundwater seepage into the lakes. Dates start following the Mackenzie River flood in 2016 and 2017.

at the end of the open-water period in 2016 (Figure 3-8). In order to evaluate potential groundwater sources, a comparison was made between the groundwater contribution for Lakes 280 and 520 and the Mackenzie River height after there was no longer a surface connection from the spring flood (Figure 3-9). There were weak negative correlations between cumulative groundwater contribution and Mackenzie River height (Lake 280: R^2 = 0.05, 0.45 and Lake 520: R^2 = <0.01, 0.15 for 2016 and 2017, respectively), suggesting the Mackenzie River flood was not a source of groundwater into the lakes.

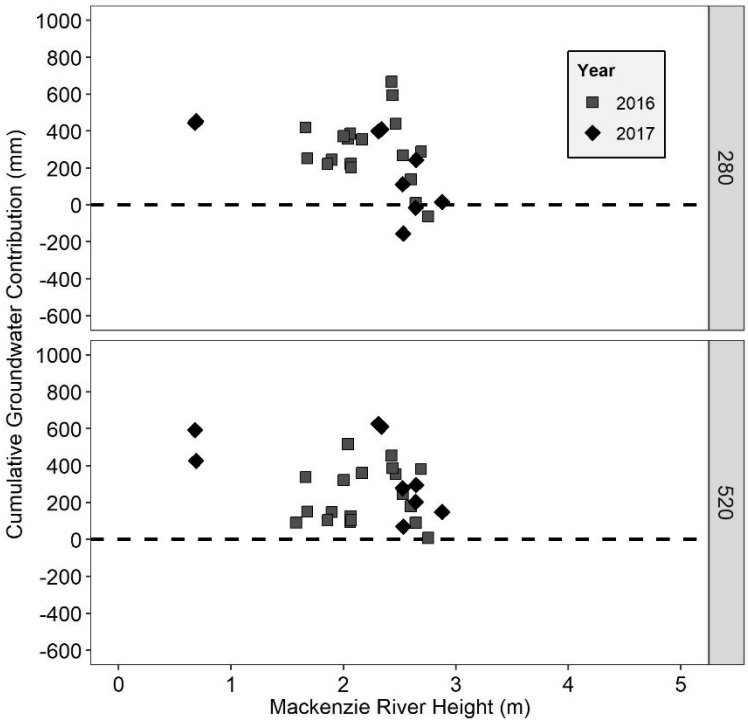

Figure 3-9. Groundwater contribution (mm) compared with the height of the Mackenzie River on the East Channel at Inuvik, NT, Canada in Lakes 280 (top) and 520 (bottom) as calculated in section 3.3.5.

3.5. Discussion

Continuous lake level data and ice-thickness were used to identify how hydrologic processes affected solute chemistry and dissolved CH_4 concentrations during open-water and ice-covered conditions in three lakes. Lake closure was hypothesized to

have the greatest influence on dissolved CH_4 concentrations, and all lakes would be evaporative basins. However, in this study, lake depth was a more important factor than lake closure, and surprisingly, only one lake was an evaporative basin while the other two were influenced by groundwater. These results have implications of increased open-water CH_4 concentrations and greater groundwater movement as lakes become deeper in a warmer and wetter Mackenzie Delta (Zhang et al., 2000). I elaborate on these points, specifically how lake depth has a strong influence on lake chemistry, biogeochemical reactions, and hydrologic behavior in individual lakes in the Mackenzie Delta.

3.5.1. Inorganic Ion and Dissolved CH_4 Concentrations Increase Due to Ice-Cover

Under ice-cover both conductivity (Figure 3-4b) and ion concentrations (Figure 3-3b, 3-4b, 3-5b) increased. Similar responses have been shown in other seasonally ice-covered lakes (Burn et al., 1998; Welch & Bergman, 1985). Ice-thickness was correlated with ion concentration increases (Figure 3-7) and conductivity increases (Lake 280: $R^2 = 0.96$) confirming the influence of salt-exclusion by ice formation on salt and ion exclusion (Lesack et al., 1990; Pieters & Lawrence, 2009). Lake depth influenced the extent to which ice exclusion affected ion concentrations by proportionally reducing liquid water volume. Since most of the water column froze in Lake 56, concentration factors for ions were greater than in Lake 520, as can be seen by the shallower slope of change in ion concentrations relative to ice-thickness (Figures 3-7d-f). Concentration factors for ions in Lake 56 are slightly less than nearby, albeit deeper, NRC Lake where Mg^{2+}, Ca^{2+}, and Cl^- concentrations factors were 3, 5, 4, respectively during ice-cover in the winter of 1986-1987 (Lesack et al., 1990). The process of ice exclusion appears to significantly affect ion concentrations in Mackenzie Delta lakes.

Timing of ice-cover was also strongly linked to dissolved CH_4 concentrations (Figures 3-3c, 3-4c, 3-5c). Dissolved CH_4 increases were observed in all three lakes once ice formed and gas exchange with the atmosphere was suppressed, which allowed CH_4 to build-up without being consumed by methanotrophs (Martinez-Cruz et al., 2015; McIntosh Marcek et al., *Submitted*). $\delta^{13}C$-CH_4 values for all three lakes were consistent with a microbial CH_4 source of primarily methyl-type fermentation (Whiticar, 1999). While most of the CH_4 increase is due to diffusion of microbial CH_4 produced in the sediments and/or water column methanogenesis in Lake 520 (McIntosh Marcek et al, *Submitted*), ice-thickness could have contributed to some of this increase in the other lakes. For instance, CH_4 concentrations were highest in Lake 56, which also had the largest ion concentration factors because ice entrained a majority of the water column. In the two deeper lakes, Lakes 280 and 520, peak CH_4 concentrations were similar, indicating that the smaller ratio of ice-thickness relative to remaining liquid water column depth does not influence CH_4 concentrations in deeper lakes. Even as dissolved CH_4 concentrations increased in Lake 280 in late winter, $\delta^{13}C$-CH_4 values increased slightly suggesting under-ice anaerobic methanotrophy, as has been reported in Arctic Alaskan lake sediments (Martinez-Cruz et al., 2018). All lakes had peak CH_4 concentrations just before or right at ice-melt. Ice-cover led to increased dissolved CH_4 concentrations and when that barrier was removed, gas exchange caused dissolved CH_4 concentrations to decrease.

3.5.2. Lake Depth Controls Water Column Mixing in Summer

The lake-dependent dissolved CH_4 and inorganic ion dynamics were captured at a ~7 day resolution during ice-out and confirmed a rapid release of CH_4 from the shallow

lake (Lake 56: 51 μM CH_4 day^{-1} in 2017), but also showed that water depth plays a key role in how quickly these lakes mix. The data collected at shallow Lake 56 suggest it is well mixed while the others are not. Lake 56 exhibited the most rapid open-water decreases in ion concentration and dissolved CH_4 concentration, i.e. within days of when ice melted (Figure 3-3). Given the shallow bathymetry, Lake 56 has a lower wind speed threshold to fully mix the water column (Lesack et al., 1990). The decrease in the $\delta^{13}C$-CH_4 value immediately after ice-melt in Lake 56 indicates CH_4 in the water column is mixed very quickly with ^{13}C-depleted CH_4 from sediment pore-water after ice is removed (~-65‰; Appendix 3 Table S3-4). Ice-melt acted as a pressure release for sediment pore-water (Casper et al., 2000) and the rapid water column mixing allowed that CH_4 to evade quickly into the atmosphere. The drop in $\delta^{13}C$-CH_4 indicates CH_4 from sediment pore-water was released without much oxidation in the water column (Whiticar, 1999). Water column mixing then facilitated CH_4 oxidation by mixing dissolved oxygen to the bottom waters (Deshpande et al., 2015). Substantial CH_4 oxidation during early open-water is indicated by $\delta^{13}C$-CH_4 values reaching a maxima of -30‰ while dissolved CH_4 concentrations decreased by 51 μM CH_4 day^{-1} in 2017 (Figure 3-3c). Rapid and regular water column mixing is indicated by bottom water temperatures that are highly influenced by diel and daily temperature changes (Figure 3-3a). The jagged record of temperature in Lake 56 and the increase to ~20ºC by late June (Figure 3-3a), suggests the entire water column is regularly mixed and highly influenced by the atmosphere.

Ion concentration, conductivity, and dissolved CH_4 concentration decreases were delayed until later in the open-water period in the deeper Lakes 280 and 520 (Figure 3-4 and 3-5), which was delayed until mid-July (McIntosh Marcek et al, *Submitted*). Bottom

water temperatures were slower to peak in Lakes 280 (~20ºC; Figure 3-4a) and 520 (~15ºC; Figure 3-5a) by mid-July. Slower bottom water temperature increases reflect diffusion of surface water heat to the bottom water rather than wind driven mixing (Oswald & Rouse, 2004). Until the whole water column mixed in mid-July, there was only shallow, surficial water column mixing in Lakes 280 and 520. Shallow mixing left bottom water enriched in CH_4 and ions and disengaged from the diluted surface water, which included ice-melt and Mackenzie River flood water (Lesack & Marsh, 2010; Lesack et al., 1990). Bottom water dissolved CH_4 concentrations slowly decreased during early open water in Lakes 280 and 520 and were mirrored by $\delta^{13}C\text{-}CH_4$ values (Figures 3-4c and 3-5c, respectively), suggesting the decrease in concentration was from CH_4 oxidation (Whiticar, 1999). Macrophytes growing on the lake beds could provide a source of dissolved oxygen to support methanotrophy while simultaneously slowing water column mixing in these lakes (McIntosh Marcek et al., *Submitted*). Entire water column mixing, which took longer in the deeper lakes, reset the lake chemistry to pre-ice-cover concentrations from the prior fall.

3.5.3. Open-Water Lake Balances Indicate Different Hydrologic Processes

Our study indicated that $LL_{\text{-}P}$ at the end of the summer was lower than at the beginning of the summer, but the trajectory to lake level decline varied among the lakes (Figure 3-3d, 3-4d, and 3-5d). I initially hypothesized that the differences would be due to closure class (Marsh & Hey, 1989). For instance, both Lake 56 and Lake 520 are high closure lakes and were expected to have simple water balances during open-water as compared to lakes with a regular connection to the Mackenzie River where riverine inflows impact water balances (Marsh & Bigras, 1988; Marsh & Lesack, 1996). Lake 56

behaved as an evaporative basin because LL_{-P} continued to decrease throughout the summer (Figure 3-3), while the water balance here suggests Lakes 280 and 520 are both influenced by groundwater (Figure 3-8).

Ion data in this study show the different hydrologic processes affecting the lakes, with Lake 56 experiencing evaporative concentration of ions during open-water and little influence of evaporation on ions in Lake 520. Sufficient evaporation in Lake 56 is supported by ion concentration changes; following minimum levels, ion concentrations increased as lake level declined (Figure 3-3b). Evaporative concentration of ions has been observed in other lakes with no connection to the Mackenzie River during summer months (Sokal et al., 2010). By contrast, in Lake 520 there was a groundwater source to the lake during the early open-water period, and a similar increase in ion concentrations was not observed (Figure 3-5b). Groundwater inflow could dilute lake solutes, which would reduce evaporative concentration effects (Lesack et al., 1998; Sokal et al., 2010). Although, there was a slight increase in Ca^{2+} and Mg^{2+} concentrations after mixing in mid-July, it probably reflects a decrease in cumulative groundwater seepage (Table 3-2). Lake chemistry indicated hydrologic connection differences between Lakes 56 and 520 during open-water in 2016.

3.5.4. Comparison of Evaporation Estimates

Evaporation rate estimates are typically made by using climatological data and assumptions of evaporation from those data. Since evaporation estimates for Lake 56 are based on measuring lake level, results were compared to rates estimated from other studies in the Mackenzie Delta in order to verify our approach (Table 3-4). There were lower evaporation rates in the nearby NRC Lake (~200 mm yr^{-1}) and Dishwater Lake

(~350 mm yr^{-1}) in the late 1980s than measured in Lake 56 (~400 mm yr^{-1}) in this study (Table 3-4; Marsh & Bigras, 1988). The differences in evaporation rates from those studies could also be due to different lakes being examined, different methods used to estimate evaporation, or due to heterogeneous effects of temperature warming on lake-groundwater interactions (Lamontagne-Hallé et al., 2018; Lecher, 2017). The higher evaporation rates now could be due to warmer air temperatures. Between 1958 and 2012, there was a 2-3ºC increase in air temperature in the Mackenzie Delta between Fort Smith and Inuvik (Government of Northwest Territories Environment and Natural Resources, 2015). The consequences of the increased temperature and increased precipitation since the 1950s in northern Canada could thus be an increase in evaporation (Zhang et al., 2000) and an increase in hydrologic connectivity (St. Jacques & Sauchyn, 2009). Therefore, care should be taken when comparing evaporation rates and efforts should be made in future work to determine the reason for these differences.

3.5.5. Groundwater Source to Lakes

My finding that groundwater influences Mackenzie Delta lakes was surprising since these lakes have been considered evaporative basins (Bigras 1990; Marsh & Bigras, 1988). Based upon the surrounding permafrost, it was expected that the hydraulic connectivity would be low (Nguyen et al., 2009). However, if a lake is deep enough and has an even deeper thaw bulb then that could explain the groundwater seepage (Figure 3-10). The deepest part of Lake 56 extends just slightly below the active layer depth of 1.3 m (Smith et al., 2009), which could be deeper or shallower into the soil and permafrost depending on density of terrestrial plant cover surrounding the lake (Nguyen et al., 2009). Mean depth in Lakes 280 and 520 extend below the active layer, with the

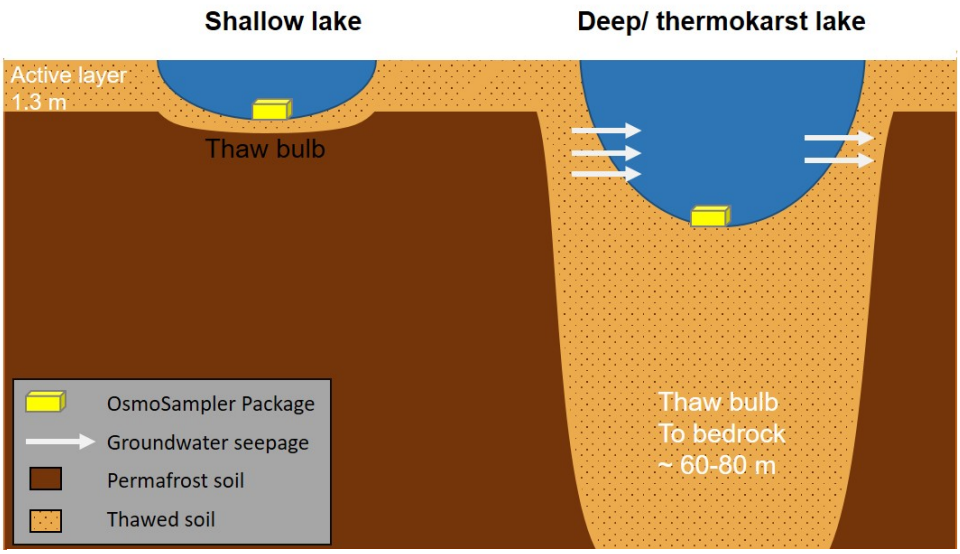

Figure 3-10. Schematic depicting difference in thaw bulb depth between a shallow lake and a deeper, thermokarst lake, and the impact on groundwater movement.

5.5 m deep location in Lake 520 extending far below (Table 3-1; McIntosh Marcek et al., *Submitted*). The thaw bulb is also expanding laterally into surrounding permafrost as both Lakes 280 and 520 exhibit active thermokarst processes (Cunada, 2016; Cunada, et al., 2018; Tank et al., 2009). Therefore, it is likely that Lakes 280 and 520 have taliks that extend through the permafrost to the bedrock~80 m below (Johnston & Brown, 1961; Johnston & Brown, 1964) and lateral expansion that allows groundwater movement via vertical and horizontal transportation (Figure 3-10).

In addition to taliks, subsurface flow through more permeable surface soil in the active layer could laterally transport water into the lake (Connon et al., 2014; Jepsen et al., 2013). Lake 280 has a marsh/ bog margin that could allow for quicker soil warming, and active layer thawing, than below the forest surrounding the rest of the lake (Marsh, 1990). The western side of Lake 280 is mostly vegetated with marsh grasses, an indicator of regular moisture and thawed, porous soil (Nguyen et al., 2009). Similarly, Lake 520 has a nearby filled channel that could connect groundwater from channels to the

northwest to the lake (Figure 3-1d; McIntosh Marcek et al., *Submitted*). Highly permeable soils, i.e. in the marsh and filled channel, allow water to be transported more effectively into and out of lakes surrounded by permafrost (Connon et al., 2014; Jepsen et al., 2013). The two formations near Lakes 280 and 520 could increase hydrologic connectivity of the thawed active layer soil, whereas Lake 56 is completely surrounded by white and black spruce forest and has no indicator of higher permeability soil.

3.5.6. Does Groundwater Carry CH_4 to Lakes 280 and 520?

Groundwater enters Lakes 280 and 520 at the same time that winter-derived CH_4 persists in the bottom water (Figures 3-4, 3-5, 3-8). Because groundwater transports dissolved CH_4 through the active layer in other Arctic regions, e.g. Toolik Lake (Lecher et al., 2017; Paytan et al., 2015) and to the Arctic and North Pacific Oceans (Lecher et al., 2016), it is plausible that the elevated CH_4 in Lakes 280 and 520 could come from this source. There is not a significant difference in the $\delta^{13}C$-CH_4 values for CH_4 produced in lake sediments compared to the surrounding groundwater, because both CH_4 pools are produced via methyl fermentation (Lecher et al., 2017). There are specific potential approaches, such as δD_{CH4} measurements, which can identify CH_4 as coming from a groundwater source (Lecher et al., 2017; Whiticar, 1999). δD_{CH4} measurements were not undertaken as a part of this project, but $\Delta^{14}C$-CH_4 data were used as a proxy to identify if groundwater transported dissolved CH_4 into Lakes 280 and 520.

It was expected that groundwater transported CH_4 would have $\Delta^{14}C$-CH_4 values indicative of aged permafrost carbon from active layer thaw. If groundwater was transporting significant amounts of labile carbon from thawing permafrost (Mueller et al., 2015; Vonk et al., 2013; Walvoord & Striegl, 2007), then it would be incorporated into

the microbial degradation byproduct of CH_4 (Walter Anthony et al., 2016). Thawed permafrost carbon is anticipated to be an accessible and labile source of carbon because it is not substantially decomposed while frozen (Schuur et al., 2009; Walter Anthony et al., 2018; Walter et al., 2008). In Arctic Alaskan lakes where permafrost carbon is available for CH_4 production, up to 25% of the diffusive CH_4 is from permafrost derived carbon (Elder et al., 2018) and the ebullitive flux has a ^{14}C age up to 40,000 YBP (Walter et al., 2008).

Radiocarbon analysis on CH_4 from Lakes 280 and 520 showed surface water dissolved CH_4 was modern aged suggesting recently produced organic matter was the primary carbon precursor, not aged permafrost carbon (Table 3-3). Macrophyte biomass and trees falling into the lakes contribute the modern carbon used by methanogens to produce near-modern aged CH_4 (McIntosh Marcek et al., *Submitted*; Squires & Lesack, 2003). Although there is evidence of groundwater contributions to Lakes 280 and 520, there is no evidence that groundwater contained significant volumes of dissolved CH_4 that was formed from permafrost carbon assimilated by microbes.

While CH_4 in Lakes 280 and 520 was near-modern, Lake 56 had slightly aged (~150 YBP) CH_4 in 2016 and within error of a modern-age in 2017 (Table 3-3). Lake 56 has the largest surface area of the study lakes so a greater amount of aged fluvial sediment (~5000 YBP; McClelland et al., 2016) is deposited on the lake bed during the spring flood (Marsh et al., 1999). Because there was no groundwater connection, the slightly aged CH_4 in Lake 56 was most likely due to slightly aged sediment and organic matter contributions from pore-water (Elder et al., 2018).

3.6. Further Analysis for Manuscript Publication

This study shows that lake depth has a significant impact on the amount of CH_4 that is removed from the systems via mixing and CH_4 oxidation. This conclusion is supported by continuous data on dissolved CH_4 concentrations and $\delta^{13}C$-CH_4 data. Future work will include calculating a dissolved CH_4 mass balance, as was done in Chapter 2, for both Lakes 56 and 280. By expanding this mass balance, I will quantify the rates and extent of methanotrophy in these lakes during the ice-melt and open-water periods. These additional analyses will help provide quantitative results to the biogeochemical reactions and physical processes that influence CH_4 concentrations.

3.7. Conclusion

Lake closure class – e.g. low closure, high closure – was anticipated to have the largest impact on open-water hydrology and would directly relate to the changes in lake chemistry and CH_4 concentrations that were seen in the lower water column of the study lakes. This study shows that rather than closure class, lake depth is the major influence on water column mixing and the hydrologic connection of the lakes. Lake 56 is a shallow lake and so it rapidly mixes and is primarily influenced by evaporation. By contrast, Lakes 280 and 520 are deeper and it is likely that their thaw bulbs extend the full depth of the permafrost allowing groundwater seepage into and out of the lake depending on the soil conditions surrounding the lake during the warm-season. Groundwater seepage into the lakes is likely not transporting CH_4 nor was thawed permafrost carbon used by methanogens since CH_4 in Lakes 280 and 520 has a near-modern age. This study

highlights the importance of understanding hydrologic connections in Arctic lakes and their influence on lake chemistry.

3.8. Acknowledgements

The above work would not have been possible without the help of numerous individuals in the field including Mitchell Bergstresser, Trevor Fournier, Kim Geeves, Nilou Rajaei, and the staff at the Aurora Research Institute and in the laboratory including Aimee Beardmore, Jessica Loveless, Mary Oster, and Maureen Strauss. Radiocarbon sample preparation was aided by Jeff Chanton and his lab, Ann McNichol, and the members of the NOSAMS Radiocarbon facility. This chapter benefitted from collaborations with Laura Lapham, C. Geoff Wheat, Lance Lesack, Beth Orcutt, Scott Dallimore, and Karen Prestegaard. Funding for this project came from an American Geophysical Union Horton Research Grant (HAMM), a Geological Society of America Research Grant (HAMM), a Presidential Fellowship from the University of Maryland Center for Environmental Science (HAMM), an Ann G. Wylie Dissertation Fellowship from the University of Maryland (HAMM), and National Science Foundation Grant PLR-1416961 (LLL). This research was conducted under research permits: NWT Scientific Research License Numbers 15724, 15851, and 16066. The data supporting the conclusions in this paper are available at the National Science Foundation Arctic Data Center (Orcutt, 2017a).

Chapter 4

Radiocarbon and stable carbon isotopes used to discern source, age and migration pathways of methane from lakes in the Mackenzie River Delta, Northwest Territories, Canada

Abstract

Ancient and modern sources of methane were assessed in lake waters using a dual isotope approach where radiocarbon and stable carbon isotope measurements were made on different pools of methane (dissolved and gas bubbles). This approach provides a whole-lake perspective of methane transport that has rarely been done in Arctic lakes. Samples were collected in the Mackenzie River Delta (Northwest Territories, Canada); an ideal location to contrast the effects of geology and permafrost cover. The Mackenzie River Delta is a productive, lake-rich region with discontinuous permafrost and the outer delta overlies natural gas and oil reserves. Radiocarbon ($\Delta^{14}C\text{-}CH_4$) and stable carbon isotope ($\delta^{13}C\text{-}CH_4$) values are presented for dissolved methane from surface water (8 lakes) and methane captured in bubbles (3 lakes). Data support the hypothesis that methane diffusing out of the lakes is near-modern in age from microbial decomposition of recent organic matter. Bubbles in the outer delta have significantly older methane formed by thermogenic processes (radiocarbon-dead). Within one lake, a two-year time-series shows dissolved methane concentrations are linked to dissolved oxygen presence, and during ice-cover CH_4 source composition shifts from a microbial diffusive

source of CH_4 to thermogenic bubble dissolution. Results from this study expand our knowledge of methane source and migration pathways within an important Arctic delta.

4.1. Introduction

Atmospheric methane (CH_4) concentrations have increased in the past few decades, but there has been uncertainty in the sources of that CH_4 (Howarth, 2019; Saunois et al., 2016; Saunois et al., 2019). Stable isotope plots of atmospheric $\delta^{13}C$-CH_4 suggest a greater contribution from microbial sources over the last decade (Nisbet et al., 2016). Northern freshwater systems may explain some of the recent increasing atmospheric trend (Schaefer et al., 2016) because of the high density of lakes at boreal and arctic latitudes and most of their CH_4 is of microbial origin. Currently lakes north of 50^{o}N release 16.5 Tg CH_4 yr^{-1} (Wik et al., 2016b) or 6% of the global natural CH_4 emissions that are expected to increase in the future (Bastviken et al., 2011; Heslop et al., 2019; Kirschke et al., 2013; Treat et al., 2015).

While most of the CH_4 in Arctic lakes is from *in situ* microbial decomposition of organic carbon in anoxic lakes, it can also come from evasion from deep sources produced by thermogenic or microbial processes (Etiope & Klusman, 2002; Saunois et al., 2016; Walter et al., 2008). Thermogenically produced CH_4 is found in areas of the Arctic that contain large reserves of oil and natural gas trapped below the cryosphere (Gautier et al., 2009) and/or frozen gas hydrate (Dallimore & Collett, 1995). Stable carbon isotope ratios ($\delta^{13}C$-CH_4) have been extensively used in Arctic lakes to discern CH_4 source (Hershey et al., 2014; Lecher et al., 2017; Matheus Carnevali et al., 2015; Neumann et al., 2016; Sriskantharajah et al., 2012). $\delta^{13}C$-CH_4 values can separate

thermogenic (-30 to -50‰) from microbial (-50 to -100‰) sources of CH_4, as shown in Figure 4-1, because of greater incorporation of ^{12}C into CH_4 during methanogenesis than during catagenesis (Conrad, 2005; Etiope & Klusman, 2002; Whiticar et al., 1986; Whiticar, 1999).

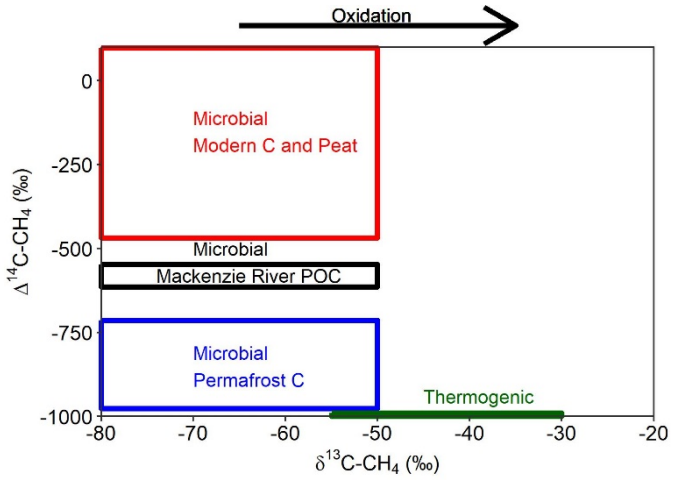

Figure 4-1. Expected $\Delta^{14}C$ (‰) and $\delta^{13}C$ (‰) of CH_4 collected from lakes within the Mackenzie Delta from different sources. The red box indicates microbially formed CH_4 with precursor carbon sources that are modern C, e.g. peat (Garnett et al., 2011; Turnbull et al., 2017; Whiticar, 1999). The black box indicates microbially formed CH_4 with Mackenzie River particulate organic carbon (POC) as the precursor carbon source (McClelland et al., 2016). The blue box indicates microbially formed CH_4 from a permafrost carbon source (Walter Anthony et al., 2012; Walter et al., 2008). The green line indicates thermogenically produced CH_4 formed via catagenesis (Etiope & Klusman, 2002; Whiticar, 1990). $\delta^{13}C$ shifts due to fractionation of CH_4 during oxidation are up to 30‰, as is indicated by the black arrow (Cadieux et al., 2016; Kankaala et al., 2007; Whiticar & Faber, 1986).

The limitation with $\delta^{13}C$ is that if the CH_4 pool has been reduced due to significant CH_4 oxidation there can be up to 30‰ fractionation between the ^{12}C and ^{13}C isotopes (Cadieux et al., 2016; Kankaala et al., 2007). The residual CH_4 will have a $\delta^{13}C$-CH_4 value similar to that of CH_4 produced thermogenically (Figure 4-1, Whiticar & Faber, 1986). Additionally, microbial degradation of peat or thawed permafrost soil produces CH_4 with similar $\delta^{13}C$-CH_4 values, which can make $\delta^{13}C$ values alone a difficult tool to distinguish precursor carbon sources (Figure 4-1).

However, by combining measurements of the radiocarbon content ($\Delta^{14}C$-CH_4) of CH_4 with those of the stable carbon isotope ratios, it should be possible to more effectively constrain CH_4 sources and precursor carbon sources (Figure 4-1). Methane formed from microbial degradation will have a ^{14}C age similar to its organic carbon source, such as recent organic matter (OM) (e.g. modern plants, peat; Martens et al., 1992; Nakagawa et al., 2002), old OM (e.g. thawed permafrost, 10,000-30,000 years old; Walter et al., 2008; Zimov et al., 1997), or intermediate aged OM (e.g. glacial soils, fluvial sediment for lakes with connections to Arctic rivers; Elder et al., 2018); all of which are younger than CH_4 formed from carbon thermally degraded in ancient sedimentary basins (Walter Anthony et al., 2012; Walter et al., 2008). For example, the oldest thermogenic CH_4 accumulations found within the Mackenzie Delta are from the Cretaceous period, as determined by the stratigraphic sequence (Collett & Dallimore, 1999). Paired ^{13}C and ^{14}C analyses have been used in systems like shallow alasses (temporary shallow lakes formed by permafrost subsidence), peat bogs and lakes (Elder et al., 2019; Garnett et al., 2011; Matveev et al., 2018; Martens et al., 1992; Nakagawa et al., 2002; Negandhi et al., 2013; Walter et al., 2008). The studies found bubbles in Arctic lake surface sediments contain CH_4 with a relatively modern ^{14}C age, presumably from a young carbon source while CH_4 contained in rapidly evading bubbles is produced in deep sediments from significantly older carbon sources, such as thawed permafrost carbon. To the best of my knowledge, there have been no published ^{14}C measurements made that confirm either the source or age of the CH_4 present in the western Canadian Arctic.

The Mackenzie Delta is located in the western Canadian Arctic within an interconnected system of lakes and channels. Lakes in the delta have been classified by

the extent of their connection to the Mackenzie River or channels based on the height of the ground, or sill, between the river and lake as: no closure, connected up to half the year; low closure, connected during the spring flood; or high closure, interannually connected (Marsh & Hey, 1989; Marsh & Hey, 1994). In addition, the delta's permafrost conditions within the outer delta dictate whether thermogenic CH_4 is released to the atmosphere through direct gas seeps or if it is kept trapped below the cryosphere (Collett & Dallimore, 1999). Underlying the outer delta, including Richard's Island near Tuktoyaktuk, an estimated 292 to 356 x 10^9 m^3 of recoverable natural gas was formed at low temperature from terrestrial organic carbon and is thermally immature (Collett & Dallimore, 1999; Dixon et al., 1994; Snowdon & Powell, 1982). Permafrost in the delta generally acts as a barrier for the release of thermogenic CH_4. West of the Middle Channel of the Mackenzie modern deltaic sediments (~50 m thick) overlie Pleistocene glaciomarine sediments and consist of relatively shallow permafrost (<100 m, Dallimore & Matthews, 1997; Johnston & Brown, 1964). East of the Middle Channel in the delta, there is a thin, discontinuous layer of Holocene deltaic sediment over thick Pleistocene glacial sediments creating thicker permafrost (>600 m, Hu et al., 2013). High rates of CH_4 escaping the landscape have been measured in the thinner western outer delta (>5 mg m^{-2} hr^{-1}) and this region has been previously explored for natural gas and oil reserves (Kohnert et al., 2017). Whereas in the southeastern delta with thicker permafrost, CH_4 evasion rates are significantly dampened and expected to be of a modern, microbial origin (Kohnert et al., 2017). Overall, the delta releases 38 Gg CH_4 yr^{-1} to the atmosphere from ebbulitive and diffusive CH_4 fluxes (Kohnert et al., 2017), but the sources of that CH_4 flux are not clarified.

Therefore, it is important to understand the source of CH_4 in both ebullitive and diffusive CH_4 fluxes to know which processes are contributing to the CH_4 being released to the atmosphere from these lakes. Surface water dissolved $\Delta^{14}C\text{-}CH_4$ indicated that the source of the carbon was from a potentially different production pathway or depth of production than ebullition (Elder et al., 2019; Elder et al., 2018). Previously, radiocarbon measurements on dissolved CH_4 were challenging because >12.5 μmol C was needed (Pearson et al., 1998) which meant large volumes of water would be necessary for $\Delta^{14}C\text{-}CH_4$ analyses. New methods and improved precision of ^{14}C measurements on small amounts of carbon (<2 μmol C) dictate more reasonable volumes of water, on the order of 10's of liters, can be collected for $\Delta^{14}C\text{-}CH_4$ analyses (Garnett et al., 2016; Pearson et al., 1998; Santos et al., 2007; Shah Walter et al., 2015). Our study took advantage of these recent advancements to generate the first $\Delta^{14}C\text{-}CH_4$ data, and corresponding $\delta^{13}C\text{-}CH_4$ data, for dissolved and bubble CH_4 from lakes in the Mackenzie River Delta to elucidate 1) the process by which CH_4 was formed (i.e. microbial or thermogenic) and 2) the precursor carbon source for microbially produced CH_4.

The overall study goal was to elucidate the source of CH_4 present in nine lakes, and a gas seep location located in a channel branching from the Middle Channel of the Mackenzie River, and the East Channel of the Mackenzie River. Study lakes include two which overlie thin permafrost and are in close proximity to oil and gas reserves in the outer delta, and seven lakes in the central delta with differing connections to the Mackenzie River two of which have expanding shorelines and active thermokarst processes. Based on these characteristics, I had three hypotheses of how CH_4 source and age would differ in the study lakes. First, lakes in the outer delta and the seep location

would release thermogenic, ^{13}C enriched and radiocarbon-dead CH_4 (Figure 4-1) due to conduits through thin permafrost allowing CH_4 to evade underlying gas reserves. Second, because the lakes in the central delta do not overlie gas nor oil, I hypothesized CH_4 in those lakes would be microbial in origin with the CH_4 age increasing for those lakes with longer connections to the Mackenzie River because the river transports aged particulate organic carbon (~5000 YBP, McClelland et al., 2016). Thirdly, I hypothesized lakes undergoing thermokarst enlargement would have labile permafrost carbon entering the lakes that would be readily decomposed by methanogens to produce ^{13}C depleted CH_4 with a radiocarbon-age between 10,000 and 40,000 YBP (Figure 4-1).

4.2. Materials and Methods

4.2.1. Study Site Description

The outer delta lakes – informally named Manta and Swiss Cheese – and the seep site are north of the treeline near known oil and gas deposits (Burn & Kokelj, 2009; Collett & Dallimore, 1999) (Figure 4-2). At Swiss Cheese Lake, gas bubbles break the water continuously during open water and maintain openings following ice formation that completely ice over mid-winter. Swiss Cheese Lake is Y shaped and each side of the upper prongs were sampled with site 1 being the reference site (SC-ref) and site 2 within 10 m of a gas seep (SC-seep) (Figure 4-2b). Seep 7 is located in a distributary channel adjacent the Middle Channel of the Mackenzie River near where it enters the Beaufort Sea (Table 4-1; Figure 4-2c). This site is offset from the Middle Channel such that the river bypasses it, except during periods of high river flow such as the spring flood or a Beaufort Sea storm surge.

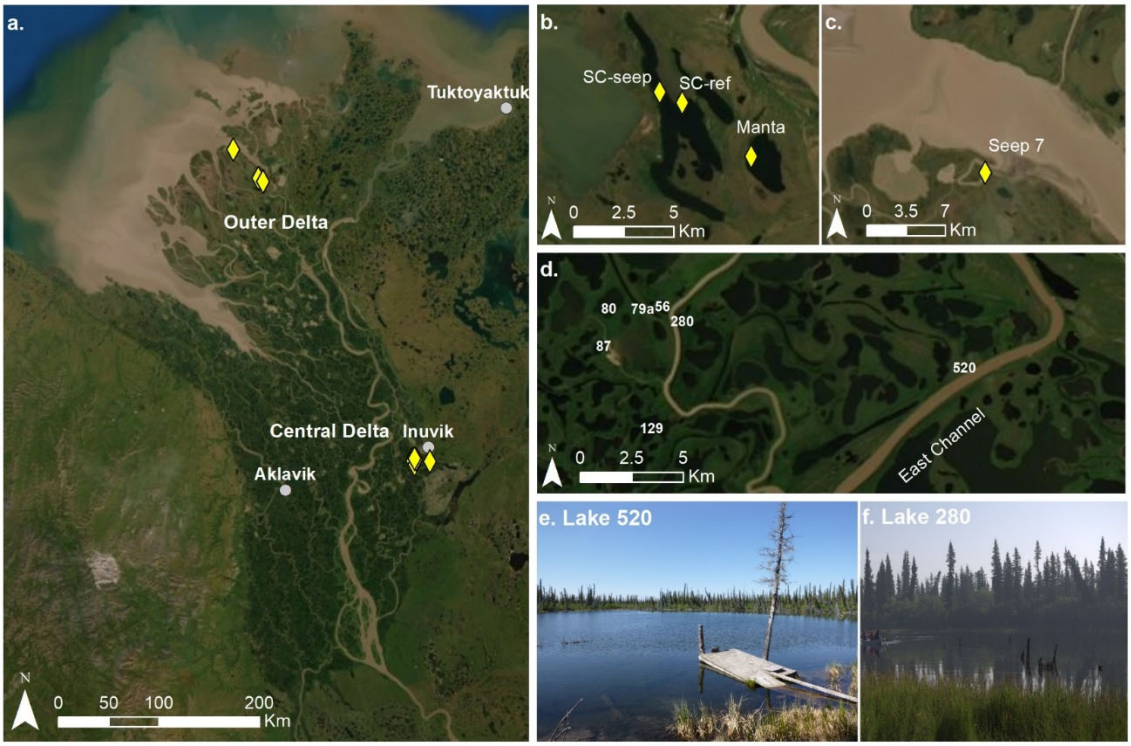

Figure 4-2. Location of sampling sites where surface water was collected for [CH_4], δ^{13}C-CH_4 and Δ^{14}C-CH_4 analyses. a) Mackenzie River Delta with yellow symbols showing the lake locations, b) Outer delta lakes Swiss Cheese Lake and Manta Lake are next to each other. At Swiss Cheese Lake there were two sites visited – SC-ref and SC-seep, which is within 10 m of a seep. c) Seep 7 situated in a channel adjacent to a larger channel of the Middle Channel. d) Lakes near Inuvik, Northwest Territories, Canada with the East Channel of the Mackenzie River to the East. e) Picture of Lake 520 from the southern perimeter showing the trees surrounding the lake falling into the lake (McIntosh Marcek et al., *Submitted*). f) Picture of Lake 280 with tree stumps present and falling trees.

The seven central delta lake sites (Lakes 129, 79a, 80, 87, 280, 56, 520) and East Channel of the Mackenzie River are near Inuvik, Northwest Territories, Canada (Figure 4-2d). They are within white spruce (*Picea glauca*) and black spruce (*Picea mariana*) forests and overlie discontinuous permafrost (Black & Bliss, 1980; Johnstone & Kokelj, 2008; Mackay, 1995; Pearce et al., 1988). The study lakes represent the three closure classes for Mackenzie Delta lakes and a range of lake sizes (Table 4-1; Cunada, 2016; Lesack & Marsh, 2010; Marsh & Hey, 1989). Lakes 280 and 520 have expanding shorelines and elevated pCO_2 representative of active thermokarst processes occurring beneath them (Cunada et al., 2018; Tank et al., 2009).

Table 4-1. Location of sampling sites and sampling dates.

Lake/ Location	Latitude (°N)	Longitude (°W)	Lake Area (ha)*	Summer Sill Height (m)*	Closure Type	Sampling Date(s)
		Inuvik Region				
129	68° 18.244’	133° 51.090’	37.8	2.363	No	10 Aug. 2016 9 Aug. 2017
79a	68° 19.393’	133° 53.078’	34.6	2.631	Low	8 May 2017
80	68° 19.395’	133° 52.204’	19.3	2.631	Low	15 Aug. 2016 11 Aug. 2017
87	68° 19.015’	133° 52.460’	3.9	3.389	Low	11 Aug. 2017
280	68° 19.276’	133° 50.309’	2.4	3.838	Low	12 Aug. 2016 9 Aug. 2017
56	68° 19.417’	133° 50.805’	2.1	4.623	High	15 Aug. 2016 9 Aug. 2017
520	68° 18.826’	133° 42.931’	0.2	4.913	High	13 Aug. 2016 12 Aug. 2017
Mackenzie River East Channel	68° 21.304’	133° 43.983’		-	-	9 Aug. 2016 15 Aug. 2017
		Outer Delta Region				
Manta	69° 13.133’	135° 12.406’	*	-	-	14 Aug. 2017
SC-ref•	69° 13.644’	135° 14.257’	*	-	-	16 Aug. 2017
SC-seep•	69° 13.745’	135° 14.765’	*	-	-	13 Aug. 2016 13 Aug. 2017
Seep 7	69 ° 19.190’	135 ° 28.430’		-	-	7 Aug. 2005

• Swiss Cheese Lake had two sites sampled, a reference site (SC-ref) and a site within 10 m of a gas bubble seep (SC-seep)

* Lake areas and summer sill heights for Inuvik Region lakes are taken from Lesack & Marsh (2010) and Cunada (2016). Lake area not measured for Manta or Swiss Cheese Lake.

4.2.2. Surface Water for Dissolved CH_4 Concentration and $\delta^{13}C$-CH_4 Determination

Discrete near-surface lake water (~0.5 m below surface) samples were gently collected from all lakes into submerged 160 mL serum vials (Wheaton) from a small boat in August 2016 and August 2017. After sealing the vials with butyl rubber septa (1.5 cm thick, GMT Stoppers #1313) and a crimped aluminum disk, 10 mL of lake water was exchanged with 10 mL air (Ultra High Purity (UHP), Airgas) to create a headspace and then basified to halt microbial activity (0.5 mL 1 M potassium hydroxide, KOH) (Magen et al., 2014). Samples were kept at ~22°C until dissolved CH_4 concentration and $\delta^{13}C$-CH_4 analyses were performed at the Chesapeake Biological Laboratory (CBL, Solomons, MD, USA).

4.2.3. Surface Water Dissolved CH_4 Samples for $\Delta^{14}C$-CH_4

Near-surface water (~1 m water depth) samples were collected from a small boat from eight lakes and the East Channel of the Mackenzie River into gas tight, Mylar bags (10 L, Tedlar) via submersible pump in August 2016 and August 2017. Replicate bags (2 to 4) were collected at each lake. Bags were returned to the Aurora Research Institution (ARI, Inuvik, NT, CAN) and kept at 4ºC and processed within 48 hours. Dissolved gases were extracted from the lake water via headspace extraction at 20ºC following Garrett et al. (2016). Briefly, 140 mL of air (UHP, Airgas) was added to each bag, which were then shaken vigorously for three minutes. Headspace was removed from the bags and transferred to 160 mL serum glass vials (Wheaton) by inverting the vials in a saturated brine (NaCl) solution and replacing brine solution with the extracted headspace. Vials were sealed (1.5 cm butyl rubber septa and aluminum disk) and inverted so the brine solution created a water seal. The process was repeated to produce two vials of extracted headspace per sample bag. Vials were stored at ~22ºC until processing for radiocarbon analysis. Methane storage using similar vials and stoppers has been maintained in tests for 3 months or longer (Magen et al., 2014).

4.2.4. Surface Water Bubble Samples for $\Delta^{14}C$-CH_4

Gas bubbles breaking the lake surface were collected from Lake 79a, SC-seep, and Seep 7 by inverting a container at the lake surface over the bubble streams. Gas was transferred into serum vials and sealed. All vials were sealed with a butyl rubber septa (1.5 cm thick, GMT Stoppers) and a crimped aluminum disk. Lake 79a was visited in May 2017 prior to ice-melt. A bubble sample was collected from a hole open in the ice ~2 m in diameter with several bubble streams of ~2 cm diameter bubbles. Bubble streams

were noted in Swiss Cheese Lake on 13 August 2016 within less than 10 m of SC-seep. The Seep 7 sample was collected on 7 August 2005.

4.2.5. Continuous Bottom Water Samples at Seep Site

To assess potential source changes over the year, bottom water was sampled from two sites in Swiss Cheese Lake (SC-ref and SC-seep) continuously and autonomously using OsmoSamplers (Jannasch et al., 2004). Methods are detailed in McIntosh Marcek et al. (*Submitted*). Briefly, OsmoSamplers are made of OsmoPumps and 300 m thin-bore tubing, either Teflon (Acid OsmoSamplers) for ion analyses or copper (Gas OsmoSamplers) for dissolved CH_4 analyses (Wheat et al., 2011). OsmoPumps and tubing were secured within plastic crates and the intakes were set at ~25 cm above the bottom of the crate. Sensors were secured to the crates and deployed at both SC-ref and SC-seep to measure continuous water temperature (Tidbit V2 temperature UTB1-001, 30-minute increments), dissolved oxygen (HOBO DO U26-001, 1-hour increments for 6 months until the batteries died), pressure (HOBO U201L-01, 1-hour increments), and for the 2015-2016 deployment conductivity (HOBO U24-001, 2-hour increments) at SC-ref.

One plastic crate was deployed from a small boat at each site in Swiss Cheese Lake at ~2.1 m water depth at SC-ref and ~2.4 m water depth at SC-seep (Figure 4-2b). The first year-long deployment was from 4 August 2015 to 13 August 2016, and the second year-long deployment from 13 August 2016 to 13 August 2017 (SC-seep) and 16 August 2017 (SC-ref). For recovery, the plastic crates were located by a weighted cable attached to the lake shore leading to the sampling packages. Immediately after sampling packages were recovered the two ends of the copper tubing were crimped and stored at 4°C until processing at the CBL. Telfon coils were capped off and subsampled at ARI.

4.2.6. Subsampling of coils and ion analytical methods

Teflon tubing was sectioned into 1 m segments and liquid expelled into plastic vials at ARI. Samples were analyzed for sulfate (SO_4^{2-}) and chloride (Cl^-) on a Dionex ICS1000 ion chromatograph (IC) at the Monterey Bay Aquarium Research Institute (Moss Landing, CA, USA) following Wheat et al. (2017). At CBL, copper tubing was sectioned into short (0.5 m) and long (2 m) segments and enclosed water was extracted with a benchtop roller (Gelesh et al., 2016). Sectioning ceased once the fresh lake water interface to the saline filling solution (40 mg L^{-1} NaCl) was reached. Salinity (Extech RF20 refractometer, 1‰ precision) and anion concentrations (SO_4^{2-}, Cl^-) were measured on separate aliquots of expelled fluid collected in 2 mL plastic vials from the short copper segments. The aliquots for SO_4^{2-} and Cl^- analysis from copper tubing (200-500 µL) were acidified (20-40 µL, 1 M phosphoric acid), diluted (1:10 to 1:27 in Milli Q in 5.4 mL vials for 2015-2016, and 1:1 for SC-ref and 1:3 for SC-seep in Milli Q in 500 µL vials for 2016-2017 samples), and analyzed on an IC (Dionex ICS1000) following Gelesh et al. (2016). Long segments were squeezed for CH_4 analyses using gas tight connections into pre-flushed (UHP air, Airgas, flushed 10-20 times vial volume) glass serum vials (13.5 mL, Wheaton) that were sealed with butyl rubber septa (1.5 cm thick, GMT Stoppers) and crimped aluminum disks.

4.2.7. Assigning Dates for Integrated Bottom Water Samples

The OsmoSampler deployments resulted in sequential time-integrated samples. To assign a date when water was drawn into the tubing, a temperature correction was made to account for the changes to osmosis pumping rates by the OsmoSamplers (Gelesh et al., 2016; Jannasch et al., 2004). To verify sampling dates, the Cl^- and SO_4^{2-} time-series

collected concurrently by OsmoSamplers connected to Teflon and copper tubing at SC-ref and SC-seep were compared with the conductivity measured from the sensor at SC-ref.

4.2.8. [CH_4] and $\delta^{13}C$-CH_4 Analysis

The discrete surface samples and bottom-water time-series samples were analyzed for CH_4 concentrations following published headspace equilibration methods (Magen et al., 2014; McIntosh Marcek et al., *Submitted*). Briefly, air (UHP, Airgas) was equilibrated with the headspace of the sample vial and an aliquot was injected into a gas chromatograph (SRI 8610C, Torrance, CA, USA with molecular sieve and HayeSep D columns and flame ionization detector) via loop injection. Samples were compared to CH_4 standards ranging from 30 ppm to 9.0% CH_4 (balance helium, Airgas). Replicate standards (n=3) and duplicate discrete surface water samples had coefficients of variance (CV) less than 2%.

Stable carbon isotopic ratios of CH_4 ($\delta^{13}C$-CH_4) were measured on the headspace of the above samples using a cavity ring-down spectrometer (CRDS G220l-i, Picarro, Santa Clara, CA, USA). Water vapor was kept to a minimum within the analyzer by pulling samples into the CRDS through a Drierite (8 mesh, W.A. Hammond Drierite Company, LTD) filled tube under vacuum. This was done to eliminate the interference of water vapor with CH_4 absorption in the CRDS. Gas aliquots were diluted with air (UHP, Airgas) so that CH_4 concentrations ranged between 15 and 500 ppm CH_4. Samples with <420 ppm CH_4 in the headspace were diluted to >15 ppm CH_4 with air (UHP, Airgas) and were processed through the CRDS Small Sample Inlet Module (Picarro Part#A0314 Picarro, Santa Clara, CA, USA). Isotopic ratios were averaged over three minutes and

corrected for instrumental offset by calibrating to certified CH_4 standards from Isometric Instruments (L-iso1 = -66.5 ± 0.2‰, T-iso1 = -38.3± 0.2‰, and H-iso1 = -23.9 ± 0.2‰, Victoria, BC, CAN) diluted between 30 and 100 ppm CH_4. Instrumental offset did not significantly vary over a 2-year period (2% CV). $\delta^{13}C$-CH_4 values are reported using the $\delta^{13}C$ notation in per mil (‰) with a precision of 1‰ for CH_4 concentrations greater than 15 ppm.

4.2.9. $\delta^{13}C$ Mass Balance

An isotope mass balance assessed the proportion of CH_4 coming from thermogenic CH_4 and microbial CH_4 for each time-integrated sample during ice-cover at SC-ref and SC-seep sites, following:

$$\delta^{13}C_{All}*C_{All} = \delta^{13}C_{Thermo}*C_{Thermo} + \delta^{13}C_{Microb}*C_{Microb} \quad (4.1)$$

where $\delta^{13}C_{All}$, $\delta^{13}C_{Thermo}$, and $\delta^{13}C_{Microb}$ are $\delta^{13}C$ values for time-integrated CH_4 samples analyzed on the CRDS, the thermogenic CH_4 source, and the microbial CH_4 source, respectively. $\delta^{13}C_{Thermo}$ was set at -30‰, since that was the most ^{13}C-enriched CH_4 value observed at SC Lake during ice-cover. This value is on the high end of the $\delta^{13}C$ range for thermogenic CH_4 (Etiope & Klusman, 2002) and is reasonable because the thermogenic CH_4 present in the outer delta is classified as thermally immature (Collet & Dallimore, 1998). $\delta^{13}C_{Microb}$ was set at -70‰ from the $\delta^{13}C$ measured in the bottom of sediment cores collected from SC-ref and SC-seep in August 2016 (Appendix 3 Table S3-4). C_{All} was the CH_4 concentration for each time-integrated sample with C_{Thermo} and C_{Microb} each contributing:

$$C_{All} = C_{Thermo} + C_{Microb} \quad (4.2)$$

Combining equations 4.1 and 4.2 leads to calculating the C_{Thermo}:

$$C_{Thermo} = (\delta^{13}C_{All} * C_{All} - \delta^{13}C_{Microb} * C_{All}) / (\delta^{13}C_{Thermo} - \delta^{13}C_{Microb}) \quad (4.3)$$

And substituting the results from equation 4.3 into equation 4.2 results in calculating the C_{Micro}:

$$C_{Microb} = C_{All} - (\delta^{13}C_{All} * C_{All} - \delta^{13}C_{Microb} * C_{All}) / (\delta^{13}C_{Thermo} - \delta^{13}C_{Microb}). \quad (4.4)$$

Once C_{Thermo} and C_{Microb} were calculated for each time-integrated sample with equations 4.3 and 4.4, the percent of CH_4 coming from those sources was determined by taking C_{Thermo} and C_{Microb} and dividing each by C_{All}, and multiplying by 100.

4.2.10. Radiocarbon Analysis

Gas headspace in vials from the large-volume bags was stripped sequentially using helium and combined on a vacuum line to create one sample per lake. To test replicate variability, each bag remained as a separate sample for Lakes 520 and 56 and was analyzed separately. Methane in the extracted headspace and from gas bubble aliquots was purified from other gases (e.g. water vapor, carbon dioxide, CO_2) on a vacuum line and combusted to CO_2 on a heated copper oxide column at Florida State University (Chanton et al., 1995). Purified CO_2 was reduced to graphite following standard procedures for normal-sized samples and formed into graphite targets for ^{14}C analysis in an accelerator mass spectrometer (AMS) at the National Ocean Sciences AMS Facility (NOSAMS) (Longworth et al., 2015; McNichol et al., 1992; Roberts et al., 2010). Ultra-microscale samples (1.5 to 2.3 μmol C, Mackenzie River in 2016, Lake 280 in 2017, and a process blank) were manually reduced to graphite in heated reactors over baked iron in a saturated hydrogen atmosphere (McIntosh et al., 2015; Shah Walter et al., 2015). Sample graphite was pressed into aluminum targets and analyzed with a combination of process blanks, primary NBS Oxalic Acid I standards, and secondary

standards (von Reden et al., 1998). A split (10 %) of the purified CO_2 was analyzed on a stable isotope mass spectrometer (VG PRISM series II) for $\delta^{13}C\text{-}CH_4$. Stable carbon isotope ratios ($\delta^{13}C\text{-}CH_4$) are presented using the per mil (‰) notation with an error of ± 0.1‰. This $\delta^{13}C\text{-}CH_4$ measurement with a second instrument also allowed me to cross-compare samples measured with two different instruments.

The Seep 7 bubble sample was prepared and analyzed on the AMS at the University of California Irvine's Keck Carbon Cycle facility (Kessler & Reeburgh, 2005; Vogel et al., 1984). An aliquot of purified CO_2 from Seep 7 was analyzed on a dual-inlet IR-MS at University of California Irvine's Stable Isotope facility for $\delta^{13}C\text{-}CH_4$ and is presented using the per mil (‰) notation with an error of ± 0.2‰.

All ^{14}C data were normalized to a constant ^{13}C (-25‰) to remove the effect of isotopic fractionation (Stuiver & Polach, 1977). Radiocarbon data are presented as a fraction modern ($F^{14}C$), $\Delta^{14}C$ (‰), and ^{14}C-age using standard conventions (Reimer et al., 2004; McNichol & Aluwihare, 2007; Stuiver & Polach, 1977).

4.2.10.1. Radiocarbon Process Blanks

A process blank was collected to assess background carbon obtained during processing of the dissolved CH_4 water samples in 2016 and 2017. Air (140mL, UHP, Airgas) was mixed into an empty 10 L Tedlar bag, removed and processed in the same way as the headspaces extracted from lake water. The carbon in the process blank was both quantified (1.6 μmol C) and run on the AMS ($F^{14}C = 0.78885$), but had too little carbon to be analyzed for $\delta^{13}C\text{-}CH_4$. Radiocarbon data were process blank corrected using an isotope mass balance and error propagation following standard procedures

(McNichol et al., 1992; Shah & Pearson, 2007; Shah Walter et al., 2015). Because of the small sample size, $\delta^{13}C\text{-}CH_4$ data were not unable to be process blank corrected.

4.2.11. Comparison of $\delta^{13}C\text{-}CH_4$ Values from CRDS and IR-MS

A comparison of $\delta^{13}C\text{-}CH_4$ values obtained from the same samples analyzed on different instruments was conducted using a CRDS (CRDS G220l-i, Picarro, Santa Clara, CA, USA) at CBL and an IR-MS (Delta V Advantage IR-MS, ThermoFisher Scientific, Bremen, Germany) at Florida State University. These CH_4 samples were collected via OsmoSamplers into copper tubing from bottom water in Lake 520 and Lake 56, lakes in the Mackenzie Delta near Inuvik, Northwest Territories, Canada, and processed in the same way as those from SC Lake (section 4.2.6). The headspaces had 490-1100 ppm CH_4 for the samples from Lake 520 and 20 ppm CH_4 for the sample from Lake 56.

4.2.12. Data Analysis

Statistical data analysis used RStudio (version 1.1.456). Pair-wise t-tests were used to compare data collected in 2016 to 2017. P-values of less than 0.05 were considered significant.

4.3. Results

Dissolved $[CH_4]$, $\delta^{13}C\text{-}CH_4$, $\Delta^{14}C\text{-}CH_4$, and sensor data are archived at the US National Science Foundation supported Arctic Data Center (Orcutt, 2017a).

4.3.1. Discrete Dissolved $[CH_4]$, $\delta^{13}C\text{-}CH_4$

Surface water dissolved CH_4 concentrations ranged from 0.22 to 3.29 μM CH_4 in August 2016 and August 2017 for all lakes (Table 4-2). All concentrations were above atmospheric equilibrium (3-4 nM at air temperatures of 7-15^{o}C; Yamamoto et al., 1976).

Table 4-2. Methane radiocarbon and stable carbon isotope data from dissolved CH_4 and gas bubbles collected from Mackenzie River Delta.

Lake/ River	Year Collected	Sample Type (number ^{14}C samples)	Dissolved CH_4 (µM)	Diffusive Flux (mg m^{-2} hr^{-1})º	Amount C Analyzed (µmol) •	Fraction modern ($F^{14}C$)†	$\Delta^{14}C$ (‰)†	^{14}C-age (YBP)†	$\delta^{13}C$-CH_4 IR-MS (‰)	$\delta^{13}C$-CH_4 CRDS (‰)
520	2016	Dissolved (4)	2.39 ± 0.05	0.63	29.18 ± 0.58	1.007 ± 0.002	-1 ± 2	0 ± 19	-46.7 ± 0.1*	-47.8 ± 0.3
					31.33 ± 0.63	1.006 ± 0.002	-2 ± 2	0 ± 18	-45.9 ± 0.1*	
					29.25 ± 0.59	1.013 ± 0.003	5 ± 3	0 ± 24	-48.7 ± 0.1*	
					20.34 ± 0.41	1.006 ± 0.003	-2 ± 3	0 ± 22	-47.7 ± 0.1*	
					Average	1.008 ± 0.004	0 ± 3	0 ± 28	-47.2 ± 1.2	
520	2017	Dissolved (2)	3.29 ± 0.05	1.04	6.63 ± 0.13	0.996 ± 0.005	-11 ± 5	26 ± 28	-40.9 ± 0.1*	-47.5 ± 0.1
					27.93 ± 0.56	1.002 ± 0.002	-6 ± 2	0 ± 18	-42.9 ± 0.1*	
					Average	0.999 ± 0.003	-9 ± 7	7 ± 27	-41.9 ± 1.4	
280	2016	Dissolved (1)	0.51 ± 0.04	0.13	2.80 ± 0.06	0.996 ± 0.017	-12 ± 17	30 ± 137	-24.3 ± 0.1*	-20.4 ± 1.8
280	2017	Dissolved (1)	0.22 ± 0.02	0.07	2.30 ± 0.05	1.002 ± 0.023	-6 ± 23	0 ± 46	-	-4.9 ± 1.1
56	2016	Dissolved (1)	2.03 ± 0.01	0.53	9.27 ± 0.19	0.981 ± 0.004	-26 ± 3	152 ± 29	-40.4 ± 0.1*	-48.1 ± 1.4
56	2017	Dissolved (2)	2.71 ± 0.12	0.58	18.24 ± 0.36	0.9541 ± 0.003	-54 ± 3	378 ± 22	-50.2 ± 0.1*	-53.0 ± 1.7
					4.57 ± 0.09	1.0170 ± 0.008	9 ± 8	0 ± 36	-49.5 ± 0.1*	
					Average	0.986 ± 0.044	-22 ± 44	120 ± 360	-49.9 ± 0.5	
River	2016	Dissolved (1)	0.72 ± 0.02	0.19	2.30 ± 0.05	0.912 ± 0.022	-95 ± 22	740 ± 195	-	-70.4 ± 0.3
River	2017	Dissolved (1)	0.45 ± 0.01	0.14	7.65 ± 0.15	0.837 ± 0.004	-169 ± 4	1425 ± 30	-35.5 ± 0.1*	-66.5 ± 0.1
87	2016	Dissolved (1)	0.82 ± 0.01	0.21	4.54 ± 0.09	0.878 ± 0.007	-129 ± 7	1047 ± 62	-51.3 ± 0.1*	-60.0 ± 0.4
87	2017	Dissolved (1)	1.46 ± 0.04	0.46	7.13 ± 0.14	0.882 ± 0.004	-125 ± 4	1009 ± 26	-47.3 ± 0.1*	-55.4 ± 0.2
129	2016	Dissolved (1)	0.82 ± 0.01	0.21	4.15 ± 0.08	0.839 ± 0.008	-167 ± 8	1407 ± 77	-58.1 ± 0.1*	-63.6 ± 0.2
129	2017	Dissolved (1)	0.86 ± 0.03	0.27	7.27 ± 0.15	0.877 ± 0.004	-130 ± 4	1051 ± 27	-48.5 ± 0.1*	-59.0 ± 0.4
80	2016	Dissolved (1)	0.51 ± 0.01	0.13	3.92 ± 0.08	0.798 ± 0.008	-208 ± 8	1808 ± 78	-52.9 ± 0.1*	-68.7 ± 0.2
80	2017	Dissolved (1)	0.90 ± 0.13	0.28	10.59 ± 0.21	0.840 ± 0.004	-166 ± 4	1398 ± 31	-56.7 ± 0.1*	-67.5 ± 0.2
Manta	2017	Dissolved (1)	1.19 ± 0.09	0.37	9.98 ± 0.20	0.963 ± 0.003	-44 ± 3	300 ± 21	-35.8 ± 0.1*	-46.9 ± 1.3
SC-ref	2017	Dissolved (1)	0.45 ± 0.01	0.14	4.36 ± 0.09	0.988 ± 0.009	-19 ± 9	93 ± 46	-43.0 ± 0.1*	-52.3 ± 0.9
SC-seep	2017	Dissolved (1)	1.03 ± 0.01	0.32	7.84 ± 0.16	0.450 ± 0.004	-554 ± 4	6419 ± 37	-39.6 ± 0.1*	-46.5 ± 0.3

Table 4-2 (continued). Methane radiocarbon and stable carbon isotope data from dissolved CH_4 and gas bubbles collected from Mackenzie River Delta

Lake/ River	Year Collected	Sample Type (number ^{14}C samples)	Dissolved CH_4 (µM)	Diffusive Flux (mg m^{-2} hr^{-1})º	Amount C Analyzed (µmol) •	Fraction modern ($F^{14}C$)†	$\Delta^{14}C$ (‰)†	^{14}C-age (YBP)†	$\delta^{13}C$-CH_4 IR-MS (‰)	$\delta^{13}C$-CH_4 CRDS (‰)
79a	2017	Bubble (1)	-		47.35 ± 0.95	0.501 ± 0.002	-503 ± 2	5557 ± 30	-72.7 ± 0.1*	-
SC-seep	2016	Bubble (1)	-		58.02 ± 1.16	-0.010 ± 0.001	-1000 ± 1	50000 ± 760	-45.6 ± 0.1*	-51.8 ± 0.4
Seep 7	2005	Bubble (1)	-		-	0.000 ± 0.0003	-1000 ± 0	>59300 ± 0	-42.6 ± 0	-
Process blank	2017	Gas(1)	-		1.6 ± 0.03	0.789 ± 0.0060	-	-	-	-

º Estimated diffusive flux calculated following methods in McIntosh Marcek et al. (Submitted)

• Error for amount C measured manometrically was estimated to be 2%

† blank-carbon corrected values

* IR-MS analytical error is 0.1‰

All values are Mean ± Standard deviation

There were no significant differences in dissolved CH_4 concentrations between August 2016 and August 2017 (p=0.14). Higher dissolved CH_4 concentrations were in surface waters for Lake 520, while the lowest dissolved CH_4 concentrations were in Lake 280 and the Mackenzie River. Surface water $\delta^{13}C$-CH_4 ranged from -20.4 to -70.4‰ in the discrete samples analyzed on the CRDS. There were not significant differences in $\delta^{13}C$-CH_4 measured on the CRDS for lakes visited both years (discrete: p=0.70).

4.3.2. Dissolved and Bubble $\Delta^{14}C$-CH_4, $\delta^{13}C$-CH_4

Dissolved CH_4 samples had $F^{14}C$ process blank errors of 0.3 to 4.5%, which were highly dependent on the amount of carbon analyzed using the AMS (Table 4-2). $\Delta^{14}C$-CH_4 of dissolved CH_4 ranged from 0 to -554‰ (0 to 6419 YBP; Figure 4-3) and

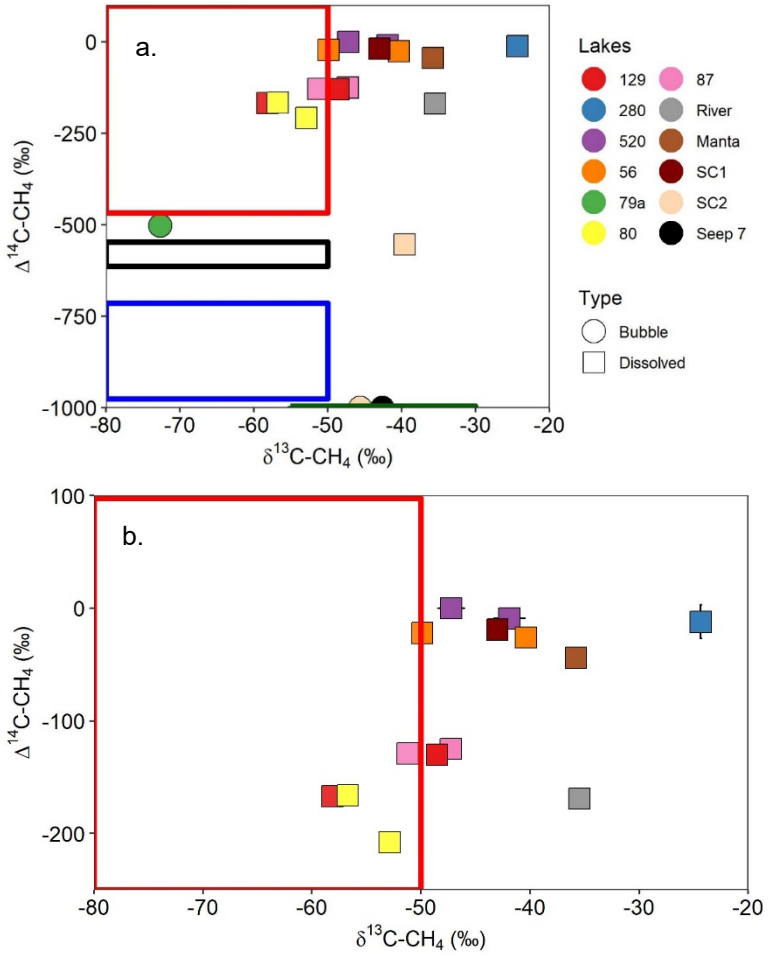

Figure 4-3. $\Delta^{14}C$ (‰) and $\delta^{13}C$ (‰) of CH_4 collected from lakes within the Mackenzie River Delta with $\Delta^{14}C$-CH_4 y-axis extending from +100 to -1000‰ in a) and an enhanced view of the $\Delta^{14}C$-CH_4 y-axis extending from +100 to -250‰ in b). Sample type is indicated with a circle for gas bubbles and squares for dissolved CH_4. Each lake is represented with a different color symbol. Error bars for $\Delta^{14}C$-CH_4 (‰) and $\delta^{13}C$-CH_4 (‰) values are standard deviation of multiple samples or process blank corrected error for single samples. Data presented are for samples processed concurrently and then split for analysis on the AMS ($\Delta^{14}C$) and the IR-MS ($\delta^{13}C$). Source boxes are the same as Figure 4-1 and references therein: microbial CH_4 with a modern carbon source (red box), microbial CH_4 from Mackenzie River POC (black box), microbial CH_4 from permafrost carbon (blue box), and thermogenically produced CH_4 (green box).

bubbles were -503‰ (5557 YBP) at Lake 79a and -1000‰ (>50,000 YBP) at SC-seep and Seep 7 (Figure 4-3, Table 4-2). Bubbles at 79a were older than dissolved CH_4 collected at any of the lakes near Inuvik and the $\delta^{13}C$-CH_4 was the most depleted in ^{13}C measured on the IR-MS. The younger ^{14}C ages in dissolved CH_4 from the lakes near Inuvik were accompanied by variable $\delta^{13}C$-CH_4 (-24.3‰ to -56.7‰) measured on the IR-MS (Figure 4-3b). Bubbles from SC-seep and Seep 7 were both enriched in ^{13}C with $\delta^{13}C$-CH_4 values of -45.6‰ and -42.6‰, respectively. Methane in SC lake had differences in CH_4 at the two sites with SC-ref dissolved $\Delta^{14}C$-CH_4 of -19‰, while SC-seep dissolved CH_4 was -554‰ and bubbles from SC-seep were radiocarbon-dead (-1000‰). The $\delta^{13}C$-CH_4 in dissolved CH_4 at SC-seep was more enriched in ^{13}C (-39.6‰) than in the bubbles (-45.6‰).

4.3.3. Comparison of $\delta^{13}C$-CH_4 values from IR-MS and CRDS

The $\delta^{13}C$-CH_4 values for the surface water samples from lakes across the Mackenzie Delta analyzed on the Picarro CRDS and the large volume water samples analyzed on the VG Prism II IR-MS had a linear relationship ($R^2 = 0.59$). There was an offset with the CRDS $\delta^{13}C$-CH_4 values depleted in ^{13}C by -8± 8‰ on average (Figure 4-4; Table 4-2). This offset could be due

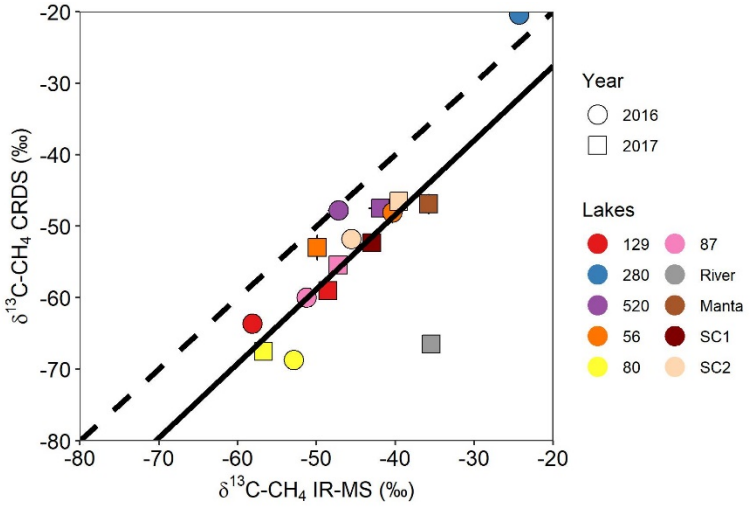

Figure 4-4. $\delta^{13}C$-CH_4 measured on discrete samples on the CRDS compared to $\delta^{13}C$-CH_4 measured on the IR-MS. The dashed line is a 1-1 line and the solid line is the regression for the surface water analyzed via both CRDS and IR-MS (y=1.04x-6.8). R^2 for the relationship is 0.59. Error bars are smaller than the size of many of the symbols.

to differences in the two instruments, differences in the way $\delta^{13}C\text{-}CH_4$ values were calculated, or differences in the way that the samples were handled prior to instrumental analysis.

First, the offset could be due to fundamental differences in the two instruments. For instance, water vapor can affect the $\delta^{13}C\text{-}CH_4$ values from the two instruments differently. Nafion dryer tubes were utilized to reduce water vapor introduction into the IR-MS and reduce artificial enhancement of the 45 ion current, which keeps IR-MS errors <0.1‰ (Leckrone & Hayes, 1998). There is not traditionally a similar component to reduce water vapor for sample introduction into the CRDS. The presence of water vapor for samples analyzed on the CRDS tends to result in more negative $\delta^{13}C\text{-}CH_4$ values (Rella et al., 2015). A maximum error of 1‰ is reported by Rella et al., (2015) with greater than 2 ppm CH_4 concentrations and water vapor concentrations between 0-2.5%. Therefore, efforts were made to achieve low water vapor concentrations in CRDS with the Drierite filled tube attached to the CRDS intake.

In order to examine the influence different instrument analysis had on $\delta^{13}C\text{-}CH_4$ values, dissolved CH_4 samples were measured on both a CRDS and IR-MS. Dissolved CH_4 samples from Lakes 520 and 56 had $\delta^{13}C\text{-}CH_4$ values with an average 1‰ difference between the two instruments (Figure 4-5). Five of 9 samples analyzed were within error of the same $\delta^{13}C\text{-}CH_4$ value (Figure 4-5). The difference in $\delta^{13}C\text{-}CH_4$ values is less than the 3‰ difference between CRDS and IR-MS measurements noted by Zare et al. (2009). Hence, it is does not appear the instrumental measurement technique contributed to the 8‰ difference between the surface samples.

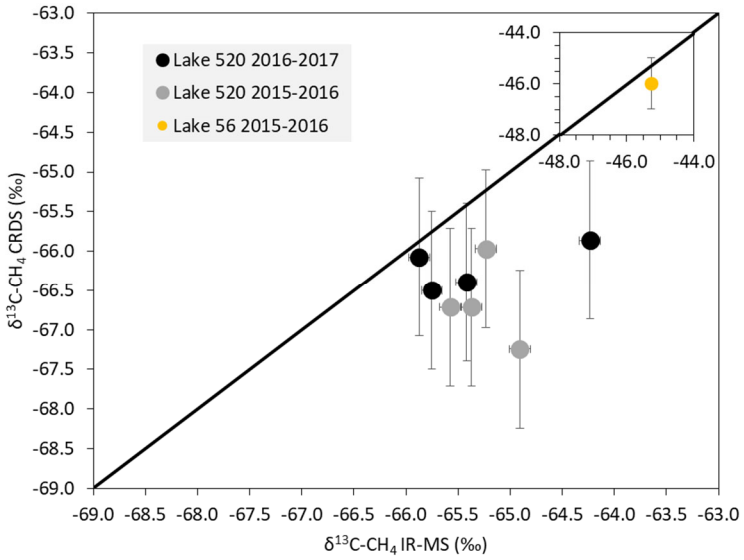

Figure 4-5. Comparison of $\delta^{13}C\text{-}CH_4$ values obtained from the same samples measured on a CRDS and an IR-MS. Error for the CRDS was ± 1‰ and for the IR-MS was ± 0.1‰. Dissolved CH_4 samples came from bottom water collected into copper tubing from Lakes 520 and 56 using OsmoSamplers deployed during the same time intervals as the Swiss Cheese Lake sampling.

Second, the offset could be due to $\delta^{13}C\text{-}CH_4$ data analysis methods. While data from both instruments was corrected with certified standards with known $^{13}C/^{12}C$ isotope ratios, the samples run on the IR-MS were not process blank corrected to account for carbon added during the large volume sample processing. The inability to correct the IR-MS data with the process blank data could contribute to some of the discrepancy, especially for the samples with the smallest amounts of CH_4.

Thirdly, the data show that the IR-MS $\delta^{13}C\text{-}CH_4$ values are more depleted in ^{13}C than the CRDS. This could be explained by the samples in the larger volume bags undergoing CH_4 oxidation. The discrete samples analyzed on the CRDS were collected, immediately capped, and basified to reduce alterations to the CH_4 sample, but the samples collected in the Tedlar bags were extracted up to 48 hours after collection. Methane oxidation could have reduced the total amount of CH_4 present in the larger volume bags and fractionated the residual CH_4 resulting in the IR-MS samples enriched

in ^{13}C compared to the CRDS samples. This would not have happened in the discrete samples collected for the CRDS because they were immediately preserved with base. Aerobic CH_4 oxidation could have occurred because surface water in the study lakes in August was likely oxygenated. Bottom water dissolved oxygen concentrations were elevated in lakes near Inuvik (data not shown). Despite the Tedlar bags being kept at 4ºC until headspace extraction, it is reasonable that methanotrophs could be active at that temperature under the presence of dissolved oxygen (Ricão Canelhas et al., 2016). The ^{13}C values could have been altered from CH_4 oxidation in the bag samples, but the ^{14}C values are not likely changed. By normalizing the ^{14}C values to a constant $\delta^{13}C$ of -25‰, isotopic fractionation affecting the ^{13}C results is removed from the ^{14}C results (Stuiver & Polach, 1977). Therefore, the $\Delta^{14}C$-CH_4 data is likely unaffected.

4.3.4. Relationship between $\Delta^{14}C$-CH_4 and Sill Height

Lakes with connections to the Mackenzie River had a strong linear relationship between $\Delta^{14}C$-CH_4 of dissolved CH_4 and their sill height ($R^2 = 0.79$, Figure 4-6a). When these same data are plotted against the duration of the river flood, there was a weak linear relationship ($R^2 = 0.34$, Figure 4-6b). The lakes with the lowest sill heights, Lakes 129 and 80, and the Mackenzie River had large variations in $\Delta^{14}C$-CH_4 between years of 37‰, 41‰, 74‰ respectively. Low and high closure class lakes had little variation in $\Delta^{14}C$-CH_4 between 2016 and 2017 (6‰).

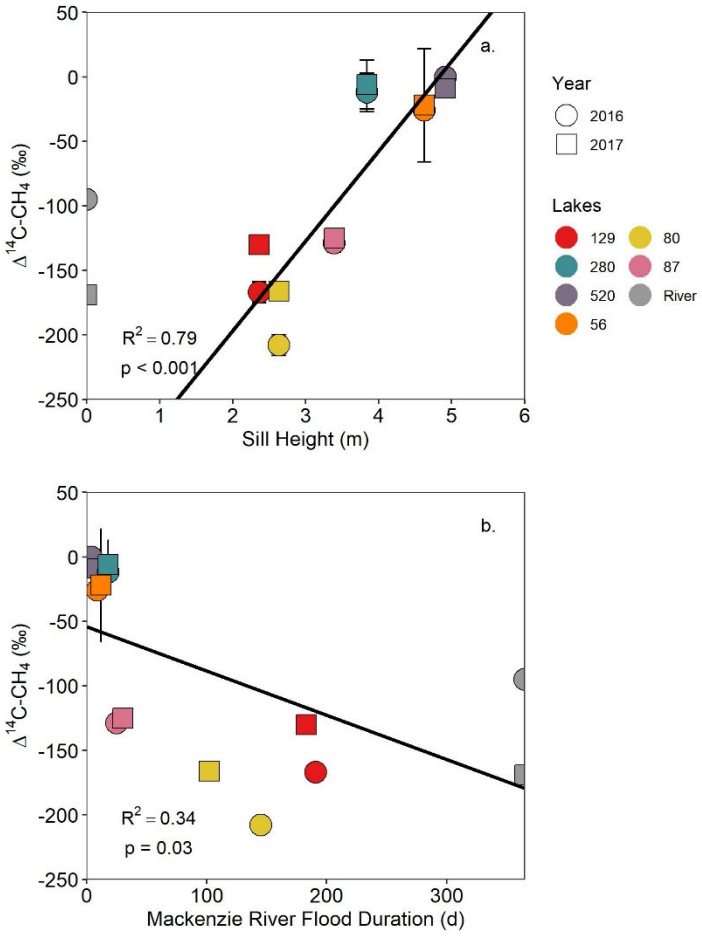

Figure 4-6. Relationship between $\Delta^{14}C\text{-}CH_4$ (‰) and Mackenzie River connection. a) $\Delta^{14}C\text{-}CH_4$ (‰) compared to sill height (m) in 2016 and 2017 for lakes with connections to the Mackenzie River and the Mackenzie River. b) $\Delta^{14}C\text{-}CH_4$ (‰) compared to sill height (m) in 2016 and 2017 for lakes with connections to the Mackenzie River and the Mackenzie River. The solid lines are the regressions for local lakes, excluding the Mackenzie River and bubbles collected at 79a. Error bars for $\Delta^{14}C\text{-}CH_4$ (‰) values are standard deviation of multiple samples (Lakes 520 and 56) or process blank corrected error for single samples (Lakes 129, 280, 80, 87, Mackenzie River).

4.3.5. Swiss Cheese Lake Time-Series

Bottom water samples were collected using OsmoSamplers from Swiss Cheese Lake for two years at a seep and a reference site. For these samples, dates were assigned with the Cl^- and SO_4^{2-} data, initially with a temperature correction used to calculate the dates from both the copper and Teflon OsmoSampler datasets (Gelesh et al., 2016). There was a mismatch when comparing the Cl^- and SO_4^{2-} time-series measured from the Teflon and copper tubing at both the SC-ref and SC-seep sites (data not shown). I think this is due to a truncation of the time-series in the copper tubing. When the dissolved CH_4 concentrations were elevated, CH_4 was able to diffuse out of the Teflon tubing whereas CH_4 was trapped within the copper tubing (Lapham et al., 2008). However, upon

recovery, it is possible that sample degassed from the slight pressure change and pushed the sample out the end of the copper tubing. This likely resulted in a loss of the most recently collected samples from the copper tubing and explains the mismatch in the Cl^- and conductivity data. Cl^- and SO_4^{2-} concentrations and conductivity increased in SC Lake during ice-cover due to ice-exclusion (Lesack et al., 1990), peaking right before ice-melt, and that allows an inter-coil comparison of Cl^- and SO_4^{2-} concentration patterns (Figure 4-7). Therefore, to assign the appropriate dates to the CH_4 data, the Cl^- and SO_4^{2-} changes in the samples collected into the copper tubing were matched to the Teflon tubing data (Figure 4-7) which resulted in shifting the date assignments for the copper time-series (SC-ref: 22, 77 days and SC-seep: 18, 75 days for 2015-2016 and 2016-2017, respectively). The shifted dates were assigned to the CH_4-related data (Figure 4-8).

At the two sites in SC Lake, bottom water lake temperature and water pressure were similar (Figure 4-8a, 4-8d). Bottom water temperatures were low in winter (~1-2ºC and high during open water (maximum 20ºC). Dissolved oxygen (DO) presence between the two sites varied (Figure 4-8b, 4-8e). SC-ref had higher DO concentrations than SC-seep during the ice-covered period during both the winters of 2015-2016 and 2016-2017.

DO presence and CH_4 dynamics were intimately linked at both sites in SC Lake. At SC-ref, dissolved CH_4 concentrations increased after ice-cover, but only following DO depletion (Figure 4-8c). Following DO removal in February 2016, CH_4 increased at 0.8 $\mu M\ d^{-1}$ to a peak of ~50 μM CH_4 (Figure 4-8c). When $\delta^{13}C$-CH_4 values were high enough to be measured in winter 2015-2016, $\delta^{13}C$-CH_4 values had an increasing pattern. In the

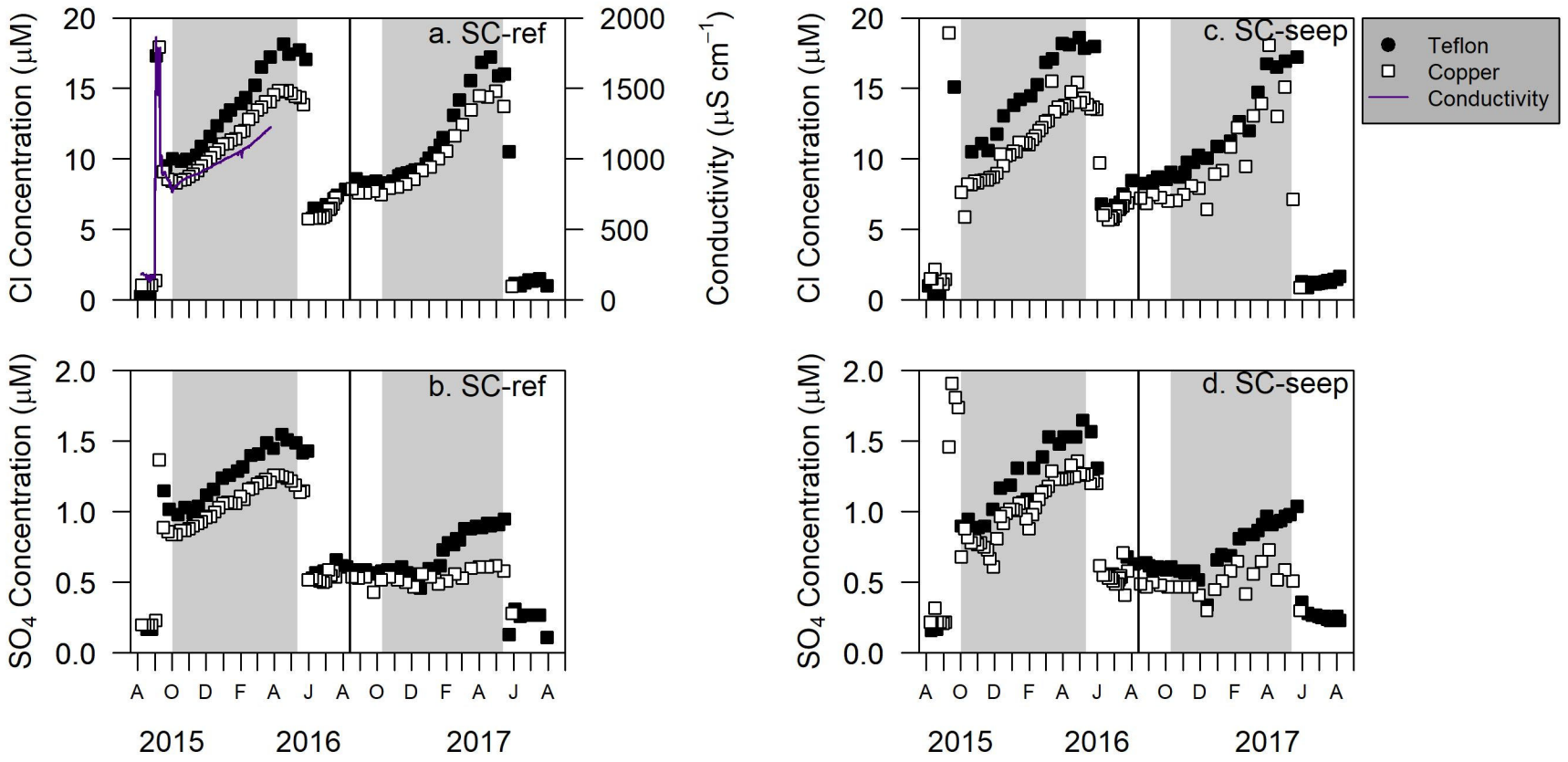

Figure 4-7. Comparison of Cl^- and SO_4^{2-} concentrations measured from lake water collected in Teflon and Copper tubing at SC-ref (a and b) and at SC-seep (c and d). Conductivity measured at SC-ref was used to match the Cl^- data for that site. Date assignments were made to the copper samples based on matching the concentrations of Cl^- and SO_4^{2-} from Teflon coils. Gray shading indicates the periods of ice-cover.

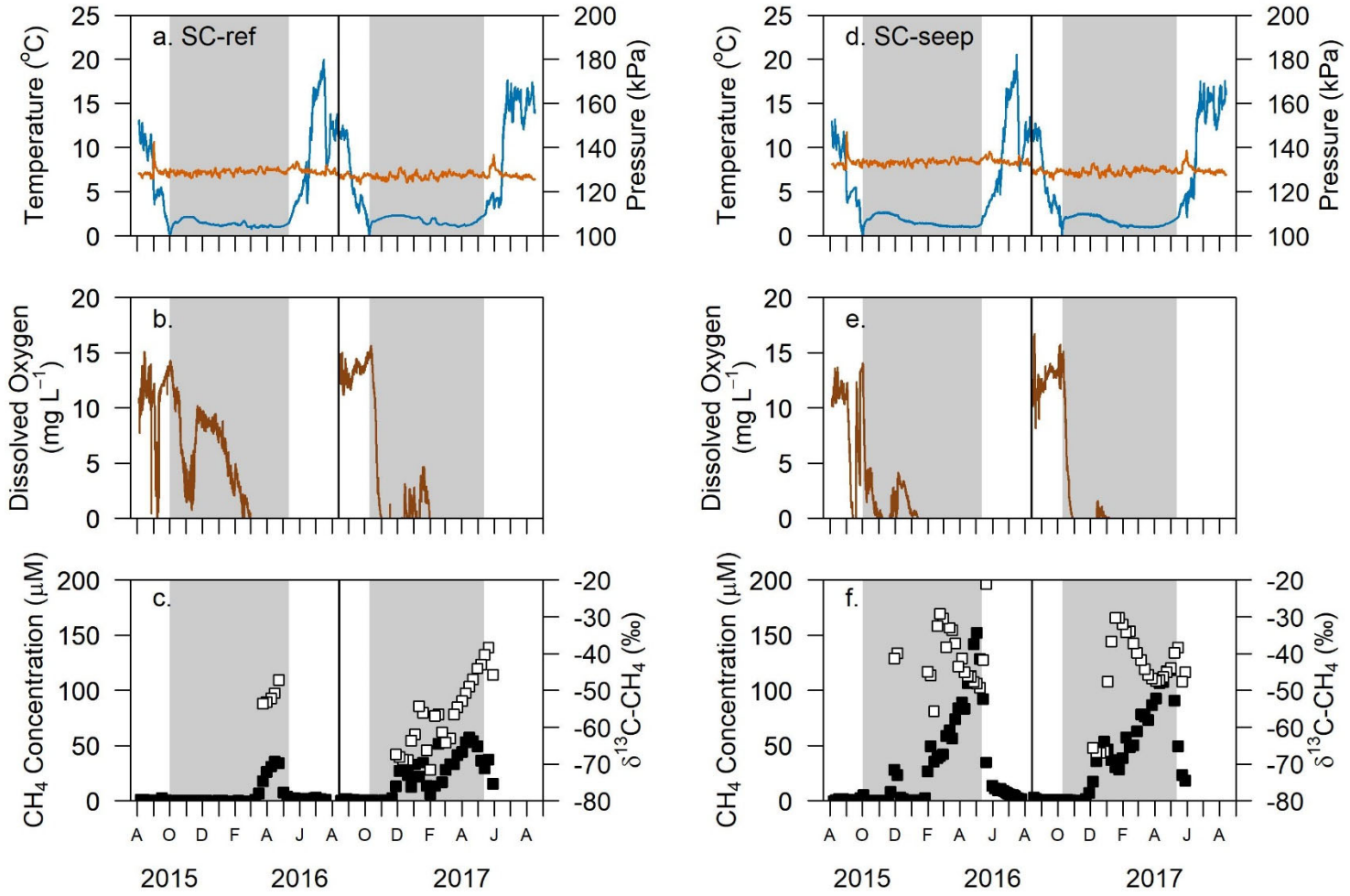

Figure 4-8. Lake characteristics and dissolved CH_4 changes during deployments of separate plastic crates in Swiss Cheese Lake at SC-ref and SC-seep from bottom water in 2015-2016. a, d) temperature (blue line) and pressure (orange line), b, e) dissolved oxygen (brown line), and c, f) dissolved CH_4 concentration (black squares, left y-axis) and $\delta^{13}C$-CH_4 values (white squares, right y-axis) measured by CRDS. Vertical black lines indicate when the second deployment began on 13 August 2016. Gray shading indicates periods of ice-cover.

winter of 2016-2017, DO was quickly exhausted following development of ice over and at that time CH_4 began to increase. Sporadic venting events increased DO concentrations in the bottom water briefly in the winter of 2016-2017 and were followed by CH_4 decreases (Figure 4-8).

Under-ice $\delta^{13}C$-CH_4 values at SC-ref were initially ~-68‰ in November and December 2016 and then rose to ~-55‰ in January 2017. Following a brief period of $\delta^{13}C$-CH_4 variability early in 2017, $\delta^{13}C$-CH_4 values increased until ice melt. The increase in $\delta^{13}C$-CH_4 values occurred both as CH_4 concentrations increased to a maximum in mid-April 2017 and continued as CH_4 concentrations decreased prior to ice_melt. Then during open water dissolved CH_4 concentrations were low at SC-ref (e.g. 2016, mean ± standard deviation, 1.4 ± 0.8 μM CH_4).

At SC-seep following ice-cover development, DO was quickly exhausted under ice both in winter of 2015-2016 and winter of 2016-2017. Once DO was gone, CH_4 concentrations increased and $\delta^{13}C$-CH_4 increased rapidly (Figure 4-8). The rate of CH_4 concentration increase was 160 μM d^{-1} in January 2016 and similar in the winter of 2016-2017 at SC-seep resulting in higher under-ice CH_4 concentrations at SC-seep (maximum ~150 μM CH_4) than at SC-ref both winters (Figure 4-8f). Otherwise during both winters in January-February $\delta^{13}C$-CH_4 values reached a maximum at ~-30‰, signifying significant influence by thermogenic CH_4 (Whiticar, 1990) and were followed by a near linear decrease in $\delta^{13}C$-CH_4 values during the middle of the winter, from February to April (Figure 4-8f). The decrease in $\delta^{13}C$-CH_4 values occurred as dissolved CH_4 concentrations were still increasing. Another reversal in $\delta^{13}C$-CH_4 values occurred during the winter of 2016-2017 and $\delta^{13}C$-CH_4 values increased from April 2017 until

ice-melt. Once ice-melt occurred in 2016, CH_4 concentrations decreased from 150 to 14 µM CH_4 over a month and $\delta^{13}C$-CH_4 values increased to -21‰.

4.3.6. Isotope Mass Balance

The isotope mass balance identified that the SC-ref site had a greater proportion of CH_4 from microbial CH_4 than the SC-seep site (Figure 4-9). Methane at SC-ref consisted of 21 to 100% microbial CH_4 while SC-seep CH_4 was 0 to 93% microbial in origin, with the remainder being thermogenically sourced. Both sites had the highest microbial contribution in the early ice-cover period. The thermogenic CH_4 source at SC-seep was greatest in late-February 2016 and late-January 2017 and increased at SC-ref during the ice-cover period both winters. Overall, the mass balance indicated that the ebullition seen at SC-seep of primarily thermogenic origin took longer to influence the SC-ref site.

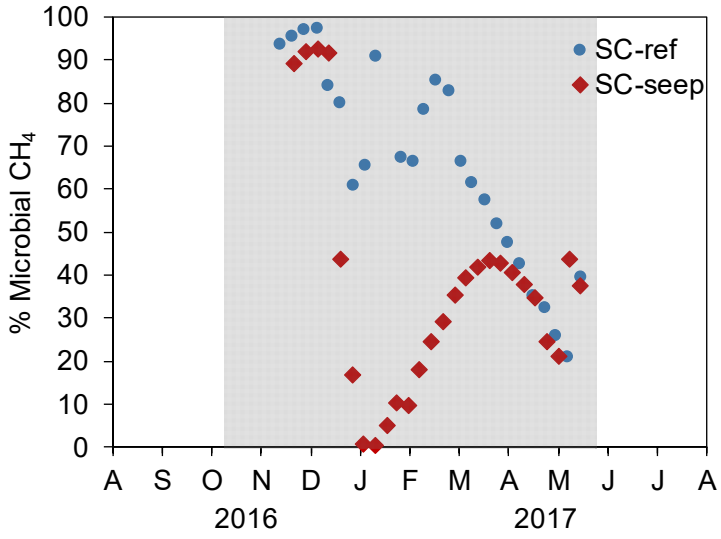

Figure 4-9. Microbial CH_4 source contribution changes in 2016 to 2017 at SC-ref (blue circles) and SC-seep (red diamonds). Thermogenic CH_4 source contributions are the inverse of microbial CH_4 contributions shown in this figure.

4.4. Discussion

This multi-lake study was conducted with stable carbon and radiocarbon isotopes to decipher the source of CH_4 emitted to the atmosphere from lakes and seeps in the Mackenzie Delta. I hypothesized that there would be differences in CH_4 source based on the lakes' location in the delta. These hypotheses were: 1) lakes in the outer delta would have primarily thermogenic CH_4, 2) lakes in the central delta would have primarily microbial CH_4 with CH_4 age related to their connection to the Mackenzie River, and 3) lakes exhibiting thermokarst enlargement would have permafrost carbon incorporated into the CH_4 present. The results of this study show that not all lakes in the central or outer delta regions had the same sources of CH_4. For instance, while there is thermogenic CH_4 present in some lakes in the outer delta, not all lakes have a thermogenic CH_4 source. Similarly while there was aged CH_4 in some of the lakes in the central delta, it is likely a function of their connection to the Mackenzie River rather than permafrost carbon incorporation, since the thermokarst lakes had the youngest dissolved CH_4. The whole-lake CH_4 dataset from Swiss Cheese Lake shows a dynamic link between DO and CH_4 concentrations, and following DO exhaustion, shows the interplay between diffusive, microbial CH_4 and ebullitive, thermogenic CH_4 sources and the influence of under-ice mixing. Overall, for lakes in the Mackenzie Delta surface water dissolved CH_4, emitted as a diffusive flux to the atmosphere, was modern, and CH_4 released from gas bubbles was formed from significantly older carbon.

4.4.1. Modern CH_4 Diffuses to Atmosphere While Ancient CH_4 is Lost Via Bubbling

Airborne surveys conducted in 2012 and 2013 found low CH_4 fluxes to the atmosphere across most of the Mackenzie Delta (Kohnert et al., 2017). An exception was

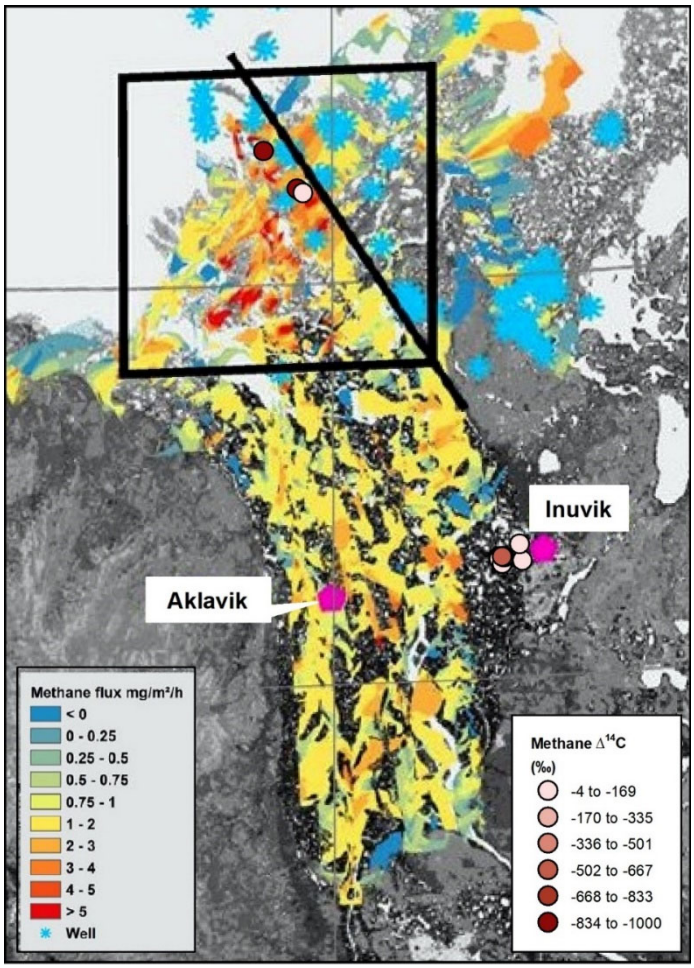

Figure 4-10. Comparison of the atmospheric CH_4 flux across the Mackenzie Delta and $\Delta^{14}C$-CH_4 (‰) from lakes and channels measured on dissolved CH_4 and bubble CH_4 samples. The $\Delta^{14}C$-CH_4 data from this study are overlaid on CH_4 fluxes to the atmosphere from Figure 2 in Kohnert et al. (2017). Black box and line are from original figure.

in the outer delta where large swaths had CH_4 emissions >5 mg m^{-2} hr^{-1} observed (Kohnert et al., 2017). The lakes I studied in the central delta near Inuvik bordered on the region of low atmospheric CH_4 flux found by Kohnert and colleagues (2017; background map in Figure 4-10). Surface water CH_4 concentrations were higher than equilibrium and indicate my study lakes were sources of CH_4 to atmosphere in late-summer (Table 4-1). The highest surface water concentration was at Lake 520 and represents a 1.0 mg m^{-2} hr^{-1} atmospheric flux (McIntosh Marcek et al., *Submitted*). This diffusive flux is below the cutoff used by Kohnert et al. (2017) of 5 mg m^{-2} hr^{-1} that delineates a modern, microbial CH_4 source rather than a geologic CH_4 source. Since all of the central delta study lakes have diffusive fluxes that fall below the threshold (Table 4-2), they were expected to have modern, microbial CH_4 fluxes (Kohnert et al., 2017). My $\delta^{13}C$-CH_4 and $\Delta^{14}C$-CH_4 data suggest that lakes in the central delta in late-summer are all sources of CH_4 to the atmosphere of near-modern origin with a majority of the CH_4 oxidized before it could be

released as an atmospheric flux. Hence, most lakes in the central Mackenzie Delta have a low flux of microbial, modern CH_4 to the atmosphere (Figure 4-10).

Within lakes in the central delta near Inuvik, winter-time CH_4 exhibits $\delta^{13}C$-CH_4 consistent with a microbial CH_4 source, such as in Lake 79a (Figure 4-3) and Lake 520 (McIntosh Marcek et al., *Submitted*). Microbially produced CH_4 dissolved in surface water was near-modern, while the bubbles collected from Lake 79a were significantly older (Figure 4-3). This follows what has been observed in Alaskan lakes with bubbles being ^{14}C depleted compared to dissolved or background CH_4 (Elder et al., 2019). Bubbles collected from Lake 79a suggest a mixture of modern carbon and aged permafrost or a single carbon source with a $\Delta^{14}C$-CH_4 value of ~-500‰, such as Mackenzie River POC. Lake 79a is a low closure lake with a regular connection to the Mackenzie River. During the ice-free season in 2016 Lake 79a was connected to the Mackenzie River for 145 days and in 2017 for 102 days. Therefore, I expect the Lake 79a sediments to contain large amounts of fluvial material, and the lower light levels limit the biomass of modern macrophyte biomass present (Marsh et al., 1999; Squires & Lesack, 2003). Mackenzie River particulate organic carbon transported into Mackenzie Delta lakes has a $\Delta^{14}C$ of -547 to -614‰ (McClelland et al., 2016). The similarity in POC values to the Lake 79a bubbles supports the primary carbon to microbes being fluvial sediments, though it is possible multiple carbon sources were integrated by methanogens including thawed permafrost carbon. From Lake 79a, it appears some lakes in the central delta have bubble fluxes of a microbial source, but are of older age.

The study lakes in the outer delta are within the region of highest atmospheric CH_4 fluxes found by Kohnert and colleagues, which they assumed were due to geologic

CH_4 fluxes from CH_4 concentrations (Figure 4-10, Kohnert et al., 2017; Kohnert et al., 2018). Bubbles collected at Seep 7 and SC-seep were relatively enriched in ^{13}C and radiocarbon-dead CH_4 and indicate the CH_4 bubbles at the bubble seep sites are comprised of geologic CH_4 formed by thermogenic processes (Figure 4-3). The $\delta^{13}C$-CH_4 time-series at SC-seep support the elevated CH_4 concentrations from bubbles in SC Lake being from thermogenically formed CH_4 (Figure 4-8f). Both Seep 7 and SC-seep are to the west of the middle Channel, where the thinner permafrost (<50 m) provides pathways of least resistance and is apparently more permeable as compared to thicker permafrost to the East (Kohnert et al., 2017). Our data confirm that regions of high CH_4 flux in the Mackenzie Delta are releasing geologic CH_4 of thermogenic origin (Figure 4-10).

It was expected that the outer delta was dominated by thermogenic CH_4, but surprisingly Manta Lake, very close to SC Lake, was observed to be releasing modern CH_4 (Figure 4-3). Manta Lake had no bubbles, however, and very low dissolved CH_4 during open-water (Table 4-2) and winter (Appendix 3 Figure S3-5), so its contribution to the atmosphere is small. Late-summer sampling of Manta Lake revealed $\delta^{13}C$-CH_4 values that were enriched in ^{13}C, although a microbial vs. thermogenic source determination cannot be made with the $\delta^{13}C$-CH_4 values because CH_4 oxidation could have significantly altered the CH_4 at that time of year (Cadieux et al., 2016). Instead, the $\Delta^{14}C$-CH_4 data showed CH_4 in Manta Lake was produced from modern carbon precursors and is similar to SC-ref in the summertime (Figure 4-3). The $\Delta^{14}C$-CH_4 analysis from Manta Lake shows that CH_4 released in the outer delta is not solely influenced by thermogenic seeps. While the outer delta has large thermogenic CH_4 reserves, they are only released to the atmosphere where permeable conduits are available, such as below relatively warm lakes

and channels (Burn and Kokelj, 2009). Not all water bodies have these conduits, as is evident from the data observed at Manta Lake. Some of the outer delta lakes have CH_4 produced primarily from methanogenesis of modern carbon and also emit much less CH_4 to the atmosphere (Table 4-2).

The results of near-modern dissolved CH_4 and aged CH_4 in gas bubbles are not unique to Mackenzie Delta lakes (Figure 4-11). In fact, in seven of 29 Arctic Alaskan lakes sampled by Elder et al. (2018), surface water dissolved CH_4 was modern, particularly within lakes with glacial and fluvial sediments. The median dissolved $\Delta^{14}C\text{-}CH_4$ of all 29 Alaskan lakes that Elder et al. (2018) studied was -80‰, very similar to the median dissolved $\Delta^{14}C\text{-}CH_4$ of -85‰ for the Mackenzie Delta lakes in this study.

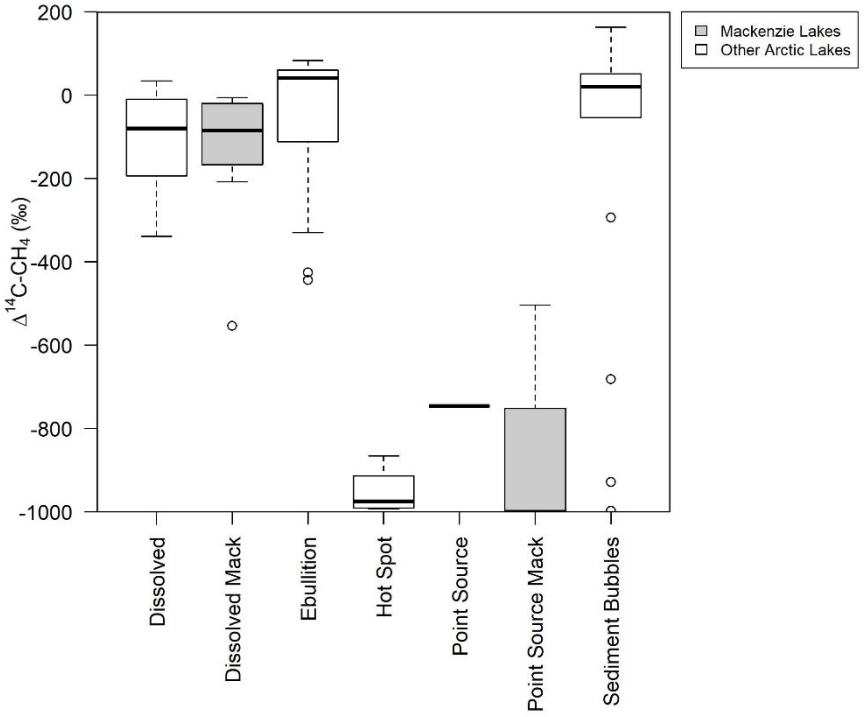

Figure 4-11. Comparison of $\Delta^{14}C\text{-}CH_4$ from Arctic lakes and their migration pathway (dissolved, ebullition, hot spot, point source, and surface sediment bubbles). Dissolved Mack and Point Source Mack in gray boxes indicate dissolved CH_4 and gas bubbles, respectively, collected from Mackenzie Delta lakes in this study. Other Arctic lake $\Delta^{14}C\text{-}CH_4$ data are in white boxes from Bouchard et al. (2015), Dean et al. (2018), Elder et al. (2018), Nakagawa et al. (2002), Martens et al. (1992), Negandhi et al. (2013), Walter et al. (2008), Walter Anthony et al. (2012), and Zimov et al. (1997).

Similarly, sediment bubbles that were extracted by disturbing the sediments in multiple studies were modern (median = +20‰, Figure 4-11; Martens et al., 1992; Nakagawa et al., 2002; Negandhi et al., 2013; Walter

et al., 2008; Zimov et al., 1997). The youngest sediment bubbles had $\Delta^{14}C\text{-}CH_4$ of +163‰ in Eastern Siberian alasses (Nakagawa et al., 2002) and the oldest bubbles had $\Delta^{14}C\text{-}CH_4$ of -998‰ from lakes in the Kolyma River basin (Zimov et al., 1997). As shown in Figure 4-11, the gas bubbling from hot spots and point sources is the oldest CH_4 released to the atmosphere. Within the Mackenzie Delta, the rapid bubbling observed at Seep 7, SC-seep, and Lake 79a is consistent with the range of $\Delta^{14}C\text{-}CH_4$ seen in other regions of rapid CH_4 bubbling where "hot spots" have been identified (Walter et al., 2008). While the number of lakes that have been studied (n= 83; Figure 4-11) is a small representation of the millions of lakes within the Arctic (Verpoorter et al., 2014), overall, fluxes of modern CH_4 to the atmosphere appear to be lower than the rapid release of old CH_4 emitted from bubble sites within northern lakes.

4.4.2. Sill height and River Connection Influence on Lake Dissolved CH_4 Trend

Lakes in the central delta near Inuvik had systematic differences in dissolved $\Delta^{14}C\text{-}CH_4$ that could be explained by sill height, but not as well by the duration of their connection to the Mackenzie River (Figure 4-6). Sill height represents a multi-year integrated impact of the Mackenzie River on the lakes, while the length of the Mackenzie River connection during the years the lakes were sampled represents individual years and does not represent the overall influence of the river on $\Delta^{14}C\text{-}CH_4$. The floods in 2015, 2016, and 2017 were intermediate (661 to 775 $m^2\ s^{-1}$; Station 10LC002, Water Survey Canada, https://wateroffice.ec.gc.ca/index_e.html) at peak flood discharge and occurred between 24 and 31 May, slightly earlier than normal (Lesack et al., 2013). These characteristics suggest that the Mackenzie River flooding for the years sampled were not extreme.

The Mackenzie River influences the composition of dissolved, sedimentary and particulate organic matter in the lakes near Inuvik (Gareis, 2018; Gareis & Lesack, 2017; Squires & Lesack, 2003; Tank et al., 2011). As lakes are connected to the river over longer periods, there is more aged sediment that is deposited on the lake bed (Marsh et al., 1999; McClelland et al., 2016). At the same time there is a greater contribution of modern DOC to the water column (Gareis, 2018). Alternatively for the lakes with shorter connections to the Mackenzie River the clarity of the water column increases as does macrophyte biomass (Squires et al., 2002; Squires & Lesack, 2003). Macrophytes are a modern source of labile carbon through their exudates and senescence of their plant biomass during the winter (Marcek McIntosh et al., *Submitted*; Tank et al., 2011). A higher sill height means more of the sediment organic carbon composition is from either the plants in the lake or allochthonous transport of plant organic matter surrounding the lakes (Hanson et al., 2011; Osburn et al., 2019). Transportation of pre-aged sediment and POC by the river, rather than modern riverine DOC, appears to strongly influence CH_4 produced in lake sediments and the incorporation of pre-aged organic carbon into CH_4 in lakes with longer connections to the Mackenzie River.

The positive relationship between sill height and $\Delta^{14}C\text{-}CH_4$ regresses at a sill height of 0 m to a $\Delta^{14}C\text{-}CH_4$ of -336‰, but the Mackenzie River $\Delta^{14}C\text{-}CH_4$ was -95‰ and -169‰ in 2016 and in 2017 (Figure 4-5). Therefore the measured relationship does not hold for lakes with a sill height of <3 m that are connected to the Mackenzie River for the majority of the ice-free season (Emmerton et al., 2007; Marsh & Hey, 1989). Those lakes, such as Lakes 129 and 80, have a $\Delta^{14}C\text{-}CH_4$ similar to dissolved CH_4 in the river surface water dissolved CH_4. While there were similarities in the $\Delta^{14}C\text{-}CH_4$ between

2016 and 2017 (p=0.92), the Mackenzie River and the lakes with a regular connection to the Mackenzie River exhibited large variability in $\Delta^{14}C\text{-}CH_4$ (Figure 4-5). McClelland et al. (2016) show variability in the $\Delta^{14}C$ POC of up to ±100‰ between 2004 and 2005 with younger POC being transported by the river later in the open water period. The large variability in $\Delta^{14}C\text{-}CH_4$ could come from interannual differences in the CH_4 and carbon transported by the river due to differences in rate of riverine discharge (4 August 2016: 191 $m^2\ s^{-1}$, 4 August 2017: 260 $m^2\ s^{-1}$), precipitation events within the watershed, and seasonal variability in nutrients (Emmerton et al., 2008; Gareis & Lesack, 2017; Lesack & Marsh, 2010).

Aged CH_4 in the central delta lakes could also be coming from the microbial incorporation of thawing permafrost. Allochthonous organic carbon sources such as thawing permafrost are present in large enough amounts to be detected in the DOC pool within central Mackenzie Delta lakes (Tank et al., 2011). Assuming permafrost carbon has an intermediate $\Delta^{14}C$ of -850‰ (Walter et al., 2008) and modern carbon from the last 20 years has an average $\Delta^{14}C$ of 50‰ (Turnbull et al., 2017), then at Lake 80, the Inuvik-region lake with the oldest dissolved CH_4, there would be less than 30% permafrost carbon incorporated into CH_4. As pointed out above, Lake 80 is strongly influenced by the Mackenzie River and is not considered to have active thermokarst processes. The two lakes in our study that are considered thermokarst lakes (Lakes 280 and 520) have some of the youngest CH_4 and, with the same assumptions for $\Delta^{14}C$ as above, as little as 5% comes from permafrost carbon (Figure 4-3). Macrophyte and autochthonous modern carbon sources are the primary precursor for CH_4 in these lakes (McIntosh Marcek et al., *Submitted*). This could be because the macrophyte carbon, such

as exudate, is highly labile and more rapidly utilized by microbes than the permafrost carbon that has been present for 10,000-30,000 years (Tank et al., 2011). While permafrost carbon is labile enough for CH_4 production in terrestrial tundra settings (Treat et al., 2015) and lakes extending into yedoma permafrost (Heslop et al., 2019), in lakes of the Mackenzie Delta other carbon sources appear to be preferentially consumed by methanogens.

4.4.3. Whole-Lake Perspective Shows Varying Impact of Thermogenic CH_4 Seep

The distinctive dataset at Swiss Cheese Lake allows us to connect what is seen in the surface water to what is occurring in the sediments and the flux of CH_4 into the water column. Different pools of CH_4 (dissolved and gas bubbles) were assessed to gain a whole-lake perspective on the migration and transport of CH_4 from a seep site (SC-seep) and reference site (SC-ref). The ^{14}C data show mixing of microbial and thermogenic sources that is examined through the year with the time-integrated year-round sampling. Figure 4-12 shows a conceptual model of the year-round whole lake perspective.

In late summer, since the water surface is ice-free, different processes affect CH_4 released at the SC-ref and SC-seep sites (Figure 4-12, top-left panel). Bubbles escape directly to the atmosphere at the bubble seep location. As the bubbles escape from the sediments and traverse through the water column, it is likely a small portion of the bubbles' CH_4 dissolves and enter the dissolved CH_4 pool (DelSontro et al., 2015; Delwiche & Hemond, 2017). Therefore, at SC-seep, bubbles released to the atmosphere emit ancient CH_4 formed by thermogenic processes and the diffusive efflux of CH_4 above the seep sites is a mixture of the background modern dissolved CH_4 pool and the

geologic-aged bubbles. Locations without seeps, like SC-ref, have dissolved CH_4 sourced directly from recently formed microbial CH_4 in the sediments.

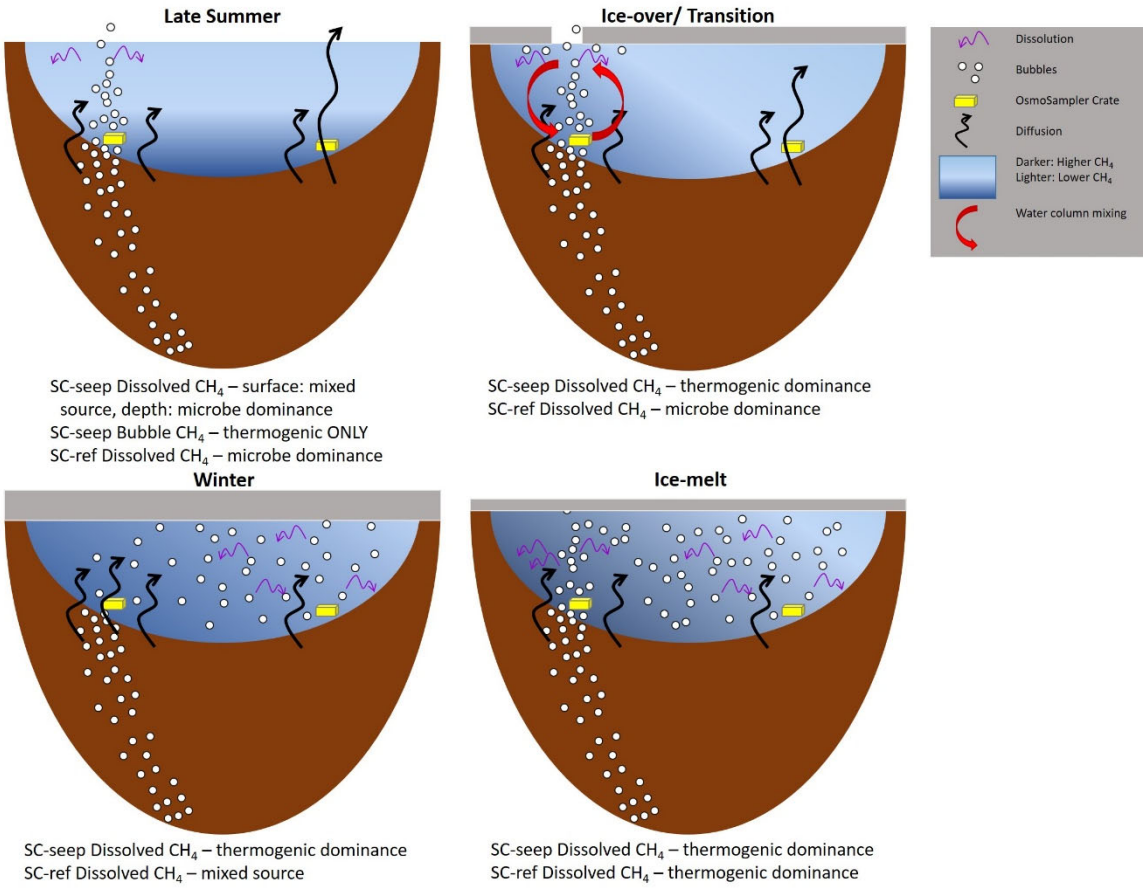

Figure 4-12. Diagram of CH_4 pathways of migration from sediments to surface water during summer, ice-cover/ transition, winter, and ice-melt in Swiss Cheese Lake. Top left panel (approximate months based on Figure 4-9) represents August to December, top right panel December to January, bottom left panel January to April, bottom right panel April to June. Ebullition is represented with white bubbles, while diffusion is represented as thick, black arrows. Bubble dissolution is identified with thin, purple arrows and the shade of blue indicates the amount of CH_4 present. Water column mixing during incomplete ice-cover are shown with red arrows.

Once ice begins to form in early winter, there is a transition period where there are holes in the ice from the seeps (Figure 4-12, top right panel). Elevated DO suggests that there was a connection between the water and the atmosphere late into the ice-cover period (Martinez-Cruz et al., 2015). These observations support what has been observed in other Arctic lakes with CH_4 "hotspots" during ice-cover (Elder et al., 2019; Walter et

al., 2006; Walter et al., 2008). The DO venting events to the bottom water provide evidence that SC Lake does not completely ice-over even though bottom water temperatures decrease, until February or March (Figure 4-8a, 4-8d). Between these DO venting events, bottom water CH_4 concentrations increased, possibly as the ice formed over the CH_4 seep holes, and the CH_4 was trapped under the ice (Figure 4-12, top right panel). Higher dissolved CH_4 concentrations during ice-cover is consistent with other Arctic lakes (Cunada et al., 2018; McIntosh Marcek et al., *Submitted*, Sepulveda-Jauregui et al., 2015; Townsend-Small et al., 2017). As seep bubbles are trapped under the ice, they dissolve into the water column at the ice-water interface (Greene et al., 2014). Methane from thermogenic bubble dissolution at the ice-water interface mixes to the SC-seep bottom water sampler during DO venting events (Figure 4-8). As DO from the atmosphere is brought to the bottom water of SC Lake from water column mixing so is dissolved CH_4 from bubble dissolution at the ice-water interface. Wind induced mixing through holes in the ice or under-ice mixing could contribute to water column mixing (Vachon et al., 2019; MacIntyre et al., 2018). Both an increase in CH_4 concentration and rapid increase in $\delta^{13}C\text{-}CH_4$ to ~-30‰ point to a thermogenic source influencing SC-seep between December and January. This is consistent with the bubbles collected at SC-seep in open-water being radiocarbon-dead and produced by thermogenic processes (Figure 4-3). Water column mixing brings CH_4 of primarily thermogenic origin to the bottom water, which leads to a minima of the microbial contribution to the CH_4 at SC-seep (Figure 4-12, top right panel).

As the winter progresses, there is a shift toward more microbial CH_4 at SC-seep and more thermogenic CH_4 at SC-ref (Figure 4-12, bottom left panel). This could be due

to the gas bubbles from SC-seep no longer escaping from the sediments as the ice thickness increases during the ice cover period as shown in Figure 4-12. This may be similar to the effects of flood of the tides in coastal locations (Chanton et al., 1989) or increases driven by atmospheric pressure (Casper et al., 2000). The thicker ice may inhibit thermogenic bubbles from escaping into the water-column due to hydrostatic pressure increases and the primary source of CH_4 shifts to microbial CH_4 diffusion during the part of the winter with the thickest ice-cover. Even as the SC-seep appears to shift toward increasing microbial methanogenesis between February and April 2017, there was a higher CH_4 concentration than at the non-seep site, SC-ref, because of proximity to the seep (Figure 4-12).

SC-ref has CH_4 primarily of thermogenic origin by the end of ice-cover, which likely occurs due to under-ice mixing of CH_4 from SC-seep and dissolution of bubbles containing thermogenic CH_4 (Figure 4-12, bottom right panel). During early "ice-melt", SC-seep and SC-ref $\delta^{13}C$-CH_4 values indicate that both sites had CH_4 of primarily thermogenic origin. This suggests there is fairly substantial under-ice mixing, since the CH_4 source composition was so drastically different just a few months prior between the two sites (Figure 4-9). Ultimately, once SC Lake is completely iced-over the under-ice pool of CH_4 is a mixture of both diffusive and ebbulitive CH_4 sources that changes depending on ice-depth (Elder et al., 2019). The high temporal resolution of the SC Lake CH_4 and $\delta^{13}C$-CH_4 dataset provides a view of processes occurring under-ice, as shown in Figure 4-12, that have not been captured before in a lake with a gas bubble seep.

4.5. Further Analysis for Manuscript Publication

In the comparison of $\delta^{13}C\text{-}CH_4$ values between the CRDS and IR-MS, I stated the importance of water vapor for the CRDS instrument. While all attempts were made to keep water vapor concentrations low for the samples analyzed, it is important to have that amount quantified. Future work should include finding the apparent water vapor contribution data for samples that were analyzed and presented here to make sure they fall below the 2.5% water vapor cutoff.

In the $\delta^{13}C\text{-}CH_4$ isotope mass balance presented here, $\delta^{13}C\text{-}CH_4$ values of -30‰ and -70‰, for microbial and thermogenic CH_4 sources, respectively, were used. These were based on peak $\delta^{13}C\text{-}CH_4$ for the thermogenic end-member and sediment $\delta^{13}C\text{-}CH_4$ for samples collected at SC-seep for the microbial end-member. A sensitivity analysis is needed to see how changes in source $\delta^{13}C\text{-}CH_4$ values modify the proportion of CH_4 from the two sources. While these quantitative data analyses are outside the scope of this chapter, the results and discussion above lead to a schematic conceptual of diffusive transport of methane to the atmospheric versus ebullition. Further data analysis will likely enhance understanding of Swiss Cheese Lake's CH_4 sources and sinks.

4.6. Conclusion

This study verifies the outer delta's high CH_4 fluxes most likely originate from geologic seeps and the associated CH_4 is produced by thermogenic processes. By contrast, diffusive release of microbially produced CH_4 is mostly from near-modern carbon sources. For lakes in the central delta, the primary carbon sources used for CH_4 production are near-modern. Lake 79a with the CH_4 bubble seep in the middle delta had

the oldest CH_4 age of nearby lakes, due to methanogens using deeper lake sediments that are slightly older than those currently transported by the Mackenzie River. There is not strong evidence to suggest that thawed permafrost carbon is being incorporated into CH_4 and producing a significant diffusive CH_4 flux out of Mackenzie Delta lakes. In SC Lake, the interplay between diffusive and ebullitive CH_4 sources produces a pool of CH_4 during the ice-cover period of mixed origin. Similarly, during open-water, as the bubbles travel upwards in the water column a minimal amount dissolves into the surrounding water, and most evades to the atmosphere.

4.7. Acknowledgements

Field assistance for this project came from Mitchell Bergstresser, Michelle Côté, Trevor Fournier, Kim Geeves, Roger MacLeod, Nilou Rajaei, and the staff at the Aurora Research Institute. Sample analysis at Chesapeake Biological Lab would not have been possible without the help of the Lapham Biogeochemistry lab members: Aimee Beardmore, Jessica Loveless, Mary Oster, and Maureen Strauss. This chapter benefitted from collaborations with Ann McNichol, Scott Dallimore, Lance Lesack, Beth Orcutt, C. Geoff Wheat, Jeff Chanton, and Laura Lapham. Financial support came from an American Geophysical Union Horton Research Grant (HAMM), a Geological Society of America Research Grant (HAMM), a Presidential Fellowship from the University of Maryland Center for Environmental Science (HAMM), a Dissertation Fellowship from the University of Maryland (HAMM), and National Science Foundation Grant PLR-1416961 (LLL).

Chapter 5

Conclusions & Future Work

Global CH_4 concentrations are increasing and this work is an attempt to understand one of the sources contributing to that increase, Arctic lake emissions. In order to do this, I focused on lakes within the Mackenzie Delta. Prior work on CH_4 distributions in Mackenzie Delta lakes by Cunada et al. (2018) and Pipke (1996) provided a strong basis for my dissertation. This prior work examined lakes with discrete sampling of the under-ice and open-water periods across a wide extent of the Mackenzie Delta and found that the length of lake connections to the Mackenzie River drives CH_4 concentrations and fluxes. In my dissertation, I provide high temporal resolution of dissolved CH_4 concentrations and $\delta^{13}C\text{-}CH_4$ in multiple lakes to understand sources of dissolved CH_4 and processes affecting diffusive CH_4 release. I revisited three of the same lakes – Lakes 280, 56, and 520 (Chapters 2 and 3) – and further expand our knowledge of outer delta lakes through Swiss Cheese Lake (Chapter 4).

This was the first time OsmoSamplers were utilized to collect water samples from multiple lake systems in the Arctic. The unique nature of these dissolved CH_4 concentration and $\delta^{13}C\text{-}CH_4$ datasets allows nearly weekly assessment of dissolved CH_4 changes in bottom water in Mackenzie Delta lakes. These data provide insights into CH_4 processes occurring during dynamic periods of the year, such as ice-cover and ice-melt, which are not traditionally sampled.

One clear result from this work is that dissolved CH_4 concentrations are highly linked to dissolved oxygen concentrations, and other electron acceptors in seasonally ice-covered lakes, as shown in Chapters 2 and 4. Oxygen comes into these lakes through a connection between the lake water and the atmosphere by diffusion and mixing. Dissolved oxygen presence provides methanotrophs electron acceptors to oxidize CH_4 as noted by higher $\delta^{13}C\text{-}CH_4$ (^{13}C enriched) values during open water than under ice-cover. One limitation is that while the $\delta^{13}C\text{-}CH_4$ data was used to calculate MOx rates, α_{ox} has not been measured in the water column of Mackenzie Delta lakes. Choosing an α_{ox} for the calculations left some uncertainty in the MOx rates I provide because published rates of α_{ox} are variable. Once the Mackenzie Delta lakes are ice-covered, the connection between the lake and atmosphere becomes limited, and aerobic respiration removes dissolved oxygen. This allows CH_4 to be retained in the water-column. The extent of the dissolved CH_4 increase during the ice-cover period was greater in the central delta lakes where sediment organic matter quality is likely higher due to inputs of seasonal macrophyte-derived carbon (Chapters 2 and 3). Whereas, in the outer delta lake, the dissolved CH_4 concentrations did not get as high, both due to an extended dissolved oxygen presence during winter and thermogenic CH_4 bubbles having a larger water volume to dissolve in SC Lake. Dissolved CH_4 concentrations increased in the study lakes until ice-melt and the Mackenzie River spring flood.

Another topic highlighted in my work is that while dissolved CH_4 concentrations are high in the winter and low during the summer, not all lakes show rapid evasion from the bottom water following ice-melt, as shown in Chapters 2 and 3. Lake depth influences whether there is a rapid loss of dissolved CH_4, such as in shallow lakes, or if

winter-derived CH_4 persists. In deeper systems, the flux to the atmosphere and MOx are limited by diffusion rather than advective mixing. Water column mixing is delayed until the later open-water period in deeper lakes. Thereby, lake depth affects the connection of bottom water CH_4 to surface waters where it is released as a flux to the atmosphere.

Lake depth also influences the hydrologic connections of lakes. Not all lakes in the Mackenzie Delta are evaporative basins. Some are, such as Lake 56, but others show groundwater contributions. The deeper delta lakes have a contribution during open-water from groundwater. While groundwater connections have been noted in other Arctic systems with permafrost present, this is the first time this has been shown in Mackenzie Delta lakes. While remote sensing has shown that there are ~45,000 lakes in the Mackenzie Delta and provided their surface area, lake depth is not well known for most. As lake depth appears to influence hydrologic and dissolved CH_4 processes, it is important that lake bathymetry be measured and is taken into account during future studies.

The timing of ice formation and ice-melt and/or Mackenzie River spring flood are critical influences on the concentration increase of dissolved CH_4 in the delta lakes during winter. If ice-melt occurs later, then CH_4 concentrations will have more time to increase and will be higher. Higher CH_4 concentrations lead to a greater flux of CH_4 to the atmosphere and are a positive feedback for climate change. In contrast, if ice-melt occurs earlier, dissolved CH_4 concentrations will be lower and will be a negative feedback to climate change.

Finally, the novel $\Delta^{14}C$-CH_4 measurements in this dissertation provide new insights into CH_4 sources in Mackenzie Delta lakes (Chapter 4). To begin with, the region

of high CH_4 flux in the Mackenzie Delta is where radiocarbon-dead, thermogenic CH_4 was measured in rapidly evading gas bubbles. I am able to confirm prior hypotheses that CH_4 seeps in the outer delta are of geologic origin, specifically thermogenically produced CH_4. Additionally, I add to the increasing body of knowledge on dissolved $\Delta^{14}C\text{-}CH_4$ in aquatic systems, showing that diffusive emissions from lakes in the Mackenzie Delta are near-modern and there is limited incorporation of old carbon by methanogens. In those lakes with a connection to the Mackenzie River, the CH_4 pool has significant inter-annual variability, but is dominated by pre-aged CH_4, possibly from the river. Overall, the $\Delta^{14}C\text{-}CH_4$ results corroborate that most of the 35 Gg CH_4 yr^{-1} atmospheric flux in the Mackenzie Delta is from a near-modern, microbial CH_4 source (Kohnert et al., 2017).

Future Work

While the work presented provides many answers to the biogeochemical cycling questions posed in the 'Introduction', particularly during the under-studied ice-cover period, there are still many questions remaining, such as: Are there differences in the rate of MOx during open-water between lakes based on either their closure class or another factor, such as depth? How representative are the lakes chosen in this study, e.g., are similar factors influencing CH_4 in lakes across the delta? What is the actual amount and $\Delta^{14}C\text{-}CH_4$ of CH_4 present in active layer and thaw bulb groundwater in lakes? And, how are the changes to the CH_4 pool reflected in CO_2 concentrations and stable carbon and radiocarbon isotopes? Below are some thoughts on future work that should be carried out to better understand the CH_4 dynamics within Mackenzie Delta lakes.

First, the importance of α_{ox} on CH_4 oxidation calculations, such as those following Chanton & Liptay (2000), cannot be under emphasized. Further work should be done within the lakes in the Mackenzie Delta to determine what the α_{ox} is for the lakes, if it changes during the open-water period, and what factors influence α_{ox} between lakes. Cunada et al. (2018) found the riverine connection had a significant impact on CH_4 production, and the extent of linkage to MOx would be helpful to improve future process knowledge. It is important to characterize the α_{ox} to constrain the mass balance model used in Chapter 2 and to improve the calculation of MOx to determine the influence MOx has on the reducing CH_4 fluxes from lakes in the Mackenzie Delta.

Second, in this dissertation I presented time-series data for four of the ~45,000 lakes in the Mackenzie Delta over a two-year period. In Appendix 3, I also provide time-series from a total of eight lakes in the delta including the central delta, outer delta, and two lakes in the northeastern outer delta on Richard's Island. More lake systems within the delta should be sampled year-round to see if what was observed in the nine lakes is consistent across the entire delta region. For instance, two high closure lakes were sampled, but one of them was a shallow lake (Lake 56) and the other a deeper, thermokarst lake (Lake 520). Future work would benefit from including another deep lake that does not exhibit thermokarst expansion as a comparison to these high closure lakes. Additionally, in the outer delta I showed that Swiss Cheese and Manta Lakes have different CH_4 sources and concentrations during ice-cover. Expanding to lakes overlying the thicker permafrost in the outer delta, but still in close proximity to the oil and gas reservoirs, would serve to show if thicker permafrost impacts thermogenic CH_4 release in a similarly heterogenous way. Since there was also no sampling in the southern delta or

in the Mackenzie uplands to the north of Inuvik– which are outside the delta but affected by a similar climate and thicker permafrost – these would be important locations to collect CH_4 and $\delta^{13}C\text{-}CH_4$ time-series to expand the regional extent of this work.

In other regions of the Arctic, e.g. Alaska along the Dalton Highway, there has been a concerted effort to increase the number of lakes being sampled, so that the interpretations being made are spatially accurate and inclusive (see Figure 1-2 for large lake studies). Research shows that many lake studies of CH_4 fluxes are subjected to limitations because they do not include enough spatiotemporal variability in CH_4 concentration changes (Wik et al., 2016a). An increased effort needs to be made not only at increasing the number of lakes sampled but also the amount of time that they are sampled. As shown in Lake 520, a mid-July CH_4 pulse to the atmosphere was noticed because I repeated the same kind of sampling Cunada et al. (2018) accomplished in 2014. The multi-year CH_4 data in this dissertation show that the patterns seen in the dissolved CH_4 concentrations are repeated over a two-year period.

Third, groundwater connections within deep lakes need to be verified and quantified in the Mackenzie Delta. Approaches that could be used to quantify lake-groundwater connections include radon or radium isotopes, $\delta D\text{-}H_2O$ and $\delta^{18}O\text{-}H_2O$, and $\delta D\text{-}CH_4$ analyses. Radon and radium gas are produced in groundwater as part of the U-Th decay series and elevated concentrations show rapid groundwater contributions, while $\delta D\text{-}H_2O$ and $\delta^{18}O\text{-}H_2O$ are distinct in groundwater sources compared to lake waters that have encountered evaporation. Another parameter to measure would be $\Delta^{14}C\text{-}CH_4$ in groundwater surrounding these lakes. In this dissertation, I assume that groundwater CH_4 has a ^{14}C-age similar to permafrost due to the incorporation of permafrost carbon, but

measuring groundwater $\Delta^{14}C\text{-}CH_4$ was outside the scope of my efforts. Quantifying the lake-groundwater interactions and CH_4 in groundwater will enhance our knowledge of the pathways by which dissolved CH_4 enters Mackenzie Delta lakes.

Finally, sampling of both dissolved CH_4 and gas bubbles, when gas bubbles are present, should be done to provide a whole-lake perspective from more lake systems. I presented $\Delta^{14}C\text{-}CH_4$ data for dissolved CH_4 and gas bubbles from one lake and $\Delta^{14}C\text{-}CH_4$ for only gas bubbles from two other sites. The gas bubble samplings presented here were opportunistic in nature, but further work to more widely sample bubbles should be made to gerneate $\Delta^{14}C\text{-}CH_4$ data for more than three locations in the delta. In addition, Elder et al. (2019) collected both CH_4 and CO_2 for $\Delta^{14}C$ analyses. This allowed the authors to follow CH_4 from production, oxidation, and evasion to the atmosphere. In particular, they were able to do a mass balance to show the proportion of CH_4 oxidized to CO_2 and emitted from the lake as CO_2. In the future, a $\delta^{13}C_{CH4}$ and $\delta^{13}C_{DIC}$ isotope mass balance will be performed for time-integrated samples collected from some of the Mackenzie Delta lakes to identify the proportion of CO_2 incorporated into CH_4 by CO_2 reduction during ice-cover and the amount of CH_4 that is converted to CO_2 by MOx during open-water. A study of $\Delta^{14}C\text{-}CH_4$ and $\Delta^{14}C\text{-}CO_2$ might be particularly insightful at SC Lake and Seep 7 to inform whether thermogenic CH_4 that dissolves out of gas bubbles is converted to radiocarbon-dead CO_2 by MOx.

Appendix 1

Supplemental Materials to Chapter 2

Text S1-1. Verifying Timing of OsmoSampler Samples

To capture a higher resolution record around the period of ice-out, a deployment was made from 21 March 2016 to 15 June 2016 with a copper Gas OsmoSampler and dissolved oxygen (DO) sensor. The faster flow OsmoSampler package had a 20-membrane (Alzet, 2ML1) OsmoPump to allow larger volumes of fluid, ~1.6 mL day^{-1} at 20°C (Jannasch et al., 2004), to be collected in a shorter period of time (Appendix 1 Figure S1-1c). Water depth at the location for the short deployment was 2.96 m. The sample intake collected water at 2.69 m (27 cm from sediments). The plastic crate was deployed through a hole cut through the frozen lake surface with an ice saw and recovered by small boat in open water. For the short deployed OsmoSamplers, temperature did not vary greatly (2.4 to 8.3°C), and time stamps were assigned by evenly distributing dates across the deployment period.

The dates of the long deployment were verified with the short deployment (Appendix 1 Figure S1-2). While CH_4 concentrations were slightly different between the short deployment at 2.69 m and the longer deployment at 2.90 m, the peak in CH_4 was within 9 days (2.69 m: 19 May 2016, 2.90 m: 28 May 2016). This assigns an error of ± 9 days for the dates associated with peak CH_4 concentrations at ice-melt. We are confident with the temperature-corrected date assignments for the 2.90 m depth because the dates

of peak CH_4 are similar between the two years (28 May 2016 at 848 μM and 29 May 2017 at 886 μM) (Appendix 1 Figure S1-6) and because of the similarity in the timing of peak CH_4 between the 2.90 m depth and the short deployment in spring 2016.

The CH_4 dates for the 2.90 m and 2.70 m water depths for the long deployment were assigned using a temperature correction rather than evenly distributing dates across the deployment period because bottom water temperatures at 2.90 m varied from 2 to 18ºC. The temperature correction was done following Gelesh et al. (2016) where bottom water temperatures were used to calculate the amount of water pulled into copper tubing each day. There is an offset in the peak CH_4 concentration between the 2.70 m and 2.90 m depths when dates were assigned with the temperature-correction. Despite the offset, the CH_4 concentrations were similar between the 2.70 m depth and the short deployment at 2.69 m prior to ice-melt (Appendix 1 Figure S1-2). There was no other way to verify the dates assigned using the temperature-correction because Cl^- and SO_4^{2-} concentrations were below the detection limit when analyzed on an ion chromatograph (ICS-1000) at Chesapeake Biological Laboratory. Therefore, Cl^- and SO_4^{2-} concentrations were not comparable between the OsmoSamplers concurrently collecting water into Teflon and copper tubing. Temperature-corrected date assignments for CH_4 data are verified by the similar CH_4 patterns seen between the two deployments at 2.90 m depth. We assume this dating is also appropriate for 2.70 m water depth. Any adjustment to the 2.70 m depth dates would result in an earlier increase in CH_4 concentrations and an earlier CH_4 peak, and would result in a poorer fit of the 1-D diffusion models and higher rates of water-column methanogenesis.

Since the CH_4 samples from the OsmoSampler time-series are integrative samples, they represent water collected over multiple days (i.e. time integrated). The middle date for each sampling period was assigned to the sample. As a result there is an uncertainty between 2 and 7 days on either end of the assigned date.

Text S1-2. Methane Oxidation Modeling

Results of modeling MOx rates were compared for two differing scenarios relative to changes in dissolved CH_4 concentrations observed at 2.90 m during open-water. During 2016, there were 15 time intervals where MOx rates could be derived from the observed changes in $\delta^{13}C$-CH_4 and paired with observed declines in dissolved CH_4 concentrations (Figure 2-3).

In Scenario (1), the α_{ox} value used in equation (2.9) was iteratively adjusted to obtain similar values between MOx rates versus observed declines in CH_4 for as many of the value-pairs as possible. With an α_{ox} of 1.020, 8 of the value-pairs (days 166, 172, 182, 186, 190, 194, 199, and 216) converged closely, yielding an average difference of only +1.4 μmol L^{-1} d^{-1} (CH_4 drop > MOx rate) and a maximum difference among the pairs of +4.5 μmol L^{-1} d^{-1} (CH_4 concentration decrease = 24.0 at that time point). On average, this scenario yields MOx rates slightly less than observed decreases in dissolved CH_4, with the difference inferred to be minor CH_4 dilution as a result of water-column mixing.

In Scenario (2), the α_{ox} value used in equation (2.9) was set to 1.011, which was the maximum value obtained in experimental MOx measurements with surface sediments from Lake 520 (Geeves, 2019). This yielded an average difference among the 8 value-pairs from scenario (1) of -8.6 μmol L^{-1} d^{-1} (CH_4 concentration decrease < MOx

rate) and a maximum difference among the pairs of -21.0 μmol L^{-1} d^{-1} (CH_4 concentration decrease = 17.7 μmol L^{-1} d^{-1} at that time point). On average, this scenario yields MOx rates substantially higher than observed decreases in dissolved CH_4, with the difference inferred to be substantial rates of (unmeasured) water-column methanogenesis.

Scenario (2) seems to be implausible because the rates of necessary methanogensis are too high relative to what was inferred to occur during the ice-cover period (Figure 2-6). However, the α_{ox} value in Scenario (1) could be too high and may overly limit the possibility of water-column methanogenesis. This issue is more fully dealt with in a subsequent mass balance comparison of all our observed and modeled processes, where MOx rates for all 15 time intervals are included. An α_{ox} of 1.020, as in Scenario (1), has also been found to be appropriate in other Arctic lake settings (Bastviken et al., 2002) and it is the best-fit for our dataset.

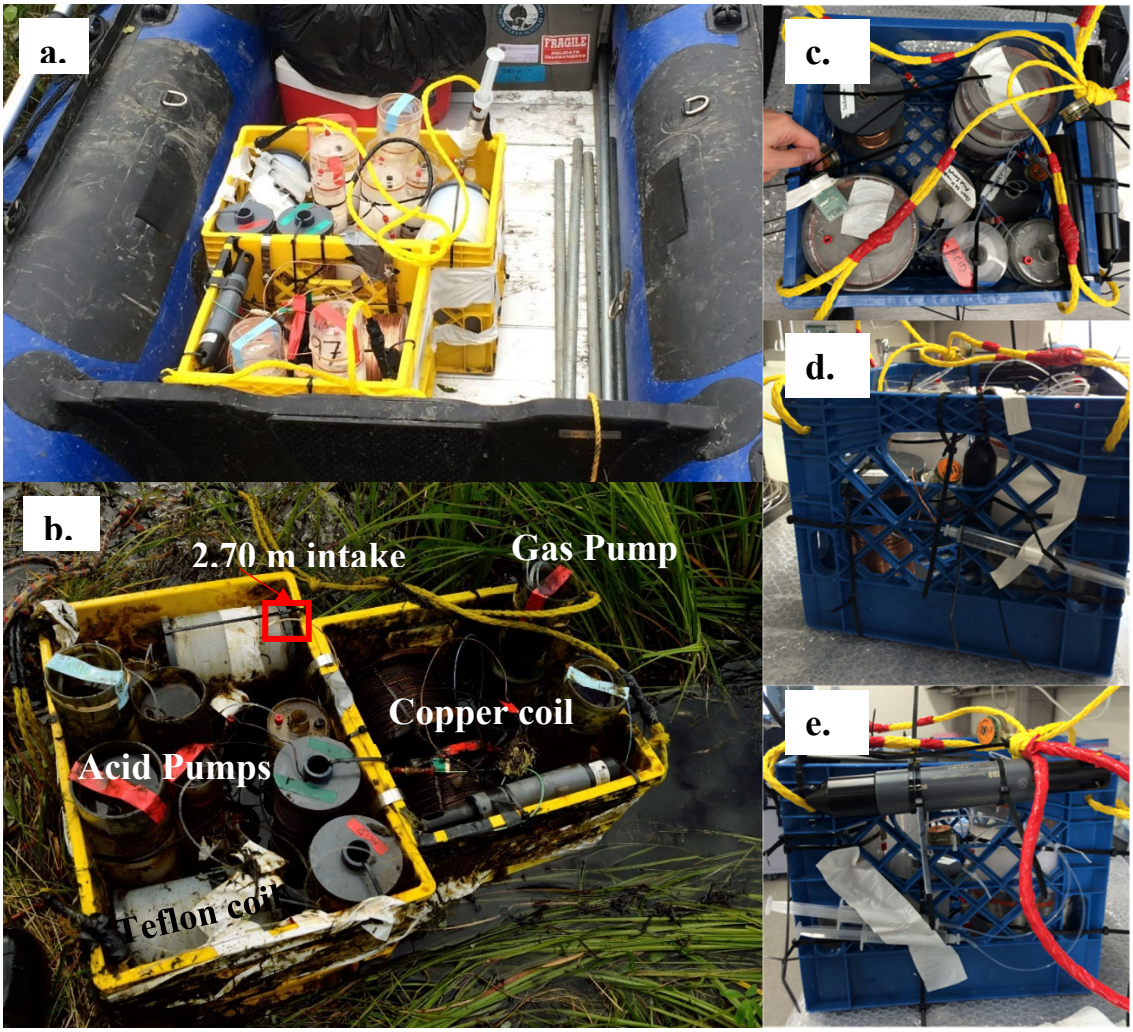

Figure S1-1. OsmoSampler packages a) prior to deployment in August 2015 at Lake 520, b) following retrieval in August 2016, and c, d, e) the fast flow package with 20 membrane pumps deployed from March to June 2016 in Lake 520 from the top and two different sides. Pictures courtesy of Beth Orcutt (a, c, d, and e) and Mitchell Bergstresser (b).

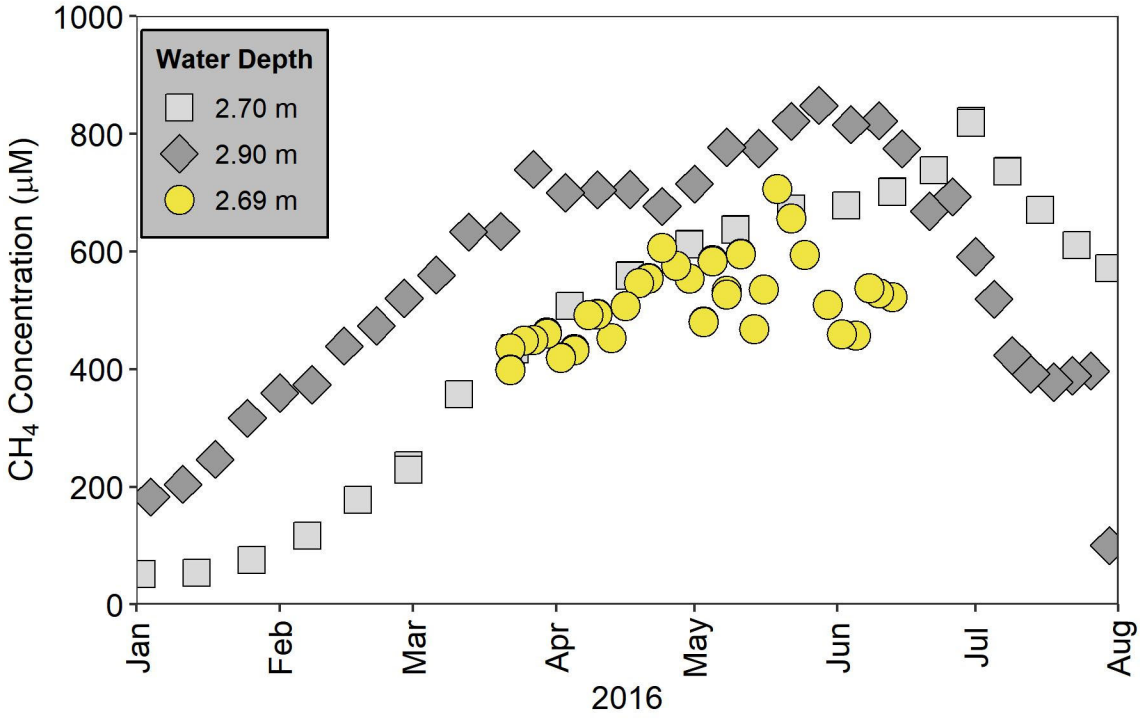

Figure S1-2. Dissolved CH_4 concentrations from January to August 2016 for Lake 520 for the short fast flow and year-long deployments. The short fast flow deployment was at 2.69 m water depth (yellow circles) and the longer deployment was at 2.70 m water depth (light gray square) and 2.90 m water depth (dark gray diamond). The timing of the peak CH_4 concentration at the 2.90 m (20 cm from the sediments) and 2.69 m (27 cm from sediments) water depths are within ± 9 days despite being placed in slightly different locations at the bottom of Lake 520. The peak at 2.70 m (40 cm from the sediments) was on 30 June 2016, and there is no reason to believe that the 2.70 m water depth dates are incorrectly assigned.

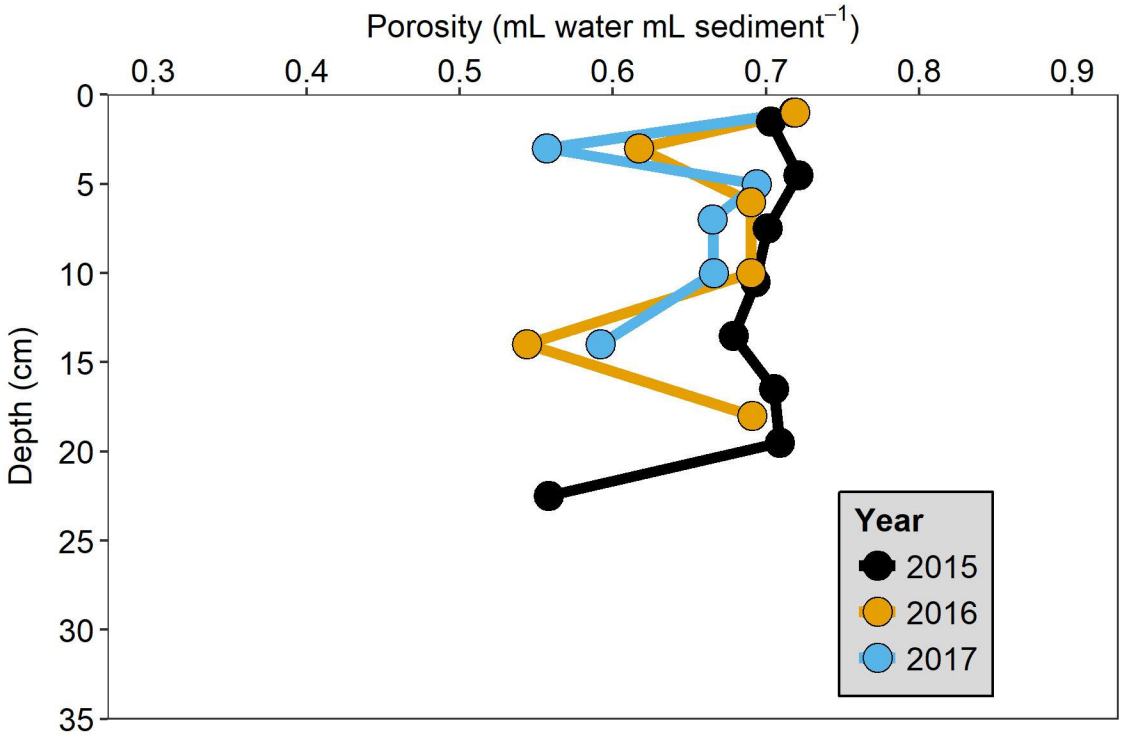

Figure S1-3. Measured sediment porosity (mL water mL sediment^{-1}) at Lake 520 in 2015 (black circles), 2016 (yellow circles), and 2017 (teal circles).

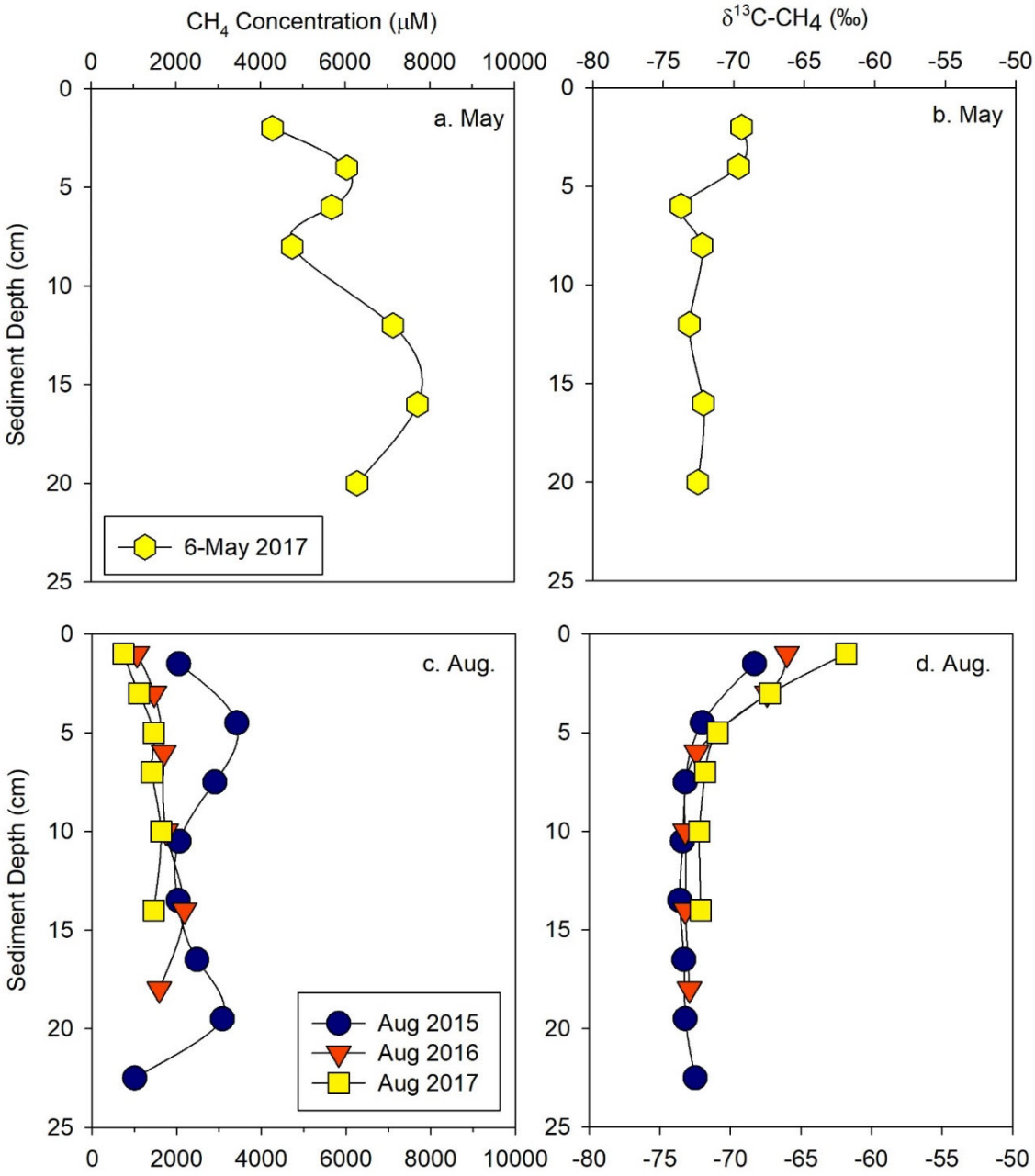

Figure S1-4. Sediment pore-water CH_4 concentration and $\delta^{13}C$-CH_4 under-ice and open-water. Under-ice sediment pore-water CH_4 concentration (μM) in May 2017 (a) and $\delta^{13}C$-CH_4 in May 2017 (b). Open-water early August sediment pore-water CH_4 (c) and $\delta^{13}C$-CH_4 (d) with 2015 in blue circles, 2016 in orange triangles, and 2017 in yellow squares. Variability in CH_4 concentrations between years could be due to the heterogeneous nature of sediment pore-water CH_4 in Lake 520, interannual variability, and spatial differences since the samples are not from exactly the same place each time.

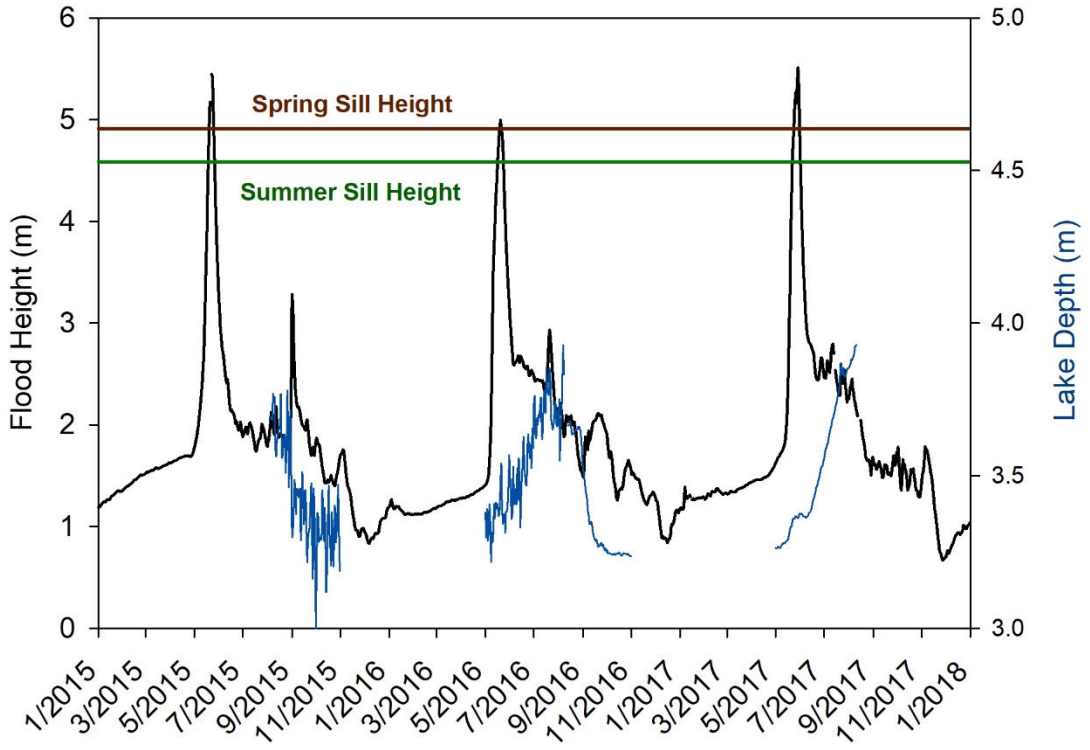

Figure S1-5. A comparison of the Mackenzie River flood height (black line) to the water depth (blue line) in Lake 520. Mackenzie River flood height was for the East Channel near Inuvik, NT, Canada (river height minus 10 m to account for the sea level contribution to the river height) from January 2015 through December 2017 (Station 10LC002, Water Survey Canada, https://wateroffice.ec.gc.ca/index_e.html). Spring sill height and summer sill height for Lake 520 are indicated in brown and green lines, respectively (Lesack & Marsh, 2010). Lake depth is presented for the periods that could be affected by water level changes (May to November).

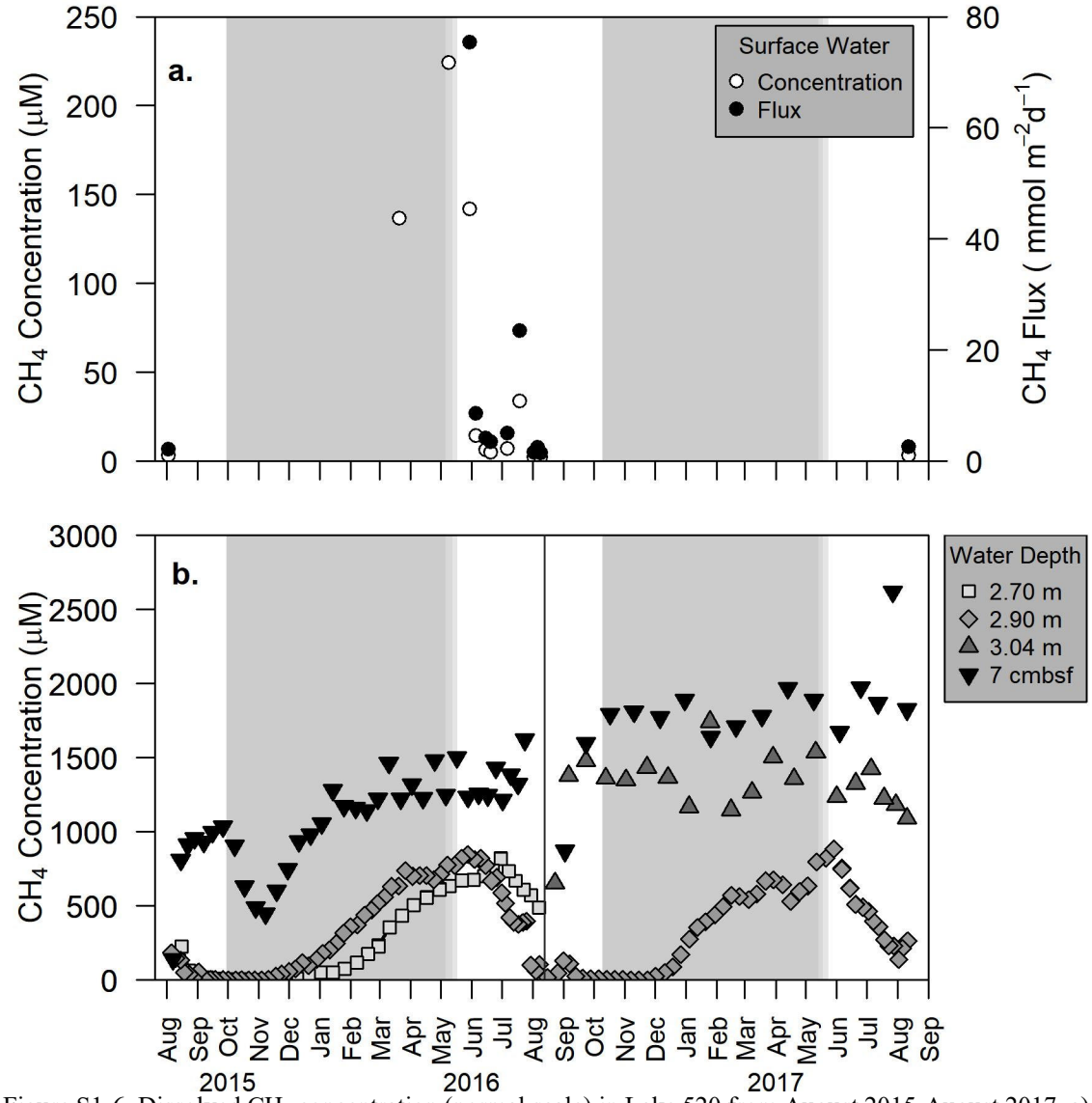

Figure S1-6. Dissolved CH_4 concentration (normal scale) in Lake 520 from August 2015-August 2017. a) discrete surface water (0.5 m) dissolved CH_4 concentration (white circles) and surface water CH_4 diffusive flux (black circles), b) time-integrated sample dissolved CH_4 concentrations. Discrete samples of surface water were taken at 0.5 m, and continuously collected samples were taken from 2.70 m, 2.90 m, 3.04 m water depth and 7 cm in the sediments (cmbsf). Note the difference in CH_4 concentration scale between a and b. Gray shaded boxes indicate when ice covered the lakes and lighter gray indicates when ice began thinning. A solid vertical line separates the two deployments in August 2016. Note this figure has a normal scale for CH_4 concentration while Figure 2-3 had CH_4 concentration presented on log scale.

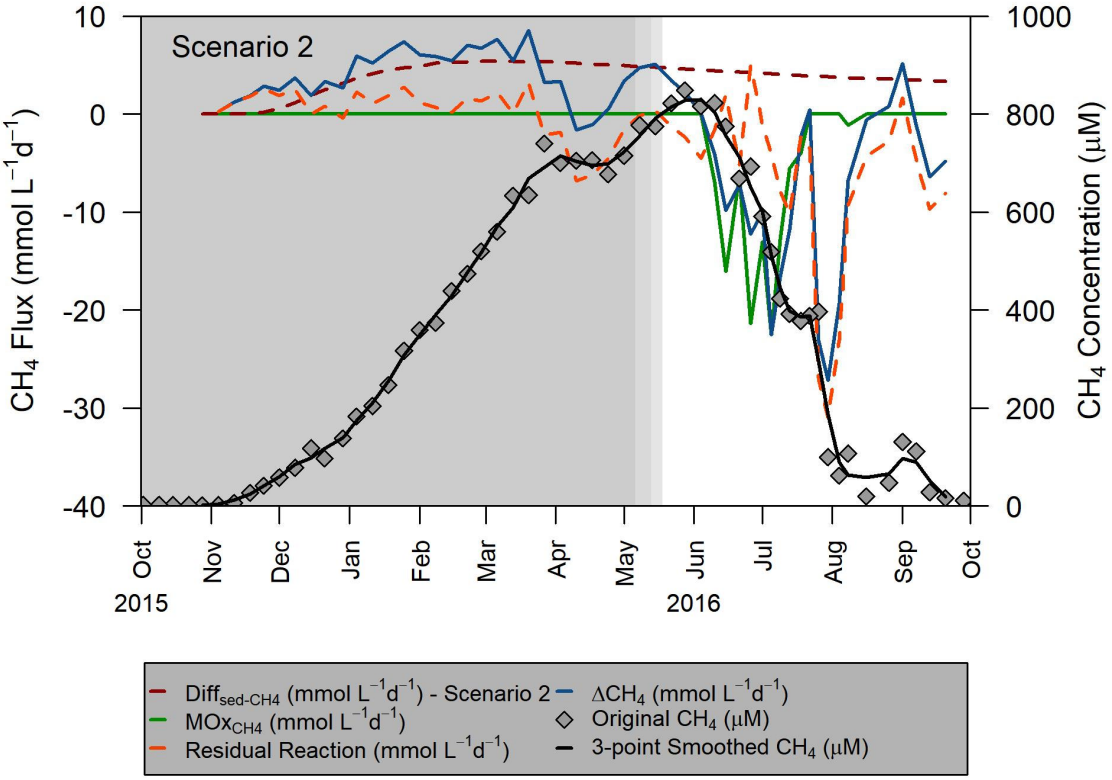

Figure S1-7. Comparison at 2.90 m water depth of dissolved CH_4 concentration and fluxes. Dissolved CH_4 concentrations (grey diamonds plotted on right hand y-axis), 3-point average smoothed CH_4 concentrations (black line, right-hand y-axis), and fluxes of CH_4 (overall change in CH_4 concentration, blue line; diffusive flux, red line; CH_4 oxidation flux, green line; residual reaction flux; dashed orange line; all plotted on left-hand y-axis) are from October 2015 to October 2016 for scenario (2) of a sediment-water interface of 4500 µM CH_4. Gray shading indicates ice-cover as in other plots.

Table S1-1. Discrete lake water sampling dates with the lakes that were sampled and method of sampling. Sampling method includes how researchers got to lakes and how the lake water was collected.

Sampling Dates	Sampling Method
31 March 2016	Transportation - Snowmobile Surface Water - Submersible pump 1 L PETG bottles without headspace Serum vial filled with canula to overfill vials
9 May 2016 5 June 2016 6 August 2016	Transportation - Helicopter Surface Water - Submersible pump into bucket, serum vial submersed in bucket
1-4 August 2015 30-31 May 2016 13, 15 June 2016 20 June 2016 7 July 2016 19-20 July 2016 1-2 August 2016 9, 10, 12 August 2016	Transportation - Small Boat Surface Water - Serum vial submersed in lake

Table S1-2. Dissolved CH_4 radiocarbon and stable carbon isotope ratios for large volume samples (10 L) taken from surface water in Lake 520 in 2016 and 2017.

Sample Date	**Duplicate vials (n)**	**Fm (mean ± s.d.)***	**Age (YBP (mean ± s.d.))***	**$\delta^{13}C$ (‰)****
13 August 2016	4	1.0081 ± 0.0035	Modern ± 27	-47.5 ± 1.2
12 August 2017	2	0.9991 ± 0.0034	6 ± 27	-41.9 ± 1.4

*Fm or fraction modern and age in years before present (YBP) were process blank carbon corrected (1.6 μmol C, Fm = 0.7885).
**$\delta^{13}C$ were not process blank carbon corrected due to insufficient process blank carbon available for $\delta^{13}C$ determinations.

Table S1-3. Surface sediment organic carbon and total nitrogen content at Lake 520 in August 2015, 2016, and 2017. Isotopic measurements were made on an elemental analyzer (Costech elemental combustion system) interfaced to an isotope ratio mass spectrometer (IR-MS, Delta V Plus Isotope Ratio Mass Spectrometer, Thermo Scientific, Waltham, MA, USA). Precision on the IR-MS was ±0.1‰ for $\delta^{13}C$ and ±0.2‰ for $\delta^{15}N$.

Depth (cm)	**Year**	**C_{org} (%)**	**TN (%)**	**$\delta^{13}C$ (‰ vs VPDB)**	**$\delta^{15}N$ (‰ vs Air)**
0-3	2015	13.0	1.1	-30.1	-2.7
0-2	2016	13.0	1.2	-31.9	-1.9
0-2	2017	9.3	0.2	-31.8	-1.2
Mean		11.8	0.8	-31.3	-1.7

Appendix 2

Supplemental Materials to Chapter 3

Text S2-1. Date Assignments to CH_4 and Ion Data

There was one method used to assign the dates to the ion data (Ca^{2+}, Cl^-, Mg^{2+}) for Lakes 56 and 520 presented in this paper and three methods used to assign the dates to the CH_4 data Lakes 56, 280, and 520 presented in this paper because of the different data collected concurrently.

For Lake 56, Cl^- and SO_4^{2-} samples were collected concurrently in copper and Teflon tubing and had concentrations above the limits of detection using the ion chromatograph. Cl^- and SO_4^{2-} from the copper segments were measured on a Dionex ICS-1000 ion chromatograph with no dilution in 500 µL autosampler vials for both the 2015-2016 and 2016-2017 samples at the Chesapeake Biological Laboratory. Teflon samples were measured as outlined in section 2.3.3. While ion samples were collected concurrently into copper and Teflon tubing, the copper tubing time-series appears truncated in comparison to the Teflon time-series (Appendix 2 Figures S2-1, S2-2). One possibility is that there is no gas exchange possible in the copper tubing and gas concentrations may be high, even though not at saturation concentrations and that when the pumps were retrieved water near the intake was expelled (noted in other locations by C.G. Wheat, personal communication). Therefore, the ion data for Lake 56 were assigned dates based on matching the peak in Cl^- and SO_4^{2-} samples extruded from the short

copper segments (0.5 and 1 m) to peaks in Cl^- and SO_4^{2-} in the samples extruded from the Teflon tubing (Appendix 2 Figure S2-1a and S2-2a). Dates for short copper segments were assigned to the adjacent long segments expressed for CH_4 analyses.

For Lake 520, Cl^- and SO_4^{2-} samples were collected concurrently in copper and Teflon tubing. Measurements were made at CBL on the ion chromatograph of the 2015-2016 samples were diluted 1:3 in 500 µL autosampler vials; no dilution was made for 2016-2017 samples in 500 µL autosampler vials, however Cl^- and SO_4^{2-} concentrations were below the limits of detection. As a result, no comparison was made between Cl^- and SO_4^{2-} measured from samples collected in the copper and Teflon tubing. Consequently, CH_4 data for Lake 520 were assigned dates based solely on the temperature correction and are outlined in Chapter 2 and Appendix 1 Text S1-1.

For Lake 280, the 2015-2016 sampling did not include OsmoSamplers with Teflon tubing. Instead conductivity measurements were made using a continuous sensor deployed from August 2015 to August 2016. The CH_4 data for Lake 280 were assigned dates based on matching the increase in conductivity in Lake 280 to the increase in Cl^- concentrations for the time-integrated samples extruded from copper tubing. Cl^- concentrations decreased in late-winter and it is unclear why. Once the early increase in conductivity was matched, the remaining dates were assigned based on a temperature correction to the pumping rates. During the 2016-2017 deployment water samples for Cl^- and SO_4^{2-} measurements were collected concurrently in copper and Teflon tubing and had concentrations above the limits of detection on the ion chromatograph. Cl^- and SO_4^{2-} from the copper segments were measured on a Dionex ICS-1000 ion chromatograph with no dilution in 500 µL autosampler vials for the 2016-2017 samples measured at CBL. There

was no truncation in the temperature-corrected Cl^- and SO_4^{2-} data-set from the copper tubing as compared to the temperature-corrected Teflon time-series (Appendix 2 Figure S2-1b and S2-2b). Therefore, no additional adjustments were made to the temperature-corrected dates assigned to the 2016-2017 CH_4 data for Lake 280.

Text S2-2. Mass Transfer Method

The mass-transfer method was used to calculate evaporation using Equation S2-1. This method calculates the exchange of water vapor between the lake surface and the atmosphere as being directly proportional to the vertical humidity gradient between those two locations and the wind speed.

$$E = N * U * (e_s - e_a) \quad \text{(S2-1)}$$

where E was the mass transfer rate in cm hr^{-1} and was scaled to cm day^{-1}, N was the mass transfer coefficient in cm $mbar^{-1}$ km^{-1}, U was average daily wind speed in km h^{-1} measured in Inuvik (Appendix 2 Figure S2-3), e_s was vapor pressure of the water surface in mbar, and e_a was vapor pressure of the air in mbar. N, mass transfer coefficient, was calculated using Equation S2-2 (Dingman, 1994). Saturated vapor pressure, e_s, was based on air temperature with Equation S2-3. Vapor pressure of air, e_a, was calculated based on average daily relative humidity and saturated vapor pressure in Equation S2-4.

$$N = 1.69 * 10^{-4} * A_L{}^{-0.05}, \quad \text{(S2-2)}$$

where A_L is lake area in km^2.

$$e_s = 6.11 * 10^{(7.5*T/237.3+T)}, \quad \text{(S2-3)}$$

where T is average daily air temperature (°C) measured in Inuvik (Appendix 2 Figure S2-3).

$$e_a = \frac{RH\ (\%) * e_s}{100}, \quad \text{(S2-4)}$$

where RH is relative humidity in percent measured in Inuvik (Appendix 2 Figure S2-3) and e_s came from Equation S2-3.

Text S2-3. Thornthwaite Method

The Thornthwaite method was used to calculated potential evapotranspiration (PET) using Equation S2-5 (Thornthwaite, 1948).

$$PET = 16 * \frac{L}{12} * \frac{N}{30} * \left(\frac{10 * T_a}{I}\right)^{\alpha}, \quad \text{(S2-5)}$$

where PET was calculated as mm month^{-1}, L is average day length in hours each month (Appendix 2 Table S2-1), N is number of days per month, T_a was average monthly air temperature in ^{o}C in Inuvik and if the temperature was below 0, then it was replaced with 0 (Appendix 2 Table S2-1). I was calculated using Equation S2-6. α was calculated using Equation S2-7.

$$I = \sum_{i=1}^{12} \left({}^{T_{ai}}/_{5}\right)^{1.514}, \quad \text{(S2-6)}$$

where T_{ai} is average monthly air temperature in ^{o}C in Inuvik.

$$\alpha = 6.75 * 10^{-7} * I^3 - 7.71 * 10^{-5} * I^3 + 1.792 * 10^{-2} * I + 0.49239. \quad \text{(S2-7)}$$

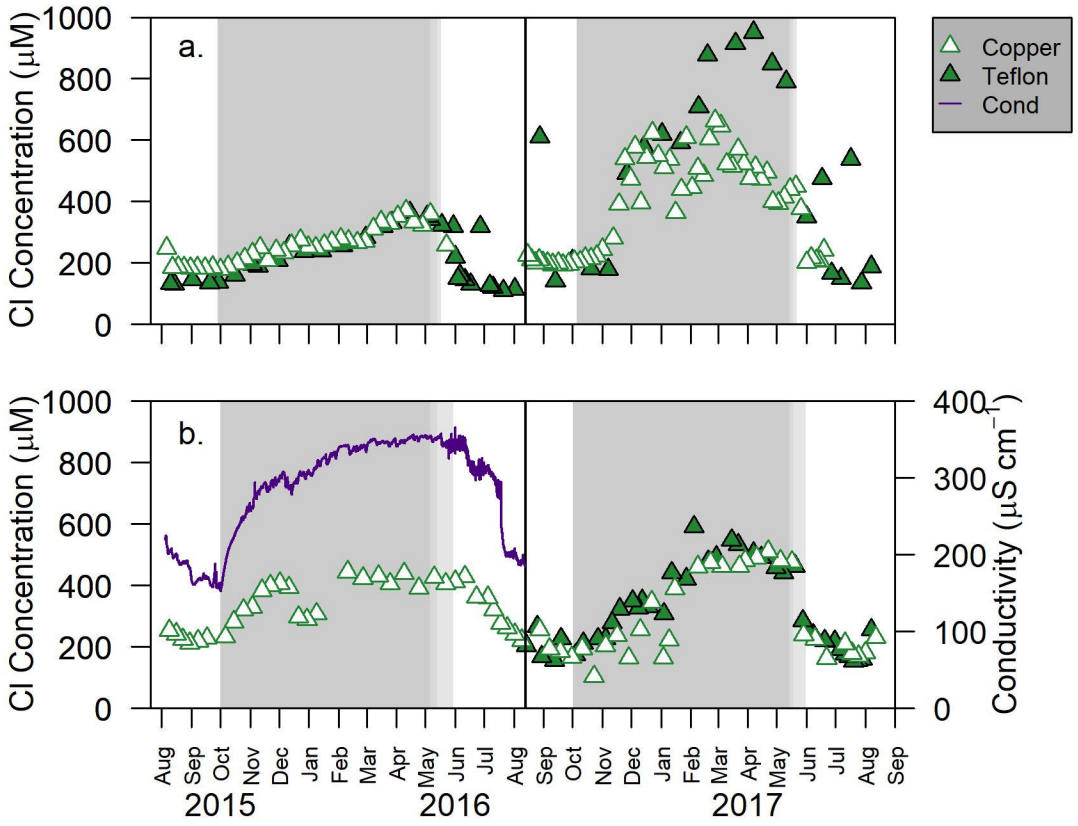

Figure S2-1. Comparison of Cl^- concentrations measured from a) Lake 56 and b) Lake 280 samples collected in copper (open triangle) and Teflon (filled triangle) tubing. Conductivity was determined instead of ion concentrations in 2015-2016 in Lake 280.

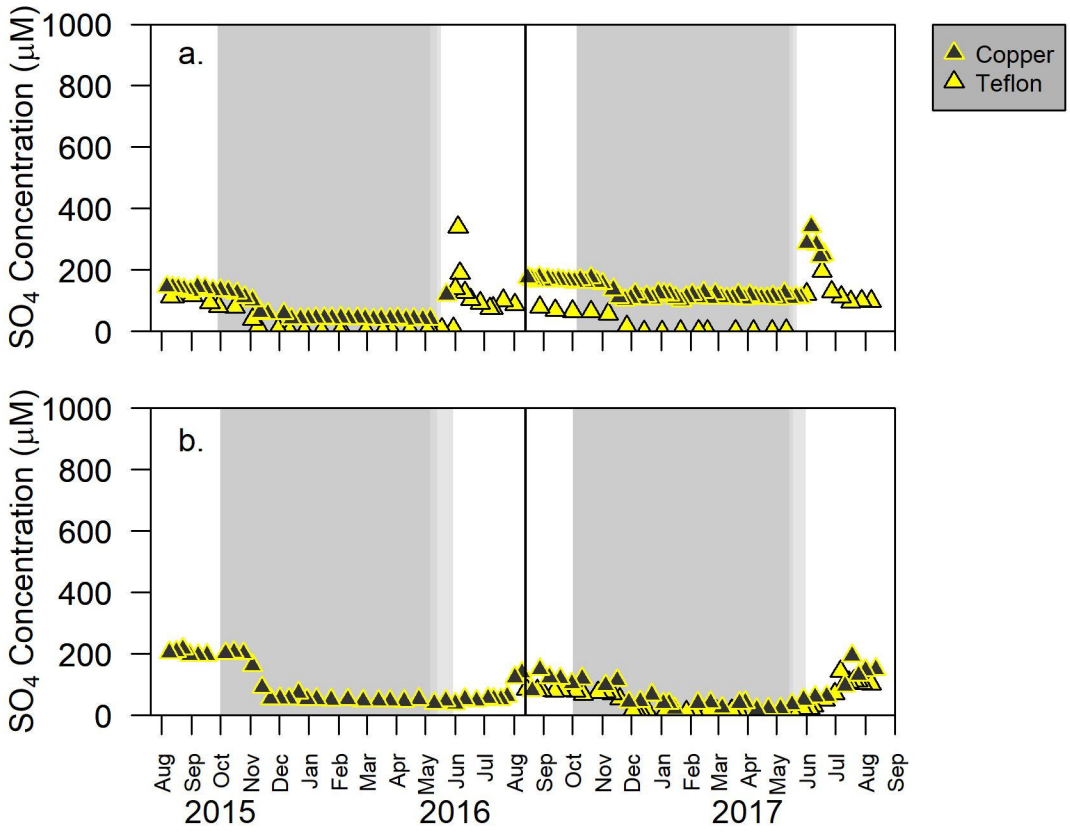

Figure S2-2. Comparison of SO_4^{2-} concentrations measured from a) Lake 56 and b) Lake 280 samples collected in copper (yellow-outlined triangle) and Teflon (yellow-filled triangle) tubing. Ion concentrations were not collected in Lake 280 in Teflon tubing.

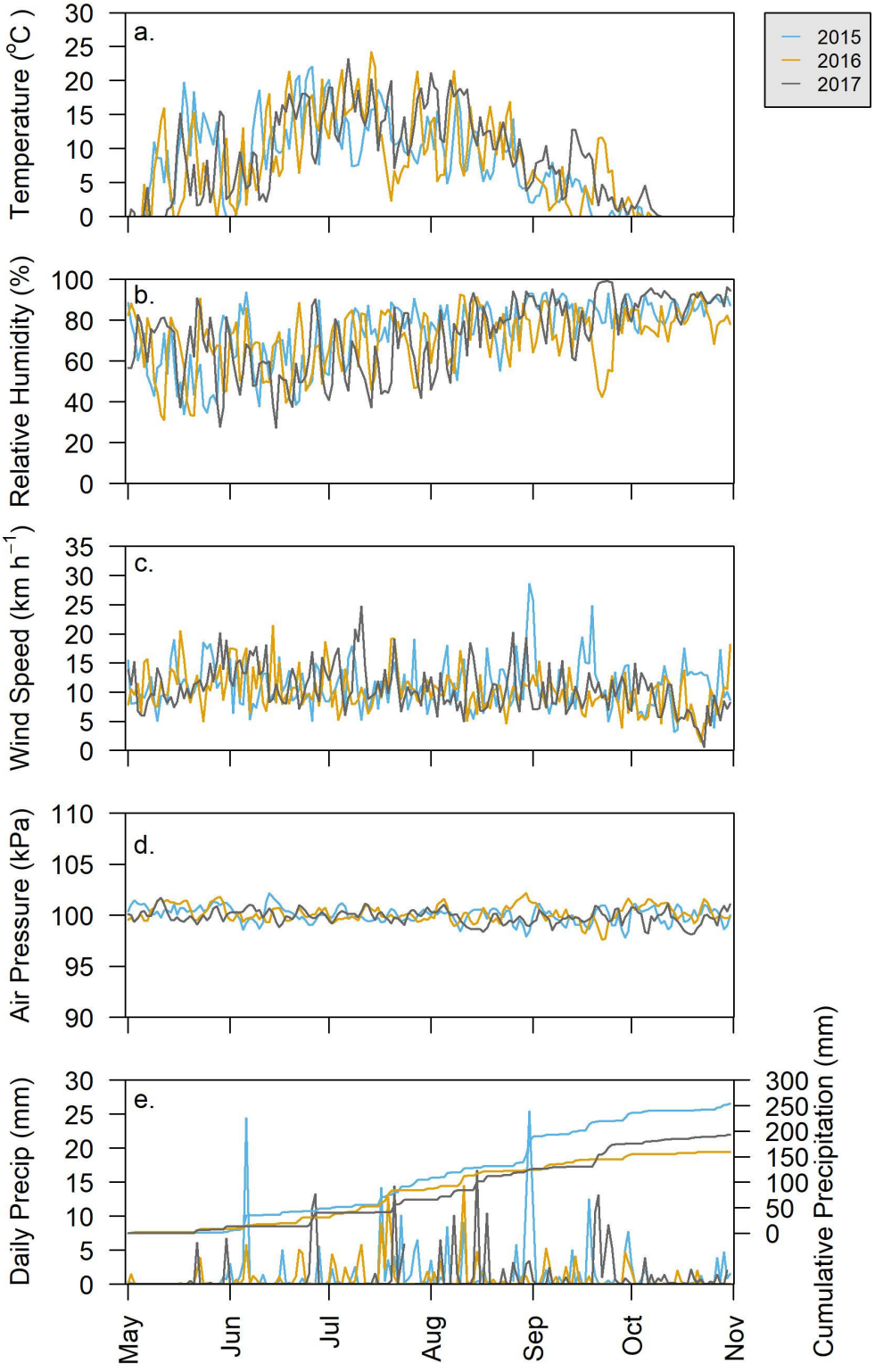

Figure S2-3. Climate near Inuvik, Northwest Territories, Canada. a) daily average wind speed (km hr^{-1}), b) daily average air temperature (°C), c) daily average relative humidity (%), d) daily average air pressure (kPa), and e) daily and cumulative precipitation during the open-water season (mm). Hourly data came from Environment Canada at the Inuvik CLIMATE Station 2202578.

Table S2-1. Regional climate air temperature, monthly precipitation, and daylight hours data used in calculating open-water evaporation. Air temperature and total monthly precipitation (mm) were measured at the Inuvik Climate station (Climate ID 2202578). Total monthly precipitation is the summation of daily precipitation (snow and rain) for each month in 2015 to 2017. Total daylight hours data are from the Naval Oceanography Portal, Astronomical Applications, Data Services, Duration of Daylight/Darkness Table for One Year at Utqiaġvik, AK, USA. Data downloaded March 22, 2018.

	Regional Climate								
	Air Temperature (^{o}C)			Precipitation (mm)			Daylight Hours		
	2015	2016	2017	2015	2016	2017	2015	2016	2017
January	-23.4	-18.4	-18.5	8.5	2.1	23.9	0.8	0.8	0.9
February	-20.1	-21.5	-22.1	6.6	0.6	23.0	6.8	6.9	6.9
March	-17.2	-17.9	-20.0	16.3	17.3	9.9	11.7	11.8	11.8
April	-6.8	-9.0	-12.0	18.2	4.6	4.0	16.7	16.9	16.8
May	6.7	5.0	3.9	2.5	8.2	13.6	23.0	23.1	23.1
June	11.8	11.0	10.6	45.9	22.2	26.0	24.0	24.0	24.0
July	12.7	14.1	15.6	56.5	56.3	25.9	24.0	24.0	24.0
August	9.6	11.0	13.4	73.3	37.6	60.1	18.9	18.7	18.8
September	2.8	4.5	6.1	55.2	28.5	50.1	13.4	13.3	13.3
October	-5.7	-6.0	-3.7	20.7	6.6	17.6	8.6	8.5	8.5
November	-14.4	-16.3	-15.5	13.4	16.4	13.6	2.4	2.2	2.3
December	-23.4	-22.0	-15.7	6.3	3.1	10.6	0.0	0.0	0.0
Annual Average	-5.6	-5.5	-4.8						
Total				323.4	203.5	278.3			

Table S2-2. Total Potential Evapotranspiration calculated for May to October with the Thornthwaite equation for lakes near Inuvik, Northwest Territories, Canada.

Total Potential Evapotranspiration (mm)			
	2015	2016	2017
January	0	0	0
February	0	0	0
March	0	0	0
April	0	0	0
May	104	83	64
June	156	146	137
July	170	180	189
August	110	118	132
September	32	43	50
October	0	0	0
November	0	0	0
December	0	0	0
Total PET	572	570	573

Table S2-3. Student's t-test p-values for the comparison of ion concentrations between open-water and ice-cover in Lake 56 and Lake 520.

Ions	Open-water to Ice-cover Student's t-test p-value	
	Lake 56	Lake 520
Ca	<0.0001	0.0001
Mg	<0.0001	<0.0001
Cl	<0.0001	0.01
Ba	<0.0001	<0.0001
Li	0.004	0.01
Sr	<0.0001	0.0001

Appendix 3

Additional Data Collected From Mackenzie Delta Lakes

Text S3-1. Bottom Water Sample Collection

This study conducted fine-scale temporal water sampling using continuous, autonomous samplers in lakes spanning a large region in the Mackenzie Delta. To do this, OsmoSamplers consisting of osmotic pumps connected to thin bore copper tubing (ID 0.8 mm or 1.1 mm) and sensors measuring water column characteristics (temperature, water pressure, dissolved oxygen, conductivity, light) were deployed in nine lakes across the Mackenzie Delta (Figure 1-3). Bottom-water was collected from these lakes for one-year or two-year periods (Appendix 3 Table S3-1). Following sampler retrieval, copper tubing was crimped and then processed at the Chesapeake Biological Laboratory (CBL, Solomons, MD, USA) for dissolved CH_4 concentrations and $\delta^{13}C\text{-}CH_4$ measurements. Data presented in Appendix 3 are for additional sensor data for the deployments in the main text and sensor, dissolved CH_4, and $\delta^{13}C\text{-}CH_4$ data for in those deployments not presented in the main text of the dissertation (Appendix Figures S3-1 to S3-9). Chapter 2 shows all time-series and sensor data for Lake 520. Chapter 3 shows the dissolved CH_4 and $\delta^{13}C\text{-}CH_4$ time-series and some of the sensor data for Lakes 280, 56, and 520. The remainder of the sensor data and time-series for Lakes 56 and 280 are shown in Appendix 3 Figures S3-3 and S3-4. Chapter 4 shows the dissolved CH_4 and $\delta^{13}C\text{-}CH_4$ time-series for Swiss Cheese Lake. Additional light data are shown in Appendix Figures S3-6 and

S3-7 for SC-ref and SC-seep. In addition, Lakes 129 (low-closure) and 80 (low-closure) were visited in the central delta, Manta Lake in the outer delta, and North Head Lakes 1 and 2 on Richard's Island in the outer delta were visited (Appendix S3-1, S3-2, S3-5, S3-8 and S3-9, respectively).

Text S3-2. Discrete Surface Water Sampling

A sampling campaign was carried out during the open-water season of 2016 to collect surface water samples from lakes near Inuvik (Lakes 129, 80, 87, 280, 56, and 520). These lakes were visited every other week and near-surface water samples (~0.5 m depth) were gently collected. Surface water dissolved CH_4 samples were also collected from the Mackenzie River and outer delta lakes when the lakes were visited for OsmoSampler deployments each August 2015, 2016, and 2017. Sample collection and analysis followed the methods outlined in Chapter 2 for dissolved CH_4 concentration and $\delta^{13}C\text{-}CH_4$ measurements. Surface water dissolved CH_4 concentration and $\delta^{13}C\text{-}CH_4$ measurements for these periods are in Appendix 3 Table S3-2 and Table S3-3.

Text S3-3. Sediment Pore-water CH_4 Concentration and $\delta^{13}C\text{-}CH_4$

Sediment cores were collected with a gravity corer (9-cm diameter, hand-held, Uwitec Corer, Mondsee, Austria) from the side of a small boat during OsmoSampler deployment and retrieval from the Lakes 129, 80, 87, 280, 56, 520, Manta Lake, Swiss Cheese Lake, North Head 1 and North Head 2. Not all lakes were visited in August 2015 nor August 2017 (Appendix 3 Table S3-4). Coring, sediment subsampling, and analytical measurements for CH_4 concentration and $\delta^{13}C\text{-}CH_4$ followed methods outlined in

Chapter 2 section 2.3.4. Sediment pore-water CH_4 concentrations and $\delta^{13}C$-CH_4 measurements were conducted at CBL. Data presented are for the full length of the sediment cores retrieved (Appendix 3 Table S3-4).

Text S3-4. Sediment OC and TN Concentrations and Stable Isotopes

Surface sediments collected from lakes in the Mackenzie Delta in August 2015, August 2016, and August 2017 were analyzed for OC and TN concentrations and $\delta^{13}C$ and $\delta^{15}N$. Sample preparation followed methods laid out in Chapter 2 section 2.3.5. Isotopic measurements were made on an elemental analyzer (Costech elemental combustion system) interfaced to an isotope ratio mass spectrometer (IR-MS, Delta V Plus Isotope Ratio Mass Spectrometer, Thermo Scientific, Waltham, MA, USA). Precision on the IR-MS was ±0.1‰ for $\delta^{13}C$ and ±0.2‰ for $\delta^{15}N$. Measurements were made in the Chesapeake Biological Lab's Stable Isotope Laboratory by Cédric Magen. Data are presented in Appendix 3 Table S3-5.

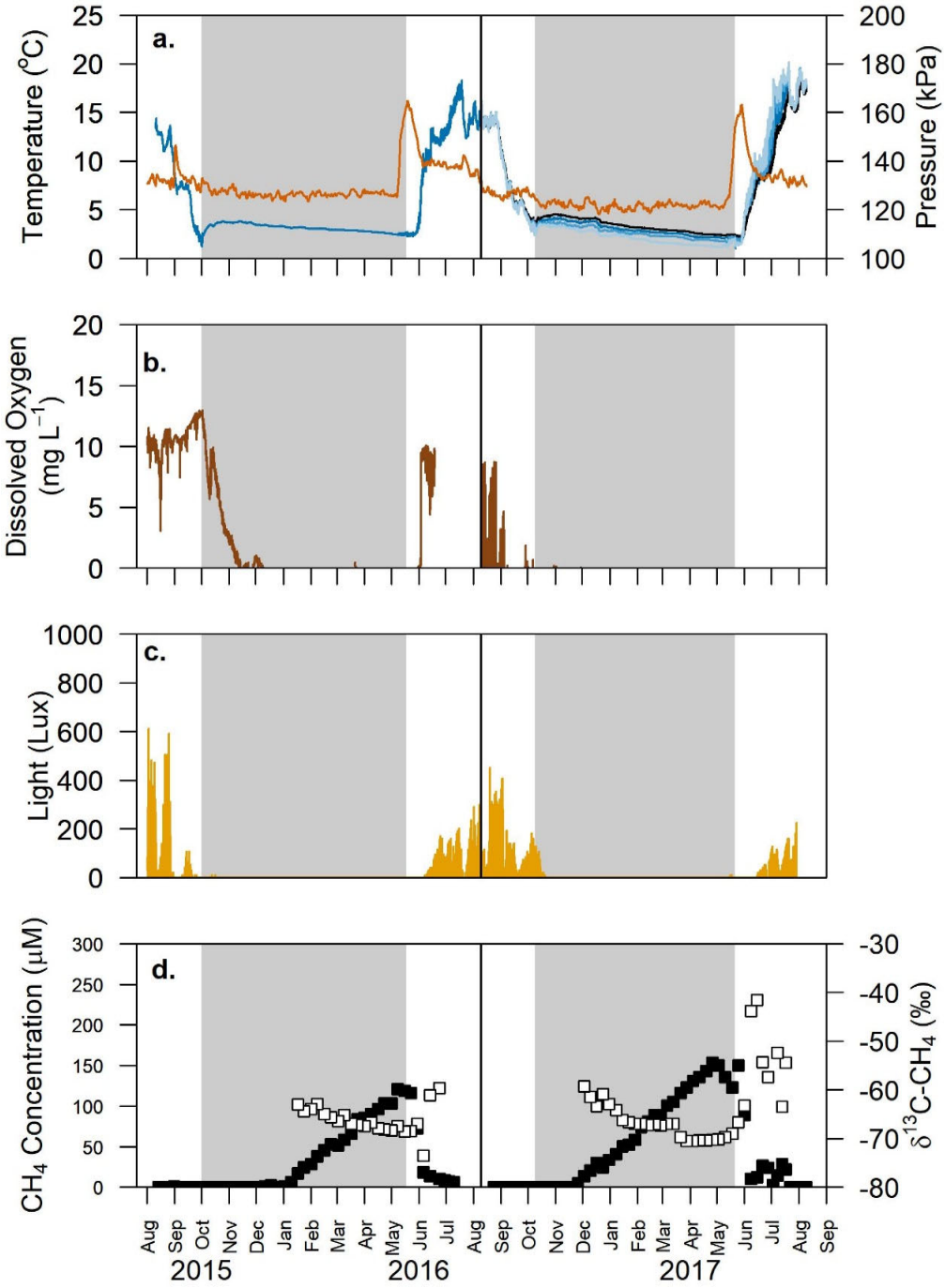

Figure S3-1. Lake 129 2015-2017 bottom-water characteristics and dissolved CH_4 changes. a) temperature (blue lines) and pressure (orange line), b) dissolved oxygen (brown line), c) light (yellow line), and d) dissolved CH_4 (black squares, left y-axis) and $\delta^{13}C$-CH_4 values (white squares, right y-axis). Different colored blue lines indicate temperature measured at different water depths. The light blue line is for temperatures measured at 2.10 m water depth, medium blue at 2.43 m, dark blue at 2.87 m, and black at 3.14 m water depth (sediment-water interface). Vertical black lines indicates the date the second deployment began 10 August 2016. Gray bars indicate the period of ice-cover. Dissolved oxygen data are not available for August 2016-August 2017 due to an instrument malfunction.

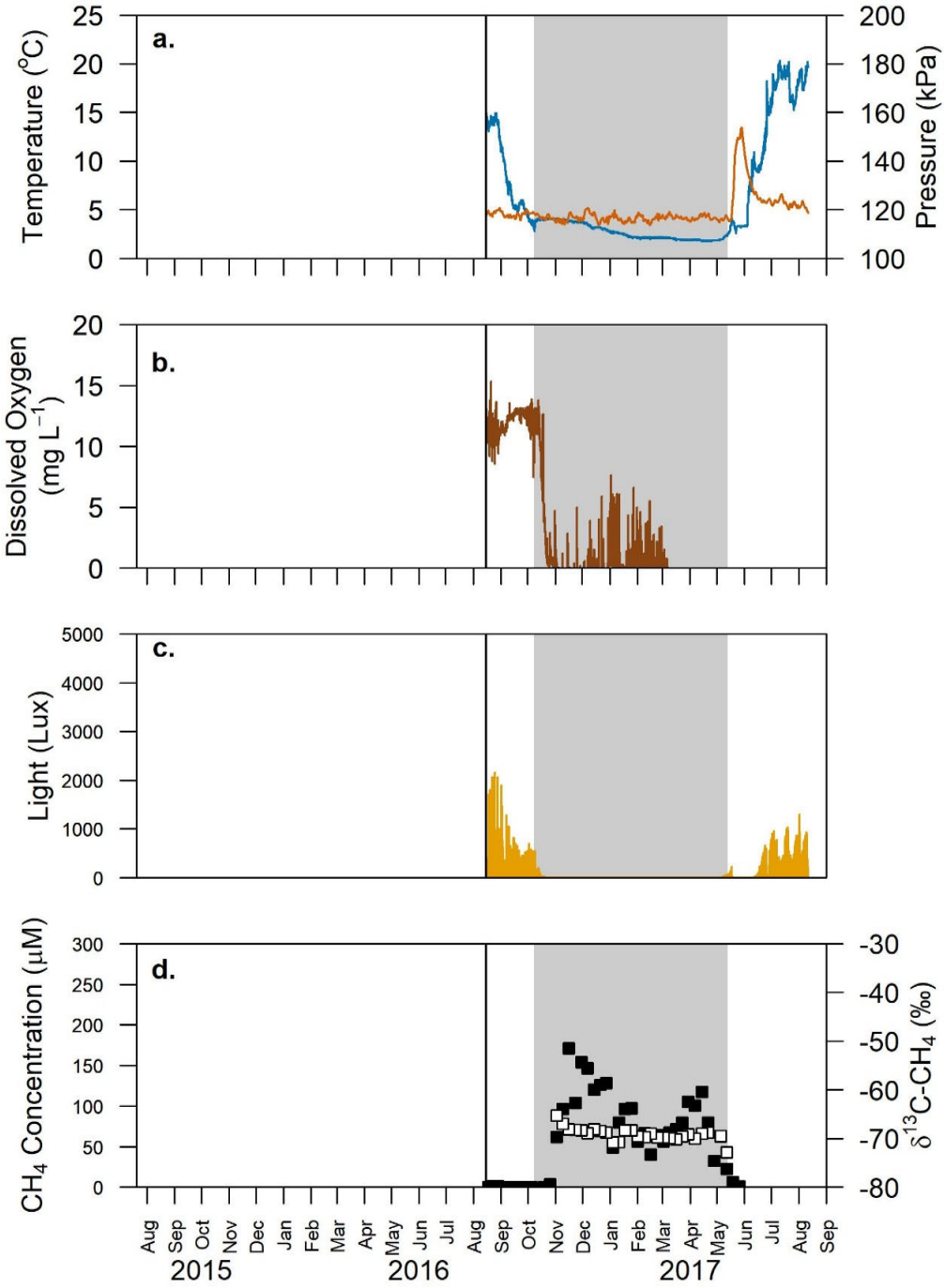

Figure S3-2. Lake 80 2016-2017 bottom-water characteristics and dissolved CH_4 changes. a) temperature (blue line) and pressure (orange line), b) dissolved oxygen (brown line), and d) dissolved CH_4 (black squares, left y-axis) and $\delta^{13}C$-CH_4 values (white squares, right y-axis). Vertical black lines indicates the date the second deployment began 15 August 2016. There were no sensors deployed from August 2015-August 2016. Gray bars indicate the period of ice-cover.

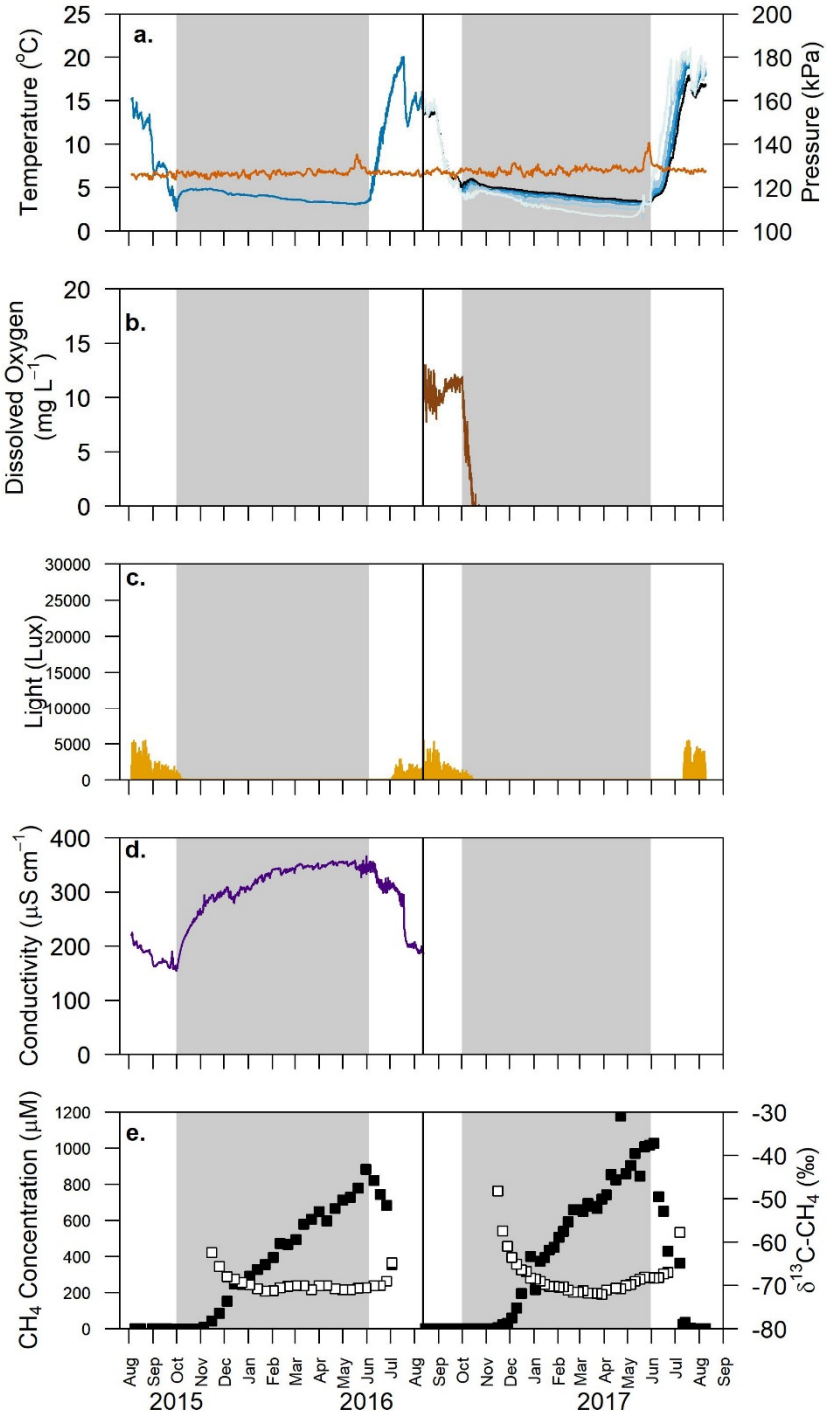

Figure S3-3. Lake 280 2015-2017 bottom-water characteristics and dissolved CH_4 changes. a) temperature (blue lines) and pressure (orange line), b) dissolved oxygen (brown line), c) light (yellow line), d) conductivity (purple line), and e) dissolved CH_4 (black squares, left y-axis) and $\delta^{13}C$-CH_4 values (white squares, right y-axis). Different colored blue lines indicate temperature measured at different water depths. Light blue are for temperatures measured at 1.48 m and 2.04 m water depth, medium blue at 2.42 m water depth, dark blue at 2.63 m water depth, and black at 2.90 m water depth (sediment-water interface). Vertical black lines indicates the date the second deployment began 13 August 2016. Gray bars indicate the period of ice-cover. There was no dissolved oxygen sensor deployed August 2015-August 2016 nor a conductivity sensor deployed August 2016-August 2017.

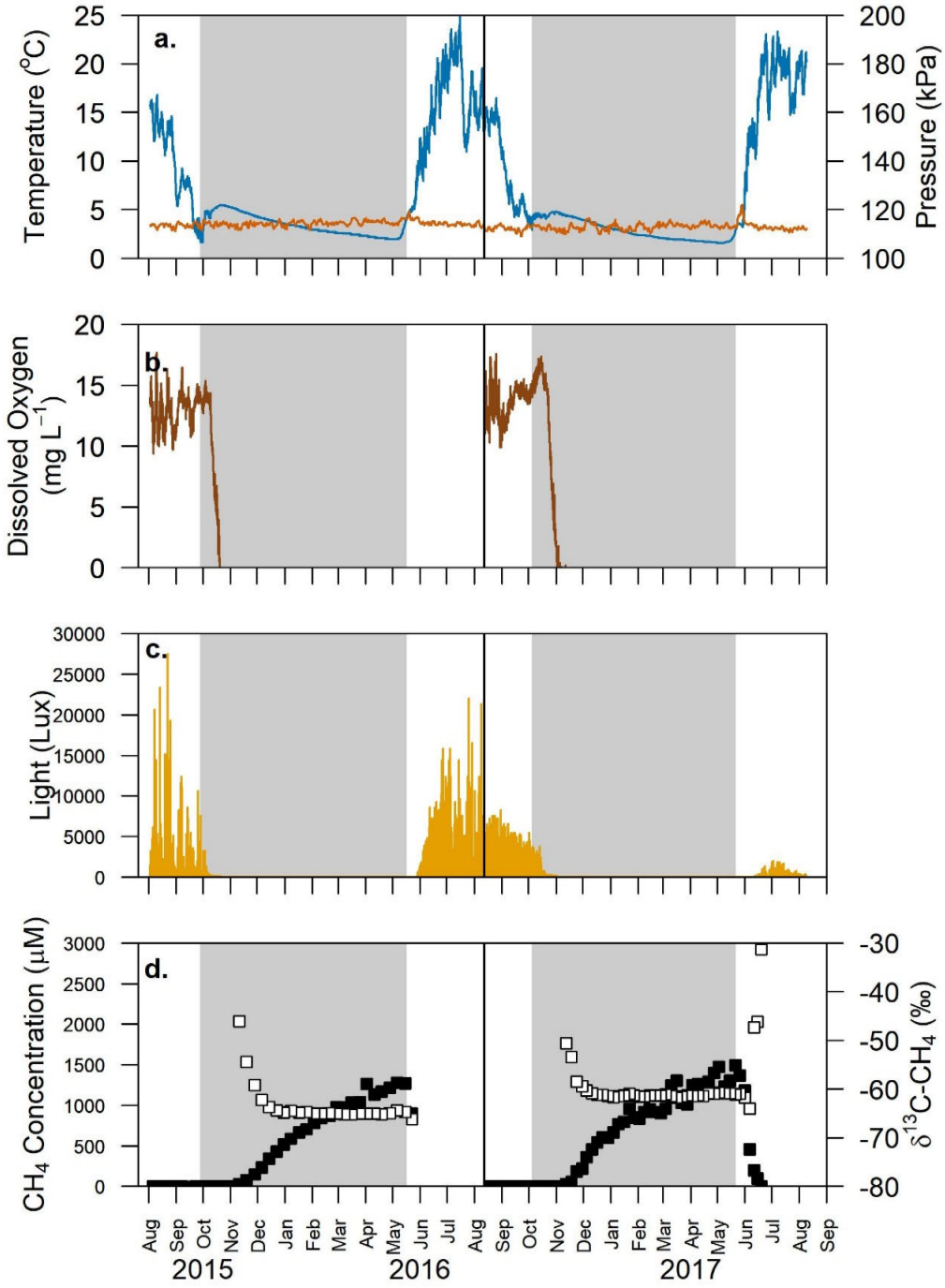

Figure S3-4. Lake 56 2015-2017 bottom-water characteristics and dissolved CH_4 changes. a) temperature (blue line) and pressure (orange line), b) dissolved oxygen (brown line), c) light (yellow line), and d) dissolved CH_4 (black squares, left y-axis) and $\delta^{13}C$-CH_4 values (white squares, right y-axis). Vertical black lines indicates the date the second deployment began 12 August 2016. Gray bars indicate the period of ice-cover.

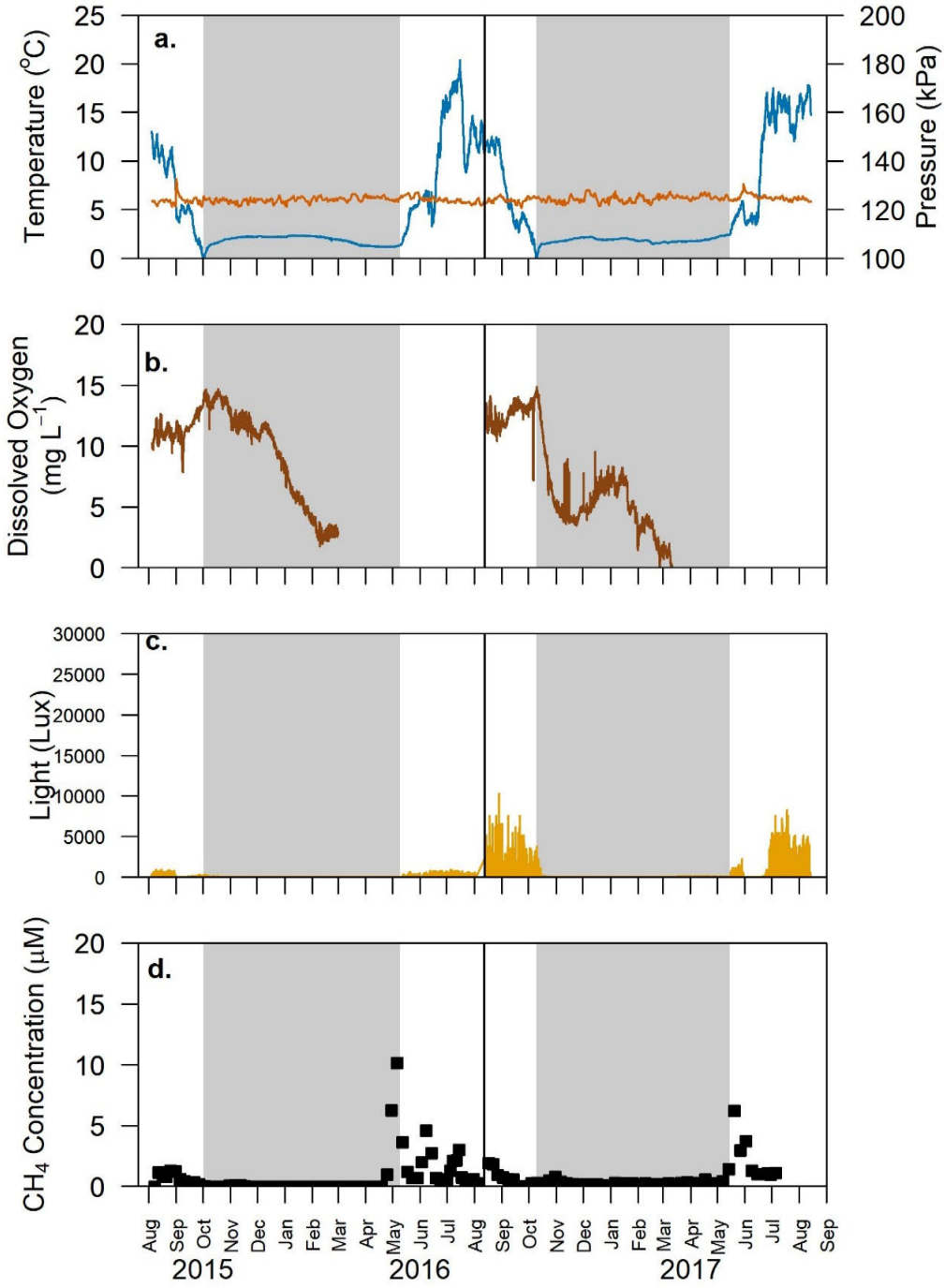

Figure S3-5. Manta Lake 2015-2017 bottom-water characteristics and dissolved CH_4 changes. a) temperature (blue line) and pressure (orange line), b) dissolved oxygen (brown line), c) light (yellow line) and d) dissolved CH_4 (black squares, left y-axis). Vertical black lines indicates the date the second deployment began 15 August 2016. Gray bars indicate the period of ice-cover.

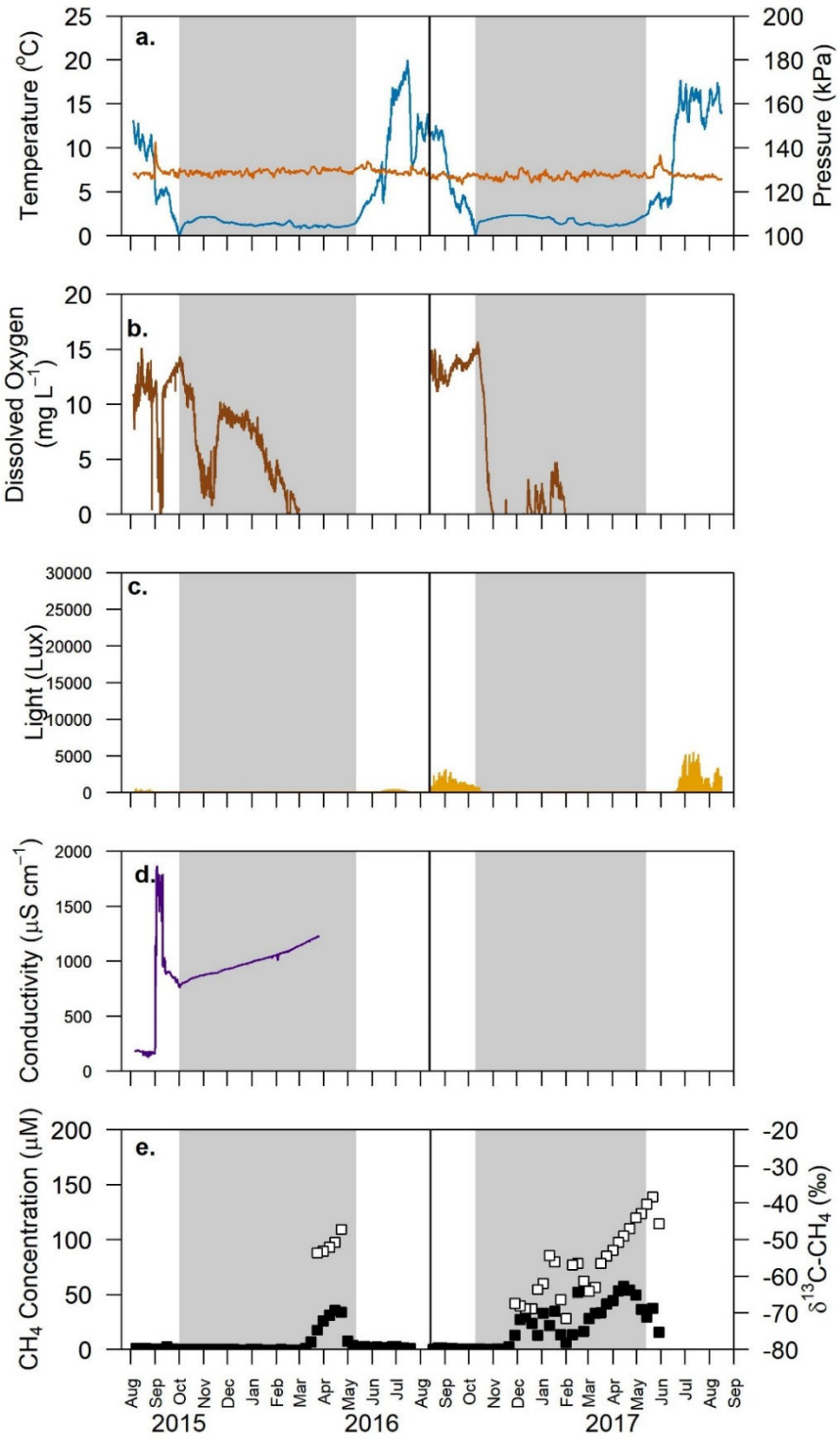

Figure S3-6. Swiss Cheese Lake SC-ref (site 1) 2015-2017 bottom-water characteristics and dissolved CH_4 changes. a) temperature (blue line) and pressure (orange line), b) dissolved oxygen (brown line), c) light (yellow line), d) conductivity (purple line), and e) dissolved CH_4 (black squares, left y-axis) and $\delta^{13}C$-CH_4 values (white squares, right y-axis). Vertical black lines indicates the date the second deployment began 13 August 2016. Gray bars indicate the period of ice-cover.

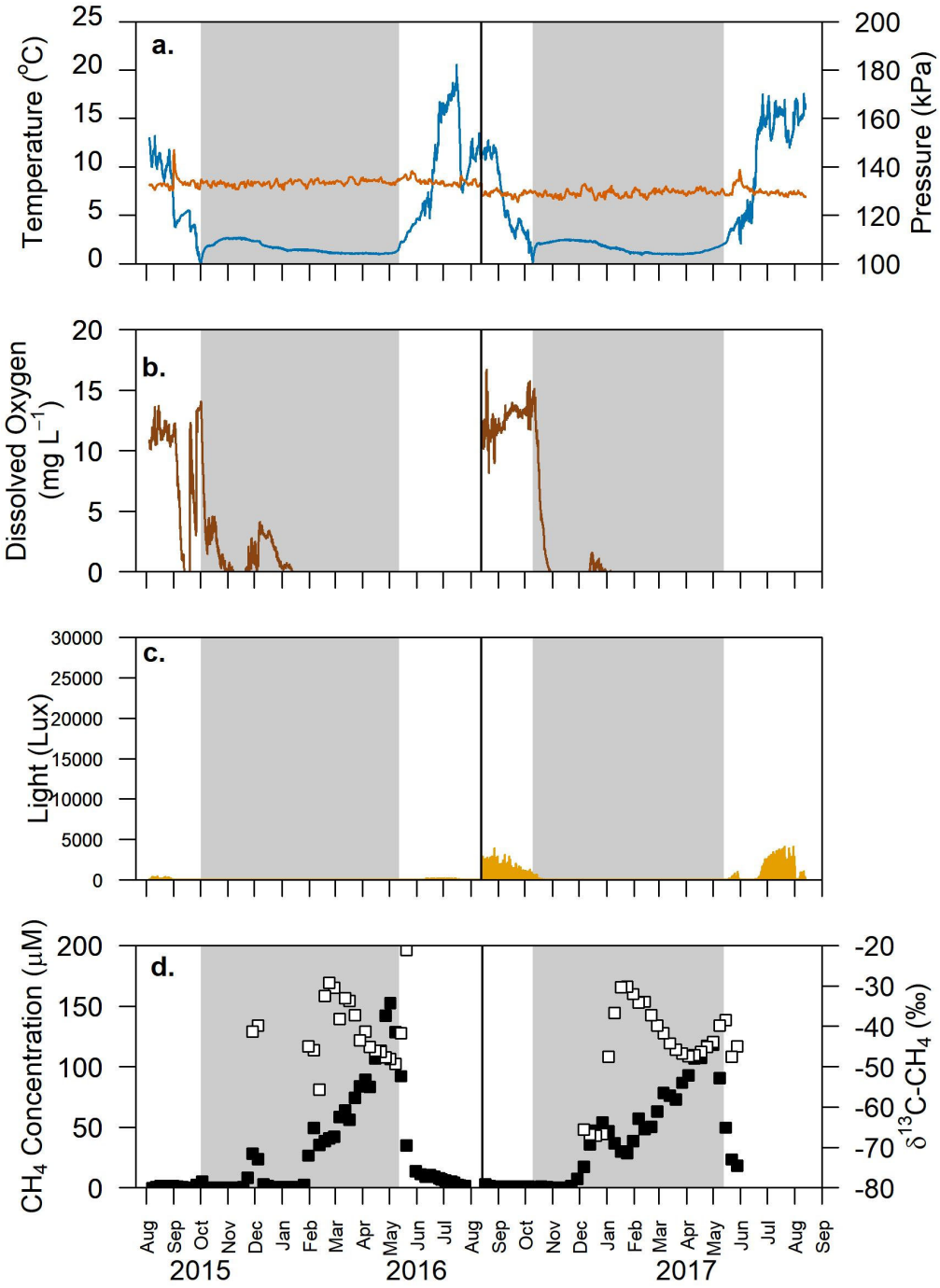

Figure S3-7. Swiss Cheese Lake SC-seep (site 2) 2015-2017 bottom-water characteristics and dissolved CH_4 changes. a) temperature (blue line) and pressure (orange line), b) dissolved oxygen (brown line), c) light (yellow line), and d) dissolved CH_4 (black squares, left y-axis) and $\delta^{13}C$-CH_4 values (white squares, right y-axis). Vertical black lines indicates the date the second deployment began 13 August 2016. Gray bars indicate the period of ice-cover.

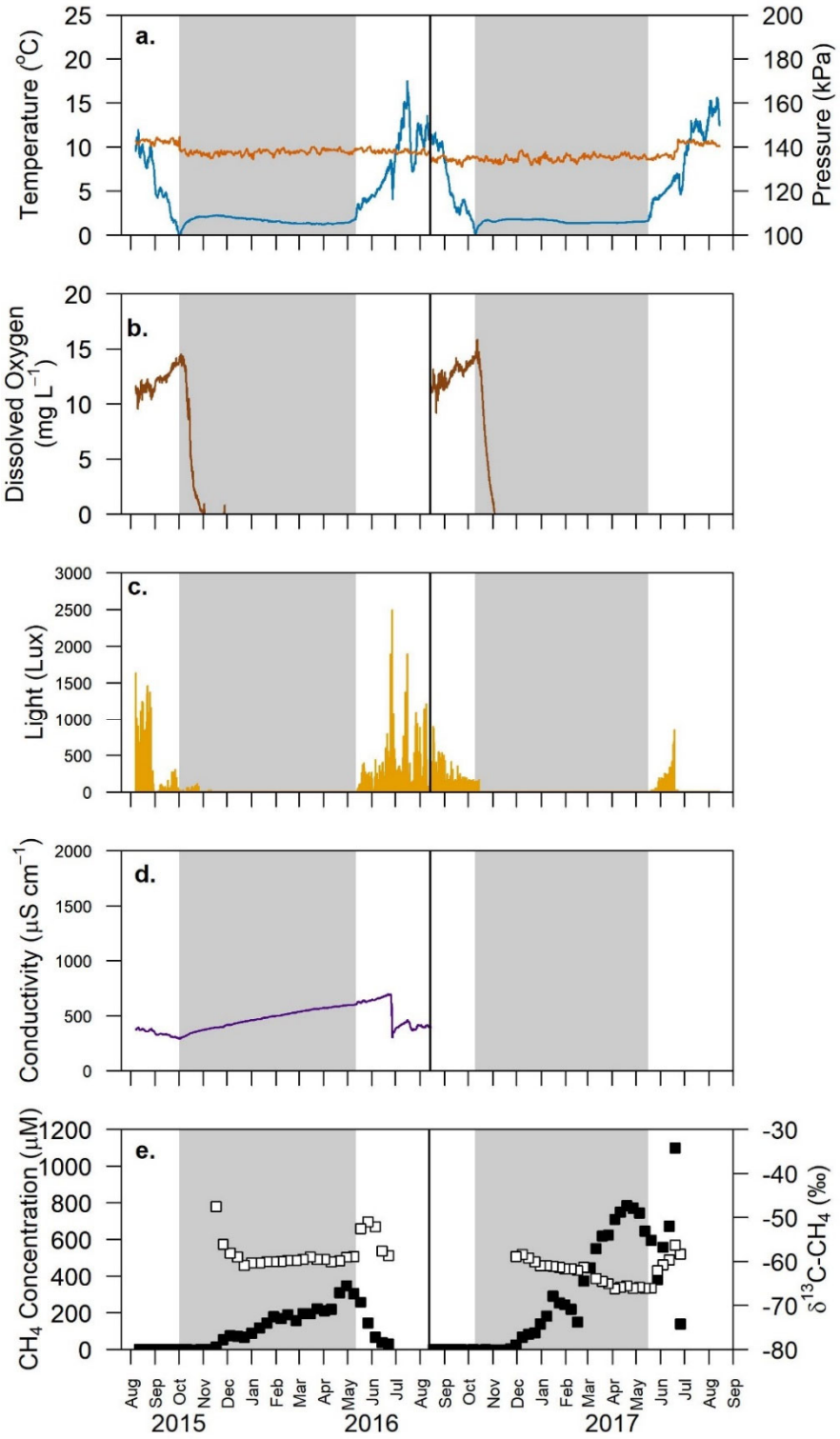

Figure S3-8. North Head Lake 1 (NH1) 2015-2017 bottom-water characteristics and dissolved CH_4 changes. a) temperature (blue line) and pressure (orange line), b) dissolved oxygen (brown line), c) light (yellow line), d) conductivity (purple line) and e) dissolved CH_4 (black squares, left y-axis) and $\delta^{13}C$-CH_4 values (white squares, right y-axis). Vertical black lines indicates the date the second deployment began 14 August 2016. There was no conductivity sensor deployed August 2016-August 2017. Gray bars indicate the period of ice-cover.

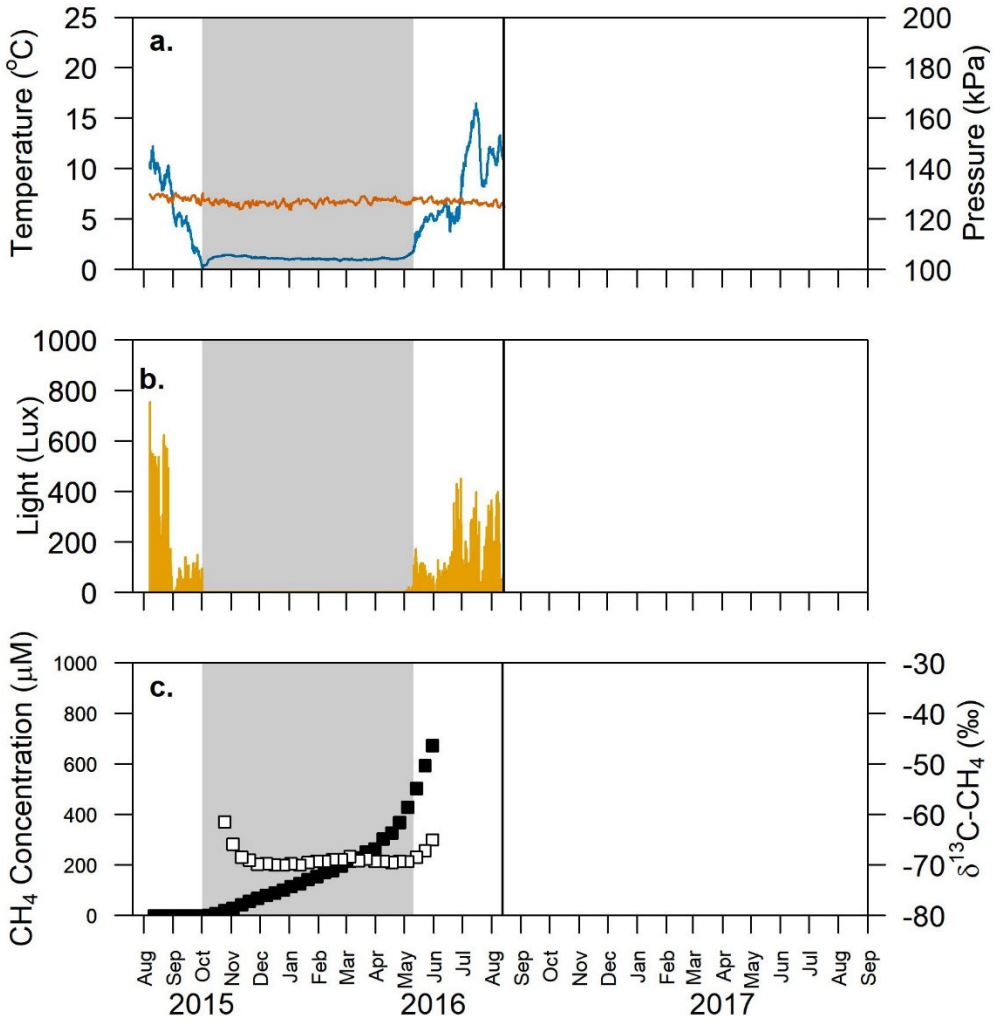

Figure S3-9. North Head Lake 2 (NH2) 2015-2016 bottom-water characteristics and dissolved CH_4 changes. a) temperature (blue line) and pressure (orange line), b) light (yellow line), and c) dissolved CH_4 (black squares, left y-axis) and $\delta^{13}C$-CH_4 values (white squares, right y-axis). Vertical black lines indicates the date the first deployment ended 14 August 2016. There were no dissolved oxygen or conductivity sensors deployed August 2015-August 2016 and no sensors deployed August 2016-August 2017. Gray bars indicate the period of ice-cover.

Table S3-1. Mackenzie Delta lake locations and sampling information for OsmoSampler deployments and retrievals in August 2015, August 2016 and August 2017.

	Lake										
	Inuvik Region						Outer delta			Richard's Island	
	129	**80**	**87**	**280**	**56**	**520**	**Swiss Cheese – ref****	**Swiss Cheese – seep****	**Manta**	**North Head 1**	**North Head 2**
Latitude (°N)	68° 18.244'	68° 19.395'	68° 19.015'	68° 19.276'	68° 19.417'	68° 18.826'	69° 13.644'	69° 13.745'	69° 13.133'	69° 42.991'	69° 40.506'
Longitude (°W)	133° 51.090'	133° 52.204'	133° 52.460'	133° 50.309'	133° 50.805'	133° 42.931'	135° 14.257'	135° 14.765'	135° 12.406'	134° 26.557'	134° 26.963'
Summer Sill Height (m)	2.363	2.631	3.389	3.838	4.623	4.913	-	-	-	-	-
Closure Class	No	Low	Low	Low	High	High	-	-	-	-	-
Lake area (km^2)	0.378	0.193	0.039	0.024	0.021	0.002	-	-	-	-	-
Deployment Depth (m)	3.10	Not Measured	-	2.90	1.50	3.10	2.10	2.40	2.30	4.10	3.10
Sampling Depths (m)	2.83	Not Measured	-	2.63	1.23	2.70 2.90 3.04 7 cmbsf	1.83	2.13	2.03	3.83	2.83
OsmoSampler 1st Deployment	1 Aug. 2015	-	-	4 Aug. 2015	2 Aug. 2015	3 Aug. 2015	4 Aug. 2015	4 Aug. 2015	4 Aug. 2015	7 Aug. 2015	7 Aug. 2015
OsmoSampler 1st Retrieval/ 2nd Deployment	10 Aug. 2016	15 Aug. 2016	-	12 Aug. 2016	12 Aug. 2016	9 Aug. 2016	13 Aug. 2016	13 Aug. 2016	13 Aug. 2016	14 Aug. 2016	-
OsmoSampler 2nd Retrieval	9 Aug. 2017	10 Aug. 2017	-	9 Aug. 2017	9 Aug. 2017	12 Aug. 2017	16 Aug. 2017	13 Aug. 2017	14 Aug. 2017	14 Aug. 2017	-
Temperature Range (°C)	1.1 – 20.0	1.8 – 20.3	-	1.6 – 20.1	1.5 – 25.2	2.4 – 17.5	-0.1 – 20.0	0.1 – 20.6	-0.1 – 20.4	0.0 – 17.5	0.0 – 16.5
Salinity Range (ppt)	0.03 – 0.10	0.01 – 0.03	-	0.01 – 0.03	0.01 – 0.04	Below Detection	0.37 – 0.95	0.07 – 1.79	0.01 – 0.12	0.04 – 0.31	0.09 – 0.20

* Lake areas and summer sill heights for Inuvik Region lakes from Lesack & Marsh (2010) and Cunada (2016).

** SC-ref and SC-seep sites are referenced as SC-1 and SC-2, respectively, in the National Science Foundation Arctic Data Center

cmbsf = cm below sediment-water interface

Table S3-2. Summer-time surface water dissolved CH_4 concentrations and $\delta^{13}C-CH_4$ in Inuvik region lakes in the Mackenzie Delta.

Date	129				80				87				280				56				520			
	Mean CH_4 (μM)	s.d. (μM)	$\delta^{13}C-CH_4$ (‰)	s.d. (‰)	Mean CH_4 (μM)	s.d. (μM)	$\delta^{13}C-CH_4$ (‰)	s.d. (‰)	Mean CH_4 (μM)	s.d. (μM)	$\delta^{13}C-CH_4$ (‰)	s.d. (‰)	Mean CH_4 (μM)	s.d. (μM)	$\delta^{13}C-CH_4$ (‰)	s.d. (‰)	Mean CH_4 (μM)	s.d. (μM)	$\delta^{13}C-CH_4$ (‰)	s.d. (‰)	Mean CH_4 (μM)	s.d. (μM)	$\delta^{13}C-CH_4$ (‰)	s.d. (‰)
1 to 7 August 2015	0.82	0.01	-61.3	0.3									2.47	0.06	-45.3	0.6	1.3	0.0	-51.2	0.3	3.29	0.03	-37.4	0.2
21 March 2016	67	1.88	-67.3	0.0																	136.69	1.55	-64.1	0.1
9 May 2016	2.42	0.26	-64.1	0.7	0.08	0.01			260	3	-61.3	0.4	162	32	-60.0	0.8	1251.0	1.4	-65.0	0.2	223.99	3.98	-64.3	0.2
31 May 2016	0.10	0.01			0.09	0.03			0.34	0.01			4.24	0.12	-12.6	3.6	68.0	0.3	-55.6	0.1	141.75	16.96	-55.2	1.0
5 June 2016	0.04	0.01			0.03	0.00			0.01	0.01			11.22	0.47	-39.6	1.1	7.5	0.2	-37.3	0.3	14.48	0.09	-51.7	0.0
13 or 15 June 2016	0.91	0.09	-53.2	0.3																	6.40	0.19	-49.7	0.0
20 June 2016	0.66	0.05	-57.1	0.5	0.33	0.00	-62.6	0.5	1.09	0.12	-53.1	1.2	9.24	1.43	-34.4	0.6	2.6	0.1	-53.9	0.5	4.92	0.78	-49.1	0.2
25 June 2016																	2.7	0.0						
7 July 2016	0.97	0.03	-60.2	1.9	0.52	0.01	-64.9	0.1	1.89	0.12	-56.8	0.8	3.96	0.02	-47.4	0.1	3.1	0.1	-47.0	0.7	7.11	0.52	-44.3	0.9
19 July 2016	0.95	0.07	-54.2	1.8	0.58	0.01	-61.3	1.8	2.19	0.24	-46.8	0.9	3.85	0.25	-43.0	0.2	2.6	0.0	-45.5	0.4	33.71	0.52	-47.3	0.3
1 to 2 August 2016	0.58	0.01	-61.4	0.1	0.50	0.01	-66.2	0.4	0.88	0.20	-53.0	1.6	2.02	0.03	-44.3	0.6	1.8	0.1	-49.8	0.4	2.38	0.21	-43.4	0.3
6 August 2016	0.47	0.01	-59.8	0.5	0.44	0.01	-65.0	0.1	0.59	0.00	-57.6	0.1	0.84	0.26	-19.7	9.8	1.5	0.0	-50.9	0.1	4.27	0.02	-47.5	0.2
9 to 15 August 2016	0.82	0.01	-63.6	0.2	0.51	0.01	-68.7	0.2	0.82	0.01	-60.0	0.4	0.51	0.04	-20.4	1.8	2.0	0.0	-48.1	1.4	2.39	0.05	-47.8	0.3
9 to 15 August 2017					0.90	0.13	-67.5	0.2	1.46	0.04	-55.4	0.2	0.22	0.02	-4.9	1.1	1.8	0.1	-50.8	0.9	3.29	0.05	-47.5	0.1

Table S3-3. Summer-time surface water dissolved CH_4 concentrations and $\delta^{13}C\text{-}CH_4$ in outer delta region lakes and the Mackenzie River in the Mackenzie Delta.

Date	Mackenzie River				SC1-ref				SC-seep				Manta				NH1				NH2			
	Mean CH_4 (μM)	s.d. (μM)	$\delta^{13}C\text{-}CH_4$ (‰)	s.d. (‰)	Mean CH_4 (μM)	s.d. (μM)	$\delta^{13}C\text{-}CH_4$ (‰)	s.d. (‰)	Mean CH_4 (μM)	s.d. (μM)	$\delta^{13}C\text{-}CH_4$ (‰)	s.d. (‰)	Mean CH_4 (μM)	s.d. (μM)	$\delta^{13}C\text{-}CH_4$ (‰)	s.d. (‰)	Mean CH_4 (μM)	s.d. (μM)	$\delta^{13}C\text{-}CH_4$ (‰)	s.d. (‰)	Mean CH_4 (μM)	s.d. (μM)	$\delta^{13}C\text{-}CH_4$ (‰)	s.d. (‰)
1 to 7 August 2015					1.10	0.06	-63.1	0.7	2.76	0.09	-54.0	0.3	1.39	0.01	-59.1	3.8	0.42	0.01			0.10	0.01		
9 to 15 August 2016	0.72	0.02	-70.4	0.3	0.60	0.01	-66.3	0.7	1.74	0.01	-51.8	0.4	0.83	0.01	-63.6	0.1	0.81	0.01	-42.1	0.5	0.33	0.010	-53.5	0.1
9 to 15 August 2017	0.45	0.01	-66.5	0.1	0.45	0.01	-52.3	0.9	1.03	0.01	-46.5	0.3	1.19	0.09	-46.9	1.3	0.26	0.00	-39.5	0.6				

Table S3-4. Mackenzie Delta lakes sediment pore-water CH_4 concentrations and $\delta^{13}C$-CH_4 from sediment cores collected in August 2015, August 2016, and August 2017.

Lake	Year	Depth (cm)	CH_4 Average (µM)	CH_4 stdev (µM)	$\delta^{13}C$-CH_4 (‰)	$\delta^{13}C$-CH_4 stdev (‰)
129	2015	0-3	27.88	0.01	-73.6	0.8
		3-6	101.21	0.15	-73.1	0.6
		6-9	112.64	0.03	-74.8	0.6
		9-12	278.41	0.15	-75.4	0.4
		12-15	353.71	0.55	-76.4	0.5
		15-18	581.14	33.42	-76.4	0.4
		18-21	780.94	0.61	-77.1	0.4
		21-24	691.52	0.41	-77.6	0.6
	2016	0-2	32.16	0.28	-66.3	0.6
		2-4	120.45	0.29	-67.2	0.8
		4-8	249.04	0.18	-68.9	0.5
		8-12	360.46	0.87	-70.3	0.5
		12-16	421.95	0.51	-71.2	0.4
		16-20	492.24	0.27	-71.8	0.5
		20-24	549.74	0.06	-61.7	0.4
	2017	0-2	48.54	*	-61.6	1.8
		2-4	132.89	*	-65.8	0.9
		4-6	173.69	*	-64.2	0.5
		6-8	256.48	*	-69.0	0.7
		8-12	334.69	*	-71.6	0.5
		12-16	472.19	*	-73.7	0.4
		16-20	527.90	*		
		20-24	623.00	*	-75.7	0.5
		24-27	532.42	*	-74.9	0.5
280	2016	0-2	385.25	1.80	-67.2	0.4
		2-4	606.15	0.56	-68.0	0.3
		4-7	1253.47	2.04	-68.3	0.3
		7-10	794.90	2.24	-69.3	0.4
		10-13	794.33	0.71	-69.8	0.4
		13-16	868.29	0.06	-70.1	0.4
		16-19	751.74	0.56	-69.9	0.4
	2017	0-2	493.18	*	-66.1	0.7
		2-4	628.08	*	-67.1	0.4
		4-6	811.64	*	-67.7	0.7
		6-8	835.87	*	-69.2	0.4
		8-12	749.22	*	-70.0	0.6
		12-13	675.55	*	-69.1	0.3

* Replicate injections not run, CV for standards was less than 2%

Table S3-4 (continued).

Lake	Year	Depth (cm)	CH_4 Average (µM)	CH_4 stdev (µM)	$\delta^{13}C$-CH_4 (‰)	$\delta^{13}C$-CH_4 stdev (‰)
80	2016	0-2	12.59	0.40	-63.7	1.0
		2-4	37.49	0.46	-64.9	0.5
		4-7	89.42	0.17	-70.6	1.1
		7-10	143.10	0.16	-73.6	0.6
		10-13	212.64	0.75	-76.4	0.4
		13-16	242.44	0.15	-77.5	0.5
		16-19	351.87	2.49	-78.7	0.5
		19-21	295.64	0.12	-78.8	0.3
	2017	0-2	54.29	*	-59.0	1.6
		2-4	135.08	*	-59.9	0.7
		4-6	180.30	*	-58.6	0.6
		6-8	148.08	*	-58.0	0.5
		8-12	369.10	*	-61.8	0.5
		12-16	385.91	*	-65.7	0.5
		16-18	398.43	*	-67.7	0.5
87	2016	0-2	29.53	0.18	-68.6	0.4
		2-4	126.54	0.22	-71.7	0.8
		4-7	244.19	0.20	-76.2	0.4
		7-10	348.20	0.67	-78.5	0.4
		10-13				
		13-16	422.00	1.12	-79.5	0.6
		16-19	388.00	0.44	-79.2	0.5
		19-22	435.60	2.10	-79.3	0.3
		22-25	451.53	0.73	-79.3	0.5
		25-28	440.51	1.21	-79.2	0.4
		28-32	479.07	1.10	-79.0	0.4
	2017	0-2	593.38	*	-55.8	0.4
		2-4	349.64	*	-58.6	0.7
		4-6	429.63	*	-59.5	0.8
		6-8	596.95	*	-59.3	0.4
		8-12	512.49	*	-60.6	0.4
		12-16	508.97	*	-61.6	0.5
		16-20	539.18	*	-63.2	0.5

* Replicate injections not run, CV for standards was less than 2%

Table S3-4 (continued).

Lake	Year	Depth (cm)	CH_4 Average (µM)	CH_4 stdev (µM)	$\delta^{13}C$-CH_4 (‰)	$\delta^{13}C$-CH_4 stdev (‰)
56	2016	0-2	1334.50	2.40	-59.7	0.3
		2-4	1289.19	2.57	-61.7	0.5
		4-7	1389.41	8.16	-63.7	0.3
		7-10	1463.43	3.35	-64.3	0.4
		10-13	700.95	1.76	-65.8	0.5
		13-16	636.81	1.77	-65.8	0.3
	2017	0-2	1167.59	*	-61.5	0.6
		2-4	1046.13	*	-62.8	0.3
		4-6	1358.25	*	-67.6	0.4
		6-8	1336.66	*	-67.6	0.4
		8-12	1319.94	*	-69.3	0.6
		12-16	845.92	*	-70.2	0.5
520	2015	0-3	1588.27	1.40	-68.3	0.4
		3-6	2729.73	3.16	-72.0	0.5
		6-9	2250.65	157.39	-73.2	0.3
		9-12	1573.98	4.35	-73.4	0.5
		12-15	1533.11	2.49	-73.6	0.3
		15-18	1922.79	0.10	-73.3	0.3
		18-21	2425.77	216.61	-73.2	0.2
		21-24	623.89	0.74	-72.5	0.4
	2016	0-2	847.22	0.09	-66.0	0.3
		2-4	1006.92	1.37	-67.4	0.2
		4-8	1298.37	5.92	-72.4	0.4
		8-12	1341.20	0.62	-73.2	0.4
		12-16	1321.63	3.91	-73.2	0.3
		16-20	1220.01	3.63	-72.9	0.4
	2017	0-2	591.90	*	-61.8	0.6
		2-4	689.61	*	-67.2	0.5
		4-6	1116.26	*	-70.9	0.3
		6-8	1052.11	*	-71.8	0.3
		8-12	1214.10	*	-72.2	0.3
		12-16	957.47	*	-72.1	0.4
Manta	2016	0-2	159.92	1.00	-58.0	0.7
		2-4	321.45	0.33	-60.1	0.3
		4-7	386.46	0.61	-60.4	0.6
		7-10	360.38	1.06	-59.3	0.5
		10-13	414.35	0.28	-59.5	0.3
		13-16	493.52	0.38	-60.8	1.0

* Replicate injections not run, CV for standards was less than 2%

Table S3-4 (continued).

Lake	Year	Depth (cm)	CH_4 Average (µM)	CH_4 stdev (µM)	$\delta^{13}C$-CH_4 (‰)	$\delta^{13}C$-CH_4 stdev (‰)
SC-ref	2016	0-2	353.08	0.27	-62.3	0.4
		2-4	475.48	0.31	-66.1	0.4
		4-7	1241.58		-67.4	0.5
		7-10	494.94	0.51	-69.7	0.4
		10-13	649.65	9.31	-70.6	0.5
		13-14	647.23	1.49	-71.0	0.2
	2017	0-2	396.62	0.94	-62.3	0.5
		2-4	547.05	1.62	-63.1	0.4
		4-6	477.69	1.63	-63.7	0.6
		6-8	592.43	0.03	-63.7	0.6
		8-12	494.27	1.63	-64.6	0.4
SC-seep	2016	0-2	363.53	0.75	-54.9	0.5
		2-4	832.95	*	-61.4	0.4
		4-7	873.02	*	-65.2	0.4
		7-10	775.48	0.46	-68.4	0.4
		10-13	644.86	1.09	-70.8	0.4
		13-16	1062.26	1.30	-71.2	0.4
		16-19	1141.47	*	-71.9	0.4
		19-22	679.49	0.44	-71.8	0.5
		22-25	1117.81	*	-71.9	0.4
		25-28	1074.14	*	-72.1	0.6
		28-32	1247.44	2.15	-71.2	0.4
		32-27	1013.04	0.35	-71.1	0.3
	2017	0-2	454.07	1.66	-64.4	0.3
		2-4	467.05	1.81	-65.1	0.5
		4-6	533.02	2.43	-65.1	0.6
		6-8	525.76	2.30	-65.0	0.5
		8-12	608.31	1.77	-66.0	0.4
		12-16	711.18	0.88	-67.2	0.4
		16-20	760.91	2.92	-64.4	0.5
		20-24	940.94	3.26	-69.5	0.3
		24-28	777.67	2.74	-69.5	0.4
		28-32	545.63	1.06	-68.2	0.3
NH1	2016	0-2	79.75	0.03	-65.3	0.4
		2-4	287.57	0.68	-68.0	0.4
		4-7	396.43	0.37	-68.6	0.5
		7-10	291.81	1.97	-69.0	0.5
		10-13	447.97	1.54	-69.7	0.5
NH2	2016	0-2	6.55	0.10	-73.4	1.8
		2-4	14.92	0.02	-68.7	0.7
		4-6	23.27	0.32	-68.8	0.8

* Replicate injections not run, CV for standards was less than 2%

Table S3-5. Mackenzie Delta lake surface sediment organic carbon (OC) and nitrogen (TN) content.

Region	Lake	Year	Sediment Depth (cm)	OC (%)	TN (%)	$\delta^{13}C$ (‰, vs VPDB)	$\delta^{15}N$ (‰, vs Air)
Inuvik	129	2015	0-2	2.8	0.2	-19.2	2.4
	129	2016	0-2	1.3	0.2	-27.8	2.7
	129	2017	0-2	1.4	0.2	-28.2	2.8
	80	2016	0-2	1.7	0.2	-27.0	3.7
	80	2017	0-2	2.1	0.1	-26.8	3.6
	87	2016	2-4	1.3	0.2	-27.2	1.8
	87	2017	0-2	1.8	0.3	-25.6	1.4
	280	2016	0-2	1.0	0.1	-23.6	1.3
	280	2017	0-2	1.2	0.1	-28.7	1.5
	56	2016	0-2	1.0	0.1	-25.7	1.5
	56	2017	0-2	2.0	0.2	-19.9	0.7
	520	2015	0-3	13.0	1.1	-30.1	-2.7
	520	2016	0-2	13.0	1.2	-31.9	-1.9
	520	2017	0-2	9.3	0.2	-31.8	-1.2
Outer Delta	Manta	2016	0-2	7.8	0.9	-27.7	2.3
	SC-ref	2016	2-4	6.9	0.6	-28.9	1.6
	SC-ref	2017	0-2	5.7	0.6	-30.4	1.6
	SC-seep	2016	0-2	4.8	0.5	-27.8	1.8
	SC-seep	2017	0-2	3.8	0.2	-26.2	1.7
Richard's Island	NH1	2016	0-2	4.8	0.6	-27.6	3.7
	NH2	2016	0-2	1.6	0.1	-26.2	2.6

References

Alperin, M. J., Reeburgh, W. S., & Whiticar, M. J. (1988). Carbon and hydrogen isotope fractionation resulting from anaerobic methane oxidation. *Global Biogeochemical Cycles, 2*(3), 279-288. https://doi.org/10.1029/GB002i003p00279

Andresen, C. G., & Lougheed, V. L. (2015). Disappearing Arctic tundra ponds: Fine-scale analysis of surface hydrology in drained thaw lake basins over a 65 year period (1948–2013). *Journal of Geophysical Research: Biogeosciences, 120*(3), 466-479. https://doi.org/10.1002/2014JG002778

Bastviken, D., Cole, J. J., Pace, M. L., & Van, d. B. (2008). Fates of methane from different lake habitats: Connecting whole-lake budgets and CH_4 emissions. *Journal of Geophysical Research: Biogeosciences, 113*, GB4009. https://doi.org/10.1029/2007JG000608

Bastviken, D., Cole, J., Pace, M., & Tranvik, L. (2004). Methane emissions from lakes: Dependence of lake characteristics, two regional assessments, and a global estimate. *Global Biogeochemical Cycles, 18*(4), GB4009. https://doi.org/10.1029/2004GB002238

Bastviken, D., Ejlertsson, J., & Tranvik, L. (2002). Measurement of methane oxidation in lakes: A comparison of methods. *Environmental Science & Technology, 36*(15), 3354-3361. https://doi.org/10.1021/es010311p

Bastviken, D., Tranvik, L. J., Downing, J. A., Crill, P. M., & Enrich-Prast, A. (2011). Freshwater methane emissions offset the continental carbon sink. *Science, 331*(6013), 50. https://doi.org/10.1126/science.1196808

Bergstresser, M. (2018). *Composition of aquatic microbial communities and their relation to water-column methane cycling among Mackenzie Delta lakes, western Canadian Arctic* (Master's thesis). Retrieved from Simon Fraser University Summit Institutional Repository. (https://summit.sfu.ca/item/18731). Burnaby, British Columbia: Simon Fraser University.

Bigras, S. C. (1990). Hydrological regime of lakes in the Mackenzie Delta, Northwest Territories, Canada. *Arctic and Alpine Research, 22*(2), 163-174. https://doi.org/10.1080/00040851.1990.12002778

Black, R. A., & Bliss, L. C. (1980). Reproductive Ecology of *Picea mariana* (Mill.) BSP, at tree line near Inuvik, Northwest Territories, Canada. *Ecolmirogical Monographs, 50*(3), 331-354. https://doi.org/10.2307/2937255

Blake, L. I., Tveit, A., Ovreas, L., Head, I. M., & Gray, N. D. (2015). Response of methanogens in Arctic sediments to temperature and methanogenic substrate availability. *Plos One, 10*(6), 1-18. https://doi.org/10.1371/journal.pone.0129733

Boereboom, T., Depoorter, M., Coppens, S., & Tison, J. (2012). Gas properties of winter lake ice in Northern Sweden: implication for carbon gas release. *Biogeosciences, 9*(2), 827-838. https://doi.org/10.5194/bg-9-827-2012

Bouchard, F., Turner, K. W., MacDonald, L. A., Deakin, C., White, H., Farquharson, N., Medeiros, A. S., Wolfe, B. B., Hall, R. I., Pienitz, R., & Edwards, T. W. D. (2013). Vulnerability of shallow subarctic lakes to evaporate and desiccate when snowmelt runoff is low. *Geophysical Research Letters, 40*(23), 6112-6117. https://doi.org/10.1002/2013GL058635

Bouchard, F., Laurion, I., Prėskienis, V., Fortier, D., Xu, X., & Whiticar, M. J. (2015). Modern to millennium-old greenhouse gases emitted from ponds and lakes of the Eastern Canadian Arctic (Bylot Island, Nunavut). Biogeosciences, 12(23), 7279-7298. https://doi.org/10.5194/bg-12-7279-2015

Boucher, O., Friedlingstein, P., Collins, B., & Shine, K. P. (2009). The indirect global warming potential and global temperature change potential due to methane oxidation. *Environmental Research Letters, 4*(4), 044007. https://doi.org/10.1088/1748-9326/4/4/044007

Burn, C. R., & Kokelj, S. V. (2009). The environment and permafrost of the Mackenzie Delta area. *Permafrost and Periglacial Processes, 20*(2), 83-105. https://doi.org/10.1002/ppp.655

Burn, C. R., Parameswaran, V. R., Kutny, L., & Boyle, L. (1998). Electrical potentials measured during growth of lake ice, Mackenzie delta area, N.W.T., Canada. In A. G. Lewkowicz, & M. Allard (Eds.), Proceedings of the 7th International Conference on Permafrost, Yellowknife, N.W.T., 23–27 June 1998 (pp. 101-106). Québec, Nordicana: Université Laval.

Cadieux, S. B., White, J. R., Sauer, P. E., Peng, Y., Goldman, A. E., & Pratt, L. M. (2016). Large fractionations of C and H isotopes related to methane oxidation in Arctic lakes. *Geochimica Et Cosmochimica Acta, 187*, 141-155. https://doi.org/10.1016/j.gca.2016.05.004

Calmels, D., Gaillardet, J., Brenot, A., & France-Lanord, C. (2007). Sustained sulfide oxidation by physical erosion processes in the Mackenzie River basin: Climatic perspectives. *Geology, 35*(11), 1003-1006. https://doi.org/10.1130/G24132A.1

Carson, M. A., Conly, F. M., & Jasper, J. N. (1999). Riverine sediment balance of the Mackenzie Delta, Northwest Territories, Canada. *Hydrological Processes, 13*(16), 2499-2518. https://doi.org/10.1002/(SICI)1099-1085(199911)13:163.0.CO;2-I

Casper, P., Maberly, S. C., Hall, G. H., & Finlay, B. J. (2000). Fluxes of methane and carbon dioxide from a small productive lake to the atmosphere. *Biogeochemistry, 49*(1), 1-19. https://doi.org/10.1023/A:1006269900174

Chanton, J. P. (2005). The effect of gas transport on the isotope signature of methane in wetlands. *Organic Geochemistry, 36*(5), 753-768. https://doi.org/10.1016/j.orggeochem.2004.10.007

Chanton, J. P., Bauer, J. E., Glaser, P. A., Siegel, D. I., Kelley, C. A., Tyler, S. C., Romanowicz, E. H., & Lazrus, A. (1995). Radiocarbon evidence for the substrates

supporting methane formation within northern Minnesota peatlands. *Geochimica Et Cosmochimica Acta, 59*(17), 3663-3668. https://doi.org/10.1016/0016-7037(95)00240-Z

Chanton, J. P., Martens, C. S., & Kelley, C. A. (1989). Gas transport from methane-saturated, tidal freshwater and wetland sediments. *Limnology and Oceanography, 34*(5), 807-819. https://doi.org/10.4319/lo.1989.34.5.0807

Chanton, J., & Liptay, K. (2000). Seasonal variation in methane oxidation in a landfill cover soil as determined by an in situ stable isotope technique. *Global Biogeochemical Cycles, 14*(1), 51-60. https://doi.org/10.1029/1999GB900087

Cole, J. J., & Caraco, N. F. (1998). Atmospheric exchange of carbon dioxide in a low-wind oligotrophic lake measured by the addition of SF_6. *Limnology and Oceanography, 43*(4), 647-656. https://doi.org/10.4319/lo.1998.43.4.0647

Cole, J. J., Prairie, Y., Caraco, N., McDowell, W., Tranvik, L., Striegl, R., Duarte, C., Kortelainen, P., Downing, J., Middelburg, J., & Melack, J. (2007). Plumbing the global carbon cycle: Integrating inland waters into the terrestrial carbon budget. *Ecosystems, 10*(1), 172-185. https://doi.org/10.1007/s10021-006-9013-8

Coleman, D. D., Risatti, J. B., & Schoell, M. (1981). Fractionation of carbon and hydrogen isotopes by methane-oxidizing bacteria. *Geochimica Et Cosmochimica Acta, 45*(7), 1033-1037. https://doi.org/10.1016/0016-7037(81)90129-0

Collett, T. S., & Dallimore, S. R. (1999). Hydrocarbon gases associated with permafrost in the Mackenzie Delta, Northwest Territories, Canada. *Applied Geochemistry, 14*(5), 607-620. https://doi.org/10.1016/S0883-2927(98)00087-0

Connon, R. F., Quinton, W. L., Craig, J. R., & Masaki, H. (2014). Changing hydrologic connectivity due to permafrost thaw in the lower Liard River valley, NWT, Canada. *Hydrological Processes, 28*(14), 4163-4178. https://doi.org/10.1002/hyp.10206

Conrad, R. (2005). Quantification of methanogenic pathways using stable carbon isotopic signatures: a review and a proposal. *Organic Geochemistry, 36*(5), 739-752. https://doi.org/10.1016/j.orggeochem.2004.09.006

Cornwell, J. C., & Kipphut, G. W. (1992). Biogeochemistry of manganese- and iron-rich sediments in Toolik Lake, Alaska. In W. J. O'Brien (Ed.), *Toolik Lake: Ecology of an aquatic ecosystem in Arctic Alaska* (pp. 45-59). Dordrecht, Netherlands: Springer. https://doi.org/10.1007/978-94-011-2720-2_5

Cunada, C. L. (2016). *Seasonal methane dynamics in lakes of the Mackenzie River Delta, Western Canadian Arctic* (Master's thesis). Retrieved from Simon Fraser University Summit Institutional Repository. (http://summit.sfu.ca/item/16714). Burnaby, British Columbia: Simon Fraser University.

Cunada, C. L., Lesack, L. F. W., & Tank, S. E. (2018). Seasonal dynamics of dissolved methane in lakes of the Mackenzie Delta and the role of carbon substrate quality. *Journal of Geophysical Research: Biogeosciences, 123*(2), 591-609. https://doi.org/10.1002/2017JG004047

Dallimore, S. R., & Collett, T. S. (1995). Intrapermafrost gas hydrates from a deep core hole in the Mackenzie Delta, Northwest Territories, Canada. *Geology, 23*(6), 527-530. https://doi.org/10.1130/0091-7613(1995)0232.3.CO;2

Dallimore, S. R., & Matthews, J. V. (1997). The Mackenzie Delta borehole project, Environmental Studies Research Funds. (No. 135). Ottowa, Ontario: Geological Survey of Canada.

Dean, J. F., van, d. V., Garnett, M. H., Dinsmore, K. J., Baxter, R., Lessels, J. S., Smith, P., Street, L. E., Subke, J., Tetzlaff, D., Washbourne, I., Wookey, P. A., & Billett, M. F. (2018). Abundant pre-industrial carbon detected in Canadian Arctic headwaters: implications for the permafrost carbon feedback. *Environmental Research Letters, 13*(3), 034024. https://doi.org/10.1088/1748-9326/aaa1fe

DelSontro, T., McGinnis, D. F., Wehrli, B., & Ostrovsky, I. (2015). Size does matter: Importance of large bubbles and small-scale hot spots for methane transport. *Environmental Science & Technology, 49*(3), 1268-1276. https://doi.org/10.1021/es5054286

Delwiche, K. B., & Hemond, H. F. (2017). Methane bubble size distributions, flux, and dissolution in a freshwater lake. *Environmental Science & Technology, 51*(23), 13733-13739. https://doi.org/10.1021/acs.est.7b04243

Denfeld, B. A., Baulch, H. M., del Giorgio, P. A., Hampton, S. E., & Karlsson, J. (2018). A synthesis of carbon dioxide and methane dynamics during the ice-covered period of northern lakes. *Limnology and Oceanography Letters, 3*(3), 117-131. https://doi.org/10.1002/lol2.10079

Denfeld, B. A., Ricão Canelhas, M., Weyhenmeyer, G. A., Bertilsson, S., Eiler, A., & Bastviken, D. (2016). Constraints on methane oxidation in ice-covered boreal lakes. *Journal of Geophysical Research: Biogeosciences, 121*(7), 1924-1933. https://doi.org/10.1002/2016JG003382

Deshpande, B. N., MacIntyre, S., Matveev, A., & Vincent, W. F. (2015). Oxygen dynamics in permafrost thaw lakes: Anaerobic bioreactors in the Canadian subarctic. *Limnology and Oceanography, 60*(5), 1656-1670. https://doi.org/10.1002/lno.10126

Dixon, J., Morrell, G. R., Dietrich, J. R., Taylor, G. C., Procter, R. M., Conn, R. F., Dallaire, S. M., & Christie, J. A. (1994). Petroleum resources of the Mackenzie Delta and Beaufort Sea. Geological Survey of Canada, Bulletin 474

Dingman, S. L. (1994). Physical Hydrology. Macmillan Publishing Company.

Dlugokencky, E. J., Crotwell, A. M., Lang, P. M., Mund, J. W., & Rhodes, M. E. (2018). Atmospheric Methane Dry Air Mole Fractions from quasi-continuous measurements at Barrow, Alaska and Mauna Loa, Hawaii, 1986-2017, Version: 2018-03-19, ftp://aftp.cmdl.noaa.gov/data/trace_gases/ch4/in-situ/surface/

Downing, J. A., Prairie, Y. T., Cole, J. J., Duarte, C. M., Tranvik, L. J., Striegl, R. G., McDowell, W. H., Kortelainen, P., Melack, J. M., & Middelburg, J. J. (2006). The global abundance and size distribution of lakes, ponds, and impoundments.

Limnology and Oceanography, 51(5), 2388-2397. https://doi.org/10.4319/lo.2006.51.5.2388

Duc, N. T., Crill, P., & Bastviken, D. (2010). Implications of temperature and sediment characteristics on methane formation and oxidation in lake sediments. *Biogeochemistry, 100*(1), 185-196. https://doi.org/10.1007/s10533-010-9415-8

Elder, C. D., Schweiger, M., Lam, B., Crook, E. D., Xu, X., Walker, J., Walter Anthony, K. M., & Czimczik, C. I. (2019). Seasonal sources of whole-lake CH_4 and CO_2 emissions from interior Alaskan thermokarst lakes. *Journal of Geophysical Research: Biogeosciences, 124*(5), 1209-1229. https://doi.org/10.1029/2018JG004735

Elder, C. D., Xu, X., Walker, J., Schnell, J. L., Hinkel, K. M., Townsend-Small, A., Arp, C. D., Pohlman, J. W., Gaglioti, B. V., & Czimczik, C. I. (2018). Greenhouse gas emissions from diverse Arctic Alaskan lakes are dominated by young carbon. *Nature Climate Change, 8*(2), 166-171. https://doi.org/10.1038/s41558-017-0066-9

Emmerton, C. A., Lesack, L. F. W., & Marsh, P. (2007). Lake abundance, potential water storage, and habitat distribution in the Mackenzie River Delta, western Canadian Arctic. *Water Resources Research, 43*(5), W05419. https://doi.org/10.1029/2006WR005139

Emmerton, C. A., Lesack, L. F. W., & Vincent, W. F. (2008). Nutrient and organic matter patterns across the Mackenzie River, estuary and shelf during the seasonal recession of sea-ice. *Journal of Marine Systems, 74*(3–4), 741-755. https://doi.org/10.1016/j.jmarsys.2007.10.001

Environment and Climate Change Canada. Meteorological Service of Canada. (24 April 2018). Inuvik Climate. Northwest Territories. Climate Identifier 2202578, WMO Identifier 71364.

ESRI."Topographic" [basemap]. Scale Not Given. "World Topographic Map". Last accessed August 2019. https://services.arcgisonline.com/ArcGIS/rest/services/World_Imagery/MapServer. 2019.

Etiope, G. (2009). Natural emissions of methane from geological seepage in Europe. *Atmospheric Environment, 43*(7), 1430-1443. https://doi.org/10.1016/j.atmosenv.2008.03.014

Etiope, G., & Klusman, R. W. (2002). Geologic emissions of methane to the atmosphere. *Chemosphere, 49*(8), 777-789. https://doi.org/10.1016/S0045-6535(02)00380-6

Ettwig, K. F., Butler, M. K., Le Paslier, D., Pelletier, E., Mangenot, S., Kuypers, M. M. M., Schreiber, F., Dutilh, B. E., Zedelius, J., de Beer, D., et al. (2010). Nitrite-driven anaerobic methane oxidation by oxygenic bacteria. *Nature, 464*(7288), 543-548. https://doi.org/10.1038/nature08883

Ettwig, K. F., Zhu, B., Speth, D., Keltjens, J. T., Jetten, M. S. M., & Kartal, B. (2016). Archaea catalyze iron-dependent anaerobic oxidation of methane. *Proceedings of*

the National Academy of Sciences, 113(45), 12792-12796. https://doi.org/10.1073/pnas.1609534113

Garcia-Tigreros Kodovska, F., Sparrow, K. J., Yvon-Lewis, S., Paytan, A., Dimova, N. T., Lecher, A., & Kessler, J. D. (2016). Dissolved methane and carbon dioxide fluxes in Subarctic and Arctic regions: Assessing measurement techniques and spatial gradients. *Earth and Planetary Science Letters, 436*, 43-55. https://doi.org/10.1016/j.epsl.2015.12.002

Gareis, J. (2018). *Arctic deltas as biogeochemical hotspots affecting the delivery of nutrients and dissolved organic matter to the Arctic Ocean*. (PhD dissertation). Retrieved from Simon Fraser University Summit Institutional Repository. (https://summit.sfu.ca/item/18759). Burnaby, British Columbia: Simon Fraser University.

Gareis, J. A. L., & Lesack, L. F. W. (2017). Fluxes of particulates and nutrients during hydrologically defined seasonal periods in an ice-affected great Arctic river, the Mackenzie. *Water Resources Research, 53*(7), 6109-6132. https://doi.org/10.1002/2017WR020623

Garnett, M. H., Gulliver, P., & Billett, M. F. (2016). A rapid method to collect methane from peatland streams for radiocarbon analysis. *Ecohydrology, 9*(1), 113-121. https://doi.org/10.1002/eco.1617

Garnett, M. H., Hardie, S. L., & Murray, C. (2011). Radiocarbon and stable carbon analysis of dissolved methane and carbon dioxide from the profile of a raised peat bog. *Radiocarbon, 53*(1), 71-83. https://doi.org/10.1017/S0033822200034366

Garnett, M. H., Hardie, S. M. L., & Murray, C. (2012). Radiocarbon analysis of methane emitted from the surface of a raised peat bog. *Soil Biology and Biochemistry, 50*, 158-163. https://doi.org/10.1016/j.soilbio.2012.03.018

Gautier, D. L., Bird, K. J., Charpentier, R. R., Grantz, A., Houseknecht, D. W., Klett, T. R., Moore, T. E., Pitman, J. K., Schenk, C. J., Schuenemeyer, J. H., Sørensen, K., Tennyson, M. E., Valin, Z. C., & Wandrey, C. J. (2009). Assessment of undiscovered oil and gas in the Arctic. *Science, 324*(5931), 1175-1179. https://doi.org/10.1126/science.1169467

Geeves, K. (2019). *Carbon quality and quantity in lake sediments and their relationship with pore-water and lake-water methane among lakes of the Makenzie River Delta, Western Canadian Arctic* (Master's thesis). Retrieved from Simon Fraser University Summit Institutional Repository. (https://theses.lib.sfu.ca/5263/show). Burnaby, British Columbia: Simon Fraser University.

Gelesh, L., Marshall, K., Boicourt, W., & Lapham, L. (2016). Methane concentrations increase in bottom waters during summertime anoxia in the highly eutrophic estuary, Chesapeake Bay, U.S.A. *Limnology and Oceanography, 61*(S1), S253-S266. https://doi.org/10.1002/lno.10272

Gibson, J. J., & Edwards, T. W. D. (2002). Regional water balance trends and evaporation-transpiration partitioning from a stable isotope survey of lakes in

northern Canada. *Global Biogeochemical Cycles, 16*(2), 10-14. https://doi.org/10.1029/2001GB001839

Gill, D. (1973). Ecological modifications caused by the removal of tree and shrub canopies in the Mackenzie Delta. *Arctic, 26*(2), 95-111. https://doi.org/10.14430/arctic2904

Government of Northwest Territories Environment and Natural Resources. (2015). Climate observations in the Northwest Territories (1957-2012): Inuvik, Norman Wells, Yellowknife, Fort Smith. Yellowknife, NT.

Greene, S., Walter Anthony, K. M., Archer, D., Sepulveda-Jauregui, A., & Martinez-Cruz, K. (2014). Modeling the impediment of methane ebullition bubbles by seasonal lake ice. *Biogeosciences, 11*(23), 6791-6811. https://doi.org/10.5194/bg-11-6791-2014

Hahn, M. W. (2004). Broad diversity of viable bacteria in 'sterile' (0.2 μm) filtered water. *Research in Microbiology, 155*(8), 688-691. https://doi.org/10.1016/j.resmic.2004.05.003

Hamilton, J. D., Kelly, C. A., Rudd, J. W. M., Hesslein, R. H., & Roulet, N. T. (1994). Flux to the atmosphere of CH_4 and CO_2 from wetland ponds on the Hudson Bay lowlands (HBLs). *Journal of Geophysical Research: Atmospheres, 99*, 1495-1510. https://doi.org/10.1029/93JD03020

Hanson, P. C., Hamilton, D. P., Stanley, E. H., Preston, N., Langman, O. C., & Kara, E. L. (2011). Fate of allochthonous dissolved organic carbon in lakes: A quantitative approach. *Plos One, 6*(7), e21884. https://doi.org/10.1371/journal.pone.0021884

He, R., Wooller, M. J., Pohlman, J. W., Quensen, J., Tiedje, J. M., & Leigh, M. B. (2012). Diversity of active aerobic methanotrophs along depth profiles of arctic and subarctic lake water column and sediments. *The ISME Journal, 6*(10), 1937-1948. https://doi.org/10.1038/ismej.2012.34

Hedges, J. I., & Stern, J. (1984). Carbon and nitrogen determinations of carbonate-containing solids. *Limnology and Oceanography, 29*(3), 657-663. https://doi.org/10.4319/lo.1984.29.3.0657

Hershey, A. E., Northington, R. M., & Whalen, S. C. (2014). Substrate limitation of sediment methane flux, methane oxidation and use of stable isotopes for assessing methanogenesis pathways in a small arctic lake. *Biogeochemistry, 117*(2), 325-336. https://doi.org/10.1007/s10533-013-9864-y

Heslop, J. K., Walter Anthony, K. M., Sepulveda-Jauregui, A., Martinez-Cruz, K., Bondurant, A., Grosse, G., & Jones, M. C. (2015). Thermokarst lake methanogenesis along a complete talik profile. *Biogeosciences, 12*(14), 4317-4331. https://doi.org/10.5194/bg-12-4317-2015

Heslop, J. K., Winkel, M., Walter Anthony, K. M., Spencer, R. G. M., Podgorski, D. C., Zito, P., Kholodov, A., Zhang, M., & Liebner, S. (2019). Increasing organic carbon biolability with depth in yedoma permafrost: Ramifications for future climate change. *Journal of Geophysical Research: Biogeosciences, 124*(7), 2021-2038. https://doi.org/10.1029/2018JG004712

Howarth, R. W. (2019). Ideas and perspectives: is shale gas a major driver of recent increase in global atmospheric methane? *Biogeosciences, 16*(15), 3033-3046. https://doi.org/10.5194/bg-16-3033-2019

Hu, K., Issler, D. R., Chen, Z., & Brent, T. A. (2013). Permafrost investigation by well logs, and seismic velocity and repeated shallow temperature surveys, Beaufort-Mackenzie Basin. Natural Resources Canada. https://doi.org/10.4095/293120

Huttula, T., Pulkkanen, M., Arkhipov, B., Leppäranta, M., Solbakov, V., Shirasawa, K., & Salonen, K. (2010). Modelling circulation in an ice-covered lake. *Estonian Journal of Earth Sciences, 59*(4), 298-309. https://doi.org/10.3176/earth.2010.4.06

Huttunen, J. T., Alm, J., Liikanen, A., Juutinen, S., Larmola, T., Hammar, T., Silvola, J., & Martikainen, P. J. (2003a). Fluxes of methane, carbon dioxide and nitrous oxide in boreal lakes and potential anthropogenic effects on the aquatic greenhouse gas emissions. *Chemosphere, 52*(3), 609-621. https://doi.org/10.1016/S0045-6535(03)00243-1

Huttunen, J. T., Alm, J., Saarijärvi, E., Matti Lappalainen, K., Silvola, J., & Martikainen, P. J. (2003b). Contribution of winter to the annual CH_4 emission from a eutrophied boreal lake. *Chemosphere, 50*(2), 247-250. https://doi.org/10.1016/S0045-6535(02)00148-0

Huttunen, J. T., Väisänen, T. S., Heikkinen, M., Hellsten, S., Nykänen, H., Nenonen, O., & Martikainen, P. J. (2002). Exchange of CO_2, CH_4 and N_2O between the atmosphere and two northern boreal ponds with catchments dominated by peatlands or forests. *Plant and Soil, 242*(1), 137-146. https://doi.org/10.1023/A:1019606410655

Huttunen, J. T., Väisänen, T. S., Hellsten, S. K., & Martikainen, P. J. (2006). Methane fluxes at the sediment-water interface in some boreal lakes and reservoirs. *Boreal Environment Research, 11*(1), 27-34.

Jammet, M., Crill, P., Dengel, S., & Friborg, T. (2015). Large methane emissions from a subarctic lake during spring thaw: Mechanisms and landscape significance. *Journal of Geophysical Research: Biogeosciences, 120*(11), 2289-2305. https://doi.org/10.1002/2015JG003137

Jammet, M., Dengel, S., Kettner, E., Parmentier, F. -J. W., Wik, M., Crill, P., & Friborg, T. (2017). Year-round CH_4 and CO_2 flux dynamics in two contrasting freshwater ecosystems of the subarctic. *Biogeosciences Discussions, 14*, 5189-5216. https://doi.org/10.5194/bg-2016-466

Jannasch, H. W., Wheat, C. G., Plant, J. N., Kastner, M., & Stakes, D. S. (2004). Continuous chemical monitoring with osmotically pumped water samplers: OsmoSampler design and applications. *Limnology and Oceanography: Methods, 2*, 102-113. https://doi.org/10.4319/lom.2004.2.102

Jansen, J., Thornton, B. F., Jammet, M. M., Wik, M., Cortés, A., Friborg, T., MacIntyre, S., & Crill, P. M. (2019). Climate-sensitive controls on large spring emissions of

CH_4 and CO_2 from northern lakes. *Journal of Geophysical Research: Biogeosciences, 124*(7), 2379-2399. https://doi.org/10.1029/2019JG005094

Jepsen, S. M., Voss, C. I., Walvoord, M. A., Rose, J. R., Minsley, B. J., & Smith, B. D. (2013). Sensitivity analysis of lake mass balance in discontinuous permafrost: the example of disappearing Twelvemile Lake, Yukon Flats, Alaska (USA). *Hydrogeology Journal, 21*(1), 185-200. https://doi.org/10.1007/s10040-012-0896-5

Johnston, G. H., & Brown, R. J. E. (1961). Effect of a lake on distribution of permafrost in the Mackenzie River Delta. *Nature, 192*(4799), 251-252. https://doi.org/10.1038/192251a0

Johnston, G. H., & Brown, R. J. E. (1964). Some observations on permafrost distribution at a lake in the Mackenzie Delta, N.W.T., Canada. *Arctic, 17*(3), 162-175. https://doi.org/10.14430/arctic3501

Johnstone, J. F., & Kokelj, S. V. (2008). Environmental conditions and vegetation recovery at abandoned drilling mud sumps in the Mackenzie Delta region, Northwest Territories, Canada. *Arctic, 61*(2), 199-211. https://doi.org/10.14430/arctic35

Jones, B. M., Grosse, G., Arp, C. D., Jones, M. C., Walter Anthony, K. M., & Romanovsky, V. E. (2011). Modern thermokarst lake dynamics in the continuous permafrost zone, northern Seward Peninsula, Alaska. *Journal of Geophysical Research: Biogeosciences, 116*, G00M03. https://doi.org/10.1029/2011JG001666

Jones, F. E., & Harris, G. L. (1992). ITS-90 Density of water formlation for volumetric standards calibration. *Journal of Research of the National Institute of Standards and Technology, 97,* 335-340. https://doi.org/10.6028/jres.097.013

Jørgensen, B. B. (2000). Bacteria and Marine Biogeochemistry. In Z. M. Schulz H.D. (Ed.), *Marine Geochemistry.* (pp. 169-206) Springer, Berlin, Heidelberg.

Joung, D., Leduc, M., Ramcharitar, B., Xu, Y., Isles, P. D. F., Stockwell, J. D., Druschel, G. K., Manley, T., & Schroth, A. W. (2017). Winter weather and lake-watershed physical configuration drive phosphorus, iron, and manganese dynamics in water and sediment of ice-covered lakes. *Limnology and Oceanography, 62*(4), 1620-1635. https://doi.org/10.1002/lno.10521

Juutinen, S., Rantakari, M., Kortelainen, P., Huttunen, J. T., Larmola, T., Alm, J., Silvola, J., & Martikainen, P. J. (2009). Methane dynamics in different boreal lake types. *Biogeosciences, 6*(2), 209-223. https://doi.org/10.5194/bg-6-209-2009

Kankaala, P., Huotari, J., Peltomaa, E., Saloranta, T., & Ojala, A. (2006). Methanotrophic activity in relation to methane efflux and total heterotrophic bacterial production in a stratified, humic, boreal lake. *Limnology and Oceanography, 51*(2), 1195-1204. https://doi.org/10.4319/lo.2006.51.2.1195

Kankaala, P., Huotari, J., Tulonen, T., & Ojala, A. (2013). Lake-size dependent physical forcing drives carbon dioxide and methane effluxes from lakes in a boreal landscape. *Limnology and Oceanography, 58*(6), 1915-1930. https://doi.org/10.4319/lo.2013.58.6.1915

Kankaala, P., Taipale, S., Nykänen, H., & Jones, R. I. (2007). Oxidation, efflux, and isotopic fractionation of methane during autumnal turnover in a polyhumic, boreal lake. *Journal of Geophysical Research: Biogeosciences, 112*, G02033. https://doi.org/10.1029/2006JG000336

Karlsson, J., Giesler, R., Persson, J., & Lundin, E. (2013). High emission of carbon dioxide and methane during ice thaw in high latitude lakes. *Geophysical Research Letters, 40*(6), 1123-1127. https://doi.org/10.1002/grl.50152

Kessler, J. D., & Reeburgh, W. S. (2005). Preparation of natural methane samples for stable isotope and radiocarbon analysis. *Limnology and Oceanography: Methods, 3*(9), 408-418. https://doi.org/10.4319/lom.2005.3.408

Kirschke, S., Bousquet, P., Ciais, P., Saunois, M., Canadell, J. G., Dlugokencky, E. J., Bergamaschi, P., Bergmann, D., Blake, D. R., Bruhwiler, L., et al. (2013). Three decades of global methane sources and sinks. *Nature Geoscience, 6*(10), 813-823. https://doi.org/10.1038/ngeo1955

Kling, G. W., Kipphut, G. W., & Miller, M. C. (1992). The flux of CO_2 and CH_4 from lakes and rivers in arctic Alaska. *Hydrobiologia, 240*(1), 23-36. https://doi.org/10.1007/BF00013449

Knoblauch, C., Beer, C., Liebner, S., Grigoriev, M. N., & Pfeiffer, E. (2018). Methane production as key to the greenhouse gas budget of thawing permafrost. *Nature Climate Change, 8*(4), 309-312. https://doi.org/10.1038/s41558-018-0095-z

Knoblauch, C., Spott, O., Evgrafova, S., Kutzbach, L., & Pfeiffer, E. (2015). Regulation of methane production, oxidation, and emission by vascular plants and bryophytes in ponds of the northeast Siberian polygonal tundra. *Journal of Geophysical Research: Biogeosciences, 120*(12), 2525-2541. https://doi.org/10.1002/2015JG003053

Kohnert, K., Juhls, B., Muster, S., Antonova, S., Serafimovich, A., Metzger, S., Hartmann, J., & Sachs, T. (2018). Toward understanding the contribution of waterbodies to the methane emissions of a permafrost landscape on a regional scale—A case study from the Mackenzie Delta, Canada. *Global Change Biology, 24*(9), 3976-3989. https://doi.org/10.1111/gcb.14289

Kohnert, K., Serafimovich, A., Metzger, S., Hartmann, J., & Sachs, T. (2017). Strong geologic methane emissions from discontinuous terrestrial permafrost in the Mackenzie Delta, Canada. *Scientific Reports, 7*(1), 5828. https://doi.org/10.1038/s41598-017-05783-2

Lamontagne-Hallé, P., McKenzie, J. M., Kurylyk, B. L., & Zipper, S. C. (2018). Changing groundwater discharge dynamics in permafrost regions. *Environmental Research Letters, 13*(8), 084017. https://doi.org/10.1088/1748-9326/aad404

Lapham, L. L., Chanton, J. P., Martens, C. S., Higley, P. D., Jannasch, H. W., & Woolsey, J. R. (2008). Measuring temporal variability in pore-fluid chemistry to assess gas hydrate stability: Development of a continuous pore-fluid array. *Environmental Science & Technology, 42*(19), 7368-7373. https://doi.org/10.1021/es801195m

Lapham, L. L., Wilson, R. M., MacDonald, I. R., & Chanton, J. P. (2014). Gas hydrate dissolution rates quantified with laboratory and seafloor experiments. *Geochimica Et Cosmochimica Acta, 125*, 492-503. https://doi.org/10.1016/j.gca.2013.10.030

Lara, M. J., Lin, D. H., Andresen, C., Lougheed, V. L., & Tweedie, C. E. (2019). Nutrient release from permafrost thaw enhances CH_4 emissions from Arctic tundra wetlands. *Journal of Geophysical Research: Biogeosciences, 124*(6), 1560-1573. https://doi.org/10.1029/2018JG004641

Laurion, I., Vincent, W. F., MacIntyre, S., Retamal, L., Dupont, C., Francus, P., & Pienitz, R. (2010). Variability in greenhouse gas emissions from permafrost thaw ponds. *Limnology and Oceanography, 55*(1), 115-133. https://doi.org/10.4319/lo.2010.55.1.0115

Lecher, A. L. (2017). Groundwater discharge in the Arctic: A review of studies and implications for biogeochemistry. *Hydrology, 4*(3), 41. https://doi.org/10.3390/hydrology4030041

Lecher, A. L., Chuang, P., Singleton, M., & Paytan, A. (2017). Sources of methane to an Arctic lake in Alaska: An isotopic investigation. *Journal of Geophysical Research: Biogeosciences, 122*(4), 753-766. https://doi.org/10.1002/2016JG003491

Lecher, A. L., Kessler, J., Sparrow, K., Garcia-Tigreros Kodovska, F., Dimova, N., Murray, J., Tulaczyk, S., & Paytan, A. (2016). Methane transport through submarine groundwater discharge to the North Pacific and Arctic Ocean at two Alaskan sites. *Limnology and Oceanography, 61*, S344-S355. https://doi.org/10.1002/lno.10118

Leckrone, K. J., & Hayes, J. M. (1998). Water-induced errors in continuous-flow carbon isotope ratio mass spectrometry. *Analytical Chemistry, 70*(13), 2737-2744. https://doi.org/10.1021/ac9803434

Ledwell, J. J. (1984). The Variation of the gas transfer coefficient with molecular diffusity. In W. Brutsaert, & G. H. Jirka (Eds.), Gas transfer at water surfaces. water science and technology library. vol. 2. Springer, Dordrecht.

Lesack, L. F. W., & Marsh, P. (2007). Lengthening plus shortening of river-to-lake connection times in the Mackenzie River Delta respectively via two global change mechanisms along the arctic coast. *Geophysical Research Letters, 34*(23), L23404. https://doi.org/10.1029/2007GL031656

Lesack, L. F. W., & Marsh, P. (2010). River-to-lake connectivities, water renewal, and aquatic habitat diversity in the Mackenzie River Delta. *Water Resources Research, 46*(12), W12504. https://doi.org/10.1029/2010WR009607

Lesack, L. F. W., Marsh, P., & Hecky, R. E. (1990). Ice cover growth and freeze-out of solutes in a Mackenzie Delta lake. In T. D. Prowse, & C. S. L. Ommanney (Eds.), Northern Hydrology: Selected Perspectives (pp. 219-236) Environ. Can.

Lesack, L. F. W., Marsh, P., & Hecky, R. E. (1998). Spatial and temporal dynamics of major solute chemistry among Mackenzie Delta lakes. *Limnology and Oceanography, 43*(7), 1530-1543. https://doi.org/10.4319/lo.1998.43.7.1530

Lesack, L., Philip, M., Hicks, F. E., & Forbes, D. L. (2013). Timing, duration, and magnitude of peak annual water-levels during ice breakup in the Mackenzie Delta and the role of river discharge. *Water Resources Research, 49*(12), 8234-8249. https://doi.org/10.1002/2012WR013198

Lofton, D. D., Whalen, S. C., & Hershey, A. E. (2014). Effect of temperature on methane dynamics and evaluation of methane oxidation kinetics in shallow Arctic Alaskan lakes. *Hydrobiologia, 721*(1), 209-222. https://doi.org/10.1007/s10750-013-1663-x

Longworth, B. E., von Reden, K. F., Long, P., & Roberts, M. L. (2015). A high output, large acceptance injector for the NOSAMS Tandetron AMS system. *Nuclear Instruments and Methods in Physics Research Section B: Beam Interactions with Materials and Atoms, 361*, 211-216. https://doi.org/10.1016/j.nimb.2015.04.005

López Bellido, J., Peltomaa, E., & Ojala, A. (2011). An urban boreal lake basin as a source of CO_2 and CH_4. *Environmental Pollution, 159*(6), 1649-1659. https://doi.org/10.1016/j.envpol.2011.02.042

López Bellido, J., Tulonen, T., Kankaala, P., & Ojala, A. (2013). Concentrations of CO_2 and CH_4 in water columns of two stratified boreal lakes during a year of atypical summer precipitation. *Biogeochemistry, 113*(1), 613-627. https://doi.org/10.1007/s10533-012-9792-2

Lundin, E. J., Klaminder, J., Bastviken, D., Olid, C., Hansson, S. V., & Karlsson, J. (2015). Large difference in carbon emission - burial balances between boreal and arctic lakes. *Scientific Reports, 5*, 14248. https://doi.org/10.1038/srep14248

MacDonald, G. M., & Gajewski, K. (1992). The northern treeline of Canada. In D. G. Janelle (Ed.), Geographical Snapshots of North America (pp. 34-37) The Guilford Press.

MacIntyre, S., Cortés, A., & Sadro, S. (2018). Sediment respiration drives circulation and production of CO_2 in ice-covered Alaskan arctic lakes. *Limnology and Oceanography Letters, 3*(3), 302-310. https://doi.org/10.1002/lol2.10083

MacIntyre, S., Jonsson, A., Jansson, M., Aberg, J., Turney, D. E., & Miller, S. D. (2010). Buoyancy flux, turbulence, and the gas transfer coefficient in a stratified lake. *Geophysical Research Letters, 37*(24), L24604. https://doi.org/10.1029/2010GL044164

Mackay, J. R. (1983). Downward water movement into frozen ground, western arctic coast, Canada. *Canadian Journal of Earth Sciences, 20*(1), 120-134. https://doi.org/10.1139/e83-012

Mackay, J. R. (1995). Active layer changes (1968 to 1993) following the Forest-Tundra Fire near Inuvik, N.W.T., Canada. *Arctic and Alpine Research, 27*(4), 323-336. https://doi.org/10.1080/00040851.1995.12003129

Magen, C., Lapham, L. L., Pohlman, J. W., Marshall, K., Bosman, S., Casso, M., & Chanton, J. P. (2014). A simple headspace equilibration method for measuring dissolved methane. *Limnology and Oceanography: Methods, 12*(9), 637-650. https://doi.org/10.4319/lom.2014.12.637

Manning, C. C., Preston, V. L., Jones, S. F., Michel, A. P. M., Nicholson, D. P., Duke, P. J., Ahmed, M., Manganini, K., Else, B. G. T., & Tortell, P. D. (2019). River inflow dominates methane emissions in an Arctic coastal system. *EarthArXiv,* https://doi.org/10.31223/osf.io/cs7nx

Marsh, P. (1990). Permafrost and lakes in the Mackenzie Delta. Proceedings of the Fifth Canadian Permafrost Conference. Quebec City, Collection Nordicana, no. 54, University of Laval. 131-136.

Marsh, P. (1991). Evaporation and ice growth in Mackenzie Delta lakes. In G. Schiller (Ed.), Hydrology of natural and manmade Lakes. Proc. Symposium, Vienna, 1991. (pp. 257-266) IAHS, Publication 206.

Marsh, P., & Bigras, S. C. (1988). Evaporation from Mackenzie Delta Lakes, N.W.T., Canada. *Arctic and Alpine Research, 20*(2), 220-229. https://doi.org/10.2307/1551500

Marsh, P., & Hey, M. (1989). The flooding hydrology of Mackenzie Delta Lakes near Inuvik, N.W.T., Canada. *Arctic, 42*(1), 41-49. https://doi.org/10.14430/arctic1638

Marsh, P., & Hey, M. (1994). Analysis of spring high water events in the Mackenzie Delta and implications for lake and terrestrial flooding. *Geografiska Annaler. Series A, Physical Geography, 76*(4), 221-234. https://doi.org/10.2307/521082

Marsh, P., & Lesack, L. F. W. (1996). The hydrologic regime of perched lakes in the Mackenzie Delta: Potential responses to climate change. *Limnology and Oceanography, 41*(5), 849-856. https://doi.org/10.4319/lo.1996.41.5.0849

Marsh, P., Lesack, L. F. W., & Roberts, A. (1999). Lake sedimentation in the Mackenzie Delta, NWT. *Hydrological Processes, 13*(16), 2519-2536. https://doi.org/10.1002/(SICI)1099-1085(199911)13:163.0.CO;2-T

Martens, C. S., & Val Klump, J. (1980). Biogeochemical cycling in an organic-rich coastal marine basin—I. Methane sediment-water exchange processes. *Geochimica Et Cosmochimica Acta, 44*(3), 471-490. https://doi.org/10.1016/0016-7037(80)90045-9

Martens, C. S., Kelley, C. A., Chanton, J. P., & Showers, W. J. (1992). Carbon and hydrogen isotopic characterization of methane from wetlands and lakes of the Yukon-Kuskokwim delta, western Alaska. *Journal of Geophysical Research: Atmospheres, 97*(D15), 16689-16701. https://doi.org/10.1029/91JD02885

Martinez-Cruz, K., Sepulveda-Jauregui, A., Casper, P., Anthony, K. W., Smemo, K. A., & Thalasso, F. (2018). Ubiquitous and significant anaerobic oxidation of methane in freshwater lake sediments. *Water Research, 144*, 332-340. https://doi.org/10.1016/j.watres.2018.07.053

Martinez-Cruz, K., Sepulveda-Jauregui, A., Walter Anthony, K., & Thalasso, F. (2015). Geographic and seasonal variation of dissolved methane and aerobic methane oxidation in Alaskan lakes. *Biogeosciences, 12*(15), 4595-4606. https://doi.org/10.5194/bg-12-4595-2015

Matheus Carnevali, P. B., Rohrssen, M., Williams, M. R., Michaud, A. B., Adams, H., Berisford, D., Love, G. D., Priscu, J. C., Rassuchine, O., Hand, K. P., & Murray, A. E. (2015). Methane sources in arctic thermokarst lake sediments on the North Slope of Alaska. *Geobiology, 13*(2), 181-197. https://doi.org/10.1111/gbi.12124

Matveev, A., Laurion, I., & Vincent, W. F. (2018). Methane and carbon dioxide emissions from thermokarst lakes on mineral soils. *Arctic Science, 4*(4), 584-604. https://doi.org/10.1139/as-2017-0047

Matveev, A., Laurion, I., Deshpande, B. N., Bhiry, N., & Vincent, W. F. (2016). High methane emissions from thermokarst lakes in subarctic peatlands. *Limnology and Oceanography, 61*, S150-S164. https://doi.org/10.1002/lno.10311

McClelland, J. W., Holmes, R. M., Peterson, B. J., & Stieglitz, M. (2004). Increasing river discharge in the Eurasian Arctic: Consideration of dams, permafrost thaw, and fires as potential agents of change. *Journal of Geophysical Research: Atmospheres, 109*, D18102. https://doi.org/10.1029/2004JD004583

McClelland, J. W., Holmes, R. M., Peterson, B. J., Raymond, P. A., Striegl, R. G., Zhulidov, A. V., Zimov, S. A., Zimov, N., Tank, S. E., Spencer, R. G. M., Staples, R., Gurtovaya, T. Y., & Griffin, C. G. (2016). Particulate organic carbon and nitrogen export from major Arctic rivers. *Global Biogeochemical Cycles, 30*(5), 629-643. https://doi.org/10.1002/2015GB005351

McIntosh Marcek, H. A., Lance F. W. Lesack, Beth N. Orcutt, C. Geoff Wheat, Scott R. Dallimore, Kimberly Geeves, Laura L. Lapham. (Submitted). Continuous sampling over two years reveals methane builds-up under-ice with substantial winter-derived methane held during summer in the bottom waters of a small Arctic lake (Mackenzie River Delta). *Journal of Geophysical Research: Biogeosciences.*

McIntosh, H. A., McNichol, A. P., Xu, L., & Canuel, E. A. (2015). Source-age dynamics of estuarine particulate organic matter using fatty acid $\delta^{13}C$ and $\Delta^{14}C$ composition. *Limnology and Oceanography, 60*(2), 611-628. https://doi.org/10.1002/lno.10053

McNichol, A. P., & Aluwihare, L. I. (2007). The power of radiocarbon in biogeochemical studies of the marine carbon cycle: Insights from studies of dissolved and particulate organic carbon (DOC and POC). *Chemical Reviews, 107*(2), 443-466. https://doi.org/10.1021/cr050374g

McNichol, A. P., Gagnon, A. R., Jones, G. A., & Osborne, E. A. (1992). Illumination of a black box: Analysis of gas composition during graphite target preparation. *Radiocarbon, 34*(3), 321-329. https://doi.org/10.2458/azu_js_rc.34.1471

Michmerhuizen, C. M., Striegl, R. G., & McDonald, M. E. (1996). Potential methane emission from north-temperate lakes following ice melt. *Limnology and Oceanography, 41*(5), 985-991. https://doi.org/10.4319/lo.1996.41.5.0985

Mueller, C. W., Rethemeyer, J., Kao-Kniffin, J., Löppmann, S., Hinkel, K. M., & Bockheim, J.,G. (2015). Large amounts of labile organic carbon in permafrost

soils of northern Alaska. *Global Change Biology, 21*(7), 2804-2817. https://doi.org/10.1111/gcb.12876

Murton, J. B. (2009). Stratigraphy and palaeoenvironments of Richards Island and the eastern Beaufort Continental Shelf during the last glacial-interglacial cycle. *Permafrost and Periglacial Processes, 20*(2), 107-125. https://doi.org/10.1002/ppp.647

Myhre, G., Shindell, D., Bréon, F.M., Collins, W., Fuglestvedt, J., Huang, J., Koch, D., Lamarque, J.F., Lee, D, Mendoza, B,. Nakajima, T., Robock, A., Stephens, G., Takemura, T., Zhang, H. (2013). Anthropogenic and Natural Radiative Forcing. In T. F. Stocker, D. Qin, G. K. Plattner, M. Tignor, S. K. Allen, J. Boschung, Nauels, A., Xia, Y., Bex, V., P. M. Midgley (Eds.), *In Climate Change 2013: The Physical Science Basis. Contribution of Working Group I to the Fifth Assessment Report of the Intergovernmental Panel on Climate Change*. (pp. 659-740). Cambridge University Press, UK and New York, NY, USA. https://doi.org/10.1017/CBO9781107415324.018

Nakagawa, F., Yoshida, N., Nojiri, Y., & Makarov, V. (2002). Production of methane from alasses in eastern Siberia: Implications from its ^{14}C and stable isotopic compositions. *Global Biogeochemical Cycles, 16*(3), 1041. https://doi.org/10.1029/2000GB001384

Natchimuthu, S., Sundgren, I., Gålfalk, M., Klemedtsson, L., Crill, P., Danielsson, Å, & Bastviken, D. (2016). Spatio-temporal variability of lake CH_4 fluxes and its influence on annual whole lake emission estimates. *Limnology and Oceanography, 61*, S13-S26. https://doi.org/10.1002/lno.10222

Negandhi, K., Laurion, I., Whiticar, M. J., Galand, P. E., Xu, X., & Lovejoy, C. (2013). Small Thaw Ponds: An unaccounted source of methane in the Canadian High Arctic. *Plos One, 8*(11), e78204. https://doi.org/10.1371/journal.pone.0078204

Neumann, R. B., Blazewicz, S. J., Conaway, C. H., Turetsky, M. R., & Waldrop, M. P. (2016). Modeling CH_4 and CO_2 cycling using porewater stable isotopes in a thermokarst bog in Interior Alaska: results from three conceptual reaction networks. *Biogeochemistry, 127*(1), 57-87. https://doi.org/10.1007/s10533-015-0168-2

Nguyen, T., Burn, C. R., King, D. J., & Smith, S. L. (2009). Estimating the extent of near-surface permafrost using remote sensing, Mackenzie Delta, Northwest Territories. *Permafrost and Periglacial Processes, 20*(2), 141-153. https://doi.org/10.1002/ppp.637

Nisbet, E. G., Dlugokencky, E. J., Manning, M. R., Lowry, D., Fisher, R. E., France, J. L., Michel, S. E., Miller, J. B., White, J. W. C., et al. (2016). Rising atmospheric methane: 2007–2014 growth and isotopic shift. *Global Biogeochemical Cycles, 30*(9), 1356-1370. https://doi.org/10.1002/2016GB005406

Nisbet, E. G., Manning, M. R., Dlugokencky, E. J., Fisher, R. E., Lowry, D., Michel, S. E., Myhre, C. L., Platt, S. M., Allen, G., Bousquet, P., et al. (2019). Very strong atmospheric methane growth in the 4 Years 2014–2017: Implications for the Paris

Agreement. *Global Biogeochemical Cycles, 33*(3), 318-342. https://doi.org/10.1029/2018GB006009

Orcutt, B. (2017a). Collaborative Research: Year-round autonomous sampling of methane in Arctic lakes, Northwest Territories, Canada, 2011-2017. Arctic Data Center. https://doi.org/10.18739/A24R81

Orcutt, B. N., Lapham, L. L., Delaney, J., Sarode, N., Marshall, K. S., Whaley-Martin, K. J., Slater, G., Wheat, C. G., & Girguis, P. R. (2017b). Microbial response to oil enrichment in Gulf of Mexico sediment measured using a novel long-term benthic lander system. *Elementa Science of the Anthropocene, 5*, 18. https://doi.org/10.1525/elementa.129

Osburn, C. L., Anderson, N. J., Leng, M. J., Barry, C. D., & Whiteford, E. J. (2019). Stable isotopes reveal independent carbon pools across an Arctic hydro-climatic gradient: Implications for the fate of carbon in warmer and drier conditions. *Limnology and Oceanography Letters*, https://doi.org/10.1002/lol2.10119

Oswald, C. J., & Rouse, W. R. (2004). Thermal characteristics and energy balance of various-size Canadian Shield lakes in the Mackenzie River Basin. *Journal of Hydrometeorology, 5*(1), 129-144. https://doi.org/10.1175/1525-7541(2004)0052.0.CO;2

Paytan, A., Lecher, A. L., Dimova, N., Sparrow, K. J., Kodovska, F. G., Murray, J., Tulaczyk, S., & Kessler, J. D. (2015). Methane transport from the active layer to lakes in the Arctic using Toolik Lake, Alaska, as a case study. *Proceedings of the National Academy of Sciences, 112*(12), 3636-3640. https://doi.org/10.1073/pnas.1417392112

Pearce, C. M., McLennan D., & Cordes, L. D. (1988). The evolution and maintenance of white spruce woodlands on the Mackenzie Delta, N.W.T., Canada. *Ecography, 11*(4), 248-258. https://doi.org/10.1111/j.1600-0587.1988.tb00807.x

Pearson, A., McNichol, A. P., Schneider, R. J., von Reden, K. F., & Zheng, Y. (1998). Microscale AMS ^{14}C measurement at NOSAMS. *Radiocarbon, 40*(1), 61-75. https://doi.org/10.1017/S0033822200017902

Phelps, A. R., Peterson, K. M., & Jeffries, M. O. (1998). Methane efflux from high-latitude lakes during spring ice melt. *Journal of Geophysical Research: Atmospheres, 103*(D22), 29029-29036. https://doi.org/10.1029/98JD00044

Pieters, R., & Lawrence, G. A. (2009). Effect of salt exclusion from lake ice on seasonal circulation. *Limnology and Oceanography, 54*(2), 401-412. https://doi.org/10.4319/lo.2009.54.2.0401

Pipke, K. J. (1996). *Under-ice methane accumulation in Mackenzie Delta lakes and potential flux to the atmosphere at ice-out* (Master's thesis). Retrieved from ProQuest Dissertations and Theses Global database. (Accession Order No. ATT MM17055). Burnaby, British Columbia: Simon Fraser University.

Preuss, I., Knoblauch, C., Gebert, J., & Pfeiffer, E.-M. (2013). Improved quantification of microbial CH_4 oxidation efficiency in arctic wetland soils using carbon isotope

fractionation. *Biogeosciences, 10*(4), 2539-2552. https://doi.org/10.5194/bg-10-2539-2013

Rasilo, T., Prairie, Y. T., & del Giorgio, P. A. (2015). Large-scale patterns in summer diffusive CH_4 fluxes across boreal lakes, and contribution to diffusive C emissions. *Global Change Biology, 21*(3), 1124-1139. https://doi.org/10.1111/gcb.12741

Raymond, P. A., Hartmann, J., Lauerwald, R., Sobek, S., McDonald, C., Hoover, M., Butman, D., Striegl, R., Mayorga, E., Humborg, C., Kortelainen, P., Durr, H., Meybeck, M., Ciais, P., & Guth, P. (2013). Global carbon dioxide emissions from inland waters. *Nature, 503(*7476), 355-359. https://doi.org/10.1038/nature12760

Reimer, P. J., Brown, T. A., & Reimer, R. W. (2004). Discussion: Reporting and calibration of post-bomb ^{14}C data. *Radiocarbon, 46*(3), 1299-1304. https://doi.org/10.1017/S0033822200033154

Rella, C. W., Hoffnagle, J., He, Y., & Tajima, S. (2015). Local- and regional-scale measurements of CH_4, $\delta^{13}CH_4$, and C_2H_6 in the Uintah Basin using a mobile stable isotope analyzer. *Atmospheric Measurement Techniques, 8*(10), 4539-4559. https://doi.org/10.5194/amt-8-4539-2015

Repo, M. E., Huttunen, J. T., Naumov, A. V., Chichulin, A. V., Lapshina, E. D., Bleuten, W., & Martikainen, P. J. (2007). Release of CO_2 and CH_4 from small wetland lakes in western Siberia. *Tellus B, 59*(5), 788-796. https://doi.org/10.1111/j.1600-0889.2007.00301.x

Ricão Canelhas, M., Denfeld, B. A., Weyhenmeyer, G. A., Bastviken, D., & Bertilsson, S. (2016). Methane oxidation at the water-ice interface of an ice-covered lake. *Limnology and Oceanography, 61*, S78-S90. https://doi.org/10.1002/lno.10288

Riley, J. P., & Skirrow, G. (Eds.). (1975). Chemical oceanography. Volume 4. New York and London: Academic Press.

Ritchie, J. C. (1985). Late-Quaternary climatic and vegetational change in the Lower Mackenzie Basin, Northwest Canada. *Ecology, 66*(2), 612-621. https://doi.org/10.2307/1940410

Roberts, M. L., Burton, J. R., Elder, K. L., Longworth, B. E., McIntyre, C. P., Reden, K. F. v., Han, B. X., Rosenheim, B. E., Jenkins, W. J., Galutschek, E., & McNichol, A. P. (2010). A high-performance ^{14}C accelerator mass spectrometry system. *Radiocarbon, 52*(2), 228-235. https://doi.org/10.1017/S0033822200045252

Rudd, J. W. M., & Hamilton, R. D. (1978). Methane cycling in a eutrophic shield lake and its effects on whole lake metabolism 1. *Limnology and Oceanography, 23*(2), 337-348. https://doi.org/10.4319/lo.1978.23.2.0337

Santos, G. M., Southon, J. R., Griffin, S., Beaupre, S. R., & Druffel, E. R. M. (2007). Ultra small-mass AMS ^{14}C sample preparation and analyses at KCCAMS/UCI Facility. *Nuclear Instruments and Methods in Physics Research Section B: Beam Interactions with Materials and Atoms, 259*(1), 293-302. https://doi.org/10.1016/j.nimb.2007.01.172

Sasaki, M., Kim, Y., Uchida, M., & Utsumi, M. (2016). Diffusive summer methane flux from lakes to the atmosphere in the Alaskan arctic zone. *Polar Science, 10*(3), 303-311. https://doi.org/10.1016/j.polar.2016.06.010

Saunois, M., Bousquet, P., Poulter, B., Peregon, A., Ciais, P., Canadell, J. G., Dlugokencky, E. J., Etiope, G., Bastviken, D., Houweling, S., et al. (2016). The global methane budget 2000-2012. *Earth System Science Data, 8*(2), 697-751. https://doi.org/10.5194/essd-8-697-2016

Saunois, M., Stavert, A. R., Poulter, B., Bousquet, P., Canadell, J. G., Jackson, R. B., Raymond, P. A., Dlugokencky, E. J., Houweling, S., Patra, P. K., et al. (2019). The global methane budget 2000--2017. *Earth System Science Data Discussions, 2019*, 1-136. https://doi.org/10.5194/essd-2019-128

Schaefer, H., Fletcher, S. E. M., Veidt, C., Lassey, K. R., Brailsford, G. W., Bromley, T. M., Dlugokencky, E. J., Michel, S. E., Miller, J. B., Levin, I., Lowe, D. C., Martin, R. J., Vaughn, B. H., & White, J. W. C. (2016). A 21st-century shift from fossil-fuel to biogenic methane emissions indicated by $^{13}CH_4$. *Science, 352*(6281), 80-84. https://doi.org/10.1126/science.aad2705

Schneider, R. J., McNichol, A. P., Nadeau, M. J., & Von Reden, K. F. (1995). Measurements of the Oxalic Acid II/Oxalic Acid I ratio as a quality control parameter at NOSAMS. *Radiocarbon, 37*(2), 693-696. https://doi.org/10.1017/S0033822200031210

Schuur, E. A. G., McGuire, A. D., Schadel, C., Grosse, G., Harden, J. W., Hayes, D. J., Hugelius, G., Koven, C. D., Kuhry, P., Lawrence, D. M., Natali, S. M., Olefeldt, D., Romanovsky, V. E., Schaefer, K., Turetsky, M. R., Treat, C. C., & Vonk, J. E. (2015). Climate change and the permafrost carbon feedback. *Nature, 520*(7546), 171-179. https://doi.org/10.1038/nature14338

Schuur, E. A. G., Vogel, J. G., Crummer, K. G., Lee, H., Sickman, J. O., & Osterkamp, T. E. (2009). The effect of permafrost thaw on old carbon release and net carbon exchange from tundra. *Nature, 459*(7246), 556-559. https://doi.org/10.1038/nature08031

Sepulveda-Jauregui, A., Walter Anthony, K. M., Martinez-Cruz, K., Greene, S., & Thalasso, F. (2015). Methane and carbon dioxide emissions from 40 lakes along a north-south latitudinal transect in Alaska. *Biogeosciences, 12*(11), 3197-3223. https://doi.org/10.5194/bg-12-3197-2015

Shah Walter, S.,R., Gagnon, A. R., Roberts, M. L., McNichol, A. P., Lardie Gaylord, M. C., & Klein, E. (2015). Ultra-small graphitization reactors for ultra-microscale ^{14}C analysis at the National Ocean Sciences Accelerator Mass Spectrometry (NOSAMS) facility. *Radiocarbon, 57*(1), 109-122. https://doi.org/10.2458/azu_rc.57.18118

Shah, S. R., & Pearson, A. (2007). Ultra-Microscale (5-25 μg C) analysis of individual lipids by ^{14}C AMS: Assessment and correction for sample processing blanks. *Radiocarbon, 49*(1), 69-82. https://doi.org/10.1017/S0033822200041904

Smith, L. C., Sheng, Y., MacDonald, G. M., & Hinzman, L. D. (2005). Disappearing Arctic lakes. *Science, 308*(5727), 1429. https://doi.org/10.1126/science.1108142

Smith, S. L., Wolfe, S. A., Riseborough, D. W., & Nixon, F. M. (2009). Active-layer characteristics and summer climatic indices, Mackenzie Valley, Northwest Territories, Canada. *Permafrost and Periglacial Processes, 20*(2), 201-220. https://doi.org/10.1002/ppp.651

Snowdon, L. R., & Powell, T. G. (1982). Immature oil and condensate: modification of hydrocarbon generation model for terrestrial organic matter. AAPG Bulletin, 66(6), 775-788. https://doi.org/10.1306/03B5A313-16D1-11D7-8645000102C1865D

Sokal, M. A., Hall, R. I., & Wolfe, B. B. (2010). The role of flooding on inter-annual and seasonal variability of lake water chemistry, phytoplankton diatom communities and macrophyte biomass in the Slave River Delta (Northwest Territories, Canada). *Ecohydrology, 3*(1), 41-54. https://doi.org/10.1002/eco.93

Squires, M. M., & Lesack, L. F. W. (2003). The relation between sediment nutrient content and macrophyte biomass and community structure along a water transparency gradient among lakes of the Mackenzie Delta. *Canadian Journal of Fisheries and Aquatic Sciences, 60*(3), 333-343. https://doi.org/10.1139/f03-027

Squires, M. M., Lesack, L. F. W., & Huebert, D. (2002). The influence of water transparency on the distribution and abundance of macrophytes among lakes of the Mackenzie Delta, Western Canadian Arctic. *Freshwater Biology, 47*(11), 2123-2135. https://doi.org/10.1046/j.1365-2427.2002.00959.x

Squires, M. M., Lesack, L. F. W., Hecky, R. E., Guildford, S. J., Ramlal, P., & Higgins, S. N. (2009). Primary production and carbon dioxide metabolic balance of a lake-rich Arctic river floodplain: partitioning of phytoplankton, epipelon, macrophyte, and epiphyton production among lakes on the Mackenzie Delta. *Ecosystems, 12*(5), 853-872. https://doi.org/10.1007/s10021-009-9263-3

Sriskantharajah, S., Fisher, R. E., Lowry, D., Aalto, T., Hatakka, J., Aurela, M., Laurila, T., Lohila, A., Kuitunen, E., & Nisbet, E. G. (2012). Stable carbon isotope signatures of methane from a Finnish subarctic wetland. *Tellus B: Chemical and Physical Meteorology, 64*(1), 18818. https://doi.org/10.3402/tellusb.v64i0.18818

St. Jacques, J., & Sauchyn, D. J. (2009). Increasing winter baseflow and mean annual streamflow from possible permafrost thawing in the Northwest Territories, Canada. *Geophysical Research Letters, 36*(1), L01401. https://doi.org/10.1029/2008GL035822

St. Pierre, K. A., St. Louis, V. L., Lehnherr, I., Schiff, S. L., Muir, D. C. G., Poulain, A. J., Smol, J. P., Talbot, C., Ma, M., Findlay, D. L., Findlay, W. J., Arnott, S. E., & Gardner, A. S. (2019). Contemporary limnology of the rapidly changing glacierized watershed of the world's largest High Arctic lake. *Scientific Reports, 9*(1), 4447. https://doi.org/10.1038/s41598-019-39918-4

Striegl, R. G., Dornblaser, M. M., McDonald, C. P., Rover, J. R., & Stets, E. G. (2012). Carbon dioxide and methane emissions from the Yukon River system. *Global Biogeochemical Cycles, 26*(4), GB0E05. https://doi.org/10.1029/2012GB004306

Stuiver, M., & Polach, H. A. (1977). Discussion: Reporting of ^{14}C data. *Radiocarbon, 19*(3), 355-363.

Tan, Z., Zhuang, Q., & Walter Anthony, K. (2015). Modeling methane emissions from arctic lakes: Model development and site-level study. *Journal of Advances in Modeling Earth Systems, 7*(2), 459-483. https://doi.org/10.1002/2014MS000344

Tank, S. E., Lesack, L. F. W. Gareis, J. A. L., Osburn, C. L., & Hesslein, R. H. (2011). Multiple tracers demonstrate distinct sources of dissolved organic matter to lakes of the Mackenzie Delta, western Canadian Arctic, *Limnology and Oceanography*, *56*(4), 1297–1309, https://doi.org/10.4319/lo.2011.56.4.1297

Tank, S. E., Lesack, L. F. W., & Hesslein, R. H. (2009). Northern delta lakes as summertime CO_2 absorbers within the Arctic landscape. *Ecosystems, 12*(1), 144-157. https://doi.org/10.1007/s10021-008-9213-5

Tarnocai, C., Canadell, J. G., Schuur, E. A. G., Kuhry, P., Mazhitova, G., & Zimov, S. (2009). Soil organic carbon pools in the northern circumpolar permafrost region. *Global Biogeochemical Cycles, 23*(2), GB2023. https://doi.org/10.1029/2008GB003327

Taylor, A. E., Dallimore, S. R., & Outcalt, S. I. (1996). Late Quaternary history of the Mackenzie-Beaufort region, Arctic Canada, from modelling of permafrost temperatures. 1. The onshore-offshore transition. *Canadian Journal of Earth Sciences, 33*(1), 52-61. https://doi.org/10.1139/e96-006

Thornthwaite, C. W. (1948). An approach toward a rational classification of climate. *Geographical Review, 38*, 55-94. https://doi.org/10.2307/210739

Thornton, B. F., Wik, M., & Crill, P. M. (2015). Climate-forced changes in available energy and methane bubbling from subarctic lakes. *Geophysical Research Letters, 42*(6), 1936-1942. https://doi.org/10.1002/2015GL063189

Thottathil, S. D., Reis, P. C. J., Giorgio, P. A., & Prairie, Y. T. (2018). The extent and regulation of summer methane oxidation in northern lakes. *Journal of Geophysical Research: Biogeosciences, 123*(10), 3216-3230. https://doi.org/10.1029/2018JG004464

Todd, B., & Dallimore, S. (1998). Electromagnetic and geological transect across permafrost terrain, Mackenzie River delta, Canada. *Geophysics, 63*(6), 1914-1924. https://doi.org/10.1190/1.1444484

Toohey, R. C., Herman-Mercer, N., Schuster, P. F., Mutter, E. A., & Koch, J. C. (2016). Multidecadal increases in the Yukon River Basin of chemical fluxes as indicators of changing flowpaths, groundwater, and permafrost. *Geophysical Research Letters, 43*(23), 12,120-12,130. https://doi.org/10.1002/2016GL070817

Townsend-Small, A., Åkerström, F., Arp, C. D., & Hinkel, K. M. (2017). Spatial and temporal variation in methane concentrations, fluxes, and sources in lakes in

Arctic Alaska. *Journal of Geophysical Research: Biogeosciences, 122*(11), 2966-2981. https://doi.org/10.1002/2017JG004002

Tranvik, L. J., Cole, J. J., & Prairie, Y. T. (2018). The study of carbon in inland waters—from isolated ecosystems to players in the global carbon cycle. *Limnology and Oceanography Letters, 3*(3), 41-48. https://doi.org/10.1002/lol2.10068

Tranvik, L. J., Downing, J. A., Cotner, J. B., Loiselle, S. A., Striegl, R. G., Ballatore, T. J., Dillon, P., Finaly, K., Fortino, K., Knoll, L., et al. (2009). Lakes and reservoirs as regulators of carbon cycling and climate. *Limnology and Oceanography, 54*(6 part 2), 2298-2314. https://doi.org/10.4319/lo.2009.54.6_part_2.2298

Treat, C. C., Natali, S. M., Ernakovich, J., Iversen, C. M., Lupascu, M., McGuire, A. D., Norby, R. J., Roy Chowdhury, T., Richter, A., Šantrůčková, H., Schädel, C., Schuur, E. A. G., Sloan, V. L., Turetsky, M. R., & Waldrop, M. P. (2015). A pan-Arctic synthesis of CH_4 and CO_2 production from anoxic soil incubations. *Global Change Biology, 21*(7), 2787-2803. https://doi.org/10.1111/gcb.12875

Turnbull, J. C., Mikaloff Fletcher, S. E., Ansell, I., Brailsford, G. W., Moss, R. C., Norris, M. W., & Steinkamp, K. (2017). Sixty years of radiocarbon dioxide measurements at Wellington, New Zealand: 1954-2014. *Atmospheric Chemistry and Physics, 17*(23), 14771-14784. https://doi.org/10.5194/acp-17-14771-2017

University of Montana. ESRI Mapping Center. (28 September 2017). http://www.arcgis.com/apps/OnePane/main/index.html?appid=b1a0c03f04994a36b93271b0c39e6c0f. Evapotranspiration Web Viewer.

Vachon, D., Langenegger, T., Donis, D., & McGinnis, D. F. (2019). Influence of water column stratification and mixing patterns on the fate of methane produced in deep sediments of a small eutrophic lake. *Limnology and Oceanography, 64*(5), 2114-2128. https://doi.org/10.1002/lno.11172

Verpoorter, C., Kutser, T., Seekell, D. A., & Tranvik, L. J. (2014). A global inventory of lakes based on high-resolution satellite imagery. *Geophysical Research Letters, 41*(18), 6396-6402. https://doi.org/10.1002/2014GL060641

Vogel, J. S., Southon, J. R., Nelson, D. E., & Brown, T. A. (1984). Performance of catalytically condensed carbon for use in accelerator mass spectrometry. *Nuclear Instruments and Methods in Physics Research Section B: Beam Interactions with Materials and Atoms*, *5*(2), 289-293. https://doi.org/10.1016/0168-583X(84)90529-9

von Reden, K. F., McNichol, A. P., Pearson, A., & Schneider, R. J. (1998). ^{14}C AMS measurements of <100 μg samples with a high-current system. *Radiocarbon*, *40*(1), 247-253. https://doi.org/10.1017/S0033822200018117

Vonk, J. E., Mann, P. J., Davydov, S., Davydova, A., Spencer, R. G. M., Schade, J., Sobczak, W. V., Zimov, N., Zimov, S., Bulygina, E., Eglinton, T. I., & Holmes, R. M. (2013). High biolability of ancient permafrost carbon upon thaw. *Geophysical Research Letters, 40*(11), 2689-2693. https://doi.org/10.1002/grl.50348

Walter Anthony, K. M., Anthony, P., Grosse, G., & Chanton, J. (2012). Geologic methane seeps along boundaries of Arctic permafrost thaw and melting glaciers. *Nature Geoscience, 5*(6), 419-426. https://doi.org/10.1038/NGEO1480

Walter Anthony, K. M., Daanen, R., Anthony, P., Schneider, v. D., Ping, C., Chanton, J. P., & Grosse, G. (2016). Methane emissions proportional to permafrost carbon thawed in Arctic lakes since the 1950s. *Nature Geoscience, 9*(9), 679-682. https://doi.org/10.1038/ngeo2795

Walter Anthony, K. M., Vas, D. A., Brosius, L., Chapin, F. S., Zimov, S. A., & Zhuang, Q. (2010). Estimating methane emissions from northern lakes using ice-bubble surveys. *Limnology and Oceanography: Methods, 8*(11), 592-609. https://doi.org/10.4319/lom.2010.8.0592

Walter Anthony, K. M., Zimov, S. A., Grosse, G., Jones, M. C., Anthony, P. M., III, F. S. C., Finlay, J. C., Mack, M. C., Davydov, S., Frenzel, P., & Frolking, S. (2014). A shift of thermokarst lakes from carbon sources to sinks during the Holocene epoch. *Nature, 511*(7510), 452-456.

Walter Anthony, K., Schneider, v. D., Nitze, I., Frolking, S., Emond, A., Daanen, R., Anthony, P., Lindgren, P., Jones, B., & Grosse, G. (2018). 21st-century modeled permafrost carbon emissions accelerated by abrupt thaw beneath lakes. *Nature Communications, 9*(1), 3262. https://doi.org/10.1038/s41467-018-05738-9

Walter, K. M., Chanton, J. P., Chapin, F. S., Schuur, E. A. G., & Zimov, S. A. (2008). Methane production and bubble emissions from arctic lakes: Isotopic implications for source pathways and ages. *Journal of Geophysical Research: Biogeosciences, 113*(G3), G00A08. https://doi.org/10.1029/2007JG000569

Walter, K. M., Zimov, S. A., Chanton, J. P., Verbyla, D., & Chapin, F. S. (2006). Methane bubbling from Siberian thaw lakes as a positive feedback to climate warming. *Nature, 443*(7107), 71-75. https://doi.org/10.1038/nature05040

Walvoord, M. A., & Kurylyk, B. L. (2016). Hydrologic impacts of thawing permafrost - a teview. *Vadose Zone Journal, 15*(6). https://doi.org/10.2136/vzj2016.01.0010

Walvoord, M. A., & Striegl, R. G. (2007). Increased groundwater to stream discharge from permafrost thawing in the Yukon River basin: Potential impacts on lateral export of carbon and nitrogen. *Geophysical Research Letters, 34*(12), D18102. https://doi.org/10.1029/2007GL030216

Welch, H. E., & Bergmann, M. A. (1985). Water circulation in small Arctic lakes in winter. *Canadian Journal of Fisheries and Aquatic Sciences, 42*(3), 506-520. https://doi.org/10.1139/f85-068

Wellman, T. P., Voss, C. I., & Walvoord, M. A. (2013). Impacts of climate, lake size, and supra- and sub-permafrost groundwater flow on lake-talik evolution, Yukon Flats, Alaska (USA). *Hydrogeology Journal, 21*(1), 281-298. https://doi.org/10.1007/s10040-012-0941-4

Westermann, S., Duguay, C. R., Grosse, G., & Kääb, A. (2015). Remote sensing of permafrost and frozen ground. In M. Tedesco (Ed.), *Remote sensing of the*

cryosphere (First ed., pp. 307-344) John Wiley & Sons, Ltd. https://doi.org/10.1002/9781118368909.ch13

Wheat, C. G., Fisher, A. T., McManus, J., Hulme, S. M., & Orcutt, B. N. (2017). Cool seafloor hydrothermal springs reveal global geochemical fluxes. *Earth and Planetary Science Letters, 476*, 179-188. https://doi.org/10.1016/j.epsl.2017.07.049

Wheat, C. G., Jannasch, H. W., Fisher, A. T., Becker, K., Sharkey, J., & Hulme, S. (2010). Subseafloor seawater-basalt-microbe reactions: Continuous sampling of borehole fluids in a ridge flank environment. *Geochemistry, Geophysics, Geosystems, 11*, Q07011. https://doi.org/10.1029/2010GC003057

Wheat, C. G., Jannasch, H. W., Kastner, M., Hulme, S., Cowen, J., Edwards, K. J., Orcutt, B. N., Glazer, B. (2011). Fluid sampling from oceanic borehole observatories: design and methods for CORK activities (1990-2010). In A. T. Fisher, T. Tsuji & Petronots, K., and the Expedition 327 Scientists (Eds.), *Proceedings of the Integrated Ocean Drilling Program*. Tokyo. Integrated Ocean Drilling Program Management International, Inc.

Whitfield, C. J., Baulch, H. M., Chun, K. P., & Westbrook, C. J. (2015). Beaver-mediated methane emission: The effects of population growth in Eurasia and the Americas. *Ambio, 44*(1), 7-15. https://doi.org/10.1007/s13280-014-0575-y

Whiticar, M. J. (1990). A geochemial perspective of natural gas and atmospheric methane. *Organic Geochemistry, 16*(1), 531-547. https://doi.org/10.1016/0146-6380(90)90068-B

Whiticar, M. J. (1999). Carbon and hydrogen isotope systematics of bacterial formation and oxidation of methane. *Chemical Geology, 161*(1–3), 291-314. https://doi.org/10.1016/S0009-2541(99)00092-3

Whiticar, M. J., & Faber, E. (1986). Methane oxidation in sediment and water column environments—Isotope evidence. *Organic Geochemistry, 10*(4), 759-768. https://doi.org/10.1016/S0146-6380(86)80013-4

Whiticar, M. J., Faber, E., & Schoell, M. (1986). Biogenic methane formation in marine and freshwater environments: CO_2 reduction vs. acetate fermentation—Isotope evidence. *Geochimica Et Cosmochimica Acta, 50*(5), 693-709. https://doi.org/10.1016/0016-7037(86)90346-7

Wik, M., Crill, P. M., Bastviken, D., Danielsson, Å, & Norbäck, E. (2011). Bubbles trapped in arctic lake ice: Potential implications for methane emissions. *Journal of Geophysical Research: Biogeosciences, 116*. G03044. https://doi.org/10.1029/2011JG001761

Wik, M., Crill, P. M., Varner, R. K., & Bastviken, D. (2013). Multiyear measurements of ebullitive methane flux from three subarctic lakes. *Journal of Geophysical Research: Biogeosciences, 118*(3), 1307-1321. https://doi.org/10.1002/jgrg.20103

Wik, M., Johnson, J. E., Crill, P. M., DeStasio, J. P., Erickson, L., Halloran, M. J., Fahnestock, M. F., Crawford, M. K., Phillips, S. C., & Varner, R. K. (2018). Sediment characteristics and methane ebullition in three subarctic lakes. *Journal*

of Geophysical Research: Biogeosciences, 123(8), 2399-2411. https://doi.org/10.1029/2017JG004298

Wik, M., Thornton, B. F., Bastviken, D., Uhlbäck, J., & Crill, P. M. (2016a). Biased sampling of methane release from northern lakes: A problem for extrapolation. *Geophysical Research Letters, 43*(3), 2015GL066501. https://doi.org/10.1002/2015GL066501

Wik, M., Varner, R. K., Anthony, K. W., MacIntyre, S., & Bastviken, D. (2016b). Climate-sensitive northern lakes and ponds are critical components of methane release. *Nature Geoscience, 9*(2), 99-105. https://doi.org/10.1038/ngeo2578

Wuebbles, D. J., & Hayhoe, K. (2002). Atmospheric methane and global change. *Earth-Science Reviews, 57*(3), 177-210. https://doi.org/10.1016/S0012-8252(01)00062-9

Yamamoto, S., Alcauskas, J. B., & Crozier, T. E. (1976). Solubility of methane in distilled water and seawater. *Journal of Chemical & Engineering Data, 21*(1), 78-80. https://doi.org/10.1021/je60068a029

Yoshikawa, K., & Hinzman, L. D. (2003). Shrinking thermokarst ponds and groundwater dynamics in discontinuous permafrost near council, Alaska. *Permafrost and Periglacial Processes, 14*(2), 151-160. https://doi.org/10.1002/ppp.451

Yvon-Durocher, G., Allen, A. P., Bastviken, D., Conrad, R., Gudasz, C., St-Pierre, A., Thanh-Duc, N., & del Giorgio, P. A. (2014). Methane fluxes show consistent temperature dependence across microbial to ecosystem scales. *Nature, 507*(7493), 488-491. https://doi.org/10.1038/nature13164

Zare, R. N., Kuramoto, D. S., Haase, C., Tan, S. M., Crosson, E. R., & Saad, N. M. R. (2009). High-precision optical measurements of $^{13}C/^{12}C$ isotope ratios in organic compounds at natural abundance. *Proceedings of the National Academy of Sciences, 106*(27), 10928-10932. https://doi.org/10.1073/pnas.0904230106

Zhang, X., Vincent, L. A., Hogg, W. D., & Niitsoo, A. (2000). Temperature and precipitation trends in Canada during the 20th century. *Atmosphere-Ocean, 38*(3), 395-429. https://doi.org/10.1080/07055900.2000.9649654

Zigah, P. K., Oswald, K., Brand, A., Dinkel, C., Wehrli, B., & Schubert, C. J. (2015). Methane oxidation pathways and associated methanotrophic communities in the water column of a tropical lake. *Limnology and Oceanography, 60*(2), 553-572. https://doi.org/10.1002/lno.10035

Zimov, S. A., Voropaev, Y. V., Semiletov, I. P., Davidov, S. P., Prosiannikov, S. F., Chapin, F. S., Chapin, M. C., Trumbore, S., & Tyler, S. (1997). North Siberian lakes: A methane source fueled by Pleistocene carbon. *Science, 277*(5327), 800-802. https://doi.org/10.1126/science.277.5327.800

Zolkos, S., Tank, S. E., Striegl, R. G., & Kokelj, S. V. (2019). Thermokarst effects on carbon dioxide and methane fluxes in streams on the Peel Plateau (NWT, Canada). *Journal of Geophysical Research: Biogeosciences, 124*(7), 1781-1798. https://doi.org/10.1029/2019JG005038

Zubov, N. N. (1945). Arctic Ice (in Russian) Istatel'sWo Glasevmorputi, Moscow.